PHASE EQUILIBRIA IN BINARY MIXTURES OF CARBON TETRAFLUORIDE AND N-ALKANES AT HIGH PRESSURES

by

João Manuel Martins Mendonça

A thesis submitted for the degree of Doctor of Philosophy of the University of London and for the Diploma of Membership of the Imperial College.

Department of Chemical Engineering and Chemical Technology,
Imperial College of Science and Technology,
London, S.W.7.

October, 1979

PHASE EQUILIBRIA IN BINARY MIXTURES OF CARBON TETRAFLUORIDE AND N-ALKANES AT HIGH PRESSURES

by

J.M.M. Mendonça

ABSTRACT

The phase behaviour of the binary system CF_4 + n-C_7H_{16} has been investigated at temperatures ranging from 323.15 K to 343.15 K and pressures up to ca. 1 300 bar. The experimental results obtained show that the critical line of this sytem goes through a minimum temperature before proceeding to very high pressures. The co-ordinates of this "critical point of double-contact" are: T^c = 330.25 K, P^c = 670 bar, x^c = 0.708.

A method based on the principle of corresponding states, originally developed by Teja and Rowlinson, has been used to correlate the experimental critical data for various CF_4 + n-alkane systems, including the data obtained in this investigation. Although the scope and flexibility of the algorithm have been improved, it fails to predict correctly the critical behaviour observed experimentally for these systems. This failure is attributed to the molecular shape factor equations commonly used to account for departures from the simple principle of corresponding states.

A simplified version of the algorithm has been used in which all the molecular shape factors are set to unity. The results thus obtained are in good agreement with the experimental evidence. In particular, the method clearly predicts a "continuous" and logical transition from the more familiar types of liquid-liquid and gas-liquid critical lines to the so-called gas-gas critical lines with increasing disparity of the component molecules.

Estimates of the numerical values of the binary interaction parameters for the CF_4 + C_3H_8 and CF_4 + n-C_4H_{10} systems have been obtained by correlating ξ_{12} and η_{12} with the number of carbon atoms in the n-alkane molecule. Thus it has been possible to predict the critical lines for these two systems, for which no experimental data are available.

Acknowledgements

I wish to express my gratitude to Dr. K.E. Bett for his unfailing friendship, encouragement and patient supervision of all the work presented in this thesis.

I should also like to thank Dr. G. Saville, Dr. R. Szczepanski and Dr. A.S. Teja for helpful discussions during the computing stages of this thesis and for permission to make use of their computer programs, and Prof. G.M. Schneider and Dr. U. Deiters for their continued interest in my work.

Thanks are also due to all members of the departmental workshop staff and glassblowers for their willing help during the experimental stages of this work, and to the departmental librarians for their invaluable help with all bibliographical matters. I am also deeply grateful to Mrs. Pat Brown for her dedication in the unenviable task of typing this thesis.

A grant from the Calouste Gulbenkian Foundation (Lisbon) and a generous leave of absence from the Department of Chemical Engineering of the University of Porto (Portugal) are gratefully acknowledged.

Finally, I wish to thank all my friends who, in one way or another, contributed towards the making of this thesis, and above all my parents for their years of patience and encouragement.

CONTENTS

		Page
	TITLE PAGE	1
	ABSTRACT	2
	ACKNOWLEDGEMENTS	3
	CONTENTS	4
	LIST OF TABLES	7
	LIST OF FIGURES	8
	LIST OF PRINCIPAL SYMBOLS	12
1.	INTRODUCTION	15
2.	CRITICAL PHENOMENA IN BINARY FLUID MIXTURES	19
	2.1 Critical States of Mixtures	19
	2.2 Retrograde Phenomena and Barotropic Inversion of Phases	23
	2.3 Classification of Binary Fluid Phase Diagrams	25
	2.4 Gas-Gas Immiscibility	35
3.	THE ANOMALOUS BEHAVIOUR OF SYSTEMS CONTAINING NON-AROMATIC FLUOROCARBONS	44
	3.1 Experimental Evidence at Low Pressures	44
	3.2 Experimental Evidence at High Pressures	47
	3.3 Interpretation of the Experimental Evidence	48
4.	DESCRIPTION OF THE APPARATUS	52
	4.1 Compression Section	52
	4.2 Equilibrium Section	55
	4.3 Analysis Section	58

(.../)

		Page
5.	EXPERIMENTAL PROCEDURE	62
	5.1 Operation of the Gas Compressor	62
	5.2 Operation of the Equilibrium Section	64
	5.3 Operation of the Phase Analysis Section	66
6.	EXPERIMENTAL RESULTS: PRESENTATION AND DISCUSSION	70
	6.1 Presentation of the Results	70
	6.2 Accuracy of Measurements	74
	6.3 Error Analysis	76
	6.4 Discussion of the Experimental Results	79
7.	CLASSICAL THERMODYNAMIC DESCRIPTION OF CRITICAL PHASES	86
	7.1 One-Component Systems	87
	7.2 Two-Component Systems	89
	7.3 Multicomponent Systems	92
	7.4 Stability of Critical Phases	94
8.	REVIEW OF EXISTING METHODS FOR CORRELATION AND PREDICTION OF CRITICAL PHENOMENA IN FLUID MIXTURES	99
	8.1 Empirical Methods	99
	8.2 Equation of State Approach	100
	8.3 Theoretically-Based Methods	104
9.	THE COMPUTATION OF THE CRITICAL LOCUS OF BINARY MIXTURES USING THE PRINCIPLE OF CORRESPONDING STATES AND ITS EXTENSIONS	114
	9.1 Theoretical Background	114
	9.2 Algorithm for the Prediction of Critical Points in Binary Fluid Mixtures	133

(.../)

Page

10. COMPUTER RESULTS AND CONCLUSIONS 139

10.1 Introduction 139

10.2 Correlation of Critical Data for Carbon Tetrafluoride + n-Alkane Systems 140

10.3 Prediction of the Critical Lines for the Systems Carbon Tetrafluoride + Propane and Carbon Tetrafluoride + n-Butane 150

10.4 Predicted Critical Behaviour at Very High Pressures 159

10.5 Conclusions and Suggestions for Further Work 161

REFERENCES 164

APPENDICES

A. PURITY OF MATERIALS 173

B. PHYSICAL PROPERTIES OF PURE SUBSTANCES 174

C. TABULATED EXPERIMENTAL RESULTS 175

D. OUTLINE OF DERIVATION OF EQUATIONS (6-3) AND (6-4) 182

E. OUTLINE OF DERIVATION OF EQUATIONS (9-36) - (9-44) 185

F. OUTLINE OF DERIVATION OF EQUATIONS (9-58) AND (9-59) 190

G. COEFFICIENTS IN EQUATION OF STATE FOR THE REFERENCE SUBSTANCE 193

H. LISTING OF ROUTINES (microfiche inside the back cover)

LIST OF TABLES

Table No.		Page
2.1	Systems found to exhibit gas-gas immiscibility of the first kind	38
2.2	Systems found to exhibit gas-gas immiscibility of the second kind	39
3.1	Thermodynamic properties of equimolar binary liquid mixtures containing a non-aromatic fluorocarbon	45
6.1	Barotropic inversion of the phases for the CF_4 + n-C_7H_{16} system	81
6.2	Critical points for the CF_4 + n-C_7H_{16} system	82
10.1	Binary interaction parameters for CF_4 + n-alkane systems	150

LIST OF FIGURES

Fig. No.		Page
2.1	(P-T-x) surface for a simple binary mixture in the gas-liquid critical region	21
2.2	Sections through the (P-T-x) surface of Fig. 2.1	22
2.3	Retrograde condensation and evaporation	24
2.4	Gas-liquid critical lines in simple binary systems	27
2.5	Positive and negative critical azeotropy	28
2.6	Systems showing distinct liquid-liquid and gas-liquid critical loci	29
2.7	Limited miscibility	31
2.8	Systems showing immiscibility at all temperatures below the critical point of the less volatile component	33
2.9	Systems showing a heterogeneous azeotrope up to the critical region	34
2.10	Typical (P^c-T^c) diagrams of systems exhibiting gas-gas immiscibility	36
2.11	Typical (P-x) diagrams of systems exhibiting gas-gas immiscibility	37
2.12	Critical loci of CO_2 + n-alkane systems	41
2.13	Critical loci of H_2O + n-alkane systems	42
2.14	Critical loci of CH_4 + n-alkane systems	43

(.../)

Fig. No.		Page
3.1	Experimental (P-x) diagrams showing liquid-liquid immiscibility in the CF_4 + CH_4 and CF_4 + C_2H_6 systems	49
4.1	Schematic diagram of gas compressor	53
4.2	Schematic diagram of equilibrium apparatus	56
4.3	Schematic diagram of analysis section	59
4.4	Vapour pressure and melting pressure curves of the pure components below atmospheric pressure	60
5.1	The two types of freezing traps used in the experiments	67
6.1	Isothermal (P-x) diagram for the CF_4 + n-C_7H_{16} system, showing the (P^c-x^c) projection of the critical line	71
6.2	Isothermal (P-ρ) diagram for the CF_4 + n-C_7H_{16} system, showing the (P^c-ρ^c) projection of the critical line	72
6.3	Isothermal (ρ-x) diagram for the CF_4 + n-C_7H_{16} system, showing the (ρ^c-x^c) projection of the critical line	73
6.4	(P^c-T^c) projection of the critical line for the CF_4 + n-C_7H_{16} system and vapour pressure curves of the pure components	83
7.1	Schematic representation of the isotherms for a pure substance, as calculated from an equation of state	88

(.../)

Fig. No.		Page
7.2	Schematic representation of the Gibbs free energy of mixing of a binary system as a function of mole fraction at constant temperature and pressure	91
7.3	Graphical procedure for location of critical end points on critical lines	96
9.1	Flow diagram of program CRITIC	136
10.1	Predicted (P^c-T^c) projection of the critical locus for the CF_4 + CH_4 system	142
10.2	Predicted (P^c-T^c) projection of the critical locus for the CF_4 + C_2H_6 system	143
10.3	Predicted (P^c-T^c) projection of the critical locus for the CF_4 + n-C_5H_{12} system	145
10.4	Predicted (P^c-T^c) projection of the critical locus for the CF_4 + n-C_6H_{14} system	146
10.5	Predicted (P^c-T^c) projection of the critical locus for the CF_4 + n-C_7H_{16} system	147
10.6	Predicted (P^c-x^c) projection of the critical locus for the CF_4 + n-C_7H_{16} system	148
10.7	Correlation of the binary interaction parameters ξ_{12} and η_{12} with the number of carbon atoms in the n-alkane molecule for CF_4 + n-alkane binary systems	151
10.8	Predicted (P^c-T^c) projection of the critical locus for the CF_4 + C_3H_8 system	153

(.../)

Fig. No.		Page
10.9	Predicted (P^c-T^c) projection of the critical locus for the CF_4 + n-C_4H_{10} system	154
10.10	Enlarged view of Fig. 10.9 in the vicinity of the critical point of pure CF_4	155
10.11	Predicted (P^c-ρ^c) projection of the critical locus for the CF_4 + n-C_4H_{10} system in the vicinity of the critical point of pure CF_4	156
10.12	Predicted behaviour of CF_4 + n-alkane systems at very high pressures	160

LIST OF PRINCIPAL SYMBOLS

Roman Capitals

A Molar Helmholtz free energy
Constants in reference substance equation of state
Constant in BWR equation of state

B Second virial coefficient
Constant in BWR equation of state

C Heat capacity
Constant in BWR equation of state

G Molar Gibbs free energy
Gaseous state

H Molar enthalpy

L Liquid state

M Molecular mass

N Number of molecules

P Pressure

Q Molecular and configurational parts of the canonical ensemble partition function

R Molar gas constant

S Molar entropy
Solid state

T Temperature

U Molar internal energy
Configurational energy

V Molar volume

Z Canonical ensemble partition function

(.../)

Roman Lower Case

a Constant in vdW, RK and BWR equations of state

b Constant in vdW, RK and BWR equations of state

c Number of components
Constant in BWR equation of state

d Density

f Corresponding states scaling parameter for energy

h Corresponding states scaling parameter for volume

k Boltzmann constant

n Number of moles

r Molecular position

u Intermolecular potential

x Mole fraction

z Compression factor

Greek Symbols

α Riedel's factor
Constant in BWR equation of state

γ Constant in reference substance equation of state
Constant in BWR equation of state

δ Excess second virial coefficient
Random experimental error

Δ Derivative of scaling parameters h and f with respect to composition at constant temperature and density

ε Characteristic energy of intermolecular potential

η Binary interaction parameter for volume

θ Temperature shape factor

(.../)

(Greek Symbols, cont.)

μ	Chemical potential
ξ	Binary interaction parameter for energy or temperature
ρ	Molar density
σ	Characteristic distance of intermolecular potential
ϕ	Volume shape factor
χ	Binary interaction parameter for distance
ω	Pitzer's acentric factor

Superscripts

c	critical
mol.	molecular
p.g.	perfect gas
e.s.	equivalent substance
R	reduced
res.	residual
σ	saturation state
E	excess
m	mixture
$\sim$	configurational

Subscripts

i,j; 1,2	component identifiers
x	constant composition partial derivative with respect to composition
v	constant volume partial derivative with respect to volume
ρ	constant molar density partial derivative with respect to molar density
o	reference substance

Chapter 1

INTRODUCTION

Phase equilibria at high pressures are of great interest to chemical engineers, especially to those in the petroleum, cryogenic and related industries. Until about 1960, however, calculations of high-pressure phase behaviour were based mainly on empirical correlations, such as the well-known K-value charts. Only in recent years has there been a move towards extending to high-pressure phase equilibria the thermodynamic concepts which for many years had been accepted for the description of equilibria at ordinary pressures.

The number of binary fluid systems which are of interest in technical processes is quite large, and if one thinks of the possible multi-component systems of interest in the chemical and petroleum industries, the number becomes very large indeed. To obtain experimental data for even a small fraction of these systems under varying conditions of pressure and temperature is an impossible task. The only practicable approach is to restrict the experimental work to a few representative systems and, on the basis of such studies, use thermodynamic analysis as a tool for correlating and generalising the experimental data.

From these generalisations it is possible to predict the phase behaviour of previously investigated systems under new conditions, and also the behaviour of new systems which have not been investigated at all. This is especially important in the prediction of properties of multi-component systems from data obtained for binary mixtures: such predictions are frequently required for rational engineering design of separation operations, as is the case with computer-aided design procedures.

Currently available methods of prediction can be roughly divided into empirical, semi-empirical and theoretically-based methods (1). The last group includes all those methods based on statistical thermodynamics, such as corresponding states methods and perturbation theory methods. In simple terms, statistical thermodynamics tries to explain

the macroscopic properties of matter in terms of the properties of the molecules. These methods therefore have a strong theoretical basis and, in principle, should be highly accurate and reliable. Unfortunately, our present knowledge of the properties of molecules is not sufficient for the methods of statistical thermodynamics to be applied in any but the simplest cases.

Progress in this field is highly desirable, but it can only be achieved if consideration is given to the experimental study of binary mixtures made up of components whose molecules differ widely in shape, size, ionisation potential and polarisability. In such cases, one might expect the phase behaviour to be very different from that found for simpler mixtures of similar molecules, because of the vast range of possible interactions between unlike molecules. This will be especially true in the critical region, where phase equilibria are characterised by large deviations from ideality, giving rise to strange phenomena such as retrograde behaviour, barotropic inversion of phases and gas-gas immiscibility. The calculation of the critical lines of mixtures provides probably the most severe test of any method of prediction, since the topology of these lines in (P,T,x) space is quite complex, even for binary systems.

Mixtures of aliphatic fluorocarbons and hydrocarbons are of special interest in this context: at atmospheric pressure these mixtures are characterised by very large values of the thermodynamic excess functions and often show liquid-liquid immiscibility with upper critical solution temperatures. The reasons for this unexpected behaviour have been ascribed to the extremely weak interaction between the unlike molecules and to differences in size and shape of the molecules (2).

Recently, the phase behaviour in the critical region of some of these mixtures of aliphatic fluorocarbons and hydrocarbons has been investigated under conditions of very high pressure over a wide range of temperatures. In particular, Sideras (3) undertook the investigation of the phase behaviour of the carbon tetrafluoride + n-heptane system at high pressures, but his work was restricted to a single isotherm (50 ^{o}C) and he found no critical points. His results, however,

seemed to suggest the possibility of the occurrence of gas-gas immiscibility in this particular system under easily-accessible experimental conditions.

The first objective of the work described in this thesis was therefore to complete the investigation initiated by Sideras and to study the phase behaviour of the CF_4 + n-C_7H_{16} system over a wide range of temperatures and pressures, including the critical region, to see whether or not this system exhibits gas-gas immiscibility.

The second objective was to compare the experimental data for this system with similar data for other aliphatic fluorocarbon + hydrocarbon systems recently investigated, with special emphasis on binary systems where one of the components is CF_4 and the other component is a normal-alkane of variable chain length. The study of such "families" of binary systems has proved to be one of the most fruitful ways of gaining insight into the complex variety of topological behaviour which characterises the critical phenomena in binary mixtures.

Finally, the main objective of the work was to use the experimental results obtained in this and other investigations to assess the validity of the existing methods for predicting critical phenomena in binary mixtures and, in particular, to see whether the principle of corresponding states will correctly predict the critical phase behaviour of these systems, so as to obtain a better understanding of the nature of the forces between the unlike molecules.

This thesis may be divided into two parts. In the first part a descriptive account is given of the variety of critical phenomena in binary fluid mixtures (Chapter 2), followed by a brief reference to the peculiar behaviour of aliphatic fluorocarbon + hydrocarbon systems and possible explanations of this behaviour (Chapter 3). After a short description of the apparatus used in this investigation (Chapter 4) and of the experimental procedure (Chapter 5), the experimental data obtained for the CF_4 + n-C_7H_{16} system are presented, together with an estimate of their accuracy (Chapter 6).

(.../)

In the second part of the thesis, after a brief reference to the classical thermodynamics of the critical phase (Chapter 7) and the description of the methods currently available for the prediction and correlation of critical phenomena in binary mixtures (Chapter 8), attention is focused on the extension of the principle of corresponding states to mixtures, and the possibilities of using this method for the prediction of critical lines in binary mixtures are explored (Chapter 9). Finally, in Chapter 10, the computer results obtained with the method described in the previous chapter are presented and compared with the experimental results obtained in this and similar investigations, and suggestions are made for possible improvements in the method.

Chapter 2

CRITICAL PHENOMENA IN BINARY FLUID MIXTURES

In the following discussion, a purely descriptive account is given of the phase behaviour of binary systems in the critical region in terms of the projections of (P-T-x) phase boundaries. On the accompanying diagrams, the (P-x) isotherms, (T-x) isobars and (P-T) isopleths are represented by thin, unbroken lines; all critical lines are represented by thick, unbroken lines; the vapour pressure lines of the pure components are shown as dashed lines; and all other equilibrium curves, like azeotropic lines and three-phase lines, are shown as dash-dot lines.

Since this investigation is concerned only with binary fluid mixtures, hardly any attention is given to solid boundaries in this discussion, although such boundaries do sometimes intrude into the critical region of binary mixtures, and possibly interfere with the critical line of the system.

Most of the examples of phase behaviour discussed in this chapter have been obtained from Rowlinson (4), Schneider (5, 6, 7, 8, 9), Hicks and Young (10), Prausnitz (11) and van Konynenburg (12), together with the comprehensive bibliography by Michaels, Green and Larsen (13) covering the period from the beginning of 1950 to the end of 1967.

2.1 Critical States of Mixtures

The critical state of a mixture, like the critical point of a pure substance, is defined as that state in which two phases co-existing in equilibrium become indistinguishable from one another in relation to all their intensive properties. Although the critical points of mixtures and the gas-liquid critical point of a pure substance are physically analogous, their thermodynamic description is quite different (4). Whereas pure substances are characterised by a single gas-liquid critical point and their fluid-phase behaviour is defined by the vapour-pressure curve, binary systems exhibit a critical line in the three-dimensional (P-T-x) space, which may have several branches. This critical line is the locus of all the critical points of the binary system.

(.../)

The representation of the (P-T-x) surfaces in the three-dimensional (P-T-x) space is difficult, and the projections of sections through those surfaces on to the (P-x), (T-x) and (P-T) planes are commonly used to facilitate the study of phase equilibria in binary systems. These projections give rise to isothermal (P-x) diagrams, isobaric (T-x) diagrams or constant-composition (P-T) diagrams, also called isopleths. Critical phenomena in binary mixtures are most easily visualised with the aid of the latter, and they will be used widely in the following discussion.

Critical points of simple binary fluid mixtures are conventionally categorised into liquid-liquid and gas-liquid critical points. Liquid-liquid critical points are normally observed at temperatures well below the critical temperature of the more volatile component and when plotted on a (P-T) diagram are often found to give a locus nearly parallel to the P-axis. Gas-liquid critical points, on the other hand, are observed at temperatures near the critical temperatures of the pure components and when plotted on a (P-T) diagram the locus of these critical points is, in the simplest possible case, a continuous smooth line joining the gas-liquid critical points of the two pure components. Fig. 2.1 shows a sketch of the (P-T-x) surfaces for a simple system in the gas-liquid critical region, and Fig. 2.2 shows the (P-T), (P-x) and (T-x) projections of sections through these surfaces. The critical point of a mixture is always at an extreme value of pressure on the isothermal (P-x) loops and at an extreme value of temperature on the isobaric (T-x) loops. It is, however, normally neither at the maximum temperature nor at the maximum pressure on the (P-T) loops at constant composition, this fact being a necessary consequence of the rounded ends of the (P-x) and (T-x) loops (4). The (P-T) projection of the critical line is in fact the envelope of all the isopleths or constant-composition (P-T) loops, as shown in Fig. 2.2(a).

(.../)

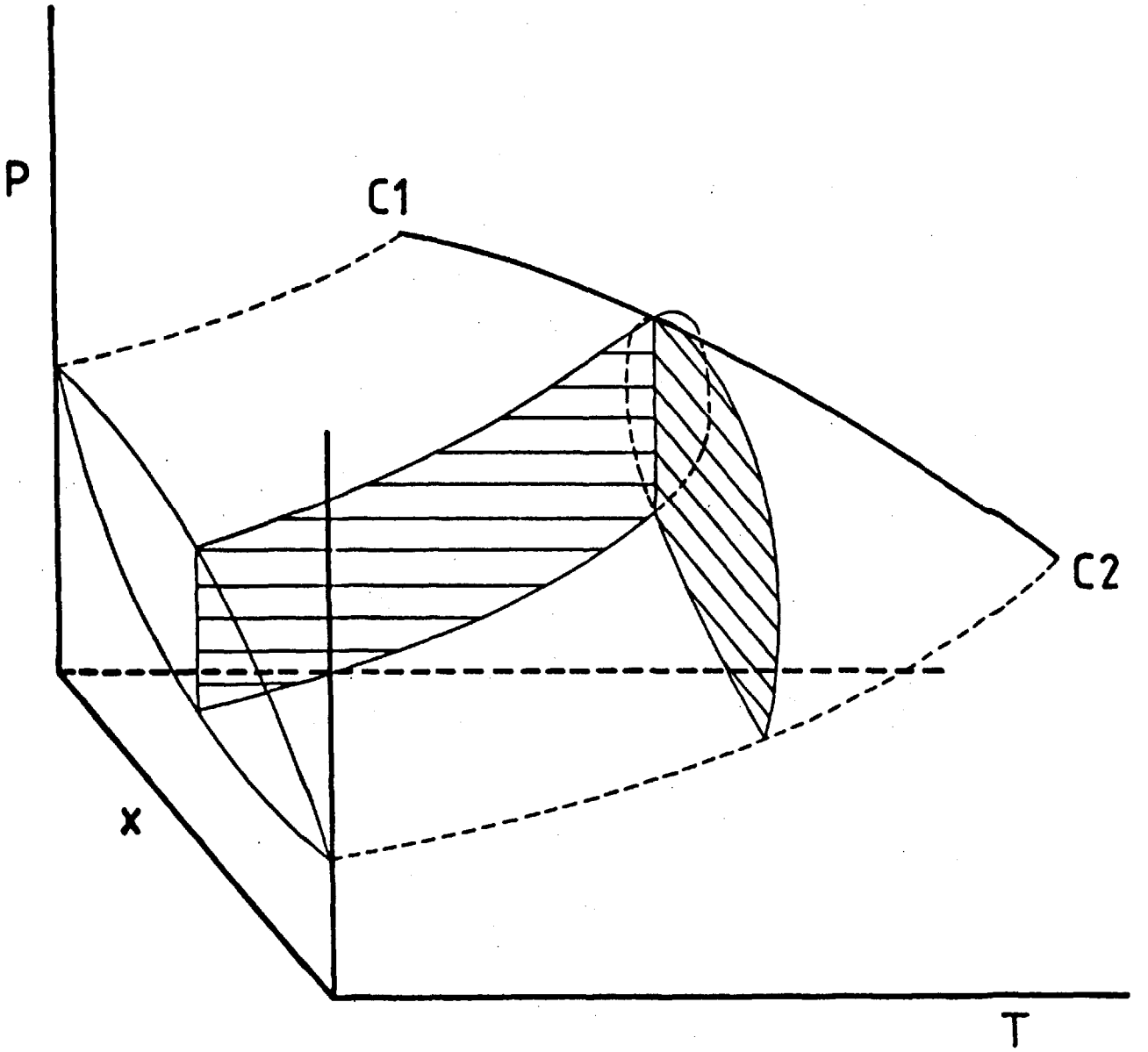


FIG. 2.1. (P-T-x) surface for a simple binary mixture in the gas-liquid critical region.

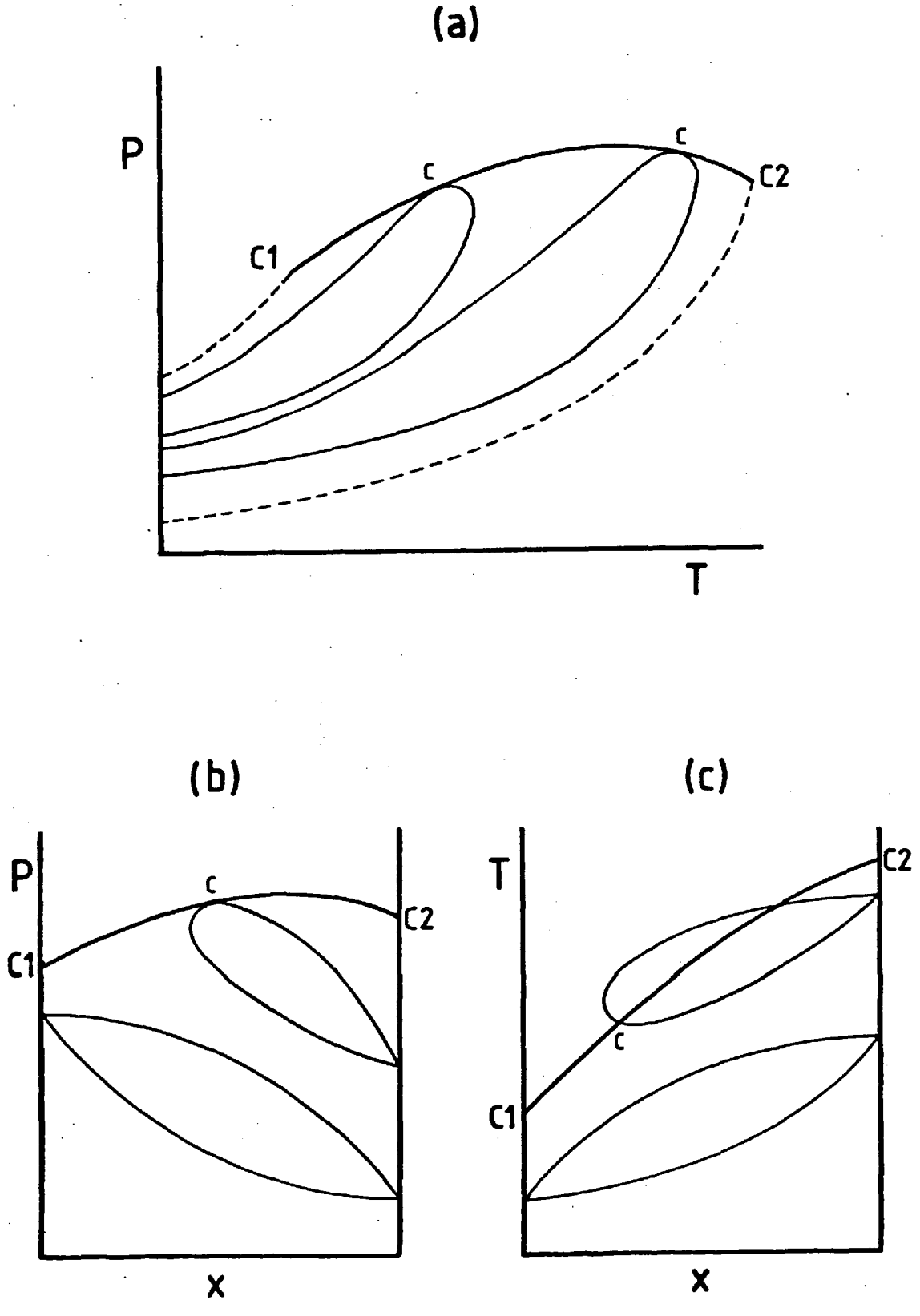


FIG. 2.2. Sections through the (P-T-x) surface of Fig. 2.1:

(a) (P-T) sections

(b) (P-x) sections

(c) (T-x) sections

2.2 Retrograde Phenomena and Barotropic Inversion of Phases

The shape of the (P-T) loops is interesting because it gives rise to the phenomena known as retrograde condensation and evaporation. Kuenen (14) was the first to observe these phenomena and to interpret them correctly.

Fig. 2.3 shows the three possible types of constant composition (P-T) loops for a binary mixture. The upper part of the loop represents the bubble-point curve and the lower part the dew-point curve. The two curves meet at the critical point (C). The point of maximum pressure (A) and that of maximum temperature (B) are usually called the cricondenbar and cricondentherm, respectively.

This mixture may be compressed isothermally in such a way that complete condensation never occurs: this is exemplified by path DD' in Figs. 2.3(a) and (b), where the temperature lies between T^C and T^B. During compression, the first drop of liquid appears at D, after which the amount of liquid increases to a maximum and then falls again to disappear completely at a second dew-point D'. This evaporation of a liquid by an isothermal increase of pressure was called retrograde behaviour of the first kind by Kuenen.

In the case of Fig. 2.3(c), however, any isothermal path between T^C and T^B will cut the (P-T) loop at two bubble-points, not two dew-points. Isothermal compression of such a mixture will therefore produce the first bubble of gas at D and, on further compression, the amount of gas will increase to a maximum and then drop, until the last bubble of gas vanishes when the isothermal path cuts the (P-T) loop at the second bubble-point, D'. This phenomenon, called retrograde behaviour of the second kind by Kuenen, is much less common than retrograde behaviour of the first kind.

Similar behaviour can be observed on changing the temperature along an isobaric path such as EE' in Fig. 2.3. When the pressure is between P^C and P^A, this path will cut the (P-T) loop at two dew-points, as in Fig. 2.3(b), or at two bubble-points, as in Fig. 2.3(a) and (c).

(.../)

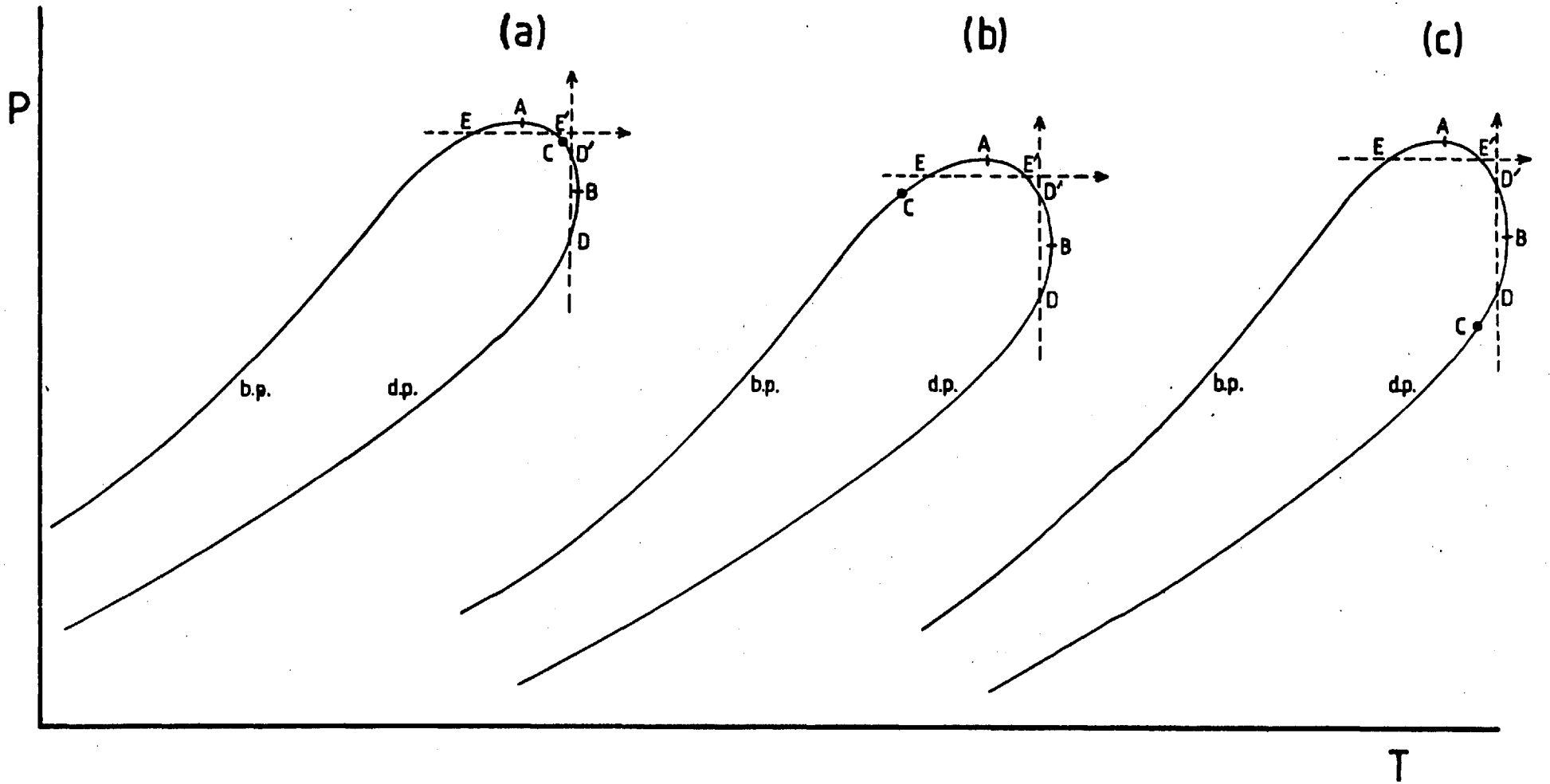


FIG. 2.3. Retrograde condensation and evaporation.

Another unusual phenomenon that occurs in some mixtures is the so-called barotropic inversion of phases: when these mixtures are compressed isothermally, above a certain pressure the "gaseous" phase becomes more dense than the "liquid" phase and sinks to the bottom of the vessel. According to Rowlinson (4), however, this effect is a consequence only of the great difference between the molecular weights of the two pure components and it is not of any fundamental significance. The barotropic inversion of phases was first found by Onnes (15) for the He + H_2 system, and it has since then been reported for various other systems, such as N_2 + NH_3 (16), Ar + NH_3 (17) and some fluorocarbon + hydrocarbon mixtures (10).

2.3 Classification of Binary Fluid Phase Diagrams

Thermodynamically speaking, there is no distinction between liquid-liquid and gas-liquid critical points in binary mixtures, since they are both points of incipient material or diffusional stability but not of mechanical stability (4). This means that the thermodynamic conditions for the existence of a critical state in a binary mixture will be exactly the same for a liquid-liquid critical point and for a gas-liquid critical point, namely that the second and third derivatives of the molar Gibbs free energy with respect to composition at constant temperature and pressure must vanish. Thus there are no thermodynamic grounds for the conventional classification of the critical points of binary mixtures into liquid-liquid and gas-liquid critical points.

Although such classification is acceptable for simple binary systems where the two loci are quite distinct, it is often impossible in more complex mixtures to speak unambiguously about two types of critical points, since the region of liquid-liquid immiscibility extends into the region of what is normally called the gas-liquid critical curve, and this interference produces a great variety of critical curves, which cannot easily be classified as liquid-liquid

or gas-liquid critical curves. The shape of these curves depends on the relative size, molecular structure and chemical nature of the two pure components. Increasing disparity between the molecules of the two components will cause the critical curves to become increasingly more complex, and this fact may be used to systematise the possible types of critical behaviour in binary fluid mixtures.

The simplest type occurs when the two pure components are very similar and their critical constants do not differ greatly. In such systems a simple continuous gas-liquid critical line is observed which connects the gas-liquid critical points of the pure components. As depicted in Fig. 2.4, the critical curve may be nearly straight, or it may have a pressure maximum, which may or may not be associated with a temperature minimum or maximum. It is found experimentally that a minimum critical temperature is normally, although not necessarily, associated with positive critical azeotropy, and a maximum critical temperature with negative critical azeotropy. In such cases the azeotropic line will be tangent to the critical line at the point where the critical temperature has an extremum, as shown in Fig. 2.5.

As the molecular disparity between the two components increases, a situation may arise where the phase diagram has a simple continuous gas-liquid critical locus, with or without azeotropy associated with it, and also a three-phase liquid-liquid-gas line (L_1L_2G) ending at an upper critical end point (UCEP) which lies below the critical temperature of either component. The liquid-liquid critical line starts from the UCEP and rapidly approaches high pressures, as shown in Fig. 2.6(a). This is the most common case, with the critical temperature either increasing or decreasing with pressure, or even showing a minimum in temperature. This is, however, by no means the only possible case: in certain systems which exhibit specific interactions, such as hydrogen bonding - usually water mixed with alcohols or amines - different types of liquid-liquid critical lines are observed, such as closed-loop critical lines between an LCEP and a UCEP, or hyperbolic-like immiscibility gaps, as represented in Figs. 2.6(b) and (c), respectively. In systems of this type it is, however, still possible to speak unambiguously of liquid-liquid and gas-liquid critical curves, since the two loci are quite distinct.

(.../)

1–CO_2+C_3H_8

2–SO_2+CH_3Cl

3–CH_4+C_3H_8

4–HCl+$(CH_3)_2O$

5–CO_2+C_2H_6

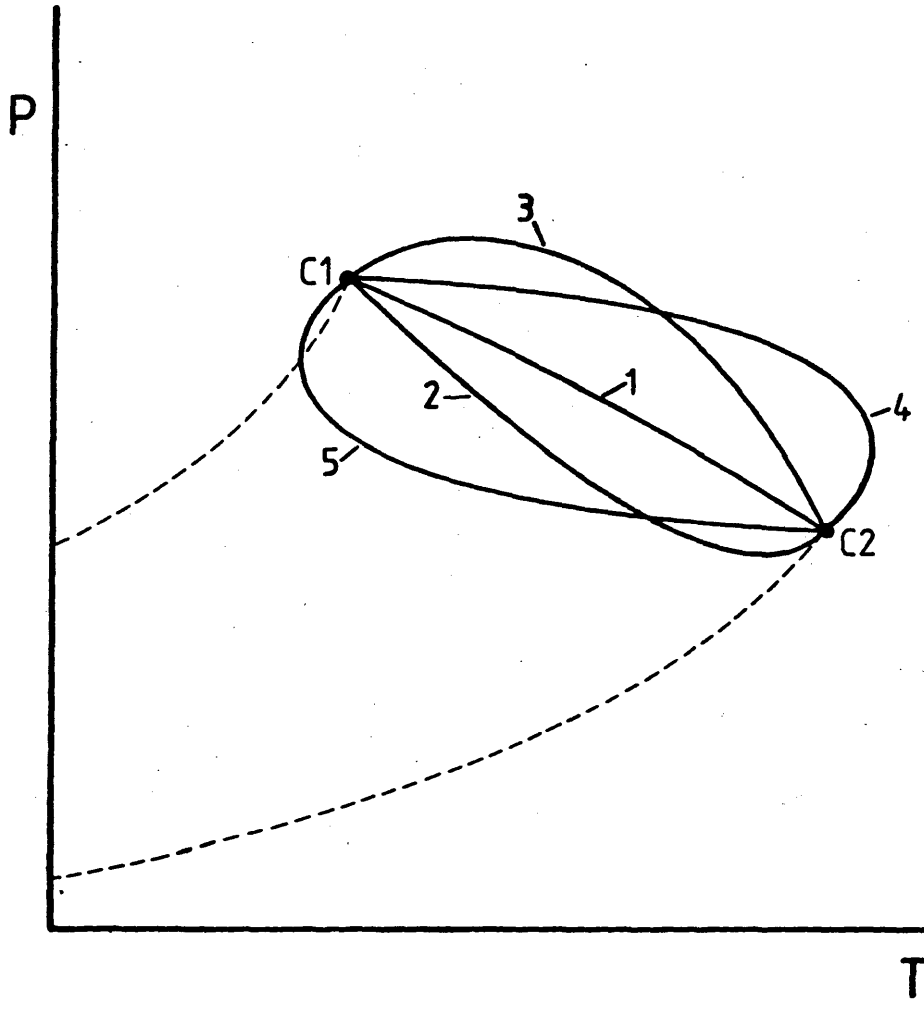


FIG. 2.4. Gas-liquid critical lines in simple binary systems.

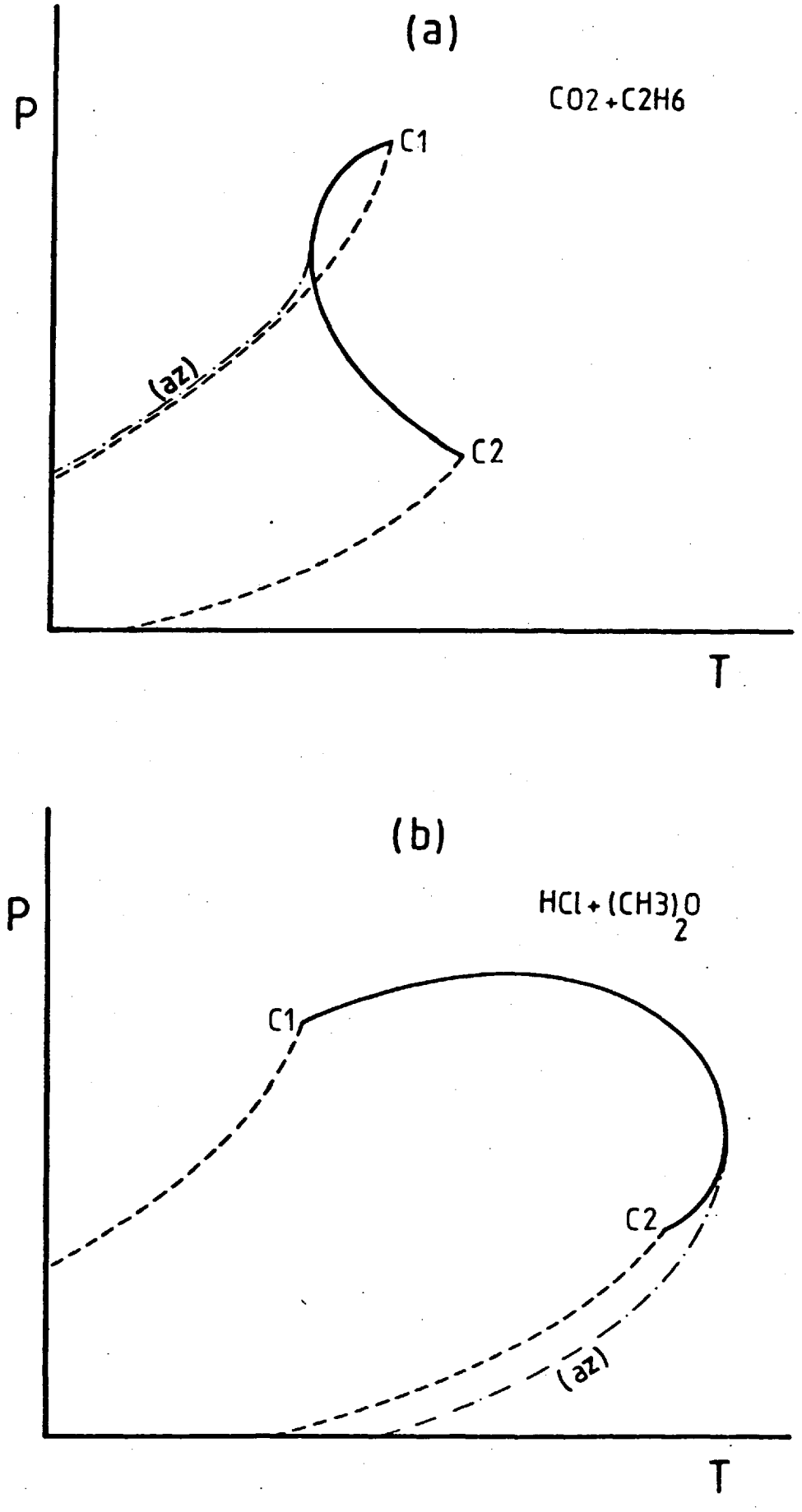


FIG. 2.5. Positive (a) and negative (b) critical azeotropy.

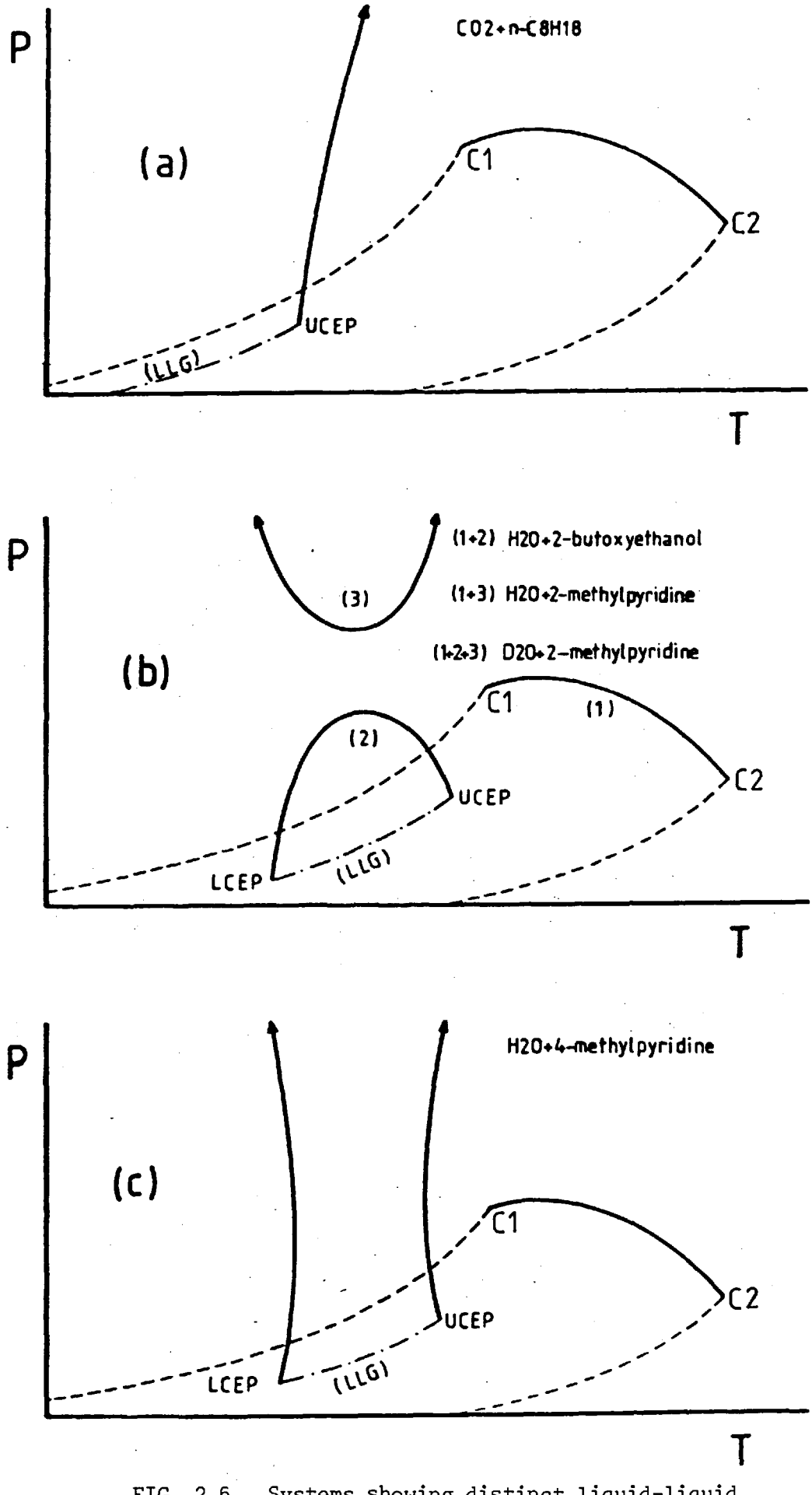
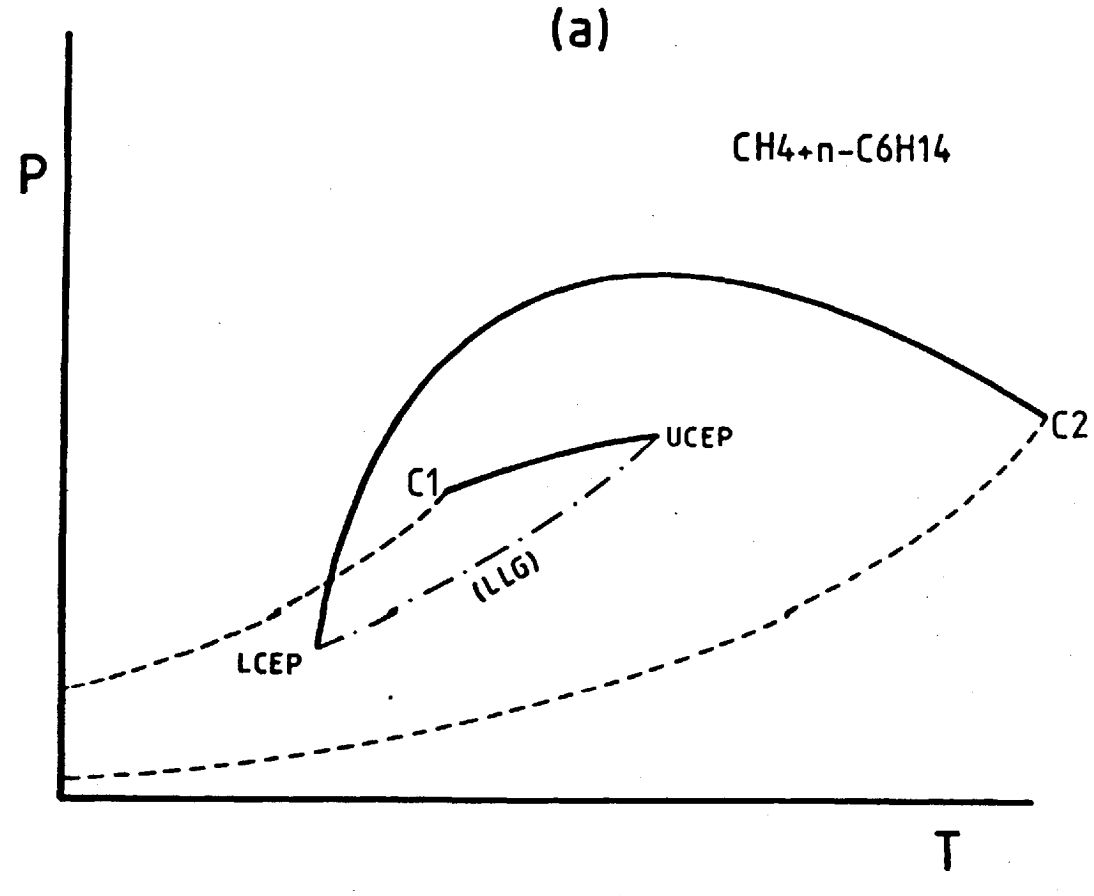


FIG. 2.6. Systems showing distinct liquid-liquid and gas-liquid critical loci.

Further disparity between the molecules of the two pure components will cause the region of liquid-liquid immiscibility to extend into and interfere with the gas-liquid critical curve, in such a way that the distinction between the two critical loci becomes very vague. This type of phase behaviour is by far the most common and complex, and can be further sub-divided into sub-categories of increasing complexity associated with increasing disparity in size and/or chemical type between the molecules of the two pure components. The following sub-division was proposed by Rowlinson (4) and is based mainly on the work of Scott and van Konynenburg (12, 18, 19) on the use of van der Waals' equation of state in predicting the phase behaviour of binary mixtures.

The simplest type of break of continuity in the gas-liquid critical line is caused by the appearance of two liquid phases over a short range of temperatures in the vicinity of the critical point of the more volatile component, as shown in Fig. 2.7(a). Systems which exhibit this behaviour provide the best example of the confusion that can arise from the conventional division of the critical points of mixtures into liquid-liquid and gas-liquid. One branch of the critical line starts at the critical point of the more volatile component and ends at a UCEP on the three-phase line L_1L_2G, whereas the other branch starts at the critical point of the less volatile component and, after normally running through a pressure maximum, ends at an LCEP on the same three-phase line L_1L_2G, where the two liquid phases become identical. Hence, along this branch of the critical line gas-liquid critical behaviour merges continuously into liquid-liquid critical behaviour. It is also possible for the LCEP, and therefore the whole of the three-phase line L_1L_2G, to be situated at temperatures higher than the critical temperature of the more volatile component.

A slight variation of this type of phase behaviour is shown in Fig. 2.7(b). Here, the critical locus has three distinct branches. The first of these, which may be unambiguously termed a liquid-liquid critical line, starts at a UCEP on the three-phase line L_1L_2G and rapidly approaches high pressures. The second branch starts at the



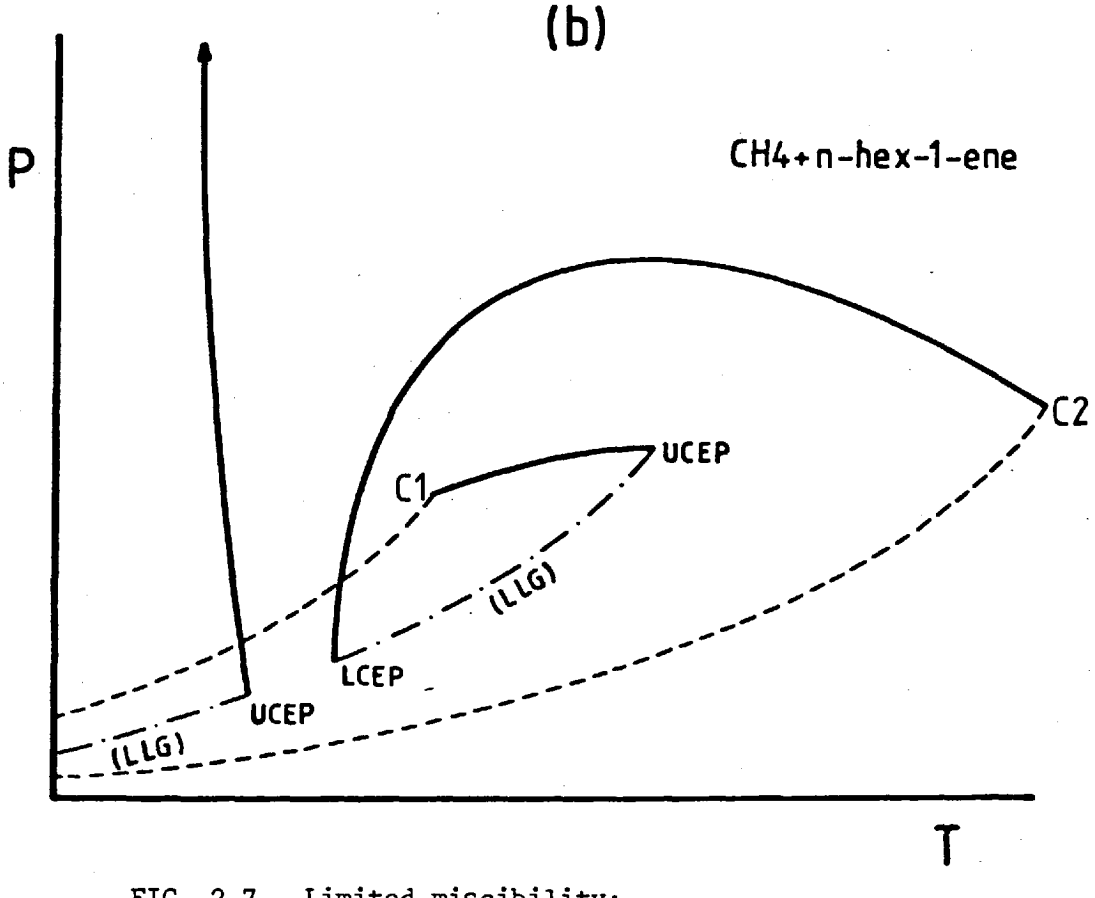


FIG. 2.7. Limited miscibility:

(a) Systems showing two liquid phases over a short range of temperatures

(b) Systems showing two distinct regions of immiscibility

critical point of the more volatile component and ends at a UCEP on a second branch of the three-phase line L_1L_2G, and has all the characteristics of a gas-liquid critical line. The third branch, however, which starts at the critical point of the less volatile component and ends at an LCEP on the second branch of the three-phase line L_1L_2G, cannot be termed liquid-liquid or gas-liquid, since there is a continuous transition from one type of behaviour to the other. Systems such as this will therefore show two distinct regions of immiscibility, separated by a narrow range of temperatures over which the two components are completely miscible.

If this small gap of complete miscibility were to disappear, the two components would then be immiscible at all temperatures below the critical point of the less volatile component, as represented in Fig. 2.8(a). This type of diagram can be thought of as having evolved from Fig. 2.7(b) by raising the minimum pressure of the critical locus so that the second branch no longer "cuts" the three-phase line (4).

Increasing disparity between the molecules will cause the minimum in pressure to become less pronounced, and the slope of the locus at very high pressures to change from negative to positive. Hence, the second branch of the critical line has to run through a minimum in temperature before proceeding to higher pressures and temperatures, as represented in Fig. 2.8(b). The three-phase line in these systems is normally, but not necessarily, situated above the vapour-pressure curve of the more volatile component, which means that these systems will have a heterogeneous azeotrope up to the critical region. The temperature of the UCEP may be higher or lower than the critical temperature of the more volatile component, leading to the two possible cases depicted in Figs. 2.9(a) and (b) respectively.

Eventually, the branch of the critical line starting from the critical point of the less volatile component will be displaced to higher temperatures and pressures, the minimum and maximum in pressure will disappear and the critical curve will have a minimum in temperature, called the "point of double contact", and there it will turn back on itself, proceeding to higher temperatures and pressures,

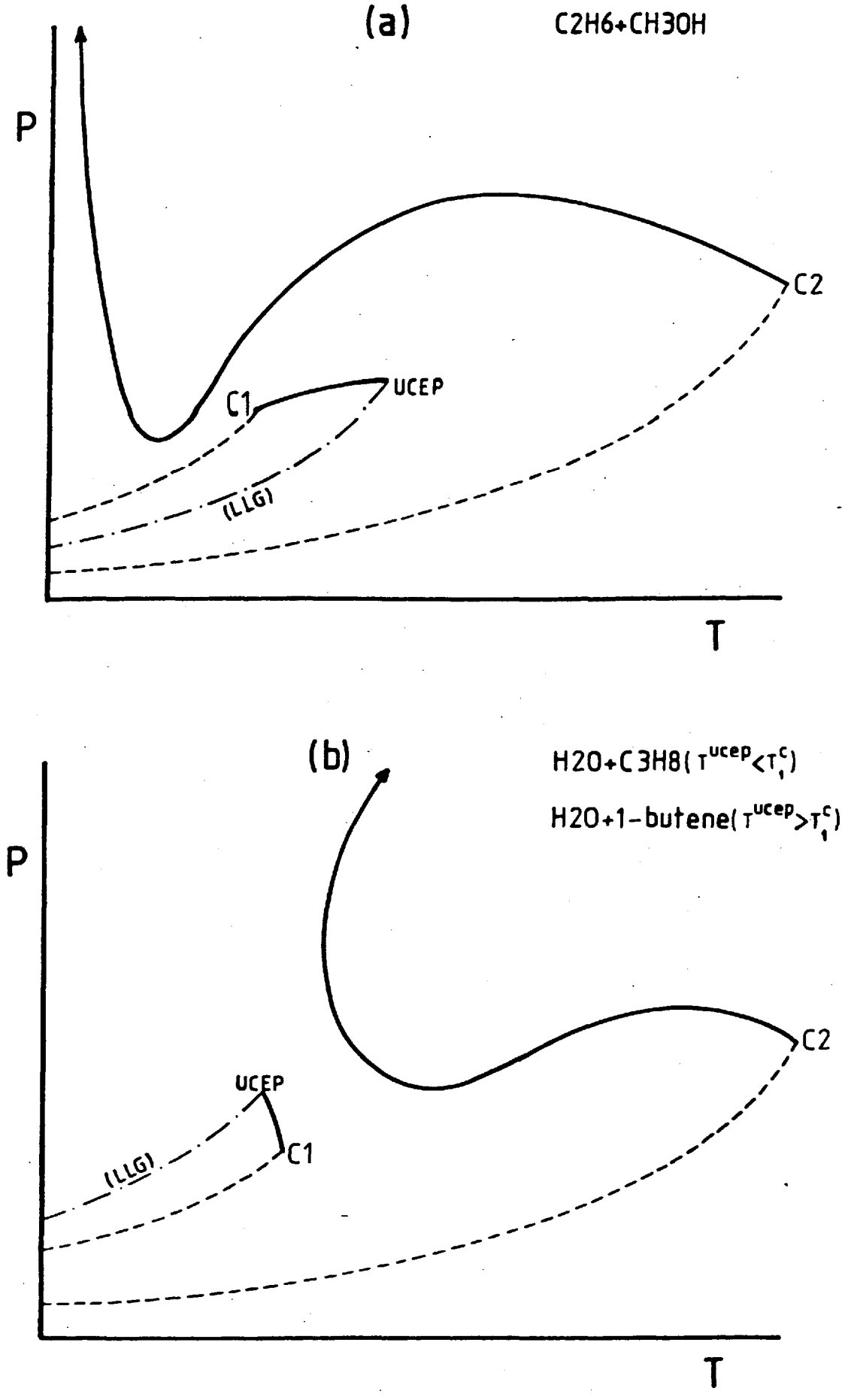


FIG. 2.8. Systems showing immiscibility at all temperatures below the critical point of the less volatile component.

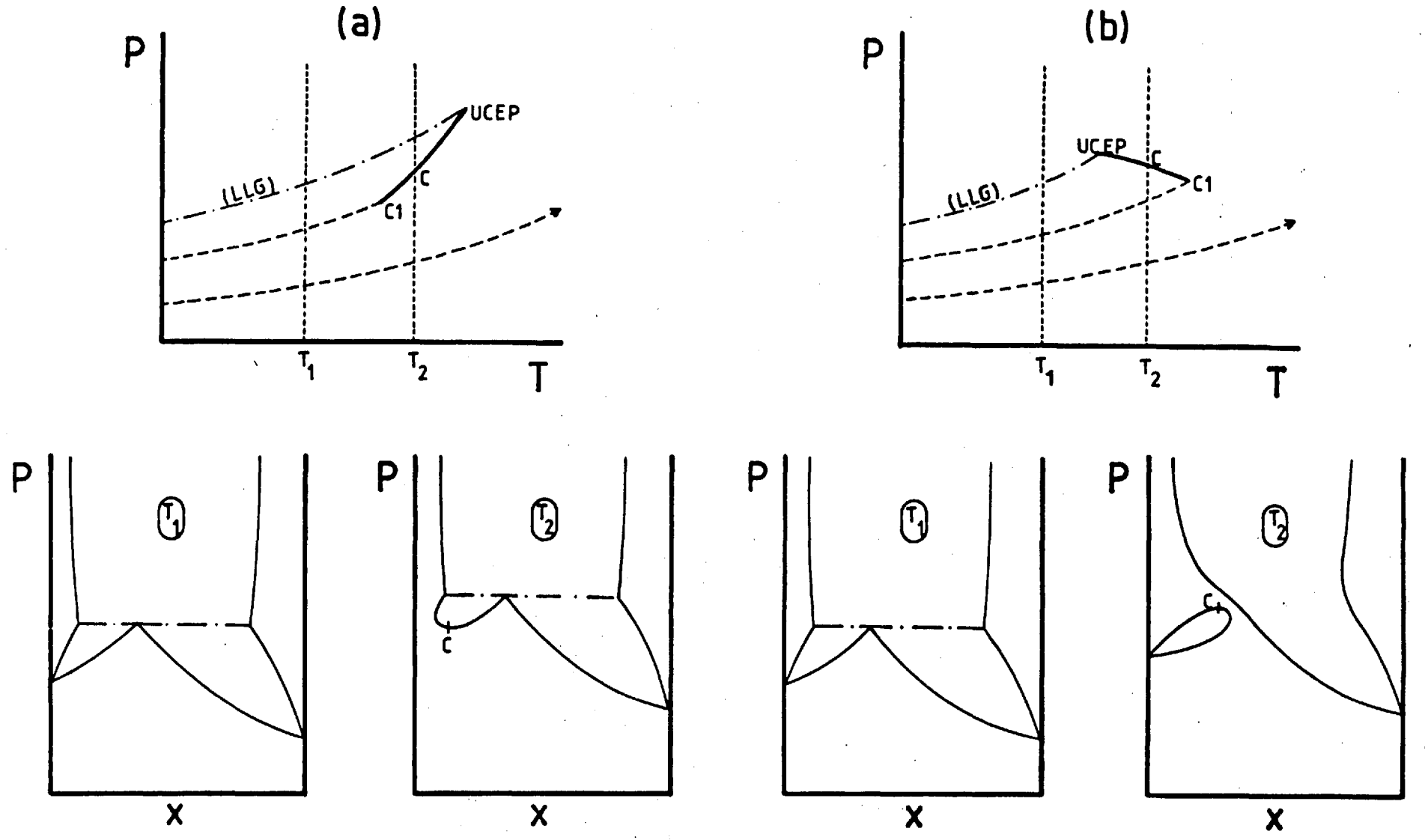


FIG. 2.9. Systems showing a heterogeneous azeotrope up to the critical region.

as depicted in Fig. 2.10(a). Further disparity between the molecules will cause even this minimum in temperature to disappear, and the critical line to rise monotonically from the critical point of the less volatile component to higher temperatures and pressures, so that $(\frac{dP}{dT})^c$ is always positive, as shown in Fig. 2.10(b). The phase diagrams sketched in Figs. 2.10(a) and (b) suggest that in these systems, sufficiently high pressures will cause the two fluids to separate at all temperatures, even at those above the critical point of the less volatile component. The term gas-gas equilibria or immiscibility of gases has been applied to these phase-separation effects in fluid mixtures at temperatures above the critical temperature of the less volatile component. The type depicted in Fig. 2.10(a) has been called gas-gas immiscibility of the second kind and that shown in Fig. 2.10(b), gas-gas immiscibility of the first kind. Typical isothermal (P-x) diagrams for these two types of binary systems are shown in Figs. 2.11(a) and (b).

2.4 Gas-Gas Immiscibility

Gas-gas immiscibility was first predicted by van der Waals in 1894 (20), and was discussed in detail by Kamerlingh Onnes and Keesom in 1907 (15). That of the second type was found for the first time by Krichevskii (21) in 1940 for the N_2 + NH_3 system and that of the first type by Tsiklis (22) in 1952 for the system He + NH_3. Since then, these phase separation effects have been found experimentally in various other systems, as shown in Tables 2.1 and 2.2. The first type is normally found in systems having He as one of the two components, whereas most of the systems found to exhibit the second kind of gas-gas immiscibility contain either H_2O or NH_3 as one of the two components. It is also found experimentally that barotropic inversion of phases is normally associated with the occurrence of gas-gas immiscibility.

Until recently, it was thought that there was no limit to the gas-gas critical curve at higher temperatures and pressures, although some authors (23, 24) have always maintained that the critical line must eventually make its way back to the critical point of the more

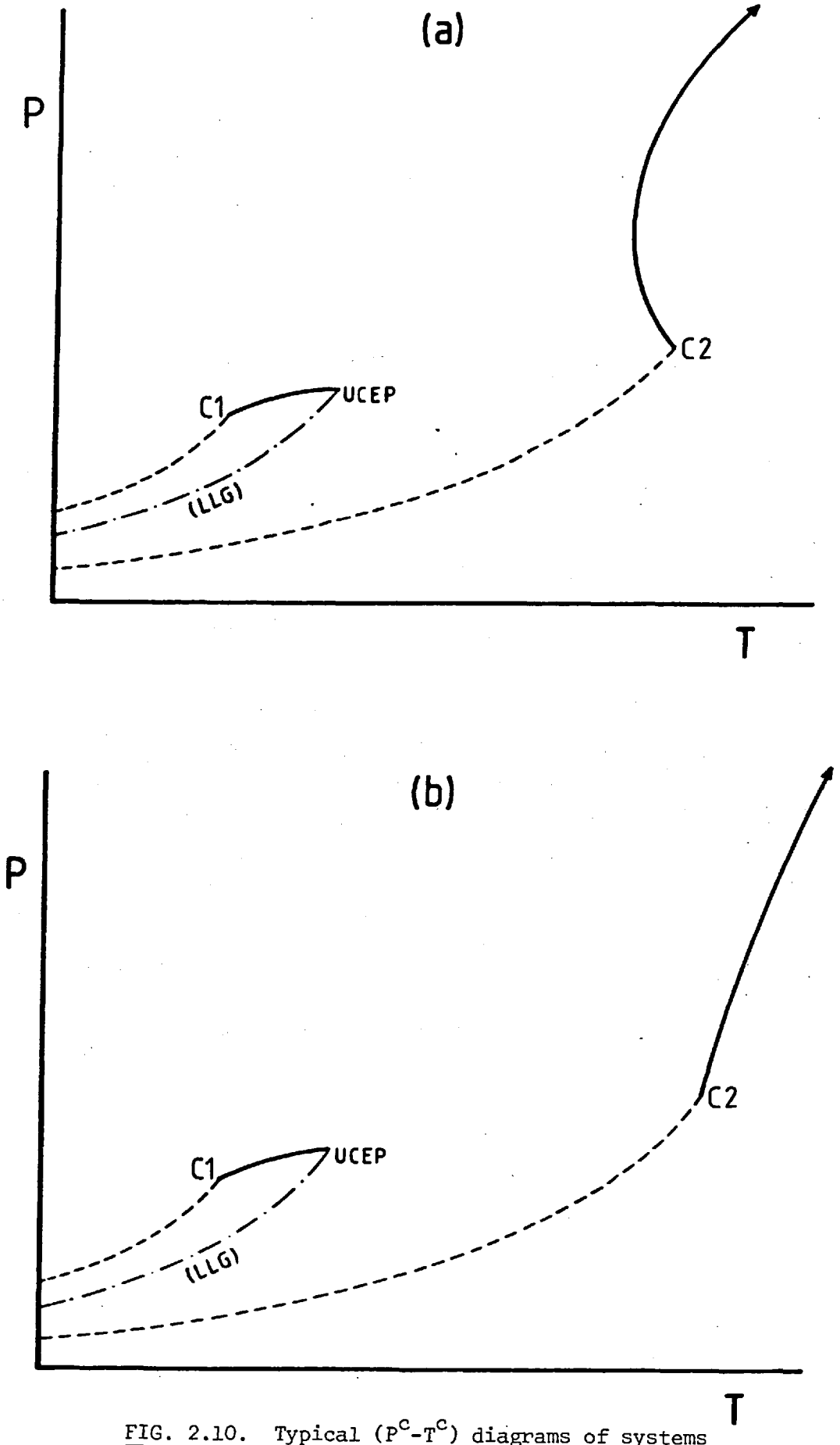
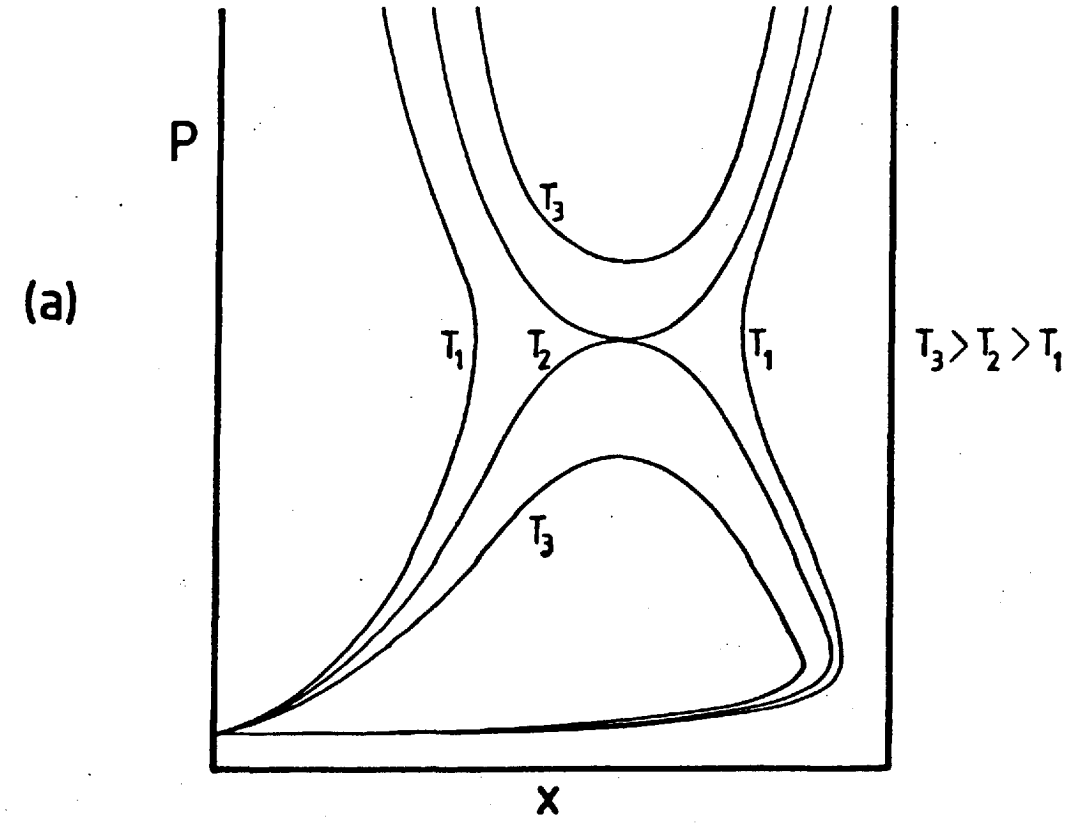


FIG. 2.10. Typical (P^C-T^C) diagrams of systems exhibiting gas-gas immiscibility:

(a) second kind

(b) first kind



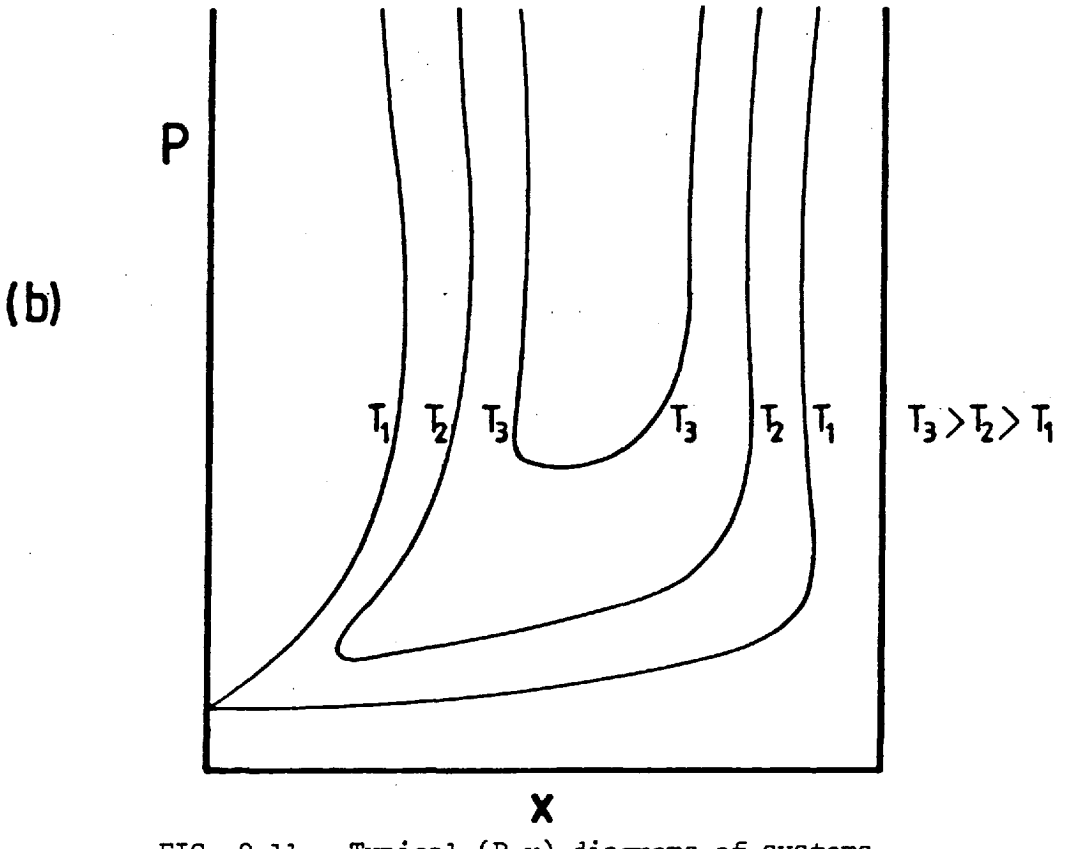


FIG. 2.11. Typical (P-x) diagrams of systems exhibiting gas-gas immiscibility:

(a) second kind

(b) first kind

TABLE 2.1

Systems found to exhibit gas-gas immiscibility of the first kind

System	Temperature range (°C)	Maximum pressure (bar)	References
He + NH_3	125 to 175	10 000	(22)
He + CO_2	25 to 100	10 000	(22)
He + C_2H_4	25 to 150	10 000	(26)
He + C_3H_8	100 to 150	7 000	(27)
He + C_6H_6	300	1 000	(27)
He + CH_3OH	245	3 000	(27)
He + SO_2	175 to 200	7 000	(27)
He + n-C_6H_{14}	245	3 000	(27)
He + Xe	5 to 65	2 000	(24)
He + C_2H_2	36	64	(27)
He + C_2H_6	32	51	(27)
He + N_2O	37	74	(27)
He + Freon 12	25 to 122	330	(28, 29)
He + Freon 22	100	330	(28, 29)
He + Freon 114B_2	216 to 223	330	(28, 29)
Ar + H_2O	270 to 440	3 000	(30)

TABLE 2.2

Systems found to exhibit gas-gas immiscibility of the second kind

System	Temperature range (°C)	Maximum pressure (bar)	References
$NH_3 + N_2$	90 to 175	16 000	(21)
$NH_3 + CH_4$	45 to 100	10 000	(27)
$NH_3 + Ar$	70 to 140	10 000	(27)
$NH_3 + N_2 + H_2$	90 to 120	5 500	(27)
$NH_3 + N_2 + CH_4$	55 to 110	5 500	(27)
$SO_2 + N_2$	35 to 40	9 000	(27)
$He + N_2$	-196 to -151	830	(31)
He + Ar	-182 to -126	650	(32)
Ne + Kr	-110 to - 63	1 800	(33, 34)
$CO_2 + n\text{-}C_{16}H_{34}$	20 to 100	1 500	(35)
$H_2O + N_2$	300 to 350	6 000	(36)
$H_2O + CO_2$	250 to 350	3 500	(37, 38)
$H_2O + C_2H_6$	200 to 400	3 700	(39)
$H_2O + n\text{-}C_4H_{10}$	355 to 364	1 100	(39, 40)
$H_2O + n\text{-}C_5H_{12}$	340 to 352	620	(41)
$H_2O + 2\text{-}CH_3C_4H_9$	330 to 355	500	(41)
$H_2O + n\text{-}C_7H_{16}$	350 to 420	1 250	(41, 42)
$H_2O + C_3H_6$	325 to 350	2 500	(30)
$H_2O + c\text{-}C_6H_{12}$	130 to 410	1 800	(42, 43)
$H_2O + C_6H_6$	200 to 370	3 700	(41, 44-47)
H_2O + toluene	305 to 360	2 000	(41, 46, 47)
H_2O + o-xylene	310 to 380	2 000	(46, 47)
H_2O + ethylbenzene	310 to 380	2 000	(46, 47)
H_2O + propylbenzene	320 to 400	2 000	(46, 47)
H_2O + 1,3,5-trimethylbenzene	320 to 400	2 000	(47, 47)
$He + CH_4$*	Up to - 82	170	(42)

*Transition type

volatile component, after running through a temperature maximum and a pressure maximum, as predicted by the original van der Waals equation. Such maxima have never been observed experimentally in the critical lines of binary systems which exhibit gas-gas immiscibility.

On the other hand, recent experimental work by Streett(25) on the high-pressure limits of gas-gas immiscibility in mixtures of light gases has shown that, in some cases at least, the gas-gas phase separation terminates at a UCEP on the intersection of the gas-gas critical line with a three-phase line of the type S_2-G_1-G_2, which results from the solidification of the less volatile component. The available evidence seems to suggest that, in other cases, gas-gas immiscibility may persist to very high temperatures and pressures, perhaps even to the limits at which atomic and molecular structure begin to break down.

In recent years, many aspects of gas-gas immiscibility have been explained by the work of Schneider and his collaborators (5, 6, 7, 8, 9) on critical phenomena in binary fluid mixtures at high pressures. By carrying out experiments on "families" of binary systems, such as CH_4 + n-alkanes, CO_2 + n-alkanes and H_2O + n-alkanes, Schneider has been able to show that there is a continuous and logical transition from the more familiar types of liquid-liquid and gas-liquid critical lines to the systems which exhibit gas-gas critical lines. The evidence put forward by Schneider suggests that gas-gas immiscibility is essentially a liquid-liquid type of equilibrium which has been displaced to high temperatures and finally merged continuously into the gas-liquid critical curve. Moreover, it suggests that gas-gas immiscibility is probably the rule, rather than the exception, for mixtures in which the forces between unlike molecules are relatively weak.

The results compiled by Schneider for CO_2 + n-alkanes, H_2O + n-alkanes and CH_4 + n-alkanes are shown schematically in Figs. 2.12, 2.13 and 2.14 respectively. These self-explanatory diagrams exhibit a whole pattern of critical behaviour covering many of the types referred to in this discussion, and showing quite clearly the transition between the various types with increasing disparity between the molecules of the two pure components.

(.../)

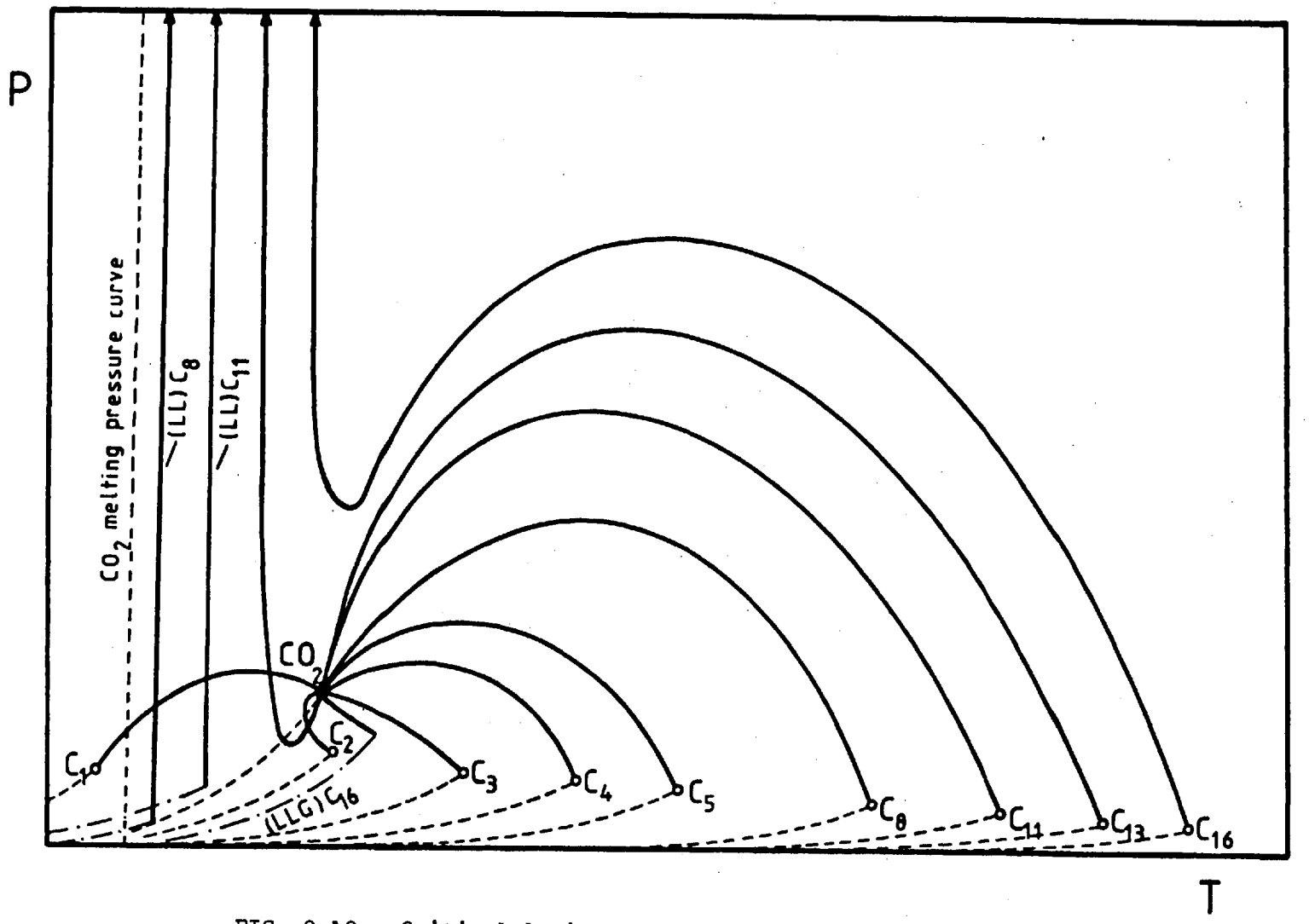


FIG. 2.12. Critical loci of CO_2 + n-alkane systems (not to scale).

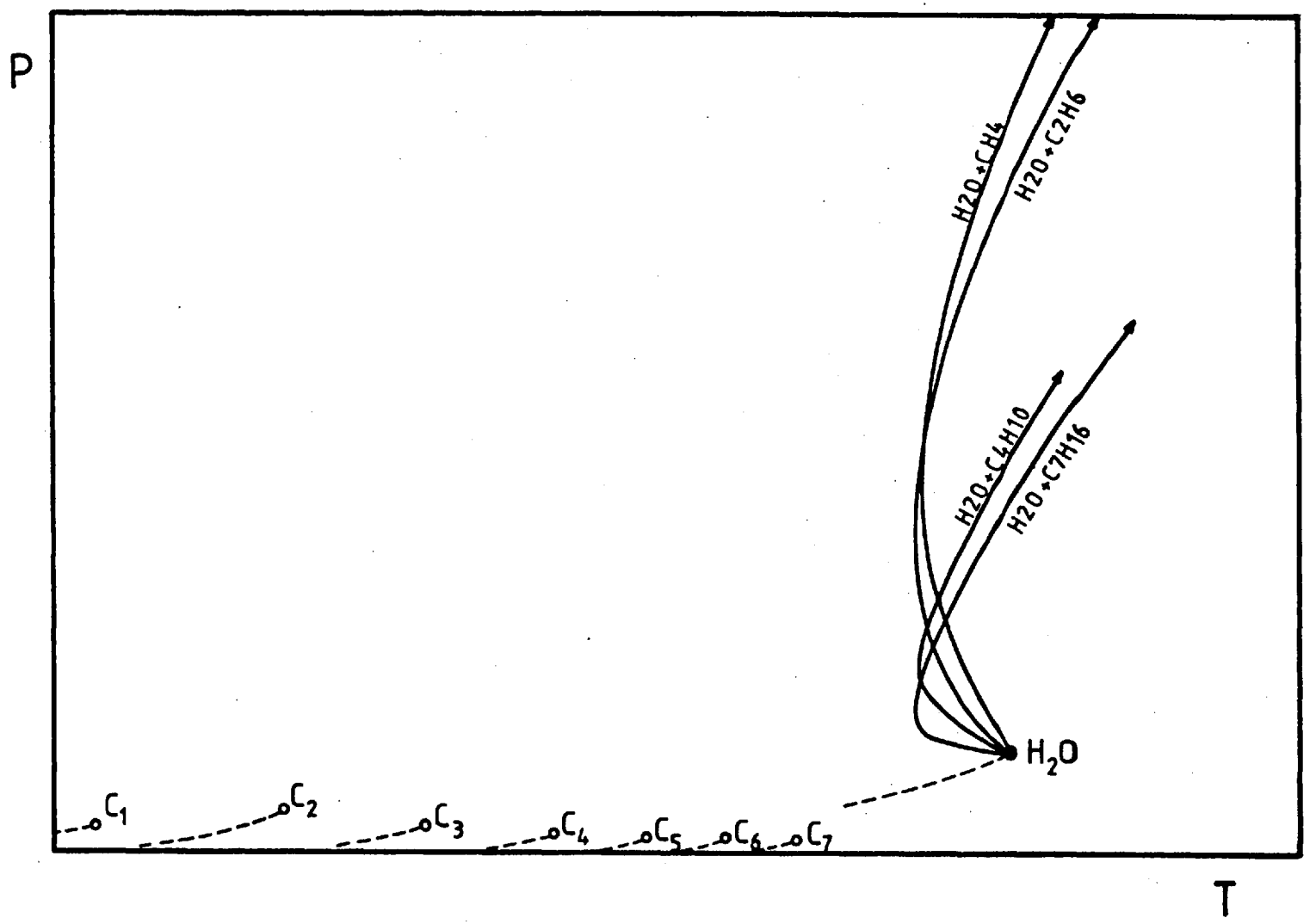


FIG. 2.13. Critical loci of H_2O + n-alkane systems (not to scale).

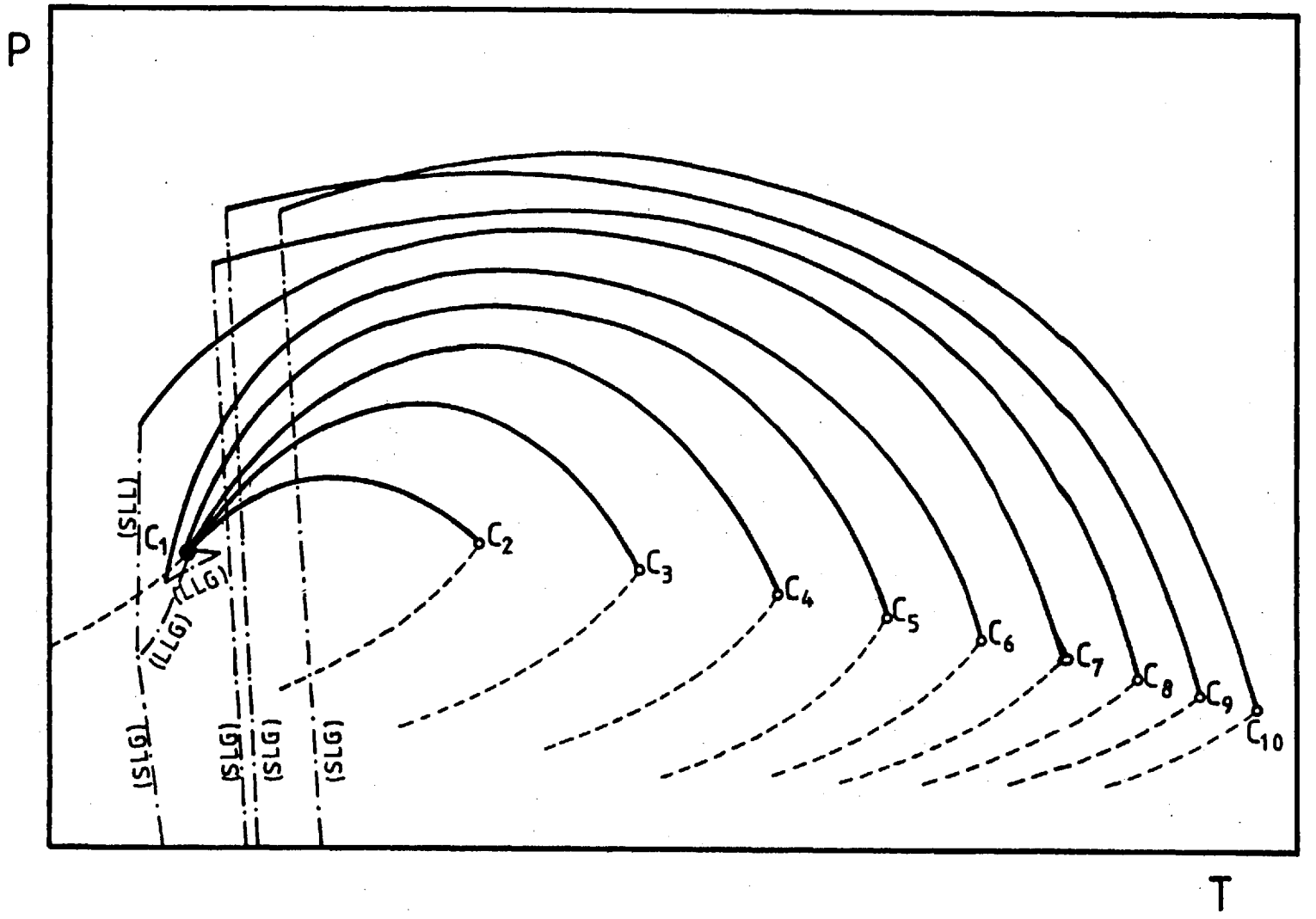


FIG. 2.14. Critical loci of CH_4 + n-alkane systems (not to scale).

Chapter 3

THE ANOMALOUS BEHAVIOUR OF SYSTEMS CONTAINING NON-AROMATIC FLUOROCARBONS

Aliphatic and alicyclic fluorinated compounds of carbon first became available in commercial quantities about forty years ago and, in complete contradiction to the predictions of the existing liquid theories, it was found that these non-aromatic fluorocarbons were only partially miscible with hydrocarbons of comparable molecular weight. This anomalous behaviour gave rise to a large amount of experimental work, especially by Scott and co-workers, in an attempt to obtain a better understanding of these systems. In 1958, Scott (2) reviewed the experimental data then available and considered the possible explanations for the disagreement between theory and experiment. More recently, Swinton (48) has published a comprehensive survey of all the literature in this field from the beginning of 1970 up to late 1976.

3.1 Experimental Evidence at Low Pressures

Binary liquid mixtures of non-aromatic fluorocarbons with hydrocarbons are characterised by large positive deviations from ideality, i.e. by large positive values of the thermodynamic excess functions G^E, H^E, S^E and V^E. In many cases, the large deviations in these mixtures lead to liquid-liquid immiscibility at temperatures below a UCST. Experimental values of the thermodynamic excess functions and UCST of some of these mixtures are given in Table 3.1.

The experimental data for these systems can be summarised as follows (4): equimolar liquid mixtures of non-aromatic fluorocarbons with hydrocarbons or with other simple non-polar molecules possess excess free energies of about $\frac{1}{2}RT$ at the normal boiling point, excess enthalpies lying between $\frac{1}{2}RT$ and RT, and positive excess volumes representing a volume expansion of 2 to 10 per cent. These systems separate into two partially miscible liquid phases below a UCST, unless prevented from doing so by the formation of a solid phase.

(.../)

TABLE 3.1

Thermodynamic properties of equimolar binary liquid mixtures containing a non-aromatic fluorocarbon (48)

System	T (K)	G^E ($kJ.mol^{-1}$)	H^E ($kJ.mol^{-1}$)	TS^E ($kJ.mol^{-1}$)	V^E ($cm^3.mol^{-1}$)	UCST (K)	References
$CF_4 + CH_4$	110	0.36	0.537	0.177	0.88	94.5	(49,50,51,52)
$n\text{-}C_6F_{14} + n\text{-}C_6H_{14}$	308	1.329	2.157	0.828	5.38	296	(53,54,55)
$c\text{-}C_6F_{12} + c\text{-}C_6H_{12}$	338	1.35	2.07	0.72	-	316	(56)
$c\text{-}C_7F_{14} + c\text{-}C_7H_{14}$	338	1.39	2.80	1.41	7.5	319	(56)

Data on the virial coefficients of gaseous mixtures of non-aromatic fluorocarbons and hydrocarbons are much more scarce than data on the corresponding liquid mixtures. To date, there have been few experimental determinations of sufficient accuracy which have been carried out over a large enough temperature range for meaningful conclusions to be obtained concerning the interactions between the molecules in these systems. Two notable exceptions of particular concern in this investigation are the measurements by Douslin et al. (57) on $CF_4 + CH_4$ and those of Dantzler-Siebert and Knobler (58) on mixtures of the type $n\text{-}C_xF_{2x+2} + n\text{-}C_yH_{2y+2}$ $(1 \leqslant x, y \leqslant 6)$. The second virial coefficient of a binary mixture is given by

$$B[T,x] = x^2 B_{11}[T] + 2x(1-x)B_{12}[T] + (1-x)^2 B_{22}[T]$$

$$= xB_{11}[T] + x(1-x)\delta[T] + (1-x)B_{22}[T], \qquad (3\text{-}1)$$

where x is the mole fraction of species 1, $B_{11}[T]$ and $B_{22}[T]$ are the corresponding second virial coefficients for the pure components, and $B_{12}[T]$ is a pseudo-virial coefficient for a hypothetical gas having only unlike molecule interaction. The quantity δ, sometimes called excess second virial coefficient, is defined as:

$$\delta \equiv 2\, B_{12} - B_{11} - B_{22}. \qquad (3\text{-}2)$$

This is the most useful quantity as far as the study of unlike molecule interactions is concerned and, for this reason, a number of experimental methods has been described in the literature which enable one to measure δ directly (80). From statistical thermodynamics, the relation between the virial coefficients and the intermolecular potential is very simple in form when the interactions between molecules have no angular dependence (81):

$$B_{ij}[T] = -2\pi N_A \int_0^\infty \left(\exp\left(-\frac{u_{ij}[r]}{kT}\right) - 1\right) r^2 dr, \qquad (3\text{-}3)$$

where $u_{ij}[r]$ is the intermolecular potential for a pair of molecules of substances i and j, and r is the distance between the molecular centres.

(.../)

Once the values of B_{11} and B_{22} are known, experimental determination of the second virial coefficient of the mixture $B[x,T]$ (or of the excess quantity δ) can be used to obtain values of B_{12}. This, in turn, can be directly related to $u_{12}[r]$, the intermolecular potential for the unlike interaction. The experimental results of Douslin et al. (57) and of Dantzler-Siebert and Knobler (58) quoted above have provided additional evidence confirming the essential weakness of the unlike interaction $u_{12}[r]$ in non-aromatic fluorocarbon + hydrocarbon systems, when compared with the intermolecular potentials for the like-molecule interactions, $u_{11}[r]$ and $u_{22}[r]$. According to Scott (2), the most significant factors that can lead to this weakening of the unlike interaction in such mixtures are the presence of non-central forces, differences in ionisation potential and differences in size of the two component molecules.

Further evidence of the anomalous behaviour of the these mixtures is provided by gas-liquid solubility measurements. Hildebrand and co-workers have measured gas solubilities for a wide variety of systems, most of these being tabulated in the comprehensive review by Battino and Clever (59). The following general conclusions can be drawn from these and similar measurements on related systems (48):

(i) Under the same conditions of temperature and pressure, fluorocarbon gases are less soluble than the equivalent hydrocarbon when dissolved in the same non-polar, non-fluorinated solvent, but the opposite is true when a fluorinated solvent is used;

(ii) A fluorocarbon solvent will dissolve a much larger amount of a particular gas solute than will the equivalent hydrocarbon solvent.

3.2 Experimental Evidence at High Pressures

Although a large number of mixtures containing non-aromatic fluorocarbons has been studied at atmospheric pressure, only recently have measurements been extended to high pressures and critical lines obtained for some of these systems, in particular for He + fluorocarbon mixtures (60), n-C_7F_{16} + n-alkanes (up to n-nonane) (61),

c-C_6F_{12} + c-alkanes (62), perfluoromethylcyclohexane + various branched alkanes (63), propane + various perfluorohydrocarbons (64) and also n-hexane + n-perfluorohexane (64).

More recently, Schneider and his co-workers (65, 66) have studied the liquid-liquid immiscibility of a series of binary and ternary non-aromatic fluorocarbon + hydrocarbon mixtures. All these mixtures exhibit UCST that increase with increase of pressure. The experimental results for the CF_4 + CH_4 (67) and CF_4 + C_2H_6 (68) systems, which are particularly relevant to this investigation, are plotted in Figs. 3.1(a) and (b) in the form of (P-x) diagrams. Paas (67) also attempted to obtain the gas-liquid critical curve for the CF_4 + CH_4 system but failed because of experimental difficulties.

Sideras (3) studied the phase behaviour of the CF_4 + n-C_7H_{16} system, but his results were limited to a single isotherm (50 °C) and he found no critical point at this temperature, since the isotherm was open at the top, at least up to the highest pressure reached. Mukherjee (69) studied the CF_4 + n-C_5H_{12} and CF_4 + n-C_6H_{14} systems, and his results indicate that these systems probably exhibit gas-gas immiscibility of the second kind. The experimental evidence is, however, not very conclusive, especially for the CF_4 + n-C_5H_{12} system, where only two experimental critical points were obtained.

3.3 Interpretation of the Experimental Evidence

When interpreted in terms of intermolecular forces, all the experimental results for non-aromatic fluorocarbon + hydrocarbon systems seem to point to a considerable weakening of the unlike interaction in such mixtures, in the sense that the well-known Berthelot or geometric mean rule for the characteristic energy of the unlike interaction,

$$\varepsilon_{12} = (\varepsilon_{11}\varepsilon_{22})^{\frac{1}{2}}, \qquad (3\text{-}4)$$

is no longer applicable. The value of ε_{12} obtained from experimental data on these mixtures is found to be much smaller than the value predicted by equation (3-4). Furthermore, it also appears that the Lorentz or arithmetic combining rule for the characteristic distance (collision diameter) of the unlike interaction

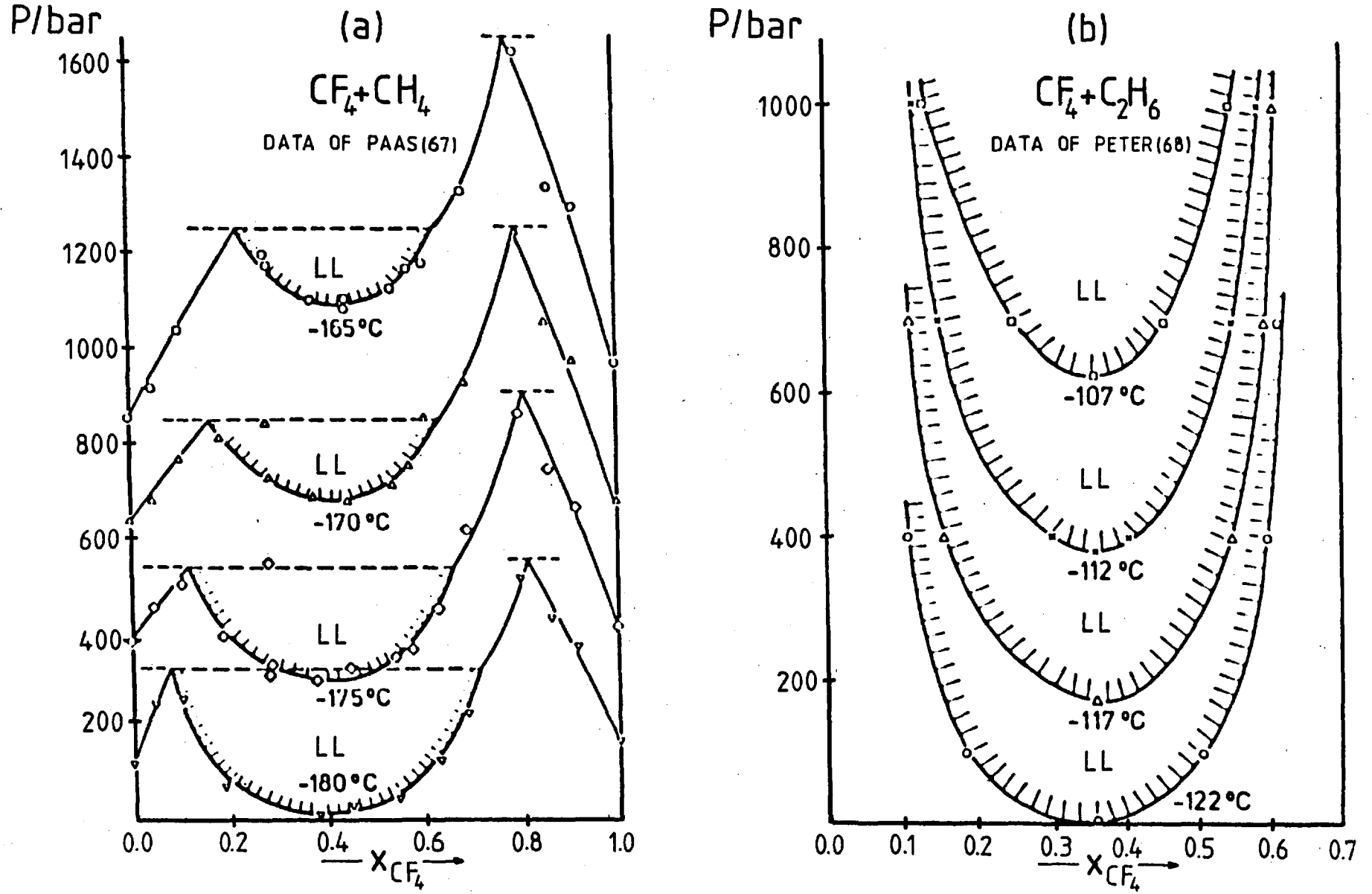


FIG. 3.1. Experimental (P-x) diagrams showing liquid-liquid immiscibility in the CF_4 + CH_4 (a) and CF_4 + C_2H_6 (b) systems.

$$\sigma_{12} = (\sigma_{11} + \sigma_{22}')/2 \qquad (3\text{-}5)$$

consistently predicts values of σ_{12} smaller than the corresponding values obtained from experimental data. Deviations of real systems from the predictions of the Lorentz-Berthelot rules are usually accounted for empirically by incorporating adjustable binary interaction parameters ξ_{12} and χ_{12} in equations (3-4) and (3-5), respectively:

$$\left.\begin{aligned} \varepsilon_{12} &= \xi_{12}(\varepsilon_{11}\varepsilon_{22})^{\frac{1}{2}} \\ \sigma_{12} &= \chi_{12}(\sigma_{11} + \sigma_{22})/2 \quad . \end{aligned}\right\} \qquad (3\text{-}6)$$

It would appear, therefore, that the considerable deviations from ideality observed in non-aromatic fluorocarbon + hydrocarbon systems can be explained if values of ξ_{12} considerably less than unity and values of χ_{12} slightly greater than unity are used in equations (3-6). For example, the values obtained from the virial coefficient data of Douslin et al. (57) for the CF_4 + CH_4 system are quoted by Swinton (48) as being: $\xi_{12} = 0.9090$ and $\chi_{12} = 1.0095$.

Recent fluid mixture theories, especially those based on the so-called van der Waals one- and two-fluid models, have been reasonably successful in representing the experimental data of fluorocarbon + hydrocarbon mixtures. The problem is that these theories require "a priori" estimates of the values of ξ_{12} and χ_{12} (or ε_{12} and σ_{12}) if they are to be used to predict the properties of mixtures. There have been various attempts (58, 70-76) to produce sophisticated "combining rules" for the prediction of these values solely from the properties of the pure components. Although some of these rules have proved to be reasonably successful, especially for very simple mixtures and for the prediction of relatively crude properties, none of them seems to be entirely satisfactory or universally valid. Rowlinson (4) has pointed out that attempts to explain the properties of mixtures solely from a knowledge of those of the pure components rest upon the fallacy that the forces (1-2) between two molecules of species 1 and 2 are always

determinable via some "averaging" of the forces (1-1) and (2-2) between the like molecules. Such "averaging" is, however, unsatisfactory for the detailed interpretation of even the simplest of mixtures. In other words, the unlike interaction parameters are not available from experiments on the pure components, since they represent interactions which only occur in the mixture. Thus the observed properties of a binary mixture should be taken as the source of information about the unlike interactions, and ξ_{12} and χ_{12} should be treated simply as adjustable parameters.

Chapter 4

DESCRIPTION OF THE APPARATUS

The apparatus used in this investigation was originally designed by Reynolds (77) and used for the investigation of vapour-liquid equilibria in binary systems of permanent non-polar gases with non-polar liquids up to pressures of 3 000 bar. It is an apparatus of the constant-volume type similar to that used by Graham (78), but in addition to stirring the heavy phase, the light phase is continually circulated through the heavy phase, thus producing complete saturation of both phases. Another important feature of the apparatus is that it allows for the determination of the density of both phases, thus providing a complete picture of the (P-ρ-T-x) properties of the system under study.

Essentially, the apparatus consists of three main parts:

(i) The compression section, which provides a means for developing gas pressures up to a few thousand bars;

(ii) The equilibrium section, where equilibrium between the two phases is attained;

(iii) The analysis section, in which the composition and density of the two phases are accurately measured.

A brief description of each of these three sections follows: a more detailed description can be found elsewhere (77).

4.1 Compression Section

The gas compressor used in this investigation is of the mercury-piston type and has two stages, as shown diagrammatically in Fig. 4.1. It has been described in detail by Bett and Reynolds (79).

The first stage compresses the gas from cylinder pressures to ca. 1 000 bar. It consists of two cylinders, A and B, connected at their base by a high-pressure capillary U-tube. The two cylinders each have

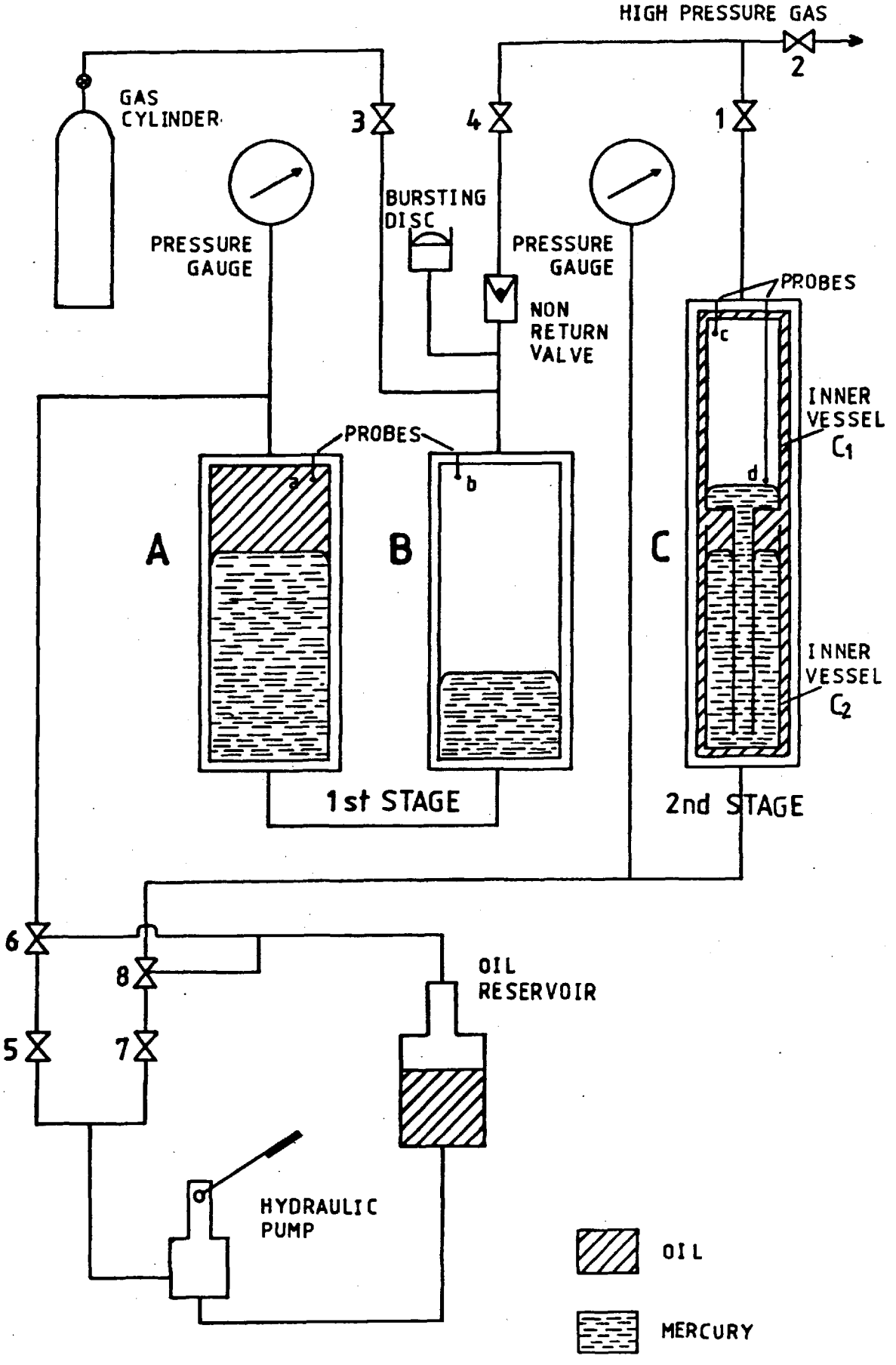


FIG. 4.1. Schematic diagram of gas compressor.

a capacity of 1 000 cm^3, with an internal diameter of 5.4 cm and an outside diameter of 12.7 cm. The second stage, which serves to boost the gas pressure to ca. 3 000 bar, differs from conventional mercury-piston compressors in that the pressure vessel is exposed only to the oil, whilst all the surfaces in contact with mercury are under hydrostatic pressure only. This design avoids the hazards associated with the embrittlement of steel by mercury at high pressures. The construction of the second stage may be seen from Fig. 4.1. It consists of a pressure vessel C, with an internal diameter of 3.4 cm and an outside diameter of 7.0 cm, inside which are located the two inner cylinders C_1 and C_2 which contain the mercury. These are made up from thin-walled stainless steel tubing which is a close fit inside the pressure vessel C. The capacity of the inner vessel C_2 is greater than the capacity of C_1, and sufficient mercury is present all the time so that a condition can never occur where oil rises through the mercury to contaminate the gas contained in C_1.

It is essential to keep the stroke of the mercury piston within certain limits to ensure that the mercury acts as an effective gas seal and prevents contamination of the gas being compressed by the oil, and also to stop the mercury contained in pressure vessels A, B and C from escaping into the pressure tubings connecting the compressor to the equilibrium section and eventually finding its way into the equilibrium section. To this end, the upper and lower limits of the permitted mercury movement are detected with the aid of the electrical probes "a", "b", "c" and "d", as shown in Fig. 4.1. When the mercury makes or, in the case of "d", breaks contact with the probes, a low-voltage electrical circuit is completed which actuates a relay and turns on an indicator light.

To operate the compressor, gas at cylinder pressure is allowed into B and C_1 and then compressed with the mercury piston by pumping oil into cylinder A using a high-pressure hydraulic pump. When the pressure reaches 1 000 bar, the first stage is isolated and oil is pumped only into C_2, until the gas pressure reaches the required value, up to a maximum of 3 000 bar. Clearly, if the required pressure is below 1 000 bar, there is no need to use the second stage of the compressor.

(.../)

These operations can be repeated as many times as necessary, until eventually the warning lights are turned on by the mercury making contact with the upper-limit probes "b" or "c". When this happens, and before carrying out any further compression of the gas, the mercury level in B or C must be lowered, by allowing oil to flow back into the oil reservoir, until the warning lights are turned on by the mercury making contact with the lower-limit probe "a" or breaking contact with the lower-limit probe "d". When this is done, gas can again be admitted from the cylinder and compression can be resumed.

4.2 Equilibrium Section

The equilibrium section, which is shown schematically in Fig. 4.2, is that part of the apparatus where the mixture under study is brought to equilibrium. It consists essentially of an equilibrium cell E, with a capacity of ca. 200 cm^3, in which the two fluid phases are well mixed, by stirring the contents of the vessel with a magnetically operated stirrer. Simultaneously, the light phase is continuously circulated around the system and bubbled through the heavy phase by means of a double-acting circulating pump, which is also magnetically operated. A small flowmeter in the form of a thermistor anemometer is inserted in the apparatus just after the circulating pump, in order to give a visual indication of whether or not the pump is operating successfully.

When equilibrium is reached, the heavy phase sample is isolated in vessel L by allowing it to flow into the vessel under gravity, and the light phase sample is isolated in vessel G. Since both sampling vessels are connected to the remainder of the high-pressure apparatus, the change in the pressure of the system arising from the closing of the relevant valves is negligible.

The relative positions of the two sampling vessels with respect to the equilibrium cell E are such that the whole of the sampling vessel L is below and the whole of the sampling vessel G is above the interface level in E. This avoids the possibility of some of the light phase being trapped in the heavy phase sampling vessel L, or some of

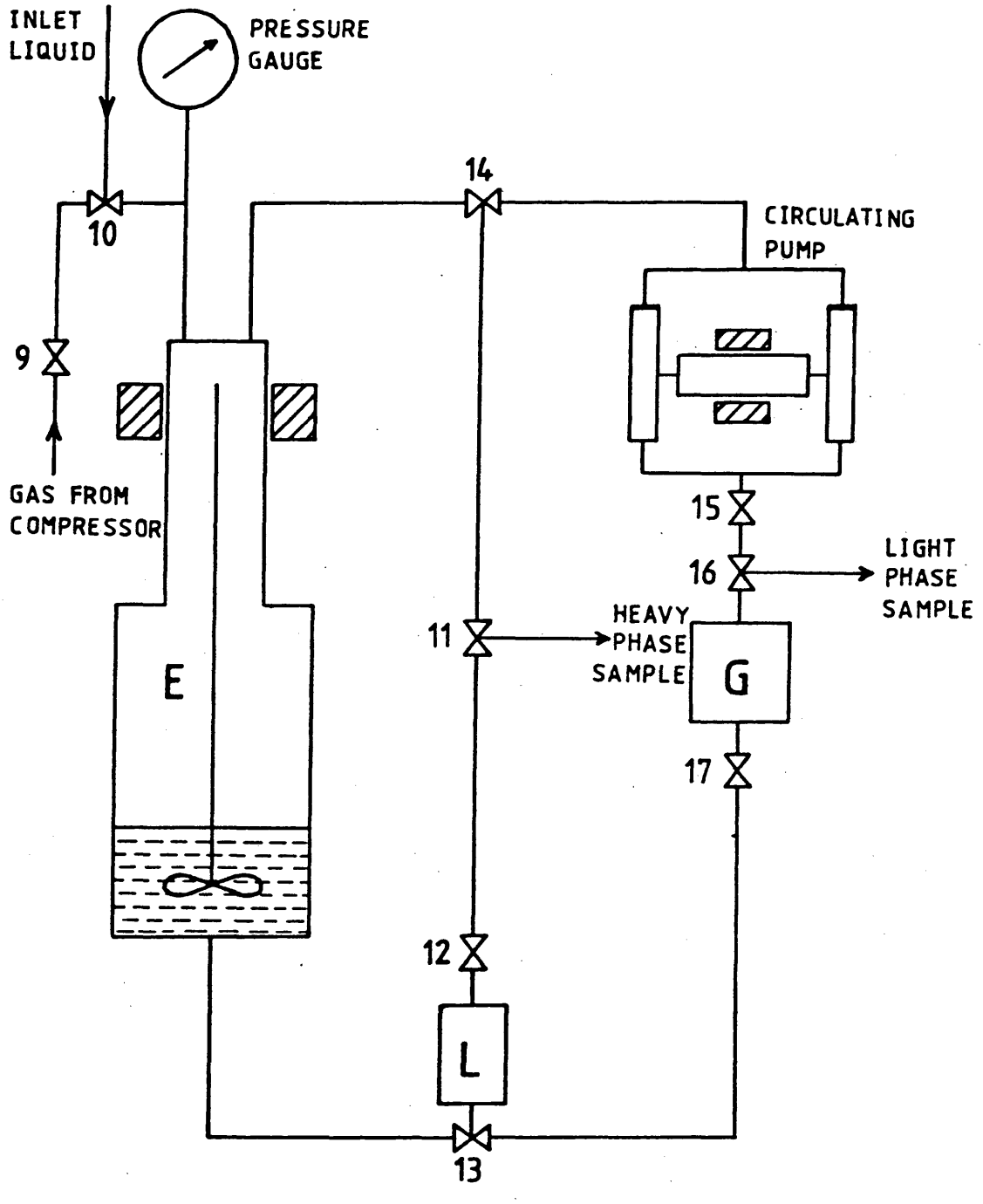


FIG. 4.2. Schematic diagram of equilibrium apparatus.

the heavy phase being trapped in the light phase sampling vessel G. The internal volume of the sampling vessel L, plus the high-pressure tubing between valves 12 and 13, is 4.47 cm^3; that of the sampling vessel G, plus the high-pressure tubing between valves 15 and 17, is 10.02 cm^3. These values, which are required to calculate the densities of both phases, were obtained by Reynolds (77), who calibrated the sampling vessels using argon.

The equilibrium pressure of the system is measured by means of a calibrated Bourdon-tube pressure gauge of appropriate range, which is directly connected to the top of the equilibrium cell E.

The equilibrium apparatus is mounted on a frame to one side of which all the valves are clamped. This frame is immersed in an oil tank, and the valves are operated by extension spindles which pass through special seals on the front face of the tank. The oil tank, which acts as a thermostating bath, is constructed from a 0.64 cm steel plate and has a detachable lid, thermal insulation being provided by a 2.5 cm thick layer of rigid asbestos. The oil used as the thermostating liquid is Shell Telus 23: it has a relatively low viscosity at ambient temperature and only fumes to a limited degree even at 100 °C. Circulation of the oil inside the tank is obtained with a propeller 7.6 cm in diameter rotating centrally 20.3 cm from the bottom of the tank and driven at 960 r.p.m. by a $\frac{1}{4}$ h.p. AC motor. In order to increase the efficiency of circulation, baffles 10.2 cm high are welded to the base of the tank along the diagonals.

Heat is supplied to the oil by means of two immersion heaters each having a maximum power dissipation of 2 kw, which may be reduced to 1 kw or 0.5 kw with a three-way series-parallel switch. The temperature of the bath is controlled using a Gallenkamp electronic relay which is actuated by a mercury-toluene thermoregulator. With this control, the temperature variation of the oil does not exceed $\pm$0.05 °C over the temperature range 25 - 100 °C. The actual temperature of the bath is measured with a calibrated mercury-in-glass thermometer engraved in 0.1 °C, the range of which depends upon the working temperature.

(.../)

Both the magnetic stirrer and the magnetic circulating pump are connected to a time switch, allowing equilibrium between the phases to be reached overnight and the sampling and analysis of the phases to be done during day-time.

4.3 Analysis Section

In this section, represented schematically in Fig. 4.3, both the heavy and the light phase samples are analysed by condensing out and weighing the less volatile component in the mixture, and then measuring the volume of the remaining gas in calibrated vessels at room temperature and pressure.

This simple procedure can be used only when there is a considerable difference between the two components and when a suitable freezing mixture can be found which will condense all the heavy component in the freezing trap without condensing any of the light component. The freezing mixture chosen in this case was a slurry of solid CO_2 in methanol, the temperature of which is in the range of -86 ^{o}C to -88 ^{o}C. In Fig. 4.4, the vapour pressure and melting curves for CF_4 and n-heptane have been plotted from their respective triple points up to atmospheric pressure. It may be seen from this diagram that in the range of temperatures from -86 ^{o}C to -88 ^{o}C all the heptane should condense out and all the CF_4 should pass through the trap, at pressures ranging from atmospheric down to a vacuum of almost 10^{-3} mm of Hg. Complete separation is, however, possible only if the residence time of the mixture in the freezing trap is sufficiently long to allow all the heptane to condense. Hence a rotameter is attached to the outlet of the freezing trap to ensure that the rate of flow of CF_4 through the trap is under control at all times.

After passing through the freezing trap and rotameter, the residual gas flows into the mercury gas burettes and calibrated spherical glass vessels, where its volume is measured under standard conditions of pressure and temperature. Two mercury gas burettes are used for gas volumes up to ca. 500 cm^3; one of these has four calibrated bulbs

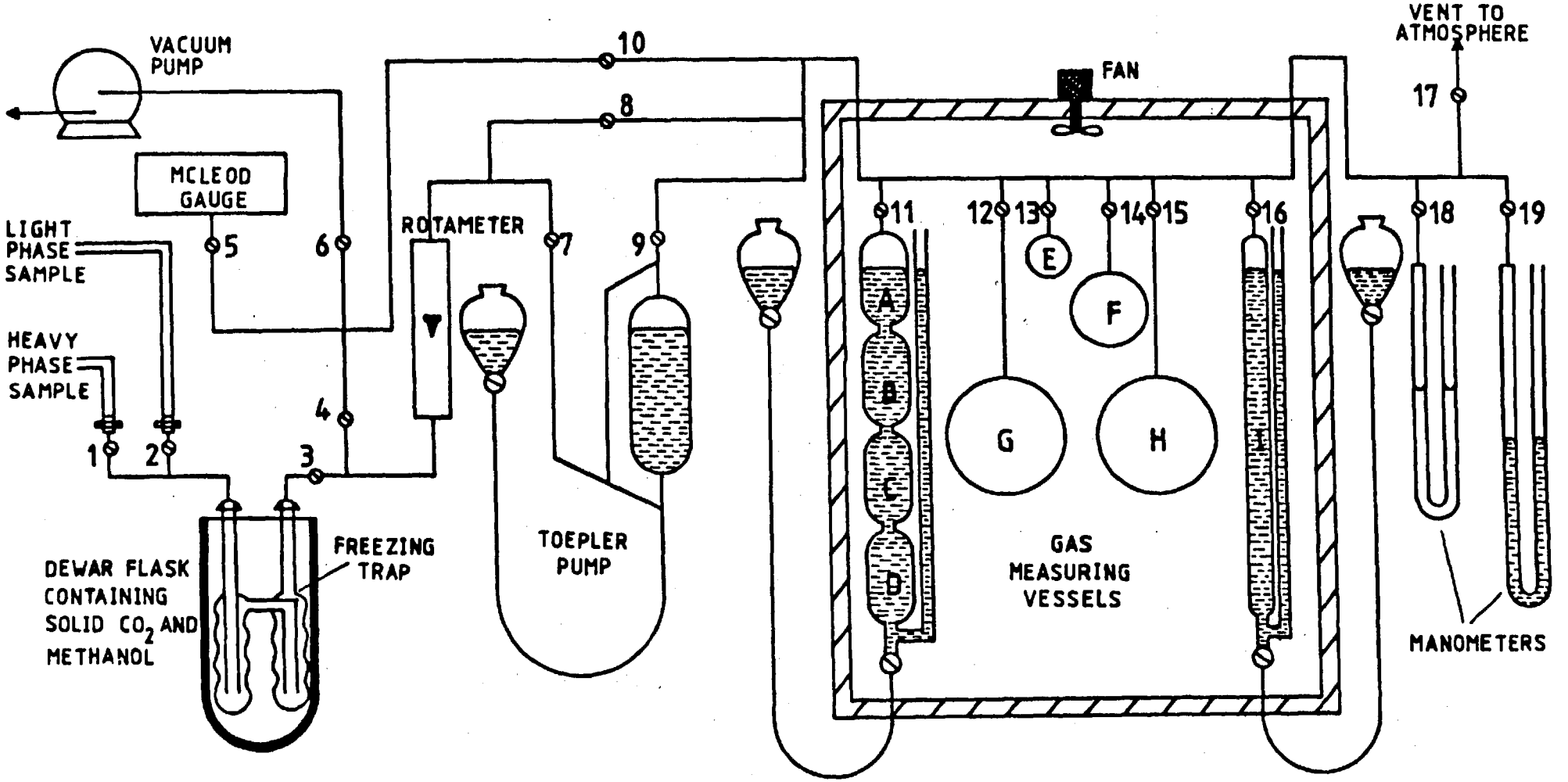


FIG. 4.3. Schematic diagram of analysis section.

Capacity of vessels: A = 98.7 cm^3; B = 97.7 cm^3; C = 99.8 cm^3; D = 101.0 cm^3; E = 547.8 cm^3; F = 1 128.1 cm^3; G = 2 240.6 cm^3; H = 2 249.1 cm^3; I = 100.0 cm^3.

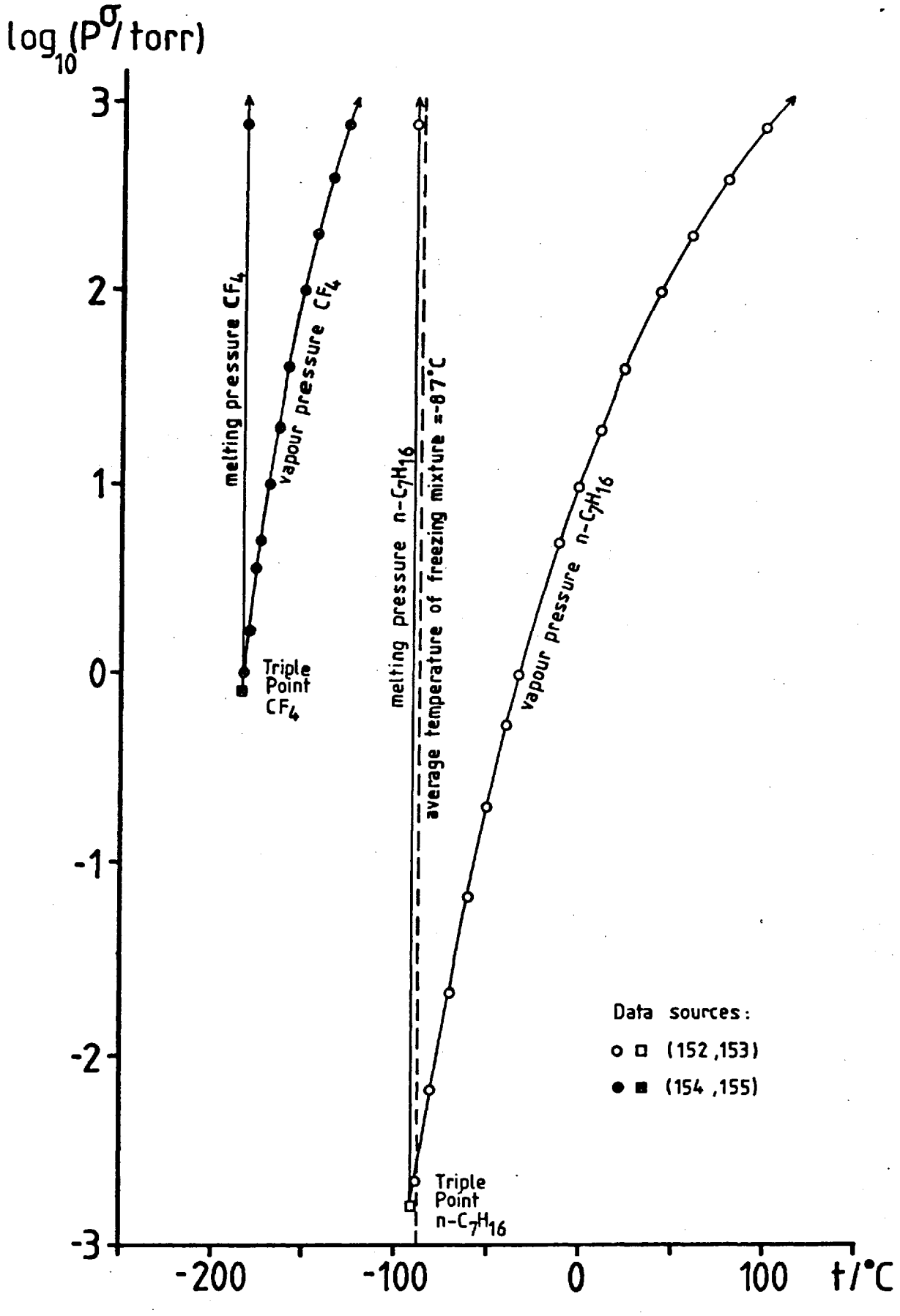


FIG. 4.4. Vapour pressure and melting pressure curves of the pure components below atmospheric pressure.

of approximately 100 cm^3 each, whereas the other has a capacity of 100 cm^3 engraved in 0.2 cm^3. For larger volumes of gas, the mercury burettes are used in conjunction with four calibrated spherical vessels having volumes ranging from ca. 500 cm^3 to ca. 2 000 cm^3. All the gas-measuring vessels and burettes are enclosed in a wooden box in which the air is circulated by means of an electric fan in order to maintain an even temperature. This box is provided with a perspex front with small hinged doors, through which the various taps are operated.

When the pressure in the sampling vessel is reduced to that in the analysis apparatus, no further flow of gas takes place spontaneously. In order to evacuate the sampling vessel and freezing trap, a Toepler pump is then used to transfer the remaining gas into the measuring vessels.

Two manometers, one filled with mercury and the other with di-butyl phthalate, enable the gas-measuring system to be adjusted to atmospheric pressure before each reading of volume is taken. The mercury manometer provides a rough adjustment of the pressure, the di-butyl phthalate one then being used for a more accurate adjustment of the pressure inside the measuring vessels.

Finally, since the entire analysis section has to be evacuated before any measurements are carried out, a vacuum pump capable of producing a vacuum of 10^{-2} mm of Hg is attached to the line, as shown in Fig. 4.3. The pressure of the vacuum produced by the pump can be read on a McLeod gauge, also shown in the same diagram.

Chapter 5

EXPERIMENTAL PROCEDURE

5.1 Operation of the Gas Compressor

Before starting the experimental runs, it was necessary to purge the compressor of any residual gas from previous experiments. Once this was done and the compressor was filled with pure CF_4, there was no need to repeat this purging operation so long as the compression section was kept completely enclosed.

5.1.1 Purging

To displace residual gas from the compressor, valves 3, 6 and 8 were shut and the remaining valves were left open (see Fig. 4.1). Oil was then pumped through valves 5 and 7 into vessels A and C_2 until the mercury levels in B and C_1 made contact with probes "b" and "c" respectively. Valves 2, 5 and 7 were then closed, leaving only valves 1 and 4 open. After opening valve 3, pure CF_4 from a gas cylinder was allowed to enter vessels B and C_1 at cylinder pressure (about 120 bar). When this was done, valve 3 was closed and, by opening valve 2, the gas was vented to the atmosphere. This procedure was repeated several times, to ensure that all the residual gas was purged from the system.

5.1.2 Normal operation

After purging the compressor, valves 6 and 8 were opened slowly, allowing the gas at cylinder pressure to push the mercury down and displace oil into the reservoir, until the mercury made contact with probes "a" and "d", as shown by the indicator bulbs. Then, with valves 1, 3 and 4 open and all other valves closed, CF_4 was introduced into vessels B and C_1 at cylinder pressure.

(.../)

After closing valve 3, valve 5 was opened and oil was pumped into vessel A so that the mercury piston compressed the CF_4 in vessels B and C_1 to a pressure not exceeding 1 000 bar, as read on the Bourdon-tube pressure gauges connected to cylinders A and C. The first stage of the compressor was then isolated by closing valves 4 and 5.

To boost the gas pressure above 1 000 bar, valve 7 was opened and oil was pumped into vessel C_2, thereby displacing mercury from C_2 to C_1 and compressing the gas in container C_1. As soon as the desired working pressure was reached, valve 7 was closed, and the compressed CF_4 was allowed to pass directly into the equilibrium section by opening valve 2. For many experiments the working pressure was below 1 000 bar and there was no need to use the second stage of the compressor, which was then completely isolated from the system by closing valves 1, 7 and 8. When only the first stage was used, valve 2 was kept open, and the compressed CF_4 from vessel B was transferred directly to the equilibrium section by opening valve 4.

5.1.3 Reloading

When the mercury surfaces reached the upper limits, as detected by probes "b" and/or "c", it was necessary to reload the compressor. This was done by opening very slowly let-down valves 6 and/or 8, keeping all the other valves closed. This caused the mercury levels to be forced down by the high-pressure gas remaining in B and C_1, hence displacing the oil into the reservoir, as previously described. Great care was taken during this operation to keep the oil flow rate under close control, in order to ensure that no mercury was expelled from vessels A and C.

When the mercury levels reached their lowest positions, as indicated by probes "a" and/or "d", valves 6 and 8 were again closed, valve 3 was opened and vessels B and C_1 were refilled with CF_4 from the cylinder. The compressor was then ready to be used again.

(.../)

5.2 Operation of the Equilibrium Section

The first step consisted in bringing the oil bath to the working temperature, for which purpose the oil stirrer was switched on and the two immersion heaters were set to dissipate 2 kw. When the required temperature had been reached, the energy input to the two immersion heaters was reduced to 0.5 kw and the mercury-toluene thermoregulator was switched on to control the temperature of the oil bath to within ± 0.05 °C of the desired temperature.

When the temperature had remained constant for several hours, the equilibrium apparatus was evacuated to a pressure of 10^{-2} mm of Hg using the vacuum pump attached to the analysis section. CF_4 was transferred from the compressor to the equilibrium apparatus, until the pressure increased to atmospheric, or slightly above.

5.2.1 Filling the apparatus with solvent

With valves 9 and 13 closed and all the other valves open (see Fig. 4.2), a measured amount of pure n-heptane was introduced very slowly into the apparatus via valve 10. The position of this valve was such that the liquid flowed by gravity into the equilibrium vessel E, an equivalent volume of CF_4 being displaced through valves 11 and 16.

The amount of n-heptane introduced into the equilibrium apparatus was critical, since the level of the interface in the equilibrium vessel E had to be kept between the levels of valves 12 and 17 at all times. Of the two components, only CF_4 could be introduced into the equilibrium vessel under pressure. It was therefore important to introduce as much n-heptane into the apparatus as feasible, in order that the maximum possible number of experiments could be completed before the level of the interface in vessel E was located above valve 17 or below valve 12. When this happened, the equilibrium apparatus had to be emptied and refilled.

(.../)

It was not easy to determine the optimum amount of n-heptane, since the position of the interface also depended on the working pressure, i.e. on the amount of high-pressure CF_4 introduced into the equilibrium apparatus, and this was not measured. It was, however, found by trial and error that between 100 and 150 cm^3 of n-heptane were needed, and that 5 to 10 experiments could be completed before the apparatus had to be emptied and refilled.

After the n-heptane had been introduced into the apparatus, it was repeatedly saturated with CF_4, and the gas vented to the atmosphere, in order to remove any small quantity of air that might have been dissolved in the n-heptane.

5.2.2 Attainment of equilibrium and sampling

After introduction of the solvent, valves 10, 11 and 16 were closed and all the other valves were kept open. CF_4 from the gas compressor was then allowed to enter the equilibrium section through valve 9 until a pressure 5 to 10 bar in excess of the required equilibrium pressure was reached. Valve 9 was then closed, and the magnetic stirrer and circulating pump were switched on. As soon as this was done, the pressure inside the apparatus decreased, as a result of the CF_4 dissolving in the n-heptane. After 15 to 20 minutes, the pressure would stabilise at a value 5 to 10 bar below the initial value, indicating that the system had probably reached equilibrium. In order to make sure that both phases were completely saturated, however, the operation of the magnetic stirrer and circulating pump was continued for another 3 to 4 hours. In the meantime, to check that the circulating pump was operating successfully, the anemometer was switched on periodically. This intermittent operation of the anemometer was necessary so as not to affect the isothermal conditions of the system.

When equilibrium had been established, the magnetic stirrer and circulating pump were switched off and the two phases were allowed to separate. Normally, 1 to 2 hours were allowed for complete separation, but at conditions under which the densities of the two phases were almost identical, such as those near the critical pressure or near the pressure of barotropic inversion, the separation time was increased to 3 or 4 hours.

(.../)

Before sampling the two phases, the equilibrium pressure of the system was read on the Bourdon-tube pressure gauge connected to vessel E. The light phase sample was then isolated in sampling vessel G by closing valves 15 and 17. At the same time, valve 13 was opened and the heavy phase was allowed to flow under gravity into sampling vessel L and also into the tubing above valve 12.

As soon as the light phase sample had been analysed (see section 5.3), valves 13, 12 and 14 were closed in that order, thus isolating the heavy phase sample in vessel L. Valve 11 was then opened to the atmosphere, and the tubing between valves 12 and 14 was evacuated using the vacuum pump attached to the phase analysis section. When this was done, valve 11 was again closed and valve 12 opened, thus allowing the heavy phase sample trapped in vessel L to expand into the line between valves 13 and 14, prior to analysis.

5.3 Operation of the Phase Analysis Section

The two types of freezing traps used in the experiments are shown in Fig. 5.1. Type A was employed when the quantity of solvent was expected to be large, as was the case with the heptane-rich samples. Otherwise, type B was employed, because of its larger surface area.

5.3.1 Preparation

Before either trap was connected to the phase analysis system, it was thoroughly cleaned, dried, stoppered and weighed. The ground conical connections through which the sample flowed were lubricated with Apiezon grease in such a way as to leave only a very thin film of grease on the mating surfaces, thereby minimising the error caused by the n-heptane coming into direct contact with the grease and dissolving it.

The appropriate trap was then connected to the system (see Fig. 4.3), which was evacuated to a pressure of 10^{-2} mm of Hg, as indicated by the McLeod gauge. It was important at this stage to make sure that the vacuum was maintained, since any air entering the system would

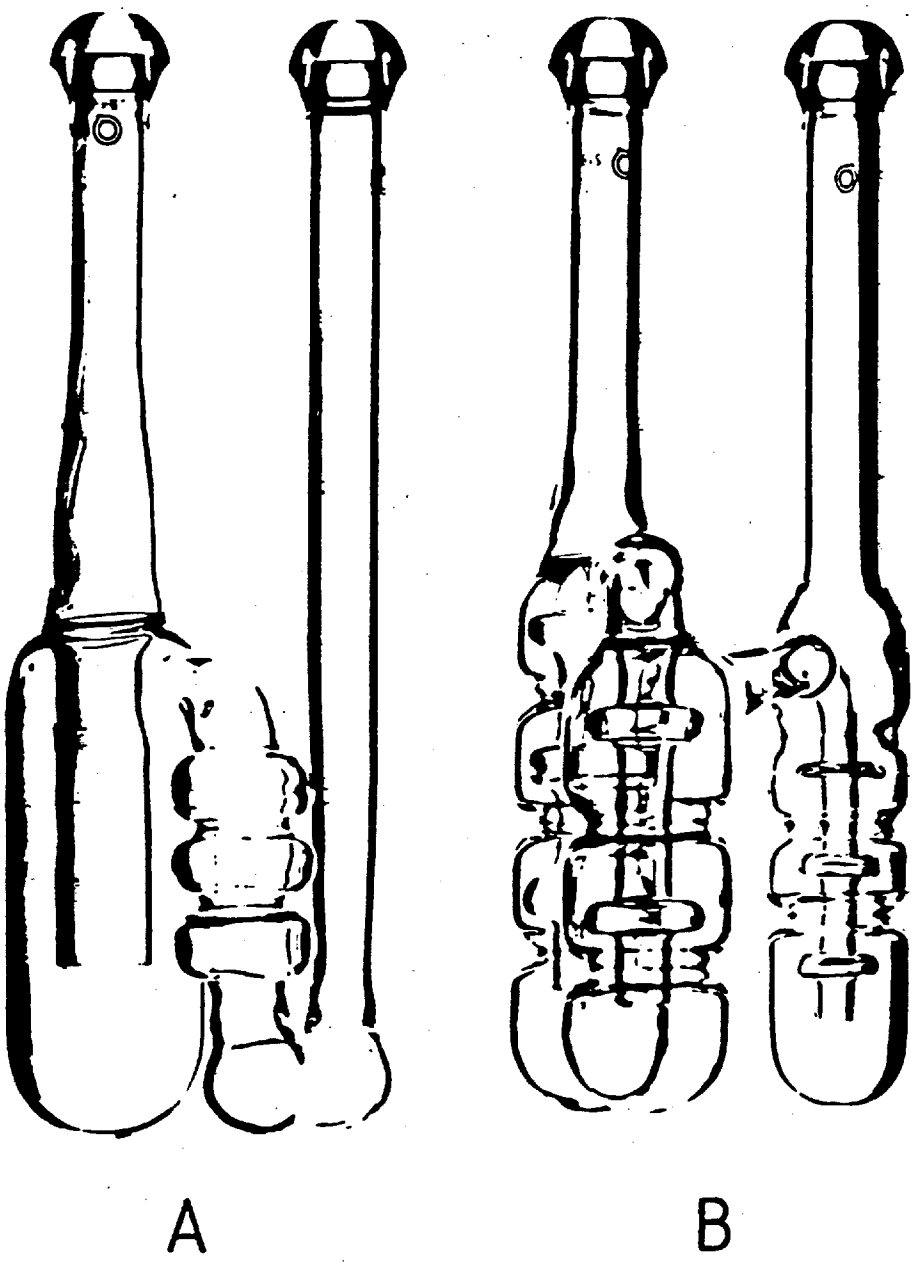


FIG. 5.1. The two types of freezing traps used in the experiments.

cause an error in the final gas volume. While the system was being evacuated, taps 7, 9, 11, 16, 17 and 18 were kept closed whilst all the others were open. When the required vacuum was reached in a leak-tight system, taps 4 and 6 were closed, together with tap 1 or 2, according to which phase was to be analysed.

Since the measuring vessels and mercury gas burettes were calibrated up to their respective taps and the volume of the line between taps 8-10 and taps 17-19 could not be determined accurately, it was necessary to compensate for this "dead volume" in order to avoid errors in the measured final volume. This was done by closing taps 8, 10 and 12-15, and then allowing air at atmospheric pressure to fill the "dead volume" by opening tap 17. When atmospheric pressure had been reached inside the "dead volume", tap 17 was again closed and tap 8 opened.

The validity of this compensation procedure rests on the following assumptions:

(i) Air and CF_4 form an ideal mixture at atmospheric temperature and pressure, with no change of volume on mixing;

(ii) Ambient temperature and pressure remain unchanged over the period between the "dead volume" being filled and the completion of the analysis of the sample. Since the analysis of a sample rarely took more than two hours, this assumption is reasonable, and the error in the measurement of the gas volume due to this compensation procedure was assumed to be negligible.

The technique for measuring the volume of CF_4 varied according to the quantity of gas that the sample was expected to produce. For volumes over 500 cm^3, the gas was drawn directly into an evacuated vessel or vessels having a volume slightly less than that expected from the sample, whereas for gas volumes under 500 cm^3 only the mercury gas burettes were used. In the former case, clearly, the taps leading to the pre-selected calibrated vessels had to be opened prior to analysis. Great care was taken not to open taps 11 or 16 unless the pressure was the same on both sides of these taps, as otherwise mercury from the gas burettes could be displaced into the calibrated vessels, with disastrous results.

(.../)

5.3.2 Analysis of the samples

Having prepared the phase analysis section in the manner described above, either valve 11 (heavy phase sample) or valve 16 (light phase sample) was very carefully cracked open, and the sample was allowed to expand through the freezing trap and rotameter into the measuring system at such a rate that all the solvent was condensed in the trap. According to Reynolds (77), provided the gas flow rate is not greater than 60 $cm^3.min^{-1}$, the loss of solvent vapour does not exceed 10^{-8} $mol.cm^{-3}$. The rotameter used in this investigation was calibrated in order to estimate the flow rate of gas at full deflection. This was found to be ca. 20 $cm^3.min^{-1}$, which is well within the limit recommended by Reynolds.

The opening of valves 11 and 16 was the most critical step in the whole experiment, since a sample initially under a pressure which could be as high as 1 300 bar was allowed to expand into the measuring system at a pressure below atmospheric. Bearing in mind that the flow rate of gas had to be kept under close control at all times, it was essential to maintain those two valves in perfect condition, since otherwise the success of this operation could not be guaranteed.

After 1 to 2 hours, the pressure inside the phase analysis section was equal to the pressure inside the sampling vessel and the flow of gas ceased. Tap 8 was then closed, and the remaining gas left in the sampling vessel was transferred via the Toepler pump to the gas burettes and calibrated vessels by careful manipulation of taps 7 and 9. The system was then adjusted to atmospheric pressure using the mercury and di-butyl phthalate manometers in conjunction with the mercury gas burettes, and the volume of CF_4 was measured at ambient temperature and pressure, as recorded respectively on a mercury-in-glass thermometer and a Fortin barometer.

Taps 1, 2 and 3 were closed and the freezing trap was disconnected from the system, stoppered and warmed up to room temperature. Any grease left on the ground conical connections to the trap was carefully removed with a suitable solvent, as were traces of condensation on the outside of the trap. Finally, the trap was accurately weighed to determine the mass of solvent present in the sample.

Chapter 6

EXPERIMENTAL RESULTS: PRESENTATION AND DISCUSSION

6.1 Presentation of the Results

Fluid phase equilibria for the binary system CF_4 + n-C_7H_{16} were determined at six different temperatures ranging from 323.15 K to 343.15 K and at pressures up to ca. 1 300 bar. The measurements recorded in the experiments are tabulated in Appendix C, together with the calculated values of the mole fraction of CF_4 and molar density for both phases. A brief discussion on the purity of the materials used in the experiments is given in Appendix A. The experimental results tabulated in Appendix C are also presented in Figs. 6.1 to 6.3 in the form of isothermal pressure-composition, pressure-molar density and molar density-composition diagrams respectively.

The mole fraction of CF_4 and the molar density of each phase were calculated from the recorded measurements in the following way:-

$$x = \frac{\text{moles of } CF_4}{\text{moles of } CF_4 + \text{moles of n-}C_7H_{16}} = \frac{(V/V^*)^{S.T.P.}}{(V/V^*)^{S.T.P.} + (W/M)} \quad (6\text{-}1)$$

$$\rho = \frac{\text{moles of } CF_4 + \text{moles of n-}C_7H_{16}}{\text{volume of sampling vessel}} = \frac{(V/V^*)^{S.T.P.} + (W/M)}{V_S} \quad (6\text{-}2)$$

where:

x = mole fraction of CF_4 in either phase

ρ = molar density of either phase, mole. dm^{-3}

$(V)^{S.T.P.}$ = experimentally measured volume of CF_4 present in either sampling vessel, cm^3, reduced to standard conditions of temperature and pressure (0 °C, 1 atm)

$(V^*)^{S.T.P.}$ = molar volume of pure CF_4 at standard conditions of temperature and pressure = 22 303.3 $cm^3.mol^{-1}$

(.../)

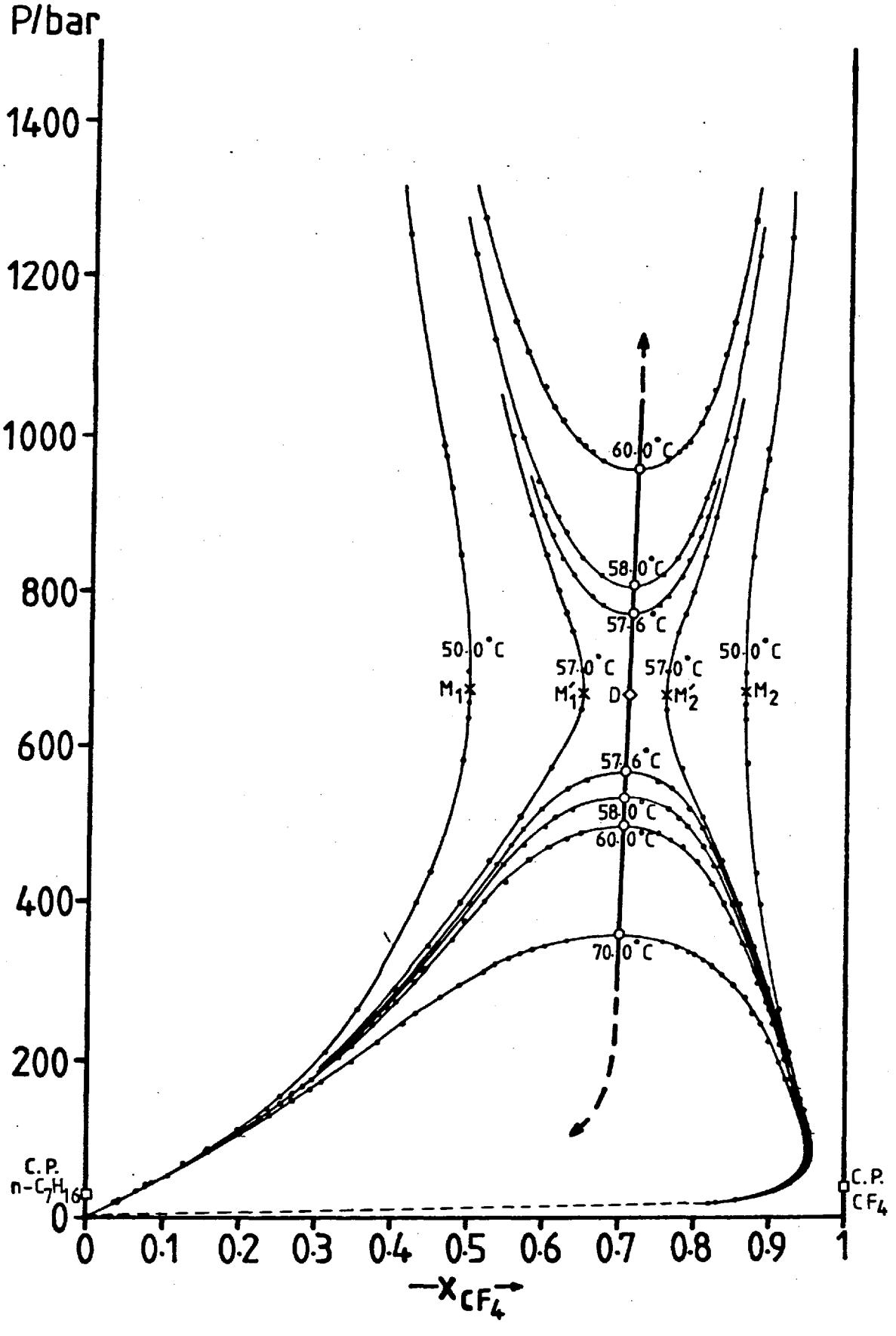


FIG. 6.1. Isothermal (P-x) diagram for the CF_4 + n-C_7H_{16} system, showing the (P^c-x^c) projection of the critical line.

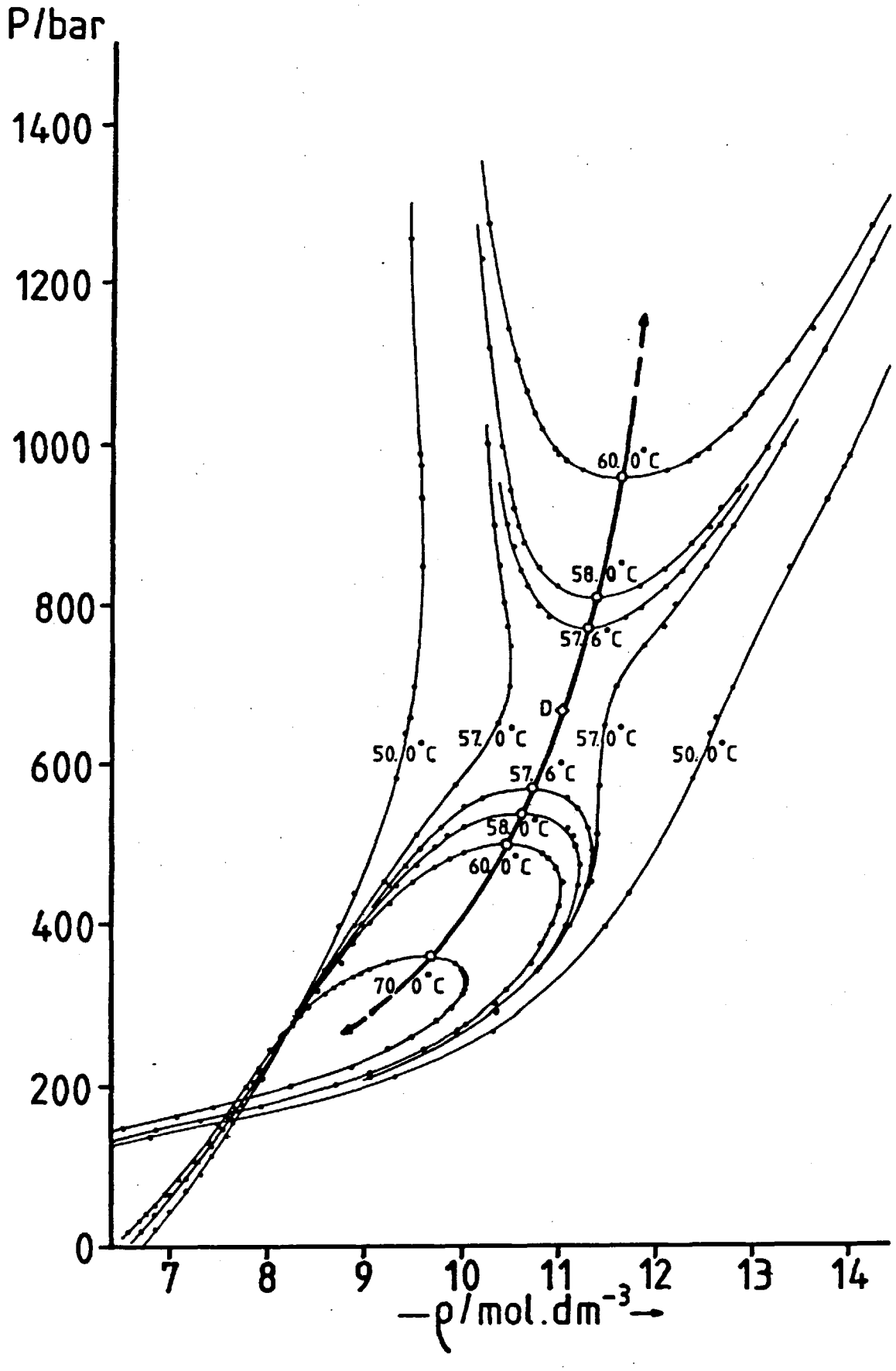


FIG. 6.2. Isothermal (P-ρ) diagram for the CF_4 + n-C_7H_{16} system, showing the (P^c-ρ^c) projection of the critical line.

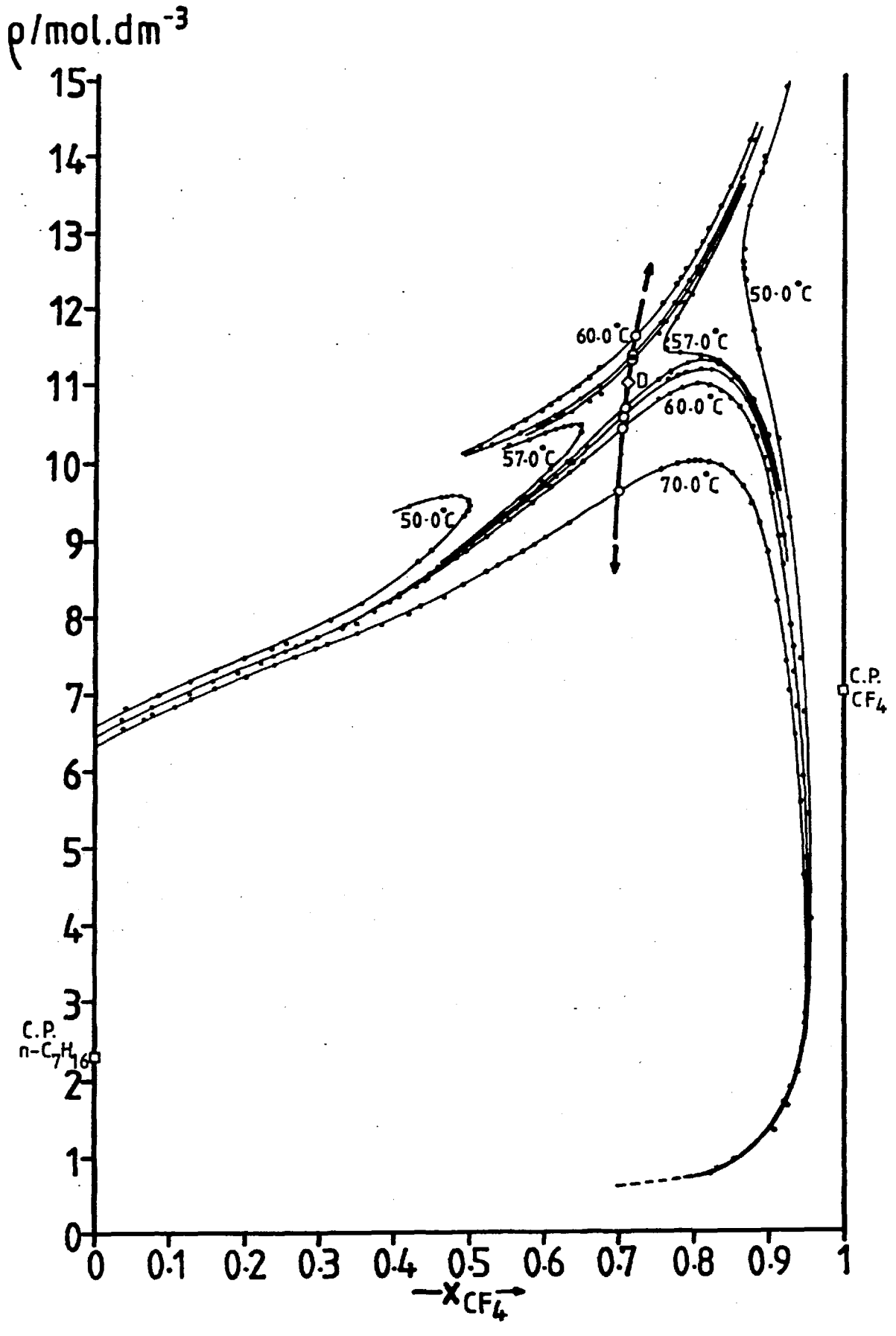


FIG. 6.3. Isothermal (ρ-x) diagram for the CF_4 + n-C_7H_{16} system, showing the (ρ^c-x^c) projection of the critical line.

W = experimentally measured mass of $n\text{-}C_7H_{16}$ present in either sampling vessel, g

M = molecular mass of $n\text{-}C_7H_{16}$ = 100.2 $g.mol^{-1}$

V_s = volume of either sampling vessel, dm^3.

The two sampling vessels were calibrated by Reynolds (77) by filling them with argon at a known temperature and pressure and measuring the corresponding volume of gas at S.T.P. From the (P-V-T) data for argon (82), Reynolds obtained the following values for the volumes of the sampling vessels:

Heavy phase sampling vessel: V_s = 0.004 47 dm^3 ($\pm$2.0%)

Light phase sampling vessel: V_s = 0.010 02 dm^3 ($\pm$2.0%).

6.2 Accuracy of Measurements

During the course of each experimental run, the following measurements were recorded:

(i) Equilibrium pressure;
(ii) Equilibrium temperature;
(iii) Mass of n-heptane in both samples;
(iv) Volume of carbon tetrafluoride in both samples;
(v) Ambient temperature and pressure at which the volume of CF_4 was measured.

6.2.1 Equilibrium pressure

The equilibrium pressure was measured by means of a Bourdon-tube pressure gauge having a range of 0 - 1 500 atm, directly connected to the top of the equilibrium cell. The scale of the gauge was divided into increments of 10 atm, and the pressure was read to $\pm$2 atm. The gauge was calibrated against a dead-weight tester to ensure that no systematic error was present, and it was found to be reproducible to $\pm$3 atm up to 1 200 atm. The measurement of the equilibrium pressure using this gauge was therefore subject to an overall uncertainty of $\pm$5 atm.

(.../)

6.2.2 Equilibrium temperature

The equilibrium temperature was read to ±0.05 °C in one of two mercury-in-glass thermometers, according to the value of the working temperature. Both thermometers were engraved in 0.1 °C, one having a range of 20 °C to 70 °C and the other a range of 60 °C to 110 °C. Since the temperature was controlled to ±0.05 °C with the mercury-toluene thermoregulator, the overall uncertainty in the measured equilibrium temperature was unlikely to be greater than ±0.1 °C.

6.2.3 Mass of n-heptane

The mass of n-heptane was measured by weighing the relevant freezing trap on a sensitive analytical balance before and after the experiment, and then subtracting the two results. Since the balance was accurate to ±0.000 5 g, the uncertainty in the value of W was unlikely to exceed ±0.001 g.

6.2.4 Volume of CF_4

According to Reynolds (77), the accuracy of the calibration of the gas-measuring vessels was better than ±0.1%. Other possible errors in the measurement of the volume of CF_4 include:

(i) A difference between the ambient temperature and the temperature (20 °C) at which the calibration was carried out, resulting in an expansion or contraction of the vessels;

(ii) The error incurred in bringing the system to atmospheric pressure using the di-butyl phthalate manometer: this was estimated to be the equivalent of ±1 mm of di-butyl phthalate.

Both these errors are negligible when compared with the error in the calibration of the measuring vessels. Taking Reynolds' calibration to be still valid, therefore, it may be assumed that the volume of CF_4 is known to ±0.1%.

(.../)

6.2.5 Ambient temperature and pressure

The ambient temperature at which the volume of CF_4 was measured varied from 15 °C to 25 °C and was read to an accuracy of ±0.1 °C on a calibrated mercury-in-glass thermometer. The ambient pressure was read on a Fortin barometer to an accuracy of ±0.1 mm of Hg. Corrections were made to this reading to account for the thermal expansion of the brass scale, the change in density of the mercury, the capillary depression of the mercury and the difference in elevation between the laboratory and the barometer.

6.3 Error Analysis

The values of the mole fraction of CF_4 and molar density of each phase calculated from equations 6-1 and 6-2 are subject to random experimental errors which may be estimated from the accuracy of the various measurements. They are also subject to indeterminate errors, which may occur as a result of failures in the experimental procedure that are not detected during the course of the experiment. Such errors can only be estimated by comparing the precision of the results with the expected total random error, for which purpose a large number of readings must obviously be taken.

6.3.1 Random errors

The percentage random error in the values of the mole fraction of CF_4 and the molar density of either phase can be obtained by using the well-known formula for the propagation of random experimental errors, together with equations (6-1) and (6-2):

$$\left(\frac{\delta x}{x}\right) = (1-x)\left\{\left(\frac{\delta V^{S.T.P.}}{V^{S.T.P.}}\right)^2 + \left(\frac{\delta W}{W}\right)^2\right\}^{\frac{1}{2}} \qquad (6\text{-}3)$$

$$\left(\frac{\delta \rho}{\rho}\right) = \left\{x^2\left(\frac{\delta V^{S.T.P.}}{V^{S.T.P.}}\right)^2 + (1-x)^2\left(\frac{\delta W}{W}\right)^2 + \left(\frac{\delta V_s}{V_s}\right)^2\right\}^{\frac{1}{2}}, \qquad (6\text{-}4)$$

where the symbol δ represents the random error in the relevant quantity, and all the other symbols have the same meaning as in equations (6-1) and (6-2). The derivation of equations (6-3) and (6-4) is set out in Appendix D.

If typical experimental values of x, $V^{S.T.P.}$, W and V_s are substituted in equations (6-3) and (6-4), together with the accuracy of these measurements, as given in section 6.2, the following conclusions can be drawn:

(i) The percentage random error in the calculated value of x, the mole fraction of CF_4 in either phase, does not exceed 0.1%, except perhaps at pressures below ca. 20 bar, i.e. at conditions that are not relevant to this investigation;

(ii) The percentage random error in ρ, the molar density of either phase, is practically independent of temperature and pressure and equal to 2.0%. Thus the error in the calibration of the sampling vessels $-(\delta V_s/V_s)$ in equation (6-4) - is by far the most dominant error.

6.3.2 Indeterminate errors

The most likely sources of indeterminate errors were:

(i) Failure to reach equilibrium;

(ii) Failure to obtain a perfect separation of the heavy and light phases, after equilibrium had been reached;

(iii) Unrepresentative sampling of one of the phases, as a result of having too much or too little n-heptane in the equilibrium apparatus, hence causing the interface to be located below the level of valve 12 or above that of valve 17 (see Fig. 4.2);

(iv) Failure to condense all the n-heptane in the freezing trap;

(v) Loss of n-heptane in the process of weighing the freezing traps.

The first two possible sources of error are especially important in the critical region and in the region of barotropic inversion, where the densities of the two phases are very similar. In the critical

region, this problem is enhanced by the fact that the concentration in the two phases is very similar and therefore the "driving force" towards equilibrium will be very small. In an attempt to eliminate any such errors, the time allowed for the system to reach equilibrium and for the two phases to separate was almost doubled when working in either of these regions.

Unrepresentative sampling of either phase was a fairly frequent occurrence, since only a limited number of experimental runs could be carried out before the interface level fell below/rose above its prescribed limit and the apparatus had to be refilled with n-heptane. The same problem would sometimes occur if too little or too much n-heptane was used in refilling the apparatus. If a visual cell were to be added to the equilibrium vessel, these problems would disappear; in addition, a visual cell would be extremely helpful in observing critical opalescence and so determining the critical pressure quickly and accurately, instead of having to interpolate between experimental results.

As regards the last two possible sources of error, extreme care was taken to keep the flow rate of CF_4 past the rotameter under close control. This was especially important when either valve 11 or valve 16 was cracked open at the beginning of the analysis of either phase. Similarly, it was essential to make sure that no loss of solvent occurred in the process of cleaning, drying and weighing the freezing traps. This might have been prevented entirely if the design of the freezing traps had been improved by incorporating Teflon taps in the necks of the traps.

It is always extremely difficult to control indeterminate errors. In this investigation, this was done by trial and error and by comparing every new result with the trend of previously obtained data: whenever a gross error was evident and the experimental points obtained did not fit into the "general picture", the run was discarded. In most cases, the cause of the error could be ascribed to unrepresentative sampling of either phase.

(.../)

As may be observed in Figs. 6.1 to 6.3, in general all the results lie within the calculated random error, which indicates that indeterminate errors were kept under close control. It is, however, possible that these errors may become more significant in the critical region, where it is more difficult to follow the trend of the results. In other words, it is not easy to find out exactly how "flat" the saturation curve is near the critical point, since it is only possible to get to within 10 to 15 bar of the critical point with the apparatus used in this investigation. Had a visual cell been incorporated in the equilibrium vessel, it would have been much easier to reduce this uncertainty, since it would have allowed a much faster and more accurate determination of the critical point.

6.4 Discussion of the Experimental Results

From the isothermal (P-x) diagram in Fig. 6.1, it is evident that the shape of the isotherms changes drastically as the temperature is increased. At 323.15 K, there are two branches to the saturation curve: no critical point was found, and the curve remains open at the top with the two branches diverging slightly up to the highest pressure attained.

The left-hand side branch represents the saturated "liquid phase", i.e. the solubility of CF_4 in n-heptane: this increases with pressure until it reaches a maximum, denoted by M_1 in Fig. 6.1, at $P \simeq 700$ bar and $x \simeq 0.5$. If the pressure is further increased isothermally, the solubility of CF_4 in n-heptane decreases, being $x \simeq 0.42$ at $P \simeq 1\,250$ bar, the highest pressure reached.

The right-hand side branch represents the saturated "gas phase", i.e. the solubility of n-heptane in CF_4. As with the other branch, this one starts off from the left-hand side axis (vapour pressure of pure n-heptane at 323.15 K), and then proceeds rapidly to lower values of the mole fraction of n-heptane (higher values of x). It goes through a solubility minimum at $P \simeq 90$ bar and $(1-x) \simeq 0.04$, and then proceeds to higher pressures. The solubility of n-heptane in CF_4 then reaches a maximum, denoted by M_2 in Fig. 6.1, at $P \simeq 700$ bar and $(1-x) \simeq 0.14$, and finally decreases with further increase in pressure.

(.../)

The solubility maxima represented by points M_1 and M_2 in Fig. 6.1, both located around 700 bar, cause the 323.15 K isotherm to have a typical "waisted" shape. The "waist" becomes more pronounced as the temperature is increased, as exemplified by the 330.15 K isotherm: the maximum in the solubility of CF_4 in n-heptane, denoted by M_1', is now located at $x \simeq 0.65$, whereas the maximum in the solubility of n-heptane in CF_4, denoted by M_2', is located at $(1-x) \simeq 0.24$.

Eventually, the two points of maximum solubility will merge into each other at the so-called "point of double contact", denoted by D in Fig. 6.1. Further increase in temperature will cause the isotherms to split into two curves: a lower curve, representing gas-liquid equilibria, which is a closed loop with an upper critical solution pressure; and an upper curve, which may be said to represent fluid-fluid equilibria, and which is open at the top, with a lower critical solution pressure. Increasing the temperature now has the effect of displacing the upper critical solution pressure to lower pressures and the lower critical solution pressure to higher pressures, as may be seen from the isotherms at 330.75 K, 331.15 K, 333.15 K and 343.15 K in Fig. 6.1. The critical mole fraction, however, remains almost constant at $x \simeq 0.7$, increasing only very slightly with increasing pressure. The upper curve at 343.15 K could not be determined experimentally because of serious leakage problems in the second stage of the gas compressor.

The isothermal (P-ρ) diagram of Fig. 6.2 shows the same general features as the isothermal (P-x) diagram, with the "waisted" shape open curves at 323.15 K and 330.15 K, splitting into upper (fluid-fluid) and lower (gas-liquid) curves as the temperature is increased above that of the "point of double contact". Unlike the critical mole fraction, the critical molar density does not remain nearly constant with increasing pressure, but increases from $\rho \simeq 9.7$ mol.dm^{-3} at $P \simeq 360$ bar to $\rho \simeq 11.6$ mol.dm^{-3} at $P \simeq 960$ bar.

The most interesting feature of the (P-ρ) diagram is the intersection of the "liquid" and "gas" branches of the various isotherms at pressures between 150 bar and 200 bar, as exemplified in Fig. 6.2 by the 323.15 K isotherm and by the lower portions of the 333.15 K and 343.15 K isotherms. This arises because barotropic inversion of the

phases occurs over this range of pressures, causing the phase rich in CF_4 to sink to the bottom of the vessel as the pressure is increased isothermally. At each temperature, barotropic inversion of the phases occurs at the pressure at which the densities (not the molar densities) of the two phases become identical. The concentration of CF_4 in the two phases is of course quite different. Table 6.1 gives the values of the pressure at which barotropic inversion of the phases occurs for the CF_4 + n-C_7H_{16} system as a function of temperature. These values were obtained by plotting the pressure P against the density d, where

$$d = \rho \{ x M_{CF_4} + (1-x) M_{C_7H_{16}} \} \qquad (6\text{-}5)$$

and M_{CF_4} and $M_{C_7H_{16}}$ represent the molecular masses of the two pure components.

TABLE 6.1

Barotropic inversion of the phases for the CF_4 + C_7H_{16} system

T/K	P/bar
323.15	182
333.15	195
343.15	211

The isothermal (ρ-x) diagram shown in Fig. 6.3 completes the graphical representation of the experimental data. It does not provide any extra information about the system which cannot be obtained by cross-plotting Figs. 6.1 and 6.2. Unlike the isothermal (P-x) and (P-ρ) diagrams, the critical points are not situated at extreme values of the isotherms on this diagram. This is because the tie-lines that join points representative of phases in equilibrium on this diagram are not constrained to be horizontal: in fact, there will be only one horizontal tie-line at each temperature, corresponding to the point on Fig. 6.2

where the two branches of the isotherm intersect. The tie-lines will have a negative slope at pressures below that corresponding to the point of intersection, and a positive slope above it.

The co-ordinates of the various critical points were obtained by graphical interpolation of the experimental data represented in Figs. 6.1 to 6.3. The values obtained are given in Table 6.2.

TABLE 6.2

Critical points for the CF_4 + n-C_7H_{16} system

T^c/K	P^c/bar	ρ^c/mol.dm^{-3}	x^c
343.15	360	9.7	0.698
333.15	500	10.4	0.703
331.15	538	10.6	0.704
330.75	570	10.7	0.705
330.25(*)	670	11.0	0.708
330.75	772	11.3	0.712
331.15	810	11.4	0.713
333.15	960	11.6	0.718

(*) Critical "point of double contact"

The critical pressure is plotted against the critical mole fraction in Fig. 6.1 and against the critical molar density in Fig. 6.2, and the critical molar density is plotted against the critical mole fraction in Fig. 6.3. Finally, the critical pressure is plotted against the critical temperature in Fig. 6.4, together with the vapour-pressure curves of the two pure components. The point of minimum critical temperature on this diagram corresponds to the "point of double contact" in Figs. 6.1 and 6.2: below this temperature, no critical points are found, whereas above it, two critical pressures exist at each temperature. The co-ordinates of this critical "point of double contact", also given in Table 6.2, were obtained by graphical interpolation from Figs. 6.1 to 6.4.

(.../)

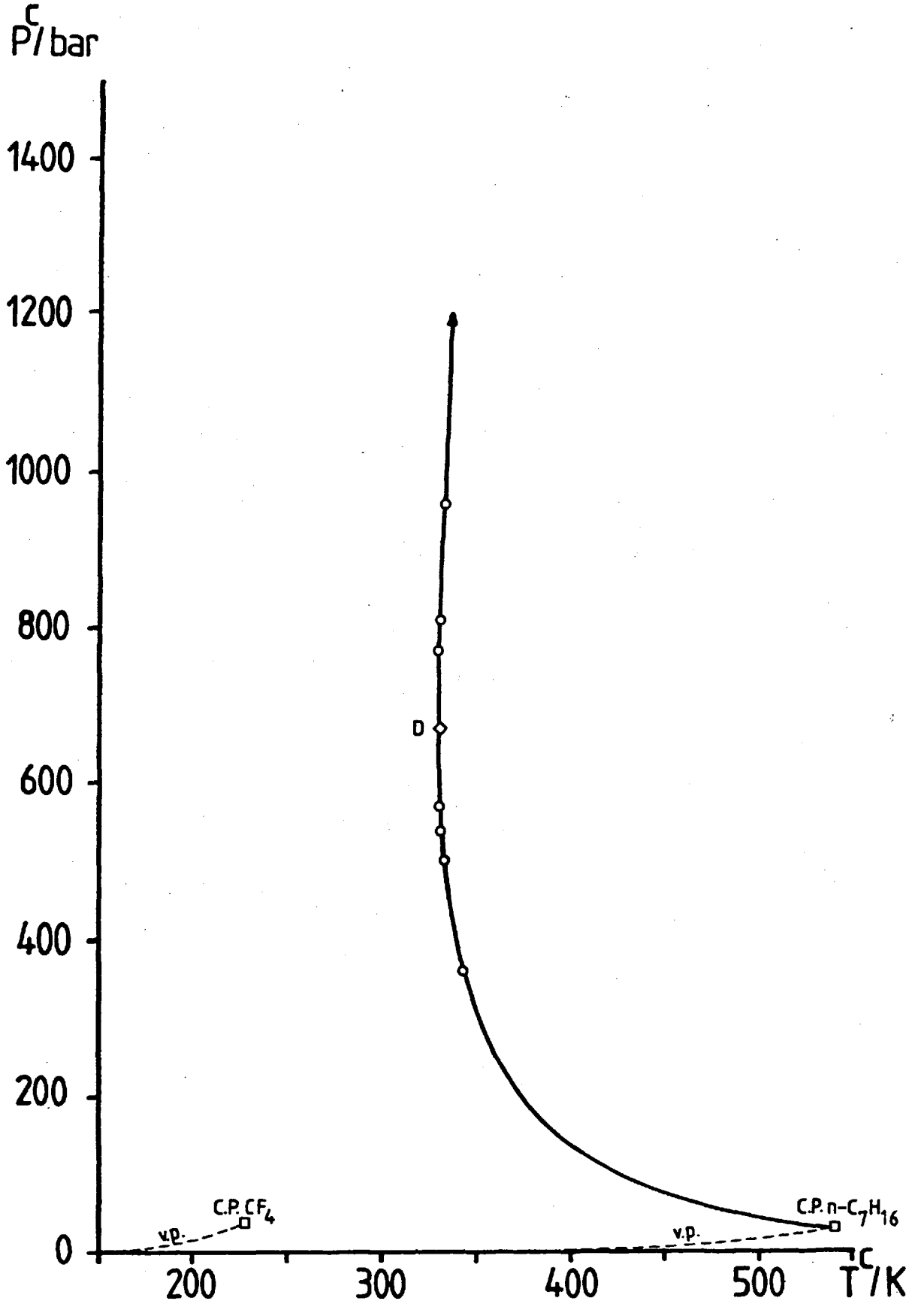


FIG. 6.4. (P^C-T^C) projection of the critical line for the CF_4 + n-C_7H_{16} system and vapour pressure curves of the pure components.

An interesting problem concerning the shape of the isotherms in this and similar systems is the fact that it has not been possible to establish experimentally what the value of the derivative $(\frac{\partial P}{\partial x})_{T,\sigma}$ is at the "point of double contact". Some investigators (83) have suggested that the two "touching" portions of the isotherm should have a common horizontal tangent at that point. Other investigators (84), however, maintain that the slope of the saturation curve is double-valued at the "point of double contact", i.e. that two branches of the isotherm intersect at that point. The evidence from this investigation does not point either way and extremely accurate measurements would be needed to arrive at a definite conclusion.

The experimental evidence suggests that the CF_4 + n-C_7H_{16} system does not have a continuous (P^c - T^c) curve joining the critical points of the two pure components. As seen from Fig. 6.4, the branch of the critical line starting at the critical point of n-heptane runs through a temperature minimum at the "point of double contact" and then proceeds steeply to higher pressures with a positive slope, which suggests that this system shows gas-gas immiscibility of the second kind (see section 2.4). This is not unexpected, in view of the great disparity between the molecules of the two pure components: the CF_4 molecule is almost spherical, in contrast to the long-chain molecular shape of n-C_7H_{16}. This fact, coupled with the large differences in polarisability and ionisation potential of the two molecules, will cause the energy of the CF_4 + n-C_7H_{16} interaction to be extremely weak compared to the energies of the corresponding like-molecule interactions.

The branch of the critical line starting from the critical point of n-heptane should extend to higher temperatures and very high pressures after going through the temperature minimum at the "point of double contact". Eventually, above the critical temperature of n-heptane, the low-pressure closed loops in the (P-x) diagram (see Fig. 6.1) should disappear altogether, and only the high-pressure open curves with a lower critical solution pressure should remain.

(.../)

It would be interesting to investigate this system at temperatures near and above the critical temperature of n-heptane. In order to do this, however, the temperature range of the equipment would have to be extended up to about 600 K and the pressure range up to possibly 5 000 or 6 000 bar. Of course, it is always possible that the critical line does not extend that far (not even past the critical temperature of n-heptane), and that it terminates at a UCEP on a three-phase line of the type S_2-G_1-G_2. The possible formation of such solid phases could be easily detected with the existing apparatus by noting the pressure at which circulation of the lighter phase stops, as detected by the flowmeter. It would not, however, be possible to withdraw samples of the solid phase for analysis, and the pressure and temperature range of the apparatus would probably have to be extended. A third possibility is a reversal in the slope of the critical line (P^C - T^C) at higher pressures, after running through a maximum in temperature. Such behaviour has never been found experimentally and, according to Rowlinson (4), it is probable that the (P-x) isotherms remain open at the top at all temperatures.

Chapter 7

CLASSICAL THERMODYNAMIC DESCRIPTION OF CRITICAL PHASES

In this and the following chapters, the classical thermodynamic description of the critical point will be presented, followed by a review of the methods currently available for the correlation and prediction of critical phenomena in binary fluid mixtures. Special emphasis is given to Teja and Rowlinson's procedure (85) based on the extension of the principle of corresponding states to mixtures, which is discussed in detail in Chapter 9, together with the corresponding algorithm for the prediction of critical points in binary mixtures.

The abbreviated notation for multiple differentiation, used by Rowlinson (4), van Konynenburg (12) and Teja (86) amongst others, will be employed henceforth in this work. In particular, for a binary mixture:

$$\left.\begin{aligned} A_{nxmv} &\equiv \left(\frac{\partial^{n+m}A}{\partial x^{n}\partial V^{m}}\right)_{T} \\ G_{lx} &\equiv \left(\frac{\partial^{l}G}{\partial x^{l}}\right)_{T,P}, \end{aligned}\right\} \qquad (7\text{-}1)$$

where $A[V,T,x]$ and $G[P,T,x]$ represent, respectively, the molar Helmholtz and Gibbs free energy functions of the mixture, and the quantities in brackets represent in each case the appropriate independent thermodynamic variables. This notation will also be applied to the composition derivatives of the scaling parameters h and f, defined in Chapter 9.

Changes in the thermodynamic state of a system may cause two co-existing phases to become identical, in the sense that all the intensive properties of the two co-existing phases become the same. The phase for which this occurs is called a critical phase, and the corresponding point on the appropriate thermodynamic surface of the phase diagram is called a critical point. Gibbs (87) proved that, in a system of c components, a critical phase which does not co-exist with other phases

must have c-1 thermodynamic degrees of freedom. Since, according to phase rule, a single phase system of c components has c+1 degrees of freedom, it follows that a critical point must necessarily be defined by two equations, the so-called criticality conditions. It also follows as a corollary of the same theorem that a critical phase in a system of c components can co-exist with, at most, c-1 other non-critical phases. When this situation occurs, the number of thermodynamic degrees of freedom is reduced to zero, which corresponds to a singular point on the phase diagram.

7.1 One-Component Systems

For a pure substance (c=1), the critical phase is represented by a singular point in phase space, since the number of degrees of freedom is zero. Consequently, the critical phase cannot co-exist with any other non-critical phase. The criticality conditions for such a system can be demonstrated by a plot of pressure vs. volume at constant temperature, or by the corresponding plot of the Helmholtz free energy vs. volume at constant temperature, as shown in Figs. 7.1(a) and (b), respectively.

If one assumes that the Helmholtz free energy is everywhere a continuous differentiable function of volume and temperature, as is the case with any analytic equation of state, then the shape of the various isotherms inside the saturation region is given by the curves $A_1B_1D_1E_1$, $A_2B_2D_2E_2$, etc., rather than by the straight lines A_1E_1, A_2E_2, etc., which join points representative of phases co-existing in equilibrium. On each of these continuous isothersm, the portion shown dotted represents states that are necessarily unstable and therefore unobtainable, since for these states $A_{2v} = -P_v < 0$ and the thermodynamic condition of mechanical stability is not satisfied. The locus of all the points for which $A_{2v} = -P_v = 0$, known as the spinodal curve, is shown as a dot-dashed line in Figs. 7.1(a) and (b). This curve defines the boundary of the unstable region of the diagram.

On each isotherm, the states lying between the saturation curve and the spinodal curve are shown dashed. These portions of the isotherms represent metastable states, i.e. states which are mechanically stable for small disturbances but unstable for large ones. These metastable states are observable experimentally as superheated liquid

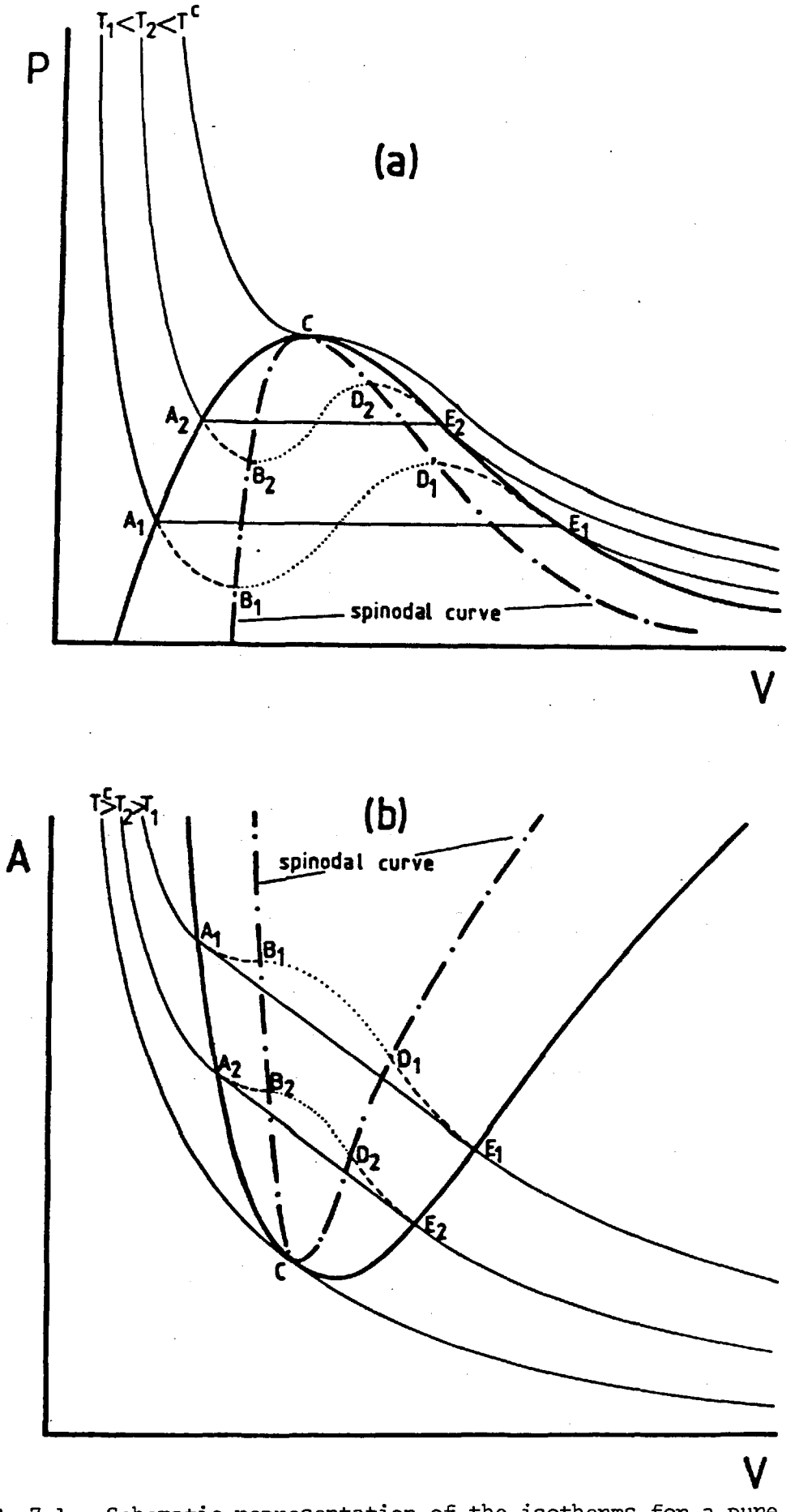


FIG. 7.1. Schematic representation of the isotherms for a pure substance, as calculated from an equation of state:

(a) (P-V) diagram

(b) (A-V) diagram

(A_1B_1, A_2B_2, etc.) and super-cooled vapour (D_1E_1, D_2E_2, etc.).

It is evident from Figs. 7.1(a) or (b) that the critical point C must lie at the boundary between the stable and unstable regions, since the saturation and spinodal curves touch at the critical point. This gives the first criticality condition for a pure substance:

$$A_{2v} = -P_v = 0. \qquad (7\text{-}2)$$

The second criticality condition can be derived by considering the variation of the critical phase at constant temperature. Since such a variation can under no circumstances go into the unstable region bounded by the spinodal curve, it can be shown (88) that this condition is given by:

$$A_{3v} = -P_{2v} = 0. \qquad (7\text{-}3)$$

In purely geometrical terms, the criticality conditions for a pure substance given in equations (7-2) and (7-3) simply express the well-known fact that, on a (P-V) diagram, the critical isotherm has a point of inflexion with a horizontal tangent at the critical point. This is equivalent to stating that the metastable and unstable portions of the isotherms will disappear simultaneously at a point C on the critical isotherm, which is the critical point.

7.2 Two-Component Systems

A critical phase in a binary system (c = 2) has one thermodynamic degree of freedom. The locus of all the critical phases of a binary system is therefore a line in the three-dimensional phase space, which may have several branches. Moreover, according to the corollary mentioned above, a critical phase in a binary system can only co-exist with another non-critical phase, in which case the variance of the system is zero. This corresponds to a singular point in the phase diagram called a critical end point.

(.../)

Critical points in binary systems, although physically similar to those of single-component systems, are governed by quite different thermodynamic considerations: whereas the critical point of a pure substance is a point of incipient mechanical instability ($A_{2v} = 0$), critical points of binary systems are points of incipient material or diffusional instability ($G_{2x} = 0$), but not of mechanical instability. This situation can be visualised by means of a plot of the Gibbs free energy of the binary system vs. mole fraction at constant temperature and pressure, as shown in Fig. 7.2. The arguments necessary to distinguish the stable phases and obtain the criticality conditions for a two-component system are similar to those used for the one-component case. Along the dashed (metastable) and dotted (unstable) portions of the curve, the system has lower free energy by splitting into two phases with compositions corresponding to A_1 and E_1, or A_2 and E_2, etc. The dot-dashed line shown in Fig. 7.2 is the locus of all points of inflexion ($G_{2x} = 0$) on the various isotherms and plays a role similar to that of the spinodal curve in one-component systems, in that it is the boundary of the unstable region of the diagram. The thermodynamic condition of stability that is violated inside this region is, however, one of material or diffusional stability ($G_{2x} < 0$), and not of mechanical stability ($A_{2v} < 0$), as was the case with a pure substance.

At the critical point of the mixture, denoted by C in Fig. 7.2, the metastable and unstable portions of the isotherms disappear at a point on the critical isotherm, as for a one-component system. By similar arguments, it can be concluded that the criticality conditions for a binary system are

$$G_{2x} = 0 \qquad (7\text{-}4)$$

and

$$G_{3x} = 0. \qquad (7\text{-}5)$$

(.../)

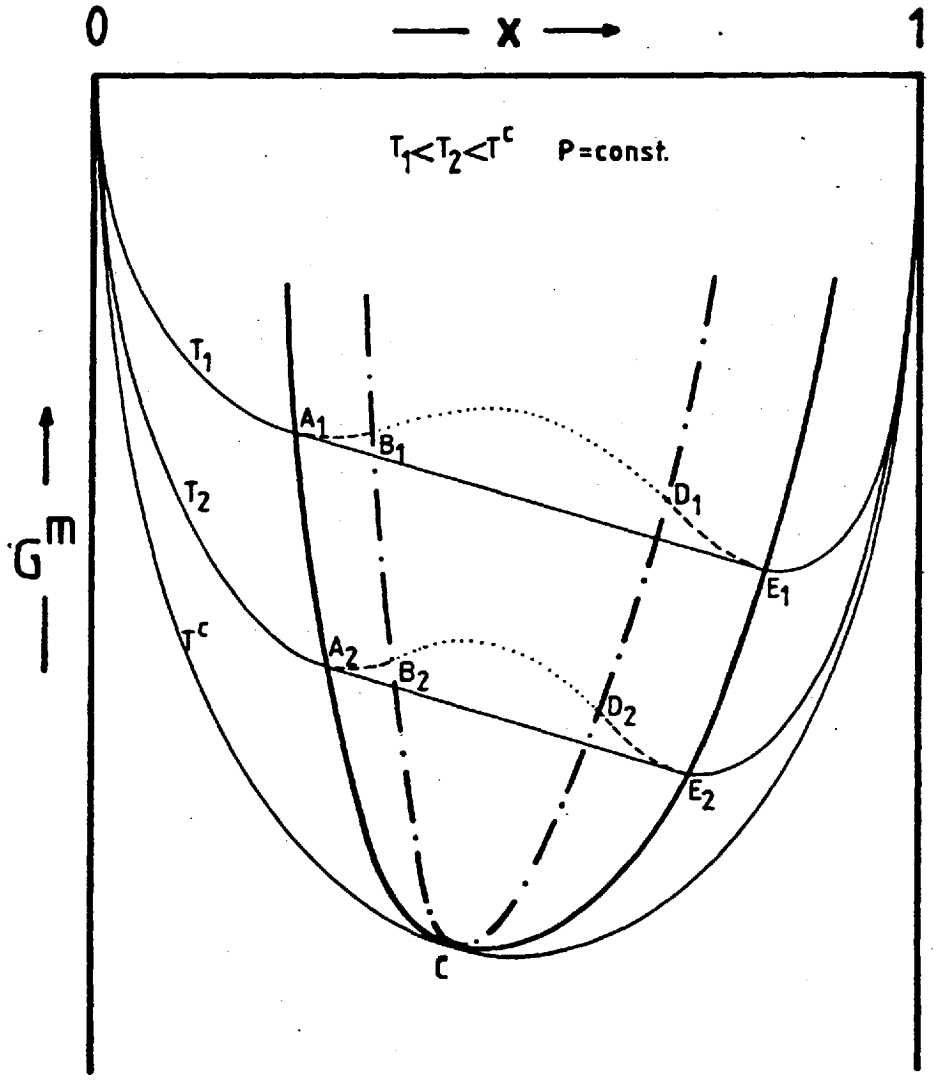


FIG. 7.2. Schematic representation of the Gibbs free energy of mixing of a binary system as a function of mole fraction, at constant temperature and pressure.

Since most equations of state capable of describing the co-existence of liquid and gas phases are more conveniently expressed in terms of V and T as independent variables, the alternative expression of the criticality conditions in terms of the Helmholtz free energy $A[V,T,x]$ is generally preferred to equations (7-4) and (7-5). These conditions can be obtained from (7-4) and (7-5) by application of the standard change of constraint partial differentiation theorem:

$$A_{2x} - \frac{A_{xv}^2}{A_{2v}} = 0 \qquad (7\text{-}6)$$

$$A_{3x} - 3\frac{A_{xv}}{A_{2v}} A_{2xv} + 3\left(\frac{A_{xv}}{A_{2v}}\right)^2 A_{x2v} - \left(\frac{A_{xv}}{A_{2v}}\right)^3 A_{3v} = 0. \qquad (7\text{-}7)$$

7.3 Multicomponent Systems

The criticality conditions for multicomponent systems are less obvious. As shown by Gibbs (87), the problem must be formulated in terms of the thermodynamic theory of stability. The two equations for the critical phase can then be deduced in various equivalent ways according to which characteristic thermodynamic function is used. For the general case of a system with c components, formulation of the problem in terms of the Helmholtz free energy of the system, $A[V,T,x_1,x_2, \ldots, x_{c-1}]$, is probably the most convenient.

Let the determinant D be defined by

$$D \equiv \begin{vmatrix} A_{2v} & A_{vx_1} & A_{vx_2} & \cdots & A_{vx_{c-1}} \\ A_{x_1v} & A_{2x_1} & A_{x_1x_2} & \cdots & A_{x_1x_{c-1}} \\ A_{x_2v} & A_{x_2x_1} & A_{2x_2} & \cdots & A_{x_2x_{c-1}} \\ \cdots & \cdots & \cdots & \cdots & \cdots \\ A_{x_{c-1}v} & A_{x_{c-1}x_1} & A_{x_{c-1}x_2} & \cdots & A_{2x_{c-1}} \end{vmatrix}, \qquad (7\text{-}8)$$

(.../)

and let D′ denote the determinant formed from D by replacing the elements of an arbitrarily chosen row by $D_v D_{x_1} D_{x_2} \ldots\ldots D_{x_{c-1}}$, where D_v represents the partial derivative of D with respect to v, D_{x_1} the partial derivative of D with respect to x_1, etc. Then it can be shown (88) that the criticality conditions of the c-component system can be simply expressed in terms of these two determinants as

$$D = 0 \tag{7-9}$$

and

$$D' = 0. \tag{7-10}$$

For a pure substance (c = 1), equations (7-2) and (7-3) are recovered, since $D = A_{2v}$ and $D' = D_v = A_{3v}$. For a binary system, the two following relations are obtained:

$$D = \begin{vmatrix} A_{2v} & A_{xv} \\ A_{xv} & A_{2x} \end{vmatrix} = 0 \tag{7-11}$$

and

$$D' = \begin{vmatrix} D_v & D_x \\ A_{xv} & A_{2x} \end{vmatrix} = 0, \tag{7-12}$$

where

$$D_v = \begin{vmatrix} A_{3v} & A_{xv} \\ A_{x2v} & A_{2x} \end{vmatrix} + \begin{vmatrix} A_{2v} & A_{x2v} \\ A_{xv} & A_{2xv} \end{vmatrix} \tag{7-13}$$

and

$$D_x = \begin{vmatrix} A_{x2v} & A_{xv} \\ A_{2xv} & A_{2x} \end{vmatrix} + \begin{vmatrix} A_{2v} & A_{2xv} \\ A_{xv} & A_{3x} \end{vmatrix}. \tag{7-14}$$

If equations (7-11) and (7-12) are written explicitly, it can be shown that the result is equivalent to equations (7-6) and (7-7). Since, however, the algorithm used in this thesis for the calculation of critical lines of binary mixtures employs the molar density ρ rather than the

equivalent molar volume $V(\equiv \frac{1}{\rho})$, it is more convenient to express the criticality conditions for a binary system in terms of $A[\rho,T,x]$ and its derivatives with respect to density and composition. When equations (7-11) and (7-12) are accordingly transformed, the following conditions are obtained:

$$A_{2x}(2A_{\rho} + \rho A_{2\rho}) - \rho(A_{x\rho})^2 = 0 \qquad (7\text{-}15)$$

and

$$\begin{aligned} &A_{3x}(2A_{\rho} + \rho A_{2\rho})^3 - 3\rho A_{x\rho}\, A_{2x\rho}(2A_{\rho} + \rho A_{2\rho})^2 \\ &+ 3\rho(A_{x\rho})^2(2A_{x\rho} + \rho A_{x2\rho})(2A_{\rho} + \rho A_{2\rho}) \\ &- \rho(A_{x\rho})^3(6A_{\rho} + 6\rho A_{2\rho} + \rho^2 A_{3\rho}) = 0. \end{aligned} \qquad (7\text{-}16)$$

7.4 Stability of Critical Phases

The thermodynamic description of critical phases given in the previous sections is a classical description, in the sense that it is based on the assumption that the Helmholtz free energy is everywhere analytic, i.e. that it is meaningful to represent A as a continuous differentiable function through stable and unstable states. It is now known that the classical description is wrong, both numerically and in principle, for the gas-liquid critical point of a pure substance, and it has been suggested that it is also wrong for the critical points of binary systems, although the experimental evidence for this is less compelling (4). The assumption that the Helmholtz free energy is everywhere analytic is, however, frequently made in practical applications of classical thermodynamics. In particular, this assumption of analyticity is inherent in the use of any analytic equation of state, since by definition these equations are continuous through metastable and unstable states.

Many of the methods currently available for the prediction of critical lines in binary mixtures use an analytic equation of state at some stage in the process of computation. Such methods will necessarily predict all gas-liquid and liquid-liquid critical points, whether

stable, metastable or unstable. Thus a procedure must be devised for the elimination of all spurious critical points, i.e. for determining which portions of the predicted critical line are thermodynamically stable.

Van Konynenburg (12) developed a graphical procedure for locating possible critical end points on a computed critical line which enables all the spurious critical points to be discarded. Consider a typical case of limited liquid miscibility near the critical point of the more volatile component, depicted in Fig. 7.3(a). The full lines represent the stable portions of the critical line, whereas the dotted lines represent the metastable and unstable portions, as predicted from an analytic equation of state. The vapour-pressure curve of the more volatile component is shown dashed and the three-phase line (L_1L_2G) is represented by dots and dashes. By definition, an upper critical end point (UCEP) occurs in fluid binary systems when the three-phase line (L_1L_2G) intersects the critical line as the temperature is increased; conversely, a lower critical end point (LCEP) occurs when the three-phase line intersects the critical line as the temperature is lowered. At the UCEP, a critical gas-liquid phase co-exists with a liquid phase, whereas at the LCEP a critical liquid-liquid phase co-exists with a gaseous phase. In either case, the critical end point can be located by observing that equations (7-15) and (7-16) are satisfied in one phase (the critical phase), whilst in the other phase (co-existing with the critical phase) the density and composition are different, but the pressure, temperature and chemical potentials of the two components have the same values as in the critical phase. From classical thermodynamics, the chemical potentials are given by

$$\mu_1 [\rho,T,x] = A + \frac{P}{\rho} - (1-x) A_x \qquad (7\text{-}17)$$

and

$$\mu_2 [\rho,T,x] = A + \frac{P}{\rho} + x A_x . \qquad (7\text{-}18)$$

In Fig. 7.3(b), typical isothermal-isobaric (G-x) plots are shown, corresponding to the temperatures and pressures of points A, B, E and D in Fig. 7.3(a); the corresponding isothermal-isobaric plots of μ_1/RT

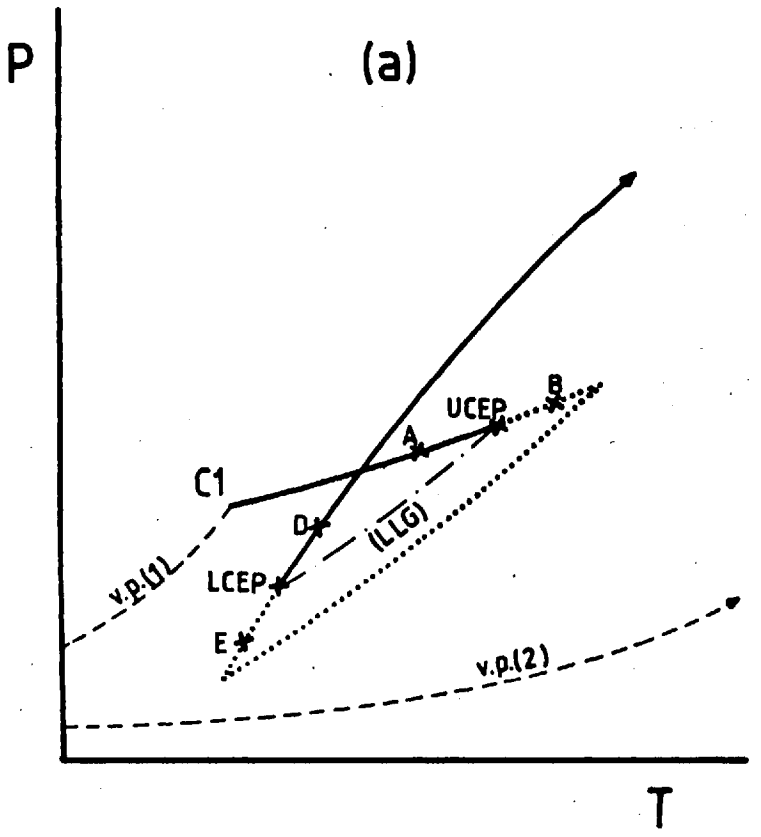
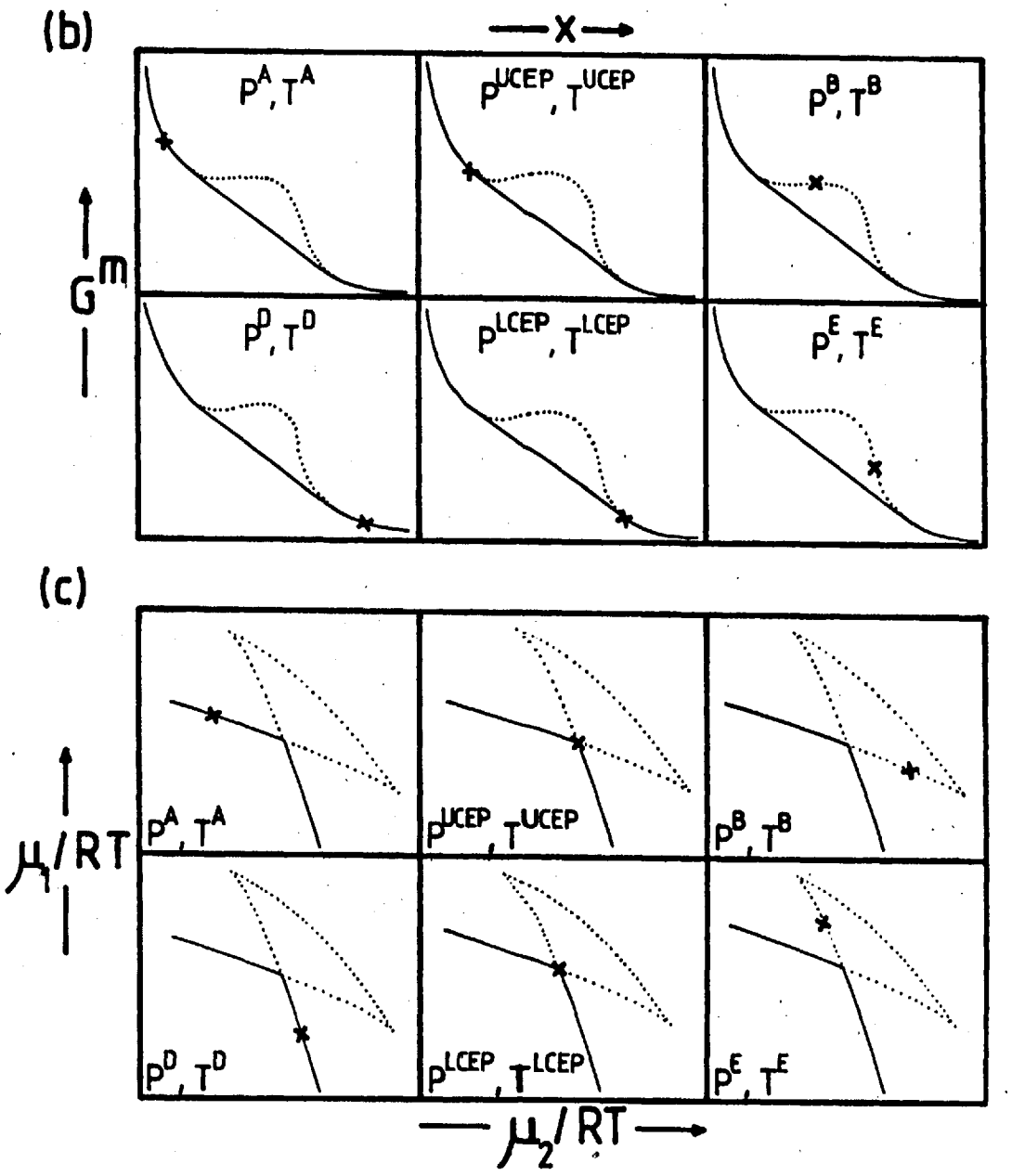


FIG. 7.3. Graphical procedure for location of critical end points on critical lines.



vs. μ_2/RT are depicted in Fig. 7.3(c). In each case, the metastable and unstable portions of the curve are shown dotted and the critical point at each temperature and pressure is marked with a cross. Points A and D, corresponding to stable critical points in Fig. 7.3(a), lie on the stable branches of the curves in Fig. 7.3(c). Conversely, points B and E, corresponding to metastable (or unstable) critical points in Fig. 7.3(a), lie on the metastable (unstable) portions of the curves in Fig. 7.3(c). The critical end points, which are located on the boundary between the stable and metastable portions of the critical line in Fig. 7.3(a), are at the intersection of the two stable branches of the curves in Fig. 7.3(c).

In the light of this discussion, the graphical procedure developed by van Konynenburg may be summarised as follows. From a knowledge of the Helmholtz free energy and its derivative with respect to composition, the chemical potentials μ_1 and μ_2 may be computed as functions of composition at each point (P^c,T^c) on the previously calculated critical line, by means of equations (7-17) and (7-18). If μ_1/RT is then plotted against μ_2/RT for each of these critical points, the critical end points can be identified by the procedure shown in Fig. 7.3(c), and it is then obvious which portions of the computed critical line are thermodynamically stable.

The problem of spurious critical points was recently discussed in detail by Hicks and Young (89). According to them, the test devised by van Konynenburg, although valid, provides more information about the general phase behaviour of the mixture than is required for a simple decision on the stability of the computed critical point. Their analysis of stability is based on the well-known result from classical thermodynamics which states that for a critical point of a binary mixture to be stable, the lowest even-order non-vanishing derivative of the Gibbs free energy of the mixture must be positive and all lower-order derivatives must be zero. It is usually assumed that the first non-vanishing derivative at the critical point is G_{4x}, whence the condition of thermodynamic stability of a critical point of a binary mixture is that

$$G_{4x} > 0. \qquad (7\text{-}19)$$

(.../)

This inequality, together with equations (7-4) and (7-5), completes the definition of a stable critical point in a binary mixture. Hence if $G_{4x} < 0$, the critical point is materially unstable and can be discarded; if $G_{4x} = 0$, the critical point lies on the unstable/metastable border-line; finally, if $G_{4x} > 0$, the critical point may be stable or metastable, since metastable points obey the condition of material stability (7-19), although they are "unstable" with respect to a separation into two phases of different compositions and lower free energy (see Fig. 7.2). The decision between stability and metastability is therefore the most difficult and in some cases requires considerable computation. According to Hicks and Young, when $G_{4x} > 0$ a detailed study of G_{2x} as a function of composition is needed, and in the more difficult cases numerical integration of the area under this curve has to be undertaken.

Chapter 8

REVIEW OF EXISTING METHODS FOR CORRELATION AND PREDICTION OF CRITICAL PHENOMENA IN FLUID MIXTURES

Methods for the correlation and prediction of critical phenomena in fluid mixtures can be roughly classified into three different groups:

(i) Empirical methods: these do not attempt to use the classical thermodynamic description of the critical phase given in the previous chapter.

(ii) Methods that use the classical criticality conditions but compute the free energy of the mixture directly from an equation of state. Some of these methods make use of sophisticated combining rules to obtain the parameters of the mixture.

(ii) Methods that differ from those in group (ii) in that the free energy of the mixture is computed from one of the various equilibrium theories of liquid mixtures (90). These methods generally require a very accurate equation of state for the calculation of the properties of a reference substance.

8.1 Empirical Methods

Several empirical correlations have been developed for the estimation of the critical properties of mixtures, although many of the earlier methods were aimed only at naturally occurring hydrocarbon systems. Amongst the better known is the method of Kurata and Katz (91) for volatile hydrocarbon mixtures, and that of Organick (92) for complex hydrocarbon systems. Davies et al. (93) modified the original Kurata-Katz procedure to make it applicable to lighter natural gas systems. All of these procedures make use of graphical correlations with parameters such as pseudo-critical temperature and pressure, molar average boiling point, weight average equivalent molecular weight, or weight average critical temperature.

Most of the more recent methods are listed in the two monographs by Reid et al. (94) and also in the review by Spencer et al. (95). In practically all of these methods, the correlations developed for T^c, V^c

and P^c of the mixture are totally independent of each other. For instance, in the method of Chueh and Prausnitz (96), which is one of the best-known empirical correlation methods, the critical temperature and the critical volume of the mixture are evaluated as surface-fraction averages of the critical temperatures and critical volumes of the pure components respectively, and then the Redlich-Kwong equation of state is used to compute the critical pressure of the mixture. If the method developed by the same authors (97) is then used to carry out vapour-liquid phase equilibrium calculations, there is no assurance that the predicted critical point will be consistent with the predicted phase envelope, because the two procedures are basically independent of each other.

In addition to difficulties caused by lack of thermodynamic consistency, empirical correlations can only predict critical lines which are continuous smooth curves joining the critical points of the pure components. This limitation obviously rules out their application to the large class of mixtures which do not show this type of behaviour (see Chapter 2). Furthermore, these correlation techniques suffer from the usual drawbacks of empirical methods in that substantial data for the mixture is required in order to fit the various parameters. In view of these limitations, these methods are more useful for the correlation or interpolation of existing data than for prediction or extrapolation purposes. Their use in correlation, however, should be confined to mixtures similar to those for which they were developed originally, as otherwise erroneous results may ensue.

8.2 Equation of State Approach

Although the rigorous classical thermodynamic theory of the critical states of mixtures was formulated by Gibbs (87) over a century ago, only a few attempts have been made since then to combine the criticality conditions with an equation of state so as to make quantitative predictions, most of which were limited to binary systems.

(.../)

One of the first attempts was that of Temkin (98) in 1959. He started from the van der Waals equation of state,

$$P = \frac{RT}{V-b} - \frac{a}{V^2} , \qquad (8\text{-}1)$$

and assumed the following mixing rules for the constants a and b, originally proposed by van der Waals (99):

$$\left.\begin{aligned} a &= a_{11}\, x^2 + 2a_{12}\, x(1-x) + a_{22}(1-x)^2 \\ \text{and} \qquad b &= b_{11}\, x^2 + 2b_{12}\, x(1-x) + b_{22}(1-x)^2 \quad , \end{aligned}\right\} \qquad (8\text{-}2)$$

where a_{11}, a_{22}, b_{11} and b_{22} are the coefficients for the pure components and a_{12} and b_{12} are constants characteristic of the unlike interaction in the mixture. By further assuming the following combining rules for a_{12} and b_{12}:

$$\left.\begin{aligned} b_{12} &= \tfrac{1}{2}(b_{11} + b_{22}) \\ \text{and} \qquad a_{12} &= (a_{11}\, a_{22})^{\frac{1}{2}} \quad , \end{aligned}\right\} \qquad (8\text{-}3)$$

Temkin was able to derive the following criteria for the occurrence of gas-gas equilibria of the first type in binary fluid mixtures:

$$\left.\begin{aligned} b_{11} &\geqslant 0.42\, b_{22} \\ a_{11} &< 0.053\, a_{22} \quad . \end{aligned}\right\} \qquad (8\text{-}4)$$

Since the van der Waals equation is known to be unsuitable for a quantitative description of the (P-V-T) relationships in the critical region, these criteria are not completely satisfactory, as was pointed out by Temkin. They have, however, proved successful in predicting gas-gas equilibria of the first type in some systems containing helium as one of the components.

(.../)

A few years later, Boberg and White (100) and Redlich and Kister (101) used the criticality conditions for the prediction of the complete critical locus of mixtures. Boberg and White employed the Gibbs free energy formulation of the criticality conditions to estimate liquid-liquid critical points in binary and ternary systems. The Redlich-Kister equation (102) was used to correlate the excess Gibbs free energy of mixing to composition. Redlich and Kister discussed the prediction of the gas-liquid critical locus for binary systems using equations equivalent to (7-4) and (7-5), but instead of G they used the fugacity coefficients of the components of the mixture. In using their equations to predict the effect of composition on T^c and P^c, they first obtained the limits of the derivatives $(dT/dx)^c$ and $(dP/dx)^c$ for $x = 0$ and $x = 1$. Then, using an interpolation method in conjunction with the Redlich-Kwong equation of state (103):

$$P = \frac{RT}{V-b} - \frac{a}{T^{\frac{1}{2}}V(V+b)}, \qquad (8\text{-}5)$$

they estimated the critical temperature and pressure of the mixture as a function of composition. In a subsequent paper, Ackerman and Redlich (104) used a very similar technique with the Benedict-Webb-Rubin equation of state (105),

$$P = \frac{RT}{V} + (B_oRT - A_o - \frac{C_o}{T^2})\frac{1}{V^2} + \frac{(bRT-a)}{V^3} + \frac{a\alpha}{V^6} + \frac{c(1+\gamma/V^2)}{V^3T^2}\exp(-\frac{\gamma}{V^2}), \qquad (8\text{-}6)$$

and, more recently, Arai and Saito (106) and Sarashina and Saito (107) have modified slightly the interpolative scheme of Redlich and Kister, and have also included a binary interaction parameter in the mixing rules for the constants of the BWR equation. Reasonably good predictions were achieved for the critical temperatures of the mixtures, but often poor results were obtained for the critical pressures, especially when the critical volumes of the pure components differed appreciably. A very similar method to the one originally proposed by Redlich and

Kister has recently been used by Prokhorov (108) to derive criteria for the occurrence of gas-gas equilibria of the first type in binary mixtures.

As faster, more reliable computers became available, Joffe and Zudkevitch (109), Hissong and Kay (110), Pak and Kay (111), Huron (112), Spear, Robinson and Chao (113), van Konynenburg (12) and Deiters and Schneider (114) applied the rigorous criticality conditions formulated by Gibbs to the prediction of critical points in binary mixtures. Spear et al. (115) also investigated the critical locus of ternary mixtures, and Peng et al. (116) calculated critical properties of multi-component hydrocarbon and related mixtures. The equations of state used to relate pressure to volume, temperature and composition at the critical point ranged from the simple van der Waals equation to the more complex BWR equation, but that most frequently used was the Redlich-Kwong equation or some variation of it. Either the Gibbs free energy criteria (equations (7-4) and (7-5)) or the equivalent Helmholtz free energy criteria (equations (7-6) and (7-7)) were employed for the criticality conditions. The accuracy of the predictions varied from one investigator to another, as did the computation techniques used for the solution of the criticality conditions. In most cases, the method was applied only to hydrocarbon binaries and, by employing one or two binary interaction parameters optimised from experimental data, it was possible in some cases to estimate critical temperatures to ± 2 K and critical pressures to ± 1 bar (117).

In only two of the investigations cited above was an attempt made to predict the wide variety of critical lines that binary fluid mixtures are known to exhibit. The first of these attempts was that of van Konynenburg (12), who was able to show that all the critical (P-T-x) diagrams obtained experimentally could be qualitatively represented by means of the van der Waals equation of state. More recently, Deiters and Schneider (114) used the original equation of state proposed by Redlich and Kwong which, like the van der Waals equation of state, has only two constants but fits the experimental (P-V-T) data in both liquid and vapour phases surprisingly well. Both van Konynenburg and

Deiters used the original mixing rules proposed by van der Waals (equations (8-2)); the cross coefficients a_{12} and b_{12} were evaluated from the pure component coefficients using two adjustable interaction parameters. The results obtained by Deiters and Schneider are surprisingly good: not only are they able to predict qualitatively the different kinds of phase behaviour in binary fluid mixtures, including critical azeotropy, liquid-liquid and gas-gas immiscibility, but they also claim that the accuracy of the computed critical and azeotropic lines is comparable to that obtained by corresponding states calculations. Furthermore, their method can also be applied to mixtures of strongly polar compounds, although it fails with mixtures of non-polar and strongly polar compounds.

Thus a fairly good quantitative description of critical phenomena in binary fluid mixtures can be obtained by using a simple two-constant equation of state in conjunction with the criticality criteria developed by Gibbs. The best equation of state for this purpose seems to be the Redlich-Kwong, or some variation of it. The use of more accurate, more complex equations of state does not seem to be justified, since the slight improvement in accuracy does not compensate for the loss of simplicity which is the most attractive feature of the method. Since an equation of state cannot provide any information about the properties of the constituent molecules in a mixture, attention must be directed towards prediction methods with a strong theoretical basis, i.e. methods based on the various equilibrium theories of liquids and liquid mixtures.

8.3 Theoretically-Based Methods

In recent years there has been a rapid development in the understanding of the statistical thermodynamics of mixtures, especially mixtures of simple liquids. A number of very successful theories has been formulated, but only in a few isolated cases have these theories been applied to the prediction of the critical behaviour of mixtures. In most cases, only qualitative predictions have been made and comparison with experimental results has not been attempted. One notable

exception is the group of methods known as corresponding-states theories, especially the so-called van der Waals models. These methods have found wide acceptance by chemical engineers because of their inherent simplicity and the accuracy of the predictions based on them.

For ease of classification, it is convenient to divide these theoretically-based prediction methods into four groups, according to the type of equilibrium theory on which the method is based:

(i) lattice models;

(ii) corresponding-states theories;

(iii) models based on a "generalised" van der Waals-like equation of state;

(iv) perturbation expansions.

Each of these groups of methods will now be reviewed briefly. It must be borne in mind, however, that this division is not complete, since there are connections between some of the methods in the different groups and, in the case of group (iii), connections with the methods described in the previous section.

8.3.1 Lattice models

Lattice theories of liquids are based on the assumption that each molecule spends most of its time confined by a shell of its nearest neighbours. These "cells" are formed into a three-dimensional lattice, hence the origin of the name. Lattice theories have been elaborated greatly beyond the crude model outlined above, and allowance can be made for vacant cells, for a non-spherical distribution of neighbours around each cell and for the correlation of the motion of molecules in neighbouring cells (4).

Schouten, Ten Seldam and Trappeniers (118) used a two-component lattice-gas model for the computation of critical and spinodal lines in binary systems. The two-component lattice-gas model combines the essential features of the lattice theory of Guggenheim for a two-component system (119) with the lattice gas model for a one-component

system. By using this model in conjunction with the criticality conditions for a binary system (equations (7-6) and (7-7)), they were able to predict qualitatively all kinds of critical phase behaviour that have been observed in binary mixtures, including liquid-liquid and gas-gas equilibria and critical azeotropy. In particular, for certain combinations of the energy parameters of the pure components, a transition from liquid-liquid into gas-gas equilibrium was observed, which supports the view put forward by Schneider (see Chapter 2) concerning the nature of this transition.

Bartis and Hall (83) introduced a two-component "decorated" lattice model which is a hybrid of the one-component lattice-gas model proposed by Mermin (120) and the two-component models of Widom, Clark, Neece and Wheeler (121). They used their model to study critical phenomena and phase equilibria in binary fluid mixtures, and observed that, for certain ranges of the interaction parameters, it predicts gas-gas equilibria of the first and second types. An important characteristic of their model is that it is not limited by the assumption of analyticity of the free energy in the neighbourhood of the critical point, and hence it yields non-classical critical behaviour and the correct values for the critical exponents. The model gives the correct shape of the isothermal (P-x) co-existence curves and it predicts that the two saturation curves which meet at the critical double contact point (see Chapter 6) should have a common tangent, rather than being two nearly straight lines which intersect at a finite angle.

The models are so complex that it has not been possible to apply them to real systems, and consequently it is impossible to assess their predictive capabilities in a quantitative sense. Furthermore, like all lattice theories they suffer from the drawback of being based on an unsatisfactory physical approach which over-emphasises the similarities of the solid and liquid states. Probably for this reason, there has been no great advance in this field in recent years, and the interest taken in lattice theories is now greatly reduced.

(.../)

8.3.2 Corresponding-states theories

Corresponding-states theories include all those models in which the thermodynamic properties of the mixture are obtained from those of a reference substance by application of the theorem of corresponding states. They are sometimes called "n-fluid theories' because the properties of the mixture are assumed to be those of a single imaginary "equivalent substance" (in a one-fluid theory), or an ideal mixture of two or more "equivalent components". The properties of the equivalent substance, or equivalent components, are obtained from the known properties of a reference substance by assuming that the functional form of the intermolecular potential is the same for all these substances (conformal substances). Each of these n-fluid models can be further sub-divided, according to how the intermolecular potential parameters of the equivalent substance, or equivalent components, are obtained from the parameters of the real components of the mixture.

The best-known corresponding-states theories are the random mixture approximation (one-fluid theory), the average-potential model (two-fluid theory), the so-called van der Waals one- and two-fluid models,and the three-fluid model. All these models have been discussed in great detail elsewhere (4, 90). The van der Waals one- and two-fluid models have a stronger theoretical basis than the random mixture and average-potential models, and this is confirmed by the quality of predictions of excess thermodynamic properties and critical lines of fluid mixtures based on the van der Waals models and also by the results of "computer experiments" (90). According to Gunning and Rowlinson (122), the van der Waals two-fluid model is generally no more accurate than the corresponding one-fluid model, except possibly at low temperatures and high densities. Hick (123) recently reported departures from physical reality when predicting phase equilibria and gas-liquid critical properties of binary mixtures using two- and three-fluid models.

A number of authors have used the van der Waals one-fluid model, but have eliminated the reference substance from their calculations and simply assumed that the equivalent substance follows a closed equation of state. This slightly different approach is discussed in more

detail in the next section. The same one-fluid model was used by Teja and Rowlinson (85) to compute critical and azeotropic states of binary and ternary mixtures, using methane as the reference substance. They extended the scope of the method to substances that do not conform to the simple principle of corresponding states (non-spherical molecules) by using the molecular shape factor equations developed by Leach and Leland (124). The method was applied to mixtures containing hydrocarbons and simple non-polar substances,and the agreement between prediction and experiment was very satisfactory.

Since this method seems to offer the best hope of predicting reasonably accurate results for a wide range of substances, it was used in this work. A detailed discussion of the principle of corresponding states and its extension to mixtures of non-conformal substances is therefore deferred until the next chapter. It should be pointed out, however, that the method is, in principle, restricted to non-polar substances which do not depart substantially from the simple principle of corresponding states, which rules out such technologically important substances as alcohols, lower amines, ammonia and water.

8.3.3 Methods based on specific equations of state

The methods outlined in this section differ from those of the previous section in that no explicit assumption is made about the form of the intermolecular potentials. Although a one-fluid van der Waals model is again assumed, hence the connection with the previous section, corresponding states arguments are not used to compute the properties of the equivalent substance. Instead, it is assumed that the equivalent substance obeys a specific equation of state which in most cases is a simple two-constant equation. If the two constants obey the relations

$$\left.\begin{aligned} a_{ij} &\propto \varepsilon_{ij}\,\sigma_{ij}^{3} \propto T_{ij}^{c}\,V_{ij}^{c} \\ \text{and} \qquad b_{ij} &\propto \sigma_{ij}^{3} \propto V_{ij}^{c} \end{aligned}\right\}, \tag{8-7}$$

then it can be shown that the mixing rules originally proposed by van der Waals for his equation of state (equations (8-2)) are equivalent to the prescriptions for obtaining the intermolecular parameters of the equivalent substance in the van der Waals one-fluid model. These intermolecular parameters, denoted by the superscript e.s., are given by

$$\left.\begin{aligned} \varepsilon^{e.s.} &= \frac{\sum_{ij} x_i x_j \varepsilon_{ij} \sigma_{ij}^3}{\sum_{ij} x_i x_j \sigma_{ij}^3} \\ \text{and} \qquad \sigma^{e.s.} &= \left(\sum_{ij} x_i x_j \sigma_{ij}^3\right)^{1/3} . \end{aligned}\right\} \qquad (8\text{-}8)$$

Clearly this is the case with the original van der Waals equation of state (hence the name given to this one-fluid model), and also with the Dieterici and the Guggenheim equations of state. Thus in some respects this approach is similar to that used by van Konynenburg and Scott, which was discussed in section 8.2. With other equations of state, however, e.g. the Redlich-Kwong equation, equations (8-7) are not valid and therefore the use of the mixing rules given in equations (8-2) for the constants of the equation of state is not equivalent to the van der Waals one-fluid prescriptions given in equations (8-8).

This approach was used by Hicks, Young and co-workers (125). They computed the critical properties of binary mixtures by assuming a van der Waals one-fluid model and using various equations of state for the equivalent substance. The best results were obtained with the Guggenheim equation of state, and gas-gas equilibria of the correct kind were successfully predicted for most of the systems that had been studied experimentally. In contrast, the use of the van der Waals equation of state results in the correct kind of gas-gas equilibrium being predicted in very few cases.

McGlashan and co-workers (126) used a similar approach in their attempt to predict gas-gas equilibrium in fluid mixtures. The equations of state investigated were those of Guggenheim and of Carnahan and Starling, together with the original van der Waals equation. Again, the van der Waals equation was clearly the poorest, while the other

two equations demonstrated the two kinds of gas-gas equilibria in qualitative agreement with experiment. Failure to obtain quantitative agreement may have arisen because only one adjustable parameter was used in the calculations, the arithmetic mean rule of Berthelot being assumed to be valid in all cases.

Finally, Scott (127) employed the same van der Waals one-fluid model, but he assumed that the thermodynamic properties of the equivalent substance could be represented by what he called a "generalised van der Waals-like" equation of state:

$$\frac{PV}{RT} = f(y) - \frac{4ay}{RTb} , \qquad (8\text{-}9)$$

where $y \equiv b/4V$ and the function $f(y)$ represents the hard-sphere contribution to the compression factor. Scott lists eight different forms of the function $f(y)$, including the original one proposed by van der Waals. In an attempt to predict the conditions for gas-gas equilibrium in binary mixtures, an analysis of the limiting slopes of the critical lines $(\frac{dT}{dx})^c_{x=0}$ and $(\frac{dP}{dx})^c_{x=0}$ was carried out, using the method of Redlich and Kister mentioned in section 8.2. Comparisons of theory with experiment were made for the eight "van der Waals-like" equations of state mentioned above, plus the Redlich-Kwong equation of state and an equation developed by Snider and Herrington (128). The method failed to predict the correct kind of gas-gas equilibrium for several systems and again the reason for this failure was probably the fact that the Lorentz-Berthelot combining rules were used throughout for the computation of the unlike interaction parameters.

8.3.4 Perturbation theories

One of the most significant advances in the statistical thermodynamics of liquids in the last few years has been the rapid development of perturbation theories of various types. A perturbation method is a mathematical means of obtaining an approximate solution to a given problem by the use of a suitable expansion about the known solution to another, usually simpler, problem (the reference or unperturbed

system). In most cases, the Helmholtz free energy of the real system is expanded as a Taylor series about the value of the chosen reference system. Various methods of carrying out this expansion have been proposed (129), but the results obtained are very similar. Various choices are possible for the reference system, although most of the work on perturbation theory of mixtures has used a pure or mixed hard-sphere system as the reference fluid, leading to the so-called hard-sphere perturbation expansions. In the case of a conformal mixture, i.e. a mixture in which all the intermolecular potentials are given by

$$u_{ij}[r] = \varepsilon_{ij} F\left[\frac{\sigma_{ij}}{r}\right], \qquad (8\text{-}10)$$

it is natural to attempt a perburbation expansion in which one of the components, or another conformal fluid, is taken as the reference or unperturbed system, leading to the so-called conformal solution theories.

A hard-sphere reference system provides equations that are highly flexible, in the sense that they can be applied to a wide variety of liquid mixtures, since the theory is not limited to any particular type of intermolecular force law. Rigby et al. (130) used a pure hard-sphere gas as the unperturbed reference system and applied a perturbation expansion to the prediction of critical loci in fluid mixtures, in what they called an "augmented van der Waals theory" for mixtures. They treated special systems, like mixtures of square-well molecules, and mixtures of hard-sphere and square-well molecules of the same size. Although they were able to predict all the qualitative features observed in real systems, including gas-gas immiscibility, they did not make any quantitative predictions of experimental results for real systems.

Trappeniers and Schouten (131) applied a first-order perturbation expansion to the computation of the critical line for the Ar + Kr system. They used as reference a mixture of hard-spheres of the same composition as the perturbed system, together with the equation of state for a mixture of hard-spheres proposed by Carnahan and Starling (132). In addition, they also computed the critical line for the same

system using the van der Waals and the Carnahan and Starling equations of state, and a second-order perturbation expansion assuming a square-well intermolecular potential. All the calculations were made assuming that the Lorentz rule for the unlike energy parameter was valid. Comparison with experimental results showed that agreement was satisfactory only for the second-order perturbation expansion, but none of the theories could predict the experimental critical volumes accurately. In a subsequent paper (133), they used again the first-order hard-sphere perturbation expansion to predict the critical curve for the system NH_3 + Ne. In this work, however, they introduced an adjustable correction factor in the Lorentz rule, so as to improve the flexibility of the prediction method, and the gas-gas equilibrium predicted for this system was in reasonable quantitative agreement with the experimental results.

More recently, Neff and McQuarrie (134) have combined the pure-fluid perturbation theory of Weeks, Chandler and Andersen (135) with the van der Waals n-fluid theories in an attempt to predict fluid-fluid equilibria in binary systems over wide ranges of pressure. Again, the van der Waals one-fluid theory was found to be the most reliable of the n-fluid theories and also the most convenient to use in terms of computer time. Using this theory, the authors were able to predict the occurrence of gas-gas equilibria in binary mixtures for specific ranges of the ratios

$$\frac{\sigma_{22}}{\sigma_{11}}, \quad \frac{\varepsilon_{22}}{\varepsilon_{11}} \quad \text{and} \quad \frac{\varepsilon_{12}}{(\varepsilon_{11}\,\varepsilon_{22})^{\frac{1}{2}}}.$$

Conformal solution theories involve perturbation about a pure fluid reference system. This approach has connections not only with other perturbation methods but also with the corresponding-states theories discussed in section 8.3.2. In fact, it can be shown (129) that first-order conformal solution theory leads naturally to a family of one-fluid corresponding-states theories, including the random mixture and the van der Waals one-fluid approximations. Kreglewski and Kay (136) predicted the critical temperatures and pressures of a wide variety of binary systems using conformal solution theory, but instead of the rigorous solution of the criticality conditions they used an approximate solution proposed by Rowlinson (4). In a subsequent paper (64),

they applied the same method to the prediction of critical lines in mixtures of perfluoro compounds with alkanes. In both cases, the agreement with experimental results was very satisfactory, but only continuous critical lines were predicted.

Tan et al. (137) have recently applied second-order conformal solution theory to the problem of predicting gas-gas equilibria. They were able to predict the occurrence of the phenomenon in the He + Xe system in reasonable agreement with the experimental data provided a suitable reference fluid was chosen. They derived the following criteria for the "a priori" prediction of the various types of gas-gas equilibria in binary mixtures of non-polar molecules:

$$\left.\begin{array}{lll} \dfrac{\sigma_2}{\sigma_1} > 1.50 \text{ and } 30.0 < \dfrac{\varepsilon_2}{\varepsilon_1} & : & \text{gas-gas equilibrium of the 1st type} \\ 1.50 > \dfrac{\sigma_2}{\sigma_1} > 1.41 \text{ and } 30.0 > \dfrac{\varepsilon_2}{\varepsilon_1} > 20.0 & : & \text{transition type} \\ \dfrac{\sigma_2}{\sigma_1} < 1.41 \text{ and } 20.0 > \dfrac{\varepsilon_2}{\varepsilon_1} & : & \text{gas-gas equilibrium of the 2nd type} \end{array}\right\} \quad (8\text{-}11)$$

where $\sigma_1 < \sigma_2 \equiv \sigma_o$ and $\varepsilon_1 < \varepsilon_2 \equiv \varepsilon_o$, i.e. the component of the mixture with the larger molecule is taken to be the reference fluid. These criteria are similar to those derived by Temkin from the equation of state of van der Waals, described in section 8.2.

The perturbation methods outlined above assume that the potential is independent of molecular orientation, i.e. that the molecules are effectively spherical. Furthermore, conformal solution theories can be applied only to groups of substances that conform to the same functional form of the intermolecular potential. Although molecular non-sphericity is known to have a significant effect on the thermodynamic properties of fluids, perturbation methods which account for non-central forces have received relatively little attention. One such perturbation expansion, recently presented by Gubbins and Twu (138), allows for strong directional intermolecular forces to be taken into account when calculating the thermodynamic properties of fluid mixtures.

(.../)

The theory was applied to the prediction of phase equilibrium surfaces, critical loci, three-phase lines and azeotropic lines for mixtures containing constituents with polar, quadrupolar and octopolar intermolecular forces. The relation between the type of intermolecular forces and the type of phase behaviour was explored for binary mixtures, and most of the known types of critical phase behaviour were predicted. The theory was also used to predict the properties of real binary and ternary mixtures composed of polar (HCl, HBr), quadrupolar (CO_2, C_2H_2, C_2H_4, C_2H_6) and octopolar (CH_4, CF_4) molecules. For the systems CO_2 + C_2H_4 and CO_2 + C_2H_6 in particular, excellent agreement was obtained between theory and experiment for the vapour-liquid equilibria and azeotropic lines at all temperatures, although some discrepancies occurred in the predicted critical line. It appears, therefore, that the method of Gubbins and Twu is a promising prediction method, in that it is not restricted to mixtures of non-polar substances. It remains to be seen, however, how it compares with other successful prediction methods, such as the extension of the principle of corresponding states to mixtures of non-spherical molecules, in terms of practicability and computing time, when both methods are applied to mixtures containing only non-polar constituents.

Chapter 9

THE COMPUTATION OF THE CRITICAL LOCUS OF BINARY MIXTURES USING THE PRINCIPLE OF CORRESPONDING STATES AND ITS EXTENSIONS

From the review given in the previous chapter, it was concluded that Teja and Rowlinson's method (85) was probably the best method for the prediction of critical lines in binary fluid mixtures of non-polar substances. For this reason, it was used to correlate the experimental critical data for various CF_4 + n-alkane systems, including the data for the CF_4 + n-C_7H_{16} system obtained in this investigation, since this was expected to provide a critical test of the prediction capabilities of the method. The results obtained with Teja and Rowlinson's method were, however, unsatisfactory: the algorithm would frequently diverge, and it was not possible to predict the minimum in the critical temperature observed experimentally for the systems CF_4 + n-C_5H_{12}, CF_4 + n-C_6H_{14} and CF_4 + n-C_7H_{16}. This led to a critical analysis of Teja's algorithm, which is described in section 9.2, and as a consequence of this analysis, most of the program had to be rewritten, in order to produce a more compact and efficient algorithm. In view of this fact, it was found necessary to review the theoretical background of the method, hence a detailed discussion of the principle of corresponding states and its extension to mixtures is given in section 9.1.

9.1 Theoretical Background

The canonical ensemble partition function of a system containing fixed amounts of substances at a given volume and temperature may be factorised into a molecular part, which depends only on the properties of the individual molecules, and a configurational part, which is related to the interaction between the molecules, i.e. to the configuration of the system:

$$Z = Q^{mol.} \tilde{Q}. \qquad (9\text{-}1)$$

(.../)

Total thermodynamic properties are directly related to the partition function Z via statistical thermodynamics and, according to (9-1), each total property may be considered as being made up of two parts: a molecular part, associated with $Q^{mol.}$, and a configurational part, associated with the configurational integral $\tilde{Q}$. Hence, for the Helmholtz free energy:

$$\left.\begin{aligned} A &= -k\,T\,\ln Z \\ A^{mol.} &= -k\,T\,\ln Q^{mol.} \\ \tilde{A} &= -k\,T\,\ln \tilde{Q} \\ \text{and} \qquad A &= A^{mol.} + \tilde{A} \end{aligned}\right\} \quad . \tag{9-2}$$

For the pressure:

$$\left.\begin{aligned} P &= kT\left(\frac{\partial \ln Z}{\partial V}\right)_{T,N} \\ P^{mol.} &= kT\left(\frac{\partial \ln Q^{mol.}}{\partial V}\right)_{T,N} = 0 \quad , \\ \tilde{P} &= kT\left(\frac{\partial \ln \tilde{Q}}{\partial V}\right)_{T,N} \\ P &= P^{mol.} + \tilde{P} = \tilde{P} \end{aligned}\right\} \tag{9-3}$$

since the molecular part of the partition function is independent of the volume of the system.

Two different types of residual functions can be defined, according to which independent variables are used. Throughout this work, the independent variables are density, temperature and composition; hence the residual part of any thermodynamic property is defined as the difference between the total property and the same property in the perfect gas state at the same density, temperature and composition:

$$Y^{res.}[\rho,T,x_\alpha] \equiv Y[\rho,T,x_\alpha] - Y^{p.g.}[\rho,T,x_\alpha] \; . \tag{9-4}$$

(.../)

Alternatively, since the molecular part of any thermodynamic property can be entirely ascribed to the equivalent perfect gas, the residual property can be defined in terms of configurational properties, rather than total properties:

$$Y^{res.}[\rho,T,x_\alpha] \equiv \hat{Y}[\rho,T,x_\alpha] - \hat{Y}^{p.g.}[\rho,T,x_\alpha]. \tag{9-5}$$

9.1.1 The principle of corresponding states for simple spherical molecules

In its simplest form, the principle of corresponding states is a direct consequence of the fact that the intermolecular potential for substances made up of simple spherical molecules are similar. Assuming that the intermolecular potentials of substance i and substance o (the reference substance) may be written as

$$\left.\begin{aligned} u_{ii}[r] &= \varepsilon_{ii}\, F[\sigma_{ii}/r] \\ \text{and} \qquad u_{oo}[r] &= \varepsilon_{oo}\, F[\sigma_{oo}/r] \end{aligned}\right\}, \tag{9-6}$$

where ε and σ are characteristic energies and distances, respectively, and F denotes some function common to both species, then, by using appropriate scaling factors, it is obvious that the two potentials can be represented by the same curve. In fact, from (9-6):

$$\begin{aligned} u_{ii}[r] &= \varepsilon_{oo}\cdot\frac{\varepsilon_{ii}}{\varepsilon_{oo}}\cdot F\left[\frac{\sigma_{ii}}{\sigma_{oo}}\cdot\frac{\sigma_{oo}}{r}\right] = \\ &= \frac{\varepsilon_{ii}}{\varepsilon_{oo}}\cdot\varepsilon_{oo}\cdot F\left[\frac{\sigma_{oo}}{r\,\sigma_{oo}/\sigma_{ii}}\right] = \\ &= \frac{\varepsilon_{ii}}{\varepsilon_{oo}}\cdot u_{oo}\left[r\,\frac{\sigma_{oo}}{\sigma_{ii}}\right]. \end{aligned} \tag{9-7}$$

Hence, by defining the appropriate energy and distance scaling factors:

$$\left.\begin{aligned} f_{ii} &\equiv \frac{\varepsilon_{ii}}{\varepsilon_{oo}} \\ \text{and} \qquad (h_{ii})^{1/3} &\equiv \frac{\sigma_{ii}}{\sigma_{oo}} \end{aligned}\right\}, \tag{9-8}$$

equation (9-7) becomes:

$$u_{ii}[r] = f_{ii} \cdot u_{oo}\left[\frac{r}{h_{ii}^{1/3}}\right]. \tag{9-9}$$

As was mentioned in Chapter 8, substances whose potentials are related to each other and to that of a reference substance by equation (9-9) are said to be conformal substances.

By making the further assumption that the configurational or potential energy of the system is divisible as follows:

$$U_i\left[(\underline{r}_i)_1, (\underline{r}_i)_2, \ldots, (\underline{r}_i)_N\right] = \sum_{k}^{N-1} \; \sum_{l}^{N} u_{ii}[r_{kl}], \tag{9-10}$$

it is possible to extend to this potential energy the arguments that led to (9-9) and to write

$$U_i\left[(\underline{r}_i)_1, \ldots, (\underline{r}_i)_N\right] = f_{ii} \cdot U_o\left[\frac{(\underline{r}_i)_1}{h_{ii}^{1/3}}, \ldots, \frac{(\underline{r}_i)_N}{h_{ii}^{1/3}}\right] \tag{9-11}$$

Since the configurational integral $\tilde{Q}$ is related to the configurational energy $U[\underline{r}_1, \ldots, \underline{r}_N]$ via

$$\tilde{Q} \equiv \frac{1}{N!} \int_V \cdots \int \exp\left\{-\frac{U[\ldots]}{kT}\right\} \underline{dr}_1 \cdots \underline{dr}_N, \tag{9-12}$$

then from (9-11) and (9-12) it follows that

$$\tilde{Q}_i[V,T,N] = h_{ii}^N \, \tilde{Q}_o\left[\frac{V}{h_{ii}}, \frac{T}{f_{ii}}, N\right]. \tag{9-13}$$

From (9-2) and (9-13) the configurational Helmholtz free energy of substance i will be given by

$$\tilde{A}_i[V,T,N] = f_{ii} \, \tilde{A}_o\left[\frac{V}{h_{ii}}, \frac{T}{f_{ii}}, N\right] - NkT \ln h_{ii}, \tag{9-14}$$

and from this equation all the configurational properties of substance i may be computed from a knowledge of the corresponding configurational properties of the reference substance o. In particular, the configurational pressure is given by

$$\tilde{P}_i[V,T,N] = \frac{f_{ii}}{h_{ii}} \tilde{P}_o\left[\frac{V}{h_{ii}}, \frac{T}{f_{ii}}, N\right] \qquad (9\text{-}15)$$

and, from equation (9-3):

$$P_i[V,T,N] = \frac{f_{ii}}{h_{ii}} P_o\left[\frac{V}{h_{ii}}, \frac{T}{f_{ii}}, N\right]. \qquad (9\text{-}16)$$

This means that the thermodynamic states of conformal substances i and o will be represented by geometrically similar surfaces for which the axes of pressure, volume and temperature are multiplied by f_{ii}/h_{ii}, h_{ii} and f_{ii} respectively. It also follows that all singular points on these surfaces, such as the critical point, will have values of pressure, volume and temperature in the ratio of these scaling factors:

$$\left.\begin{aligned} V_i^c &= h_{ii} V_o^c \\ T_i^c &= f_{ii} T_o^c \\ P_i^c &= \frac{f_{ii}}{h_{ii}} P_o^c \end{aligned}\right\} . \qquad (9\text{-}17)$$

9.1.2 Extension of the principle of corresponding states to non-conformal substances

One of the greatest limitations of the principle of corresponding states in the simple form stated above is that it is valid only over restricted sets of substances whose molecules are non-polar and spherically symmetrical, like the heavy inert gases and, to a lesser extent, isomers like i-C_4H_{10} and n-C_4H_{10}. Even for non-polar substances, there are departures from this simple form of the principle, which arise mainly from lack of spherical symmetry. This is reflected in the intermolecular pair potential of such molecules, because $u_{ii}[r]$, or

the parameters ε_{ii} and σ_{ii}, will now be a function of the orientation of the molecules, and this in turn will be a function of the temperature. These departures are not, however, random and can be well characterised by one additional parameter. Several different parameters have been suggested to account for non-spherical molecular symmetry, those that have produced the best practical results being:

i) Critical compression factor: $$z^c \equiv \frac{P^c V^c}{R\,T^c} \qquad (9\text{-}18)$$

ii) Riedel's factor: $$\alpha^c \equiv \frac{d\,\ln(P^\sigma/P^c)}{d\,\ln(T/T^c)} \text{ at } T = T^c \qquad (9\text{-}19)$$

iii) Pitzer's acentric factor: $$\omega \equiv -1.000 - \log_{10}\left(\frac{P^\sigma}{P^c}\right) \text{ at } \frac{T}{T^c} = 0.7. \qquad (9\text{-}20)$$

Pitzer's acentric factor ω, which is believed to be a measure of the deviation of the intermolecular potential from that of a simple fluid (139), is simply a comparison of reduced vapour pressures at a common reduced temperature. For simple spherical molecules (Ar, Kr, Xe), the value of (P^σ/P^c) at $\frac{T}{T^c}$ =0.7 is almost exactly 0.1, hence from equation (9-20) ω = 0 for these substances. For most other substances, (P^σ/P^c) is somewhat less than 0.1 at $\frac{T}{T^c}$ = 0.7, hence ω will be positive for these substances, the values usually ranging from 0 to 0.4. When ω is small, departures from the simple principle of corresponding states are approximately linear in ω and it is possible to write

$$z\left[\frac{V}{V^c}, \frac{T}{T^c}, \omega\right] = z^{(0)}\left[\frac{V}{V^c}, \frac{T}{T^c}\right] + \omega\, z^{(1)}\left[\frac{V}{V^c}, \frac{T}{T^c}\right], \qquad (9\text{-}21)$$

where $z\left[\frac{V}{V^c}, \frac{T}{T^c}, \omega\right]$ is the compression factor of the substance in question, $z^{(0)}$ is the compression factor for a simple substance (ω = 0) at the same reduced conditions of volume and temperature, and $z^{(1)}$ is an auxiliary function which must be obtained from experimental data. Once the compression factor is known, then the departures of all other configurational properties from the principle of corresponding states can be

found by the usual methods of classical thermodynamics.

An alternative but equivalent approach to the problem of departures from the simple principle of corresponding states was devised by Leland and his colleagues (124). For a pair of substances, i and o, which do not conform mutually to the principle of corresponding states, the scaling parameters h_{ii} and f_{ii} may be defined by a pair of equations such as (9-14) and (9-16). It has been shown (140) that these two equations can be satisfied simultaneously and consistently only by one pair of values (h_{ii}, f_{ii}) at each value of (V,T) for substance i. The scaling parameters h_{ii} and f_{ii} are now slowly varying functions of V and T, which are always close to the ratios of critical constants, as expressed in equations (9-17) for mutually conformal substances. Leach et al. (124) incorporated the departures of h_{ii} and f_{ii} from those constant values into slowly varying functions ϕ and θ, which they called molecular shape factors:

$$\left.\begin{aligned} h_{ii}[V,T] &\equiv \left(\frac{V_i^c}{V_o^c}\right).\phi_{ii}\left[\frac{V}{V_i^c}, \frac{T}{T_i^c}\right] \\ f_{ii}[V,T] &\equiv \left(\frac{T_i^c}{T_o^c}\right).\theta_{ii}\left[\frac{V}{V_i^c}, \frac{T}{T_i^c}\right] \end{aligned}\right\} \quad (9\text{-}22)$$

It might be thought that the dependence of ϕ_{ii} and θ_{ii} on the reduced variables

$$\left.\begin{aligned} V_i^R &\equiv \frac{V}{V_i^c} \\ \text{and} \qquad T_i^R &\equiv \frac{T}{T_i^c} \end{aligned}\right\} \quad (9\text{-}23)$$

should be specific of the pair of substances under consideration, but in practice this is not so. The value of this approach arises because departures from the principle of corresponding states are not random, but can be characterised by an additional parameter, such as Pitzer's acentric factor ω. By solving equations equivalent to (9-14) and (9-16)

using experimental data for hydrocarbons, Leach et al. (124) showed that ϕ_{ii} and θ_{ii} can be written, at least for non-polar substances, as universal functions of V_i^R, T_i^R and $(\omega_i - \omega_o)$:

$$\left.\begin{aligned} \phi_{ii} &= \left(\frac{z_o^c}{z_i^c}\right)\left(1 + (\omega_i - \omega_o)\left(0.3903(V_i^R - 1.0177) - 0.9462(V_i^R - 0.7663)\ln T_i^R\right)\right) \\ \theta_{ii} &= 1 + (\omega_i - \omega_o)\left(0.0892 - 0.8493 \ln T_i^R + \left(0.3063 - \frac{0.4506}{T_i^R}\right)(V_i^R - 0.5)\right) \end{aligned}\right\} \quad (9\text{-}24)$$

In equations (9-24), the reduced temperatures and volumes are restricted to $T_i^R < 2.0$ and $0.5 < V_i^R < 2.0$, values outside these ranges being set to the value at the limit. Clearly, if substances i and o do conform mutually to the principle of corresponding states, then $\phi_{ii} = \theta_{ii} = 1$ and, from (9-22), the constant values of h_{ii} and f_{ii} given by equations (9-17) are recovered.

9.1.3 Extension of the principle of corresponding states to mixtures

Various attempts have been made to extend the principle of corresponding states to mixtures. The problem is that the potential energy of the system will depend not only on the relative positions of the molecules, but also on the assignment of molecules by species to those positions. Of all the different models that have been proposed, the so-called van der Waals one-fluid model has been shown to be the most successful, and also one of the simplest to use. For these reasons, the van der Waals one-fluid model was adopted in all the calculations in this work and will now be briefly described.

The first assumption, which is common to any one-fluid model of mixtures, concerns the potential energy of the mixture. In a one-fluid model, this is replaced by a position-averaged potential which is the same for all components. This is equivalent to the assumption that the configurational Helmholtz free energy of the mixture, after subtraction

of the ideal mixing term, can be replaced by that of a single equivalent substance:

$$\tilde{A}^{m}[V,T,x_\alpha] = \tilde{A}^{e.s.}[V,T,x_\alpha] + RT \sum_{\alpha=1}^{c} x_\alpha \ln x_\alpha, \qquad (9\text{-}25)$$

where $\tilde{A}^{m}$ and $\tilde{A}^{e.s.}$ denote, respectively, the configurational Helmholtz free energy of the mixture of c components and that of the hypothetical equivalent substance. Clearly, this equivalent substance will be different for each mixture. Its properties can, in turn, be computed from the properties of a reference substance o by the method outlined in the previous sections. Thus, from (9-14), the configurational Helmholtz free energy of the imaginary equivalent substance will be given by

$$\tilde{A}^{e.s.}[V,T,x_\alpha] = f^{e.s.}[V,T,x_\alpha]\,\tilde{A}_o\left[\frac{V}{h^{e.s.}}, \frac{T}{f^{e.s.}}\right] - RT \ln h^{e.s.}[V,T,x_\alpha] \qquad (9\text{-}26)$$

where $f^{e.s.}$ and $h^{e.s.}$ are the scaling parameters of the equivalent substance with respect to the reference substance o, which are generally functions of the volume, temperature and composition of the mixture.

The next problem in the application of the one-fluid model to mixtures is the computation of the scaling parameters of the equivalent substance in terms of the scaling parameters of the real components of the mixture. Again, various recipes have been proposed, but undoubtedly the most successful, and the one for which there are the best theoretical arguments (141), is that originally proposed by van der Waals for use with his equation of state (99):

$$\left.\begin{aligned} h^{e.s.} &= \sum_{i=1}^{c}\sum_{j=1}^{c} x_i\, x_j\, h_{ij} \\ f^{e.s.} &= \left(\sum_{i=1}^{c}\sum_{j=1}^{c} x_i\, x_j\, f_{ij}\, h_{ij}\right) \Big/ h^{e.s.} \end{aligned}\right\} . \qquad (9\text{-}27)$$

The parameters $h^{e.s.}$ and $f^{e.s.}$ clearly depend on all the molecular interactions in the mixture, i.e. both on those between like molecules (represented by h_{ii} and f_{ii}) and those between unlike molecules (represented by h_{ij} and f_{ij}). Because of the usual assumption of pairwise additivity,

no three-body or higher order scaling parameters need be introduced. Values must, however, be assigned to the unlike interaction scaling parameters h_{ij} and f_{ij} $(i \neq j)$, and this is normally done by writing

$$\left.\begin{aligned} h_{ij} &= \eta_{ij}\left(\tfrac{1}{2}h_{ii}^{1/3} + \tfrac{1}{2}h_{jj}^{1/3}\right)^3 \\ \text{and} \quad f_{ij} &= \xi_{ij}(f_{ii}\, f_{jj})^{\frac{1}{2}} \end{aligned}\right\} , \tag{9-28}$$

where the binary interaction parameters η_{ij} and ξ_{ij} are constants, usually close to unity, which must be treated as adjustable parameters, i.e. they should be determined from experimental data on the relevant binary system of components i and j.

If the components of the mixture and reference substance o are assumed to be mutually conformal, then the various scaling parameters h_{ii} and f_{ii} will be constants given by the ratio of the appropriate critical constants, as in equations (9-17). In general, however, the components of the mixture and the reference substance will not be mutually conformal and the values of h_{ii} and f_{ii} must be obtained via the molecular shape factors, as in equation (9-22). Thus for a mixture,

$$\left.\begin{aligned} h_{ii}[V,T,x_\alpha] &\equiv \left(\frac{V_i^c}{V_o^c}\right).\phi_{ii}[V_i^R,\ T_i^R] \\ \text{and} \quad f_{ii}[V,T,x_\alpha] &\equiv \left(\frac{T_i^c}{T_o^c}\right).\theta_{ii}[V_i^R,\ T_i^R] \end{aligned}\right\} . \tag{9-29}$$

Leach et al. (124) have shown that the reduced properties V_i^R and T_i^R for the mixture must be obtained from

$$\left.\begin{aligned} V_i^R &\equiv \frac{V\,\phi_{ii}}{V_o^c h^{e.s.}} \\ \text{and} \quad T_i^R &\equiv \frac{T\,\theta_{ii}}{T_o^c f^{e.s.}} \end{aligned}\right\} \tag{9-30}$$

(.../)

if the calculated properties are to remain invariant when the reference substance is changed. Equations (9-30) must be used in conjunction with equations (9-29), and clearly iterative solutions are required, since the arguments of ϕ_{ii} and θ_{ii} in (9-29) are themselves functions of ϕ_{ii} and θ_{ii}.

Equations (9-25) to (9-30) provide a complete route for the computation of the configurational Helmholtz free energy of a mixture of c components from the known configurational Helmholtz free energy of a reference substance o, given the critical constants and acentric factors of the pure components and of the reference substance, and a knowledge of the c(c-1) interaction parameters ξ_{ij} and η_{ij}.

9.1.4 Computation of the derivatives of the Helmholtz free energy of a binary mixture

The method outlined in the previous section will now be applied to the problem of the solution of the criticality conditions for a binary fluid mixture. Since the molecular part of the Helmholtz free energy of the mixture is a linear function of the mole fractions of the various components (1), the only contribution to the various derivatives in equations (7-15) and (7-16) will come from the configurational part of the Helmholtz free energy of the mixture. Thus the criticality conditions for a binary fluid mixture can be written in terms only of the derivatives of the configurational Helmholtz free energy of the mixture:

$$\mathring{A}^m_{2x}(2\mathring{A}^m_{\rho} + \rho\mathring{A}^m_{2\rho}) - \rho(\mathring{A}^m_{x\rho})^2 = 0 \qquad (9\text{-}31)$$

and

$$\begin{aligned}&\mathring{A}^m_{3x}(2\mathring{A}^m_{\rho} + \rho\mathring{A}^m_{2\rho})^3 - 3\rho\mathring{A}^m_{x\rho}\,\mathring{A}^m_{2x\rho}(2\mathring{A}^m_{\rho} + \rho\mathring{A}^m_{2\rho})^2 \\ &+ 3\rho(\mathring{A}^m_{x\rho})^2(2\mathring{A}^m_{x\rho} + \rho\mathring{A}^m_{x2\rho})(2\mathring{A}^m_{\rho} + \rho\mathring{A}^m_{2\rho}) \\ &- \rho(\mathring{A}^m_{x\rho})^3(6\mathring{A}^m_{\rho} + 6\rho\mathring{A}^m_{2\rho} + \rho^2\mathring{A}^m_{3\rho}) = 0. \qquad (9\text{-}32)\end{aligned}$$

(.../)

Equation (9-25) can now be written for a binary mixture, with the molar density ρ replacing the equivalent molar volume V as one of the independent variables:

$$\tilde{A}^{m}_{x}[\rho,T,x] = \tilde{A}^{e.s.}[\rho,T,x] + RT\{x \ln x + (1-x) \ln(1-x)\}. \quad (9\text{-}33)$$

From this equation the following derivatives can be obtained immediately:

$$\left.\begin{aligned}
\tilde{A}^{m}_{x} &= \tilde{A}^{e.s.}_{x} + RT \ln\left(\frac{x}{1-x}\right) ; \\
\tilde{A}^{m}_{2x} &= \tilde{A}^{e.s.}_{2x} + RT\left(\frac{1}{x} + \frac{1}{1-x}\right) ; \\
\tilde{A}^{m}_{3x} &= \tilde{A}^{e.s.}_{3x} + RT\left(\frac{1}{(1-x)^2} - \frac{1}{x^2}\right) ; \\
\tilde{A}^{m}_{\rho} &= \tilde{A}^{e.s.}_{\rho} ; \\
\tilde{A}^{m}_{2\rho} &= \tilde{A}^{e.s.}_{2\rho} ; \\
\tilde{A}^{m}_{3\rho} &= \tilde{A}^{e.s.}_{3\rho} ; \\
\tilde{A}^{m}_{x\rho} &= \tilde{A}^{e.s.}_{x\rho} ; \\
\tilde{A}^{m}_{x2\rho} &= \tilde{A}^{e.s.}_{x2\rho} ; \\
\text{and} \quad \tilde{A}^{m}_{2x\rho} &= \tilde{A}^{e.s.}_{2x\rho}
\end{aligned}\right\} \quad (9\text{-}34)$$

The various derivatives of the configurational Helmholtz free energy of the equivalent substance can now be obtained from equation (9-35), which is the equivalent of equation (9-26) for a binary mixture:

$$\tilde{A}^{e.s.}[\rho,T,x] = f^{e.s.}[\rho,T,x].\tilde{A}_{o}\left[\rho h^{e.s.}, \frac{T}{f^{e.s.}}\right] - RT \ln h^{e.s.}[\rho,T,x]. \quad (9\text{-}35)$$

By simple but tedious algebraic manipulations, all the derivatives of $\tilde{A}^{e.s.}$ can be obtained from equation (9-35), and they can all be expressed in terms of configurational properties of the reference substance o, the scaling parameters $h^{e.s.}$ and $f^{e.s.}$ and the derivatives of these parameters with respect to composition up to third order:

$$\mathring{A}_x^{e.s.} = \left(\frac{fh_x}{h}\right)^{e.s.}\left(\frac{P_o}{\rho_o} - RT_o\right) + f_x^{e.s.}\,\mathring{U}_o \tag{9-36}$$

$$\begin{aligned}\mathring{A}_{2x}^{e.s.} = {} & \left(\frac{fh_x^2}{h^2}\right)^{e.s.}\left(\left(\frac{\partial P_o}{\partial \rho_o}\right)_{T_o} - 2\frac{P_o}{\rho_o} + RT_o\right) + \left(\frac{f_x^2}{f}\right)^{e.s.}\left(-T_o\mathring{C}_{vo}\right) \\ & + \left(2\frac{h_x f_x}{h}\right)^{e.s.}\left(\frac{P_o}{\rho_o} - \frac{T_o}{\rho_o}\left(\frac{\partial P_o}{\partial T_o}\right)_{\rho_o}\right) \\ & + \left(\frac{fh_{2x}}{h}\right)^{e.s.}\left(\frac{P_o}{\rho_o} - RT_o\right) + f_{2x}^{e.s.}\,\mathring{U}_o\end{aligned} \tag{9-37}$$

$$\begin{aligned}\mathring{A}_{3x}^{e.s.} = {} & \left(\frac{fh_x^3}{h^3}\right)^{e.s.}\left(\rho_o\left(\frac{\partial^2 P_o}{\partial \rho_o^2}\right)_{T_o} - 4\left(\frac{\partial P_o}{\partial \rho_o}\right)_{T_o} + 6\frac{P_o}{\rho_o} - 2RT_o\right) \\ & + \left(3\frac{f_x h_x^2}{h^2}\right)^{e.s.}\left(-T_o\left(\frac{\partial^2 P_o}{\partial \rho_o \partial T_o}\right) + 2\frac{T_o}{\rho_o}\left(\frac{\partial P_o}{\partial T_o}\right)_{\rho_o} + \left(\frac{\partial P_o}{\partial \rho_o}\right)_{T_o} - 2\frac{P_o}{\rho_o}\right) \\ & + \left(3\frac{h_x f_x^2}{h\,f}\right)^{e.s.}\left(\frac{T_o^2}{\rho_o}\left(\frac{\partial^2 P_o}{\partial T_o^2}\right)_{\rho_o}\right) + \left(\frac{f_x^3}{f^2}\right)^{e.s.}\left(2T_o\mathring{C}_{vo} + T_o^2\left(\frac{\partial \mathring{C}_{vo}}{\partial T_o}\right)_{\rho_o}\right) \\ & + \left(3\frac{fh_x h_{2x}}{h^2}\right)^{e.s.}\left(\left(\frac{\partial P_o}{\partial \rho_o}\right)_{T_o} - 2\frac{P_o}{\rho_o} + RT_o\right) \\ & + \left(3\frac{f_x h_{2x}}{h} + 3\frac{f_{2x} h_x}{h}\right)^{e.s.}\left(-\frac{T_o}{\rho_o}\left(\frac{\partial P_o}{\partial T_o}\right)_{\rho_o} + \frac{P_o}{\rho_o}\right) \\ & + \left(3\frac{f_x f_{2x}}{f}\right)^{e.s.}\left(-T_o\mathring{C}_{vo}\right) + \left(\frac{fh_{3x}}{h}\right)^{e.s.}\left(\frac{P_o}{\rho_o} - RT_o\right) + f_{3x}^{e.s.}\,\mathring{U}_o\end{aligned} \tag{9-38}$$

$$\mathring{A}_\rho^{e.s.} = (hf)^{e.s.}\left(\frac{P_o}{\rho_o^2}\right) \tag{9-39}$$

$$\mathring{A}_{2\rho}^{e.s.} = (h^2 f)^{e.s.}\left(\frac{1}{\rho_o^2}\left(\frac{\partial P_o}{\partial \rho_o}\right)_{T_o} - 2\frac{P_o}{\rho_o^3}\right) \tag{9-40}$$

$$\mathring{A}_{3\rho}^{e.s.} = (h^3 f)^{e.s.}\left(\frac{1}{\rho_o^2}\left(\frac{\partial^2 P_o}{\partial \rho_o^2}\right)_{T_o} - \frac{4}{\rho_o^3}\left(\frac{\partial P_o}{\partial \rho_o}\right)_{T_o} + 6\frac{P_o}{\rho_o^4}\right) \tag{9-41}$$

$$\mathring{A}_{x\rho}^{e.s.} = (hf_x)^{e.s.}\left(\frac{P_o}{\rho_o^2} - \frac{T_o}{\rho_o^2}\left(\frac{\partial P_o}{\partial T_o}\right)_{\rho_o}\right) + (h_x f)^{e.s.}\left(\frac{1}{\rho_o}\left(\frac{\partial P_o}{\partial \rho_o}\right)_{T_o} - \frac{P_o}{\rho_o^2}\right) \tag{9-42}$$

(.../)

$$\tilde{A}^{e.s.}_{x2\rho} = (h^2 f_x)^{e.s.}\left(\frac{1}{\rho_o^2}\left(\frac{\partial P_o}{\partial \rho_o}\right)_{T_o} - \frac{T_o}{\rho_o^2}\left(\frac{\partial^2 P_o}{\partial \rho_o \partial T_o}\right) + 2\frac{T_o}{\rho_o^3}\left(\frac{\partial P_o}{\partial T_o}\right)_{\rho_o} - 2\frac{P_o}{\rho_o^3}\right)$$

$$+ (hh_x f)^{e.s.}\left(\frac{1}{\rho_o}\left(\frac{\partial^2 P_o}{\partial \rho_o^2}\right)_{T_o} - \frac{2}{\rho_o^2}\left(\frac{\partial P_o}{\partial \rho_o}\right)_{T_o} + 2\frac{P_o}{\rho_o^3}\right) \qquad (9\text{-}43)$$

$$\tilde{A}^{e.s.}_{2x\rho} = \left(\frac{hf_x^2}{f}\right)^{e.s.}\left(\frac{T_o^2}{\rho_o^2}\left(\frac{\partial^2 P_o}{\partial T_o^2}\right)_{\rho_o}\right)$$

$$+ \left(\frac{h_x^2 f}{h}\right)^{e.s.}\left(\left(\frac{\partial^2 P_o}{\partial \rho_o^2}\right)_{T_o} - \frac{2}{\rho_o}\left(\frac{\partial P_o}{\partial \rho_o}\right)_{T_o} + 2\frac{P_o}{\rho_o^2}\right)$$

$$+ (2h_x f_x)^{e.s.}\left(-\frac{T_o}{\rho_o}\left(\frac{\partial^2 P_o}{\partial \rho_o \partial T_o}\right) + \frac{1}{\rho_o}\left(\frac{\partial P_o}{\partial \rho_o}\right)_{T_o} + \frac{T_o}{\rho_o^2}\left(\frac{\partial P_o}{\partial T_o}\right)_{\rho_o} - \frac{P_o}{\rho_o^2}\right)$$

$$+ (hf_{2x})^{e.s.}\left(-\frac{T_o}{\rho_o^2}\left(\frac{\partial P_o}{\partial T_o}\right)_{\rho_o} + \frac{P_o}{\rho_o^2}\right)$$

$$+ (h_{2x} f)^{e.s.}\left(\frac{1}{\rho_o}\left(\frac{\partial P_o}{\partial \rho_o}\right)_{T_o} - \frac{P_o}{\rho_o^2}\right). \qquad (9\text{-}44)$$

In the above equations, $\tilde{P}_o$ has been replaced by the total pressure P_o using equation (9-3) and, for simplicity, ρ_o and T_o have been defined as

$$\left.\begin{aligned} \rho_o &\equiv \rho.h^{e.s.}[\rho,T,x] \\ \text{and} \quad T_o &\equiv T/f^{e.s.}[\rho,T,x] \end{aligned}\right\} . \qquad (9\text{-}45)$$

All the configurational properties of the reference substance can be expressed as functions of the independent variables ρ_o and T_o. An outline of the derivation of equations (9-36) - (9-44) can be found in Appendix E.

Thus it is possible to express all the derivatives of the configurational Helmholtz free energy of the equivalent substance in terms of $h^{e.s.}$, $h_x^{e.s.}$, $h_{2x}^{e.s.}$, $h_{3x}^{e.s.}$, $f^{e.s.}$, $f_x^{e.s.}$, $f_{2x}^{e.s.}$, $f_{3x}^{e.s.}$ and the following

configurational properties of the reference substance o: $\tilde{U}_o$, $\tilde{C}_{vo}$, $(\partial\tilde{C}_{vo}/\partial T_o)$, P_o, $(\partial P_o/\partial\rho_o)$, $(\partial P_o/\partial T_o)$, $(\partial^2 P_o/\partial\rho_o^2)$, $(\partial^2 P_o/\partial T_o^2)$ and $(\partial^2 P_o/\partial\rho_o\partial T_o)$. The following two sections will be devoted to the computation of each of these two sets of quantities.

9.1.5 Computation of the derivatives of the scaling parameters $h^{e.s.}$ and $f^{e.s.}$ with respect to composition

The correct values of the scaling parameters of the equivalent substance may be obtained from equations (9-27) to (9-30) together with equations (9-24). For a binary mixture, equations (9-27) to (9-30) become:

$$h^{e.s.} = x^2 h_{11} + 2x(1-x)\, h_{12} + (1-x)^2\, h_{22} \qquad (9\text{-}46)$$

$$f^{e.s.} = \{x^2 h_{11} f_{11} + 2x(1-x) h_{12} f_{12} + (1-x)^2 h_{22} f_{22}\}/h^{e.s.} \qquad (9\text{-}47)$$

$$h_{12} = \eta_{12}\left(\tfrac{1}{2}h_{11}^{1/3} + \tfrac{1}{2}h_{22}^{1/3}\right)^3 \qquad (9\text{-}48)$$

$$f_{12} = \xi_{12}(f_{11}f_{22})^{\frac{1}{2}} \qquad (9\text{-}49)$$

$$h_{ii} = \left(\frac{\rho_o^c}{\rho_i^c}\right) \cdot \phi_{ii}[V_i^R, T_i^R] \qquad (i = 1,2) \qquad (9\text{-}50)$$

$$f_{ii} = \left(\frac{T_i^c}{T_o^c}\right) \cdot \theta_{ii}[V_i^R, T_i^R] \qquad (i = 1,2) \qquad (9\text{-}51)$$

$$V_i^R = \frac{\rho_o^c\, \phi_{ii}}{\rho\, h^{e.s.}} \qquad (i = 1,2) \qquad (9\text{-}52)$$

and

$$T_i^R \equiv \frac{T\, \theta_{ii}}{T_o^c\, f^{e.s.}} \qquad (i = 1,2). \qquad (9\text{-}53)$$

From (9-46) and (9-48), by differentiation with respect to x at constant ρ and T:

$$\Delta h^{e.s.} = 2x\, h_{11} + 2(1-2x)\, h_{12} - 2(1-x)\, h_{22} + x^2 \Delta h_{11} + 2x(1-x)\, \Delta h_{12} + (1-x)^2\, \Delta h_{22}, \qquad (9\text{-}54)$$

in which

$$\Delta h_{12} = \frac{\eta_{12}}{8}\left(h_{11}^{1/3} + h_{22}^{1/3}\right)^2\left(h_{11}^{-2/3}\Delta h_{11} + h_{22}^{-2/3}\Delta h_{22}\right). \quad (9\text{-}55)$$

In the above equations, and throughout this section, the symbol Δ is used to indicate partial differentiation with respect to x at constant ρ and T.

Similarly, from (9-47) and (9-49):

$$\begin{aligned}\Delta f^{e.s.} = {} & \frac{2}{h^{e.s.}} \cdot \frac{xh_{11}f_{11} + (1-x)h_{12}f_{12} - f^{e.s.}\{xh_{11} + (1-x)h_{12}\}}{1-x} \\ & + \frac{1}{h^{e.s.}}\{x^2(f_{11} - f^{e.s.})\Delta h_{11} + 2x(1-x)(f_{12} - f^{e.s.})\Delta h_{12} \\ & \qquad + (1-x)^2(f_{22} - f^{e.s.})\Delta h_{22}\} \\ & + \frac{1}{h^{e.s.}}\{x^2h_{11}\Delta f_{11} + 2x(1-x)h_{12}\Delta f_{12} + (1-x)^2h_{22}\Delta f_{22}\}\end{aligned} \quad (9\text{-}56)$$

in which

$$\Delta f_{12} = \frac{\xi_{12}}{2f_{12}}(f_{22}\Delta f_{11} + f_{11}\Delta f_{22}). \quad (9\text{-}57)$$

Equations (9-54) to (9-57) require a knowledge of the derivatives Δh_{ii} and Δf_{ii} (i = 1,2). It is possible to obtain explicit expressions for Δh_{ii} and Δf_{ii} in terms of $\Delta h^{e.s.}$ and $\Delta f^{e.s.}$, by very tedious algebraic manipulation of equations (9-50) to (9-53). The final results are:

$$\frac{\Delta h_{ii}}{h_{ii}} = \frac{\left(\frac{DL\Phi}{DLV}\frac{DL\Theta}{DLT} - \frac{DL\Theta}{DLV}\frac{DL\Phi}{DLT} - \frac{DL\Phi}{DLV}\right)_i \frac{\Delta h^{e.s.}}{h^{e.s.}} - \left(\frac{DL\Phi}{DLT}\right)_i \frac{\Delta f^{e.s.}}{f^{e.s.}}}{\left(1 - \frac{DL\Theta}{DLT} - \frac{DL\Phi}{DLV} + \frac{DL\Phi}{DLV}\frac{DL\Theta}{DLT} - \frac{DL\Theta}{DLV}\frac{DL\Phi}{DLT}\right)_i} \quad (9\text{-}58)$$

and

$$\frac{\Delta f_{ii}}{f_{ii}} = \frac{\left(\frac{DL\Phi}{DLV}\frac{DL\Theta}{DLT} - \frac{DL\Theta}{DLV}\frac{DL\Phi}{DLT} - \frac{DL\Theta}{DLT}\right)_i \frac{\Delta f^{e.s.}}{f^{e.s.}} - \left(\frac{DL\Theta}{DLV}\right)_i \frac{\Delta h^{e.s.}}{h^{e.s.}}}{\left(1 - \frac{DL\Theta}{DLT} - \frac{DL\Phi}{DLV} + \frac{DL\Phi}{DLV}\frac{DL\Theta}{DLT} - \frac{DL\Theta}{DLV}\frac{DL\Phi}{DLT}\right)_i}, \quad (9\text{-}59)$$

where:

$$\left.\begin{aligned}
\left(\frac{DL\Phi}{DLV}\right)_i &\equiv \frac{V_i^R}{\Phi_{ii}}\left(\frac{\partial \Phi_{ii}}{\partial V_i^R}\right) \\
\left(\frac{DL\Phi}{DLT}\right)_i &\equiv \frac{T_i^R}{\Phi_{ii}}\left(\frac{\partial \Phi_{ii}}{\partial T_i^R}\right) \\
\left(\frac{DL\Theta}{DLV}\right)_i &\equiv \frac{V_i^R}{\Theta_{ii}}\left(\frac{\partial \Theta_{ii}}{\partial V_i^R}\right) \\
\left(\frac{DL\Theta}{DLT}\right)_i &\equiv \frac{T_i^R}{\Theta_{ii}}\left(\frac{\partial \Theta_{ii}}{\partial T_i^R}\right)
\end{aligned}\right\} \quad , \qquad (9\text{-}60)$$

these derivatives being obtained directly from equations (9-24). An outline of the derivation of equations (9-58) and (9-59) is given in Appendix F. These two equations, together with equations (9-54) to (9-57), can now be solved by a simple iterative method to give the values of $h_x^{e.s.} \equiv \Delta h^{e.s.}$ and $f_x^{e.s.} \equiv \Delta f^{e.s.}$,

In view of the complexity of equations (9-58) and (9-59) and the computing time necessary to solve these equations, no attempt was made to obtain similar closed expressions for the second and third derivatives of h_{ii} and f_{ii} with respect to composition. Instead, the derivatives $h_{2x}^{e.s.}$, $h_{3x}^{e.s.}$, $f_{2x}^{e.s.}$ and $f_{3x}^{e.s.}$ were obtained by numerical differentiation using the values of $h_x^{e.s.}$ and $f_x^{e.s.}$ calculated previously.

9.1.6 Reference substance calculations

The computation of the configurational properties of the reference substance which appear in equations (9-36) to (9-44) involves the choice of a suitable reference substance, and a very accurate equation of state to represent its (P-V-T) properties over wide ranges of pressure and temperature. In principle, maximum accuracy can be obtained when the chosen reference substance is one of the components of the binary mixture.

(.../)

Although CF_4 might appear to be the obvious choice, since it was the component common to all the mixtures studied, in the absence of a sufficiently accurate equation of state for CF_4 methane was chosen as the reference substance. The equation of state is that used by the I.U.P.A.C. Thermodynamic Tables Project Centre in compiling their tables of the fluid state for methane (142). This is an equation of the same form as the "extended B-W-R" type used previously by Stewart and Jacobsen (143):

$$
\begin{aligned}
P_o = {} & \rho_o RT_o + \rho_o^2(A_1T_o + A_2T_o^{\frac{1}{2}} + A_3 + A_4T_o^{-1} + A_5T_o^{-2}) \\
& + \rho_o^3(A_6T_o + A_7 + A_8T_o^{-1} + A_9T_o^{-2} + \exp\{-\gamma\rho_o^2\}(A_{20}T_o^{-2} + A_{21}T_o^{-3})) \\
& + \rho_o^4(A_{10}T_o + A_{11} + A_{12}T_o^{-1}) \\
& + \rho_o^5(A_{13} + \exp\{-\gamma\rho_o^2\}(A_{22}T_o^{-2} + A_{23}T_o^{-4})) + \rho_o^6(A_{14}T_o^{-1} + A_{15}T_o^{-2}) \\
& + \rho_o^7(A_{16}T_o^{-1} + \exp\{-\gamma\rho_o^2\}(A_{24}T_o^{-2} + A_{25}T_o^{-3})) + \rho_o^8(A_{17}T_o^{-1} + A_{18}T_o^{-2}) \\
& + \rho_o^9(A_{19}T_o^{-2} + \exp\{-\gamma\rho_o^2\}(A_{26}T_o^{-2} + A_{27}T_o^{-4})) \\
& + \rho_o^{11}(\exp\{-\gamma\rho_o^2\}(A_{28}T_o^{-2} + A_{29}T_o^{-3})) \\
& + \rho_o^{13}(\exp\{-\gamma\rho_o^2\}(A_{30}T_o^{-2} + A_{31}T_o^{-3} + A_{32}T_o^{-4})). \qquad (9\text{-}61)
\end{aligned}
$$

The original range of applicability of this equation was from 0 to 10 000 bar between 90 K and 470 K, and from 0 to 4 000 bar between 470 K and 620 K (142). Szczepanski (144) has, however, recently extended the temperature range covered by this equation, by using experimentally determined (P-V-T) data for nitrogen and hydrogen to generate pseudo-data for methane which were incorporated into the fitting procedure used to evaluate the constants. He claims that his equation agrees with the experimental data much better than the original I.U.P.A.C. equation above 300 K and 400 bar, the agreement being just as good below this region. Moreover, his equation allows extrapolation to 1 300 K at 5 000 bar and to 3 000 K at 1 500 bar, and it also gave reasonable predictions down to the triple point of ethane (89.28 K). For these reasons, Szczepanski's modification of the I.U.P.A.C. equation of state for methane was finally chosen as the working reference substance equation of state. The 33 constants of this equation based on Szczepanski's work (144) are listed in Appendix G.

(.../)

Computation of the derivatives $(\partial P_o/\partial \rho_o)$, $(\partial P_o/\partial T_o)$, $(\partial^2 P_o/\partial \rho_o^2)$, $(\partial^2 P_o/\partial T_o^2)$ and $(\partial^2 P_o/\partial \rho_o \partial T_o)$ was performed by straightforward differentiations of equation (9-61). The remaining configurational properties of the reference sybstance were obtained by noting that, from (9-5):

$$\tilde{U}_o[\rho_o,T_o] = U_o^{res.}[\rho_o,T_o] + \tilde{U}_o^{p.g.} . \qquad (9\text{-}62)$$

Since the configurational internal energy of a perfect gas is zero (1), the configurational internal energy of the reference substance equals the residual internal energy, which in turn can be obtained from classical thermodynamics (145):

$$\tilde{U}_o[\rho_o,T_o] = U_o^{res.}[\rho_o,T_o] = \int_0^{\rho_o}\left(P_o - T_o\left(\frac{\partial P_o}{\partial T_o}\right)_{\rho_o}\right)\frac{d\rho_o}{\rho_o^2} , \qquad (9\text{-}63)$$

and similarly:

$$\tilde{C}_{vo}[\rho_o,T_o] = C_{vo}^{res.}[\rho_o,T_o] =$$

$$= \left(\frac{\partial U_o^{res.}}{\partial T_o}\right)_{\rho_o} = \int_0^{\rho_o}\left(-T_o\left(\frac{\partial^2 P_o}{\partial T_o^2}\right)_{\rho_o}\right)\frac{d\rho_o}{\rho_o^2} \qquad (9\text{-}64)$$

and $$\left(\frac{\partial \tilde{C}_{vo}}{\partial T_o}\right)_{\rho_o} = \left(\frac{\partial C_{vo}^{res.}}{\partial T_o}\right)_{\rho_o} =$$

$$= \left(\frac{\partial^2 U_o^{res.}}{\partial T_o^2}\right)_{\rho_o} = \int_0^{\rho_o}\left(-\left(\frac{\partial^2 P_o}{\partial T_o^2}\right)_{\rho_o} - T_o\left(\frac{\partial^3 P_o}{\partial T_o^3}\right)_{\rho_o}\right)\frac{d\rho_o}{\rho_o^2} . \qquad (9\text{-}65)$$

The computation of these three configurational properties from the equation of state $P_o[\rho_o,T_o]$ (equation (9-61))was done by straightforward differentiation and integration.

All the quantities necessary for the solution of the criticality conditions given in equations (9-31) and (9-32) have now been computed, and the complete algorithm for the prediction of critical points in binary mixtures will be described in detail.

(.../)

9.2 Algorithm for the Prediction of Critical Points in Binary Fluid Mixtures

9.2.1 Critical analysis of Teja's algorithm

As mentioned in the introduction to this chapter, in the earlier stages of this investigation Teja's program for the prediction of critical points in binary mixtures (86) was used to correlate the experimental data obtained for the CF_4 + n-C_7H_{16} system. In view of the poor results obtained with this program, however, it was decided to undertake a complete analysis of his algorithm, in order to detect possible errors and produce a more compact and efficient algorithm. The main conclusions of this analysis were as follows:

(i) Teja's program uses the Vennix equation of state for the reference substance, methane (146). The range of applicability of this equation is very restricted, in the light of recent developments in this field (142, 143, 144): the equation is applicable from 0 to 10 000 p.s.i. (ca. 680 bar) from 130 K and 0.36 $g.cm^{-3}$ up to 273 K; from 273 K to 625 K, the equation is valid only up to 6 000 p.s.i. (ca. 410 bar) and extrapolation outside this range is not recommended by the authors.

(ii) The overall structure of the program is not very flexible. It is totally orientated towards use of the Vennix equation of state and methane as a reference substance. A change of equation of state and/or reference substance would imply rewriting most of the program, which is inappropriate in view of the fact that reference substance calculations are totally independent of the other calculations performed in the algorithm.

(iii) An inconsistency was detected in the computation of the derivatives of the scaling parameters $h^{e.s.}$ and $f^{e.s.}$ with respect to composition: Teja correctly uses the molecular shape factors to compute $h^{e.s.}$ and $f^{e.s.}$, but then fails to use the same concepts in the computation of the derivatives $h_x^{e.s.}$, $f_x^{e.s.}$, etc. In other words, he starts by assuming non-conformality, but then half-way through the algorithm he assumes that h_{ii} and f_{ii} are constants,

and that the only contribution to the composition derivatives of $h^{e.s.}$ and $f^{e.s.}$ comes from the composition dependence given by the van der Waals recipes, equations (9-27). This is obviously inconsistent, since h_{ii} and f_{ii} are themselves composition dependent, as can be seen from equations (9-46) to (9-53). Furthermore, in equation (9-50), Teja uses the ratio $(T_i^c P_o^c / T_o^c P_i^c)$ rather than the correct value (ρ_o^c/ρ_i^c) or (V_i^c/V_o^c).

In view of these limitations, it was decided to rewrite the program for the calculation of the critical points of binary fluid mixtures, based on the methods described in section 9.1. Although the general search procedure is similar to that used by Teja, the similarities end there. The errors detected in Teja's program were corrected, and an improved and much more accurate equation of state was used for methane, the reference substance (see 9.1.6). All the calculations on the reference fluid were included in a single compact subroutine, so as to make a change of reference substance and/or equation of state much easier to perform. Similarly, all the calculations concerning the scaling parameters $h^{e.s.}$ and $f^{e.s.}$ and their derivatives with respect to composition were included in a single subroutine. For reasons that will be explained in the next chapter, a second simplified version of this subroutine was written for use when the substances are assumed to be mutually conformal and the shape factors are set to unity. A new, more efficient, minimisation subroutine was introduced in place of the one used by Teja to solve the criticality conditions, equations (9-31) and (9-32). Finally, a new subroutine was written which tests the thermodynamic stability of each computed critical point.

Unfortunately, due to lack of time, the task of improving the program could not be completed and, in particular, convenient algebraic manipulations to shorten the time of calculation could not be properly exploited. Nevertheless, the new scheme is much more flexible than the original one proposed by Teja and can be used over much wider ranges of pressure and temperature.

(.../)

9.2.2 Description of the new algorithm

A flow diagram of the algorithm is given in Fig. 9.1 and a listing of the complete computer program in Appendix H. Since a critical point is defined by two equations, any two variables of the set $[\rho,T,x]$ can in principle be obtained by fixing one of these variables and then solving the two criticality conditions to obtain the other two variables. In this investigation, the search procedure used by Teja was employed: the mole fraction x of one of the components of the mixture was varied parametrically and, for each value of x, the criticality conditions were solved for temperature and density. The critical pressure of the mixture was then obtained from equations (9-33) and (9-35) by noting that:

$$P^m[\rho,T,x] = \hat{P}^m[\rho,T,x] = \rho^2 \hat{A}^m_\rho =$$

$$= \rho^2 \hat{A}^{e.s.}_\rho = \hat{P}^{e.s.} = \frac{f^{e.s.}}{h^{e.s.}} \cdot P_o[\rho_o,T_o] \; . \qquad (9\text{-}66)$$

The steps in the algorithm for the prediction of critical points in binary mixtures are:

1) The input information is read in. This includes:

   (i) critical constants and acentric factors for the pure components and the reference substance;

   (ii) three guesses for critical points of the mixture, which may be experimentally determined values;

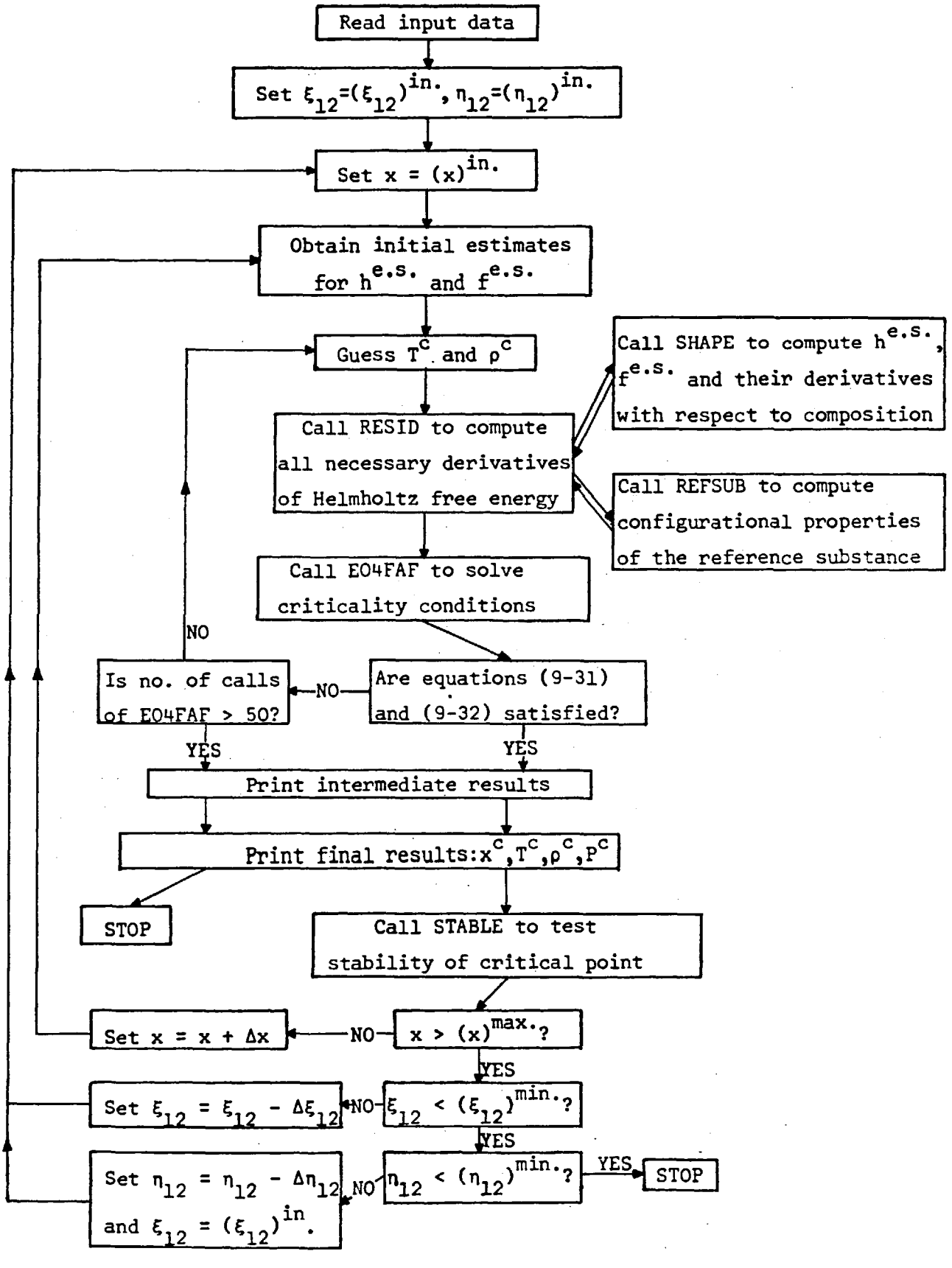
   (iii) the set of composition values (x) for which the critical points are to be computed;

   (iv) the set of binary interaction parameters (ξ_{12}, η_{12}) for which the critical lines are to be computed.

2) Initial estimates for the scaling parameters $h^{e.s.}$ and $f^{e.s.}$ are obtained by setting the shape factors to unity in equations (9-50) and (9-51).

(.../)

Fig. 9.1. Flow diagram of program CRITIC



3) For the current value of composition x, a first guess is made of the critical temperature and critical density, by extrapolation of the second degree Lagrangian polynomial through the three guesses initially read in.

4) A minimisation subroutine is used to solve the criticality conditions for the critical temperature and critical density. The subroutine chosen in this investigation has the code-name E04FAF; it is an unconstrained non-linear least-squares minimisation subroutine supplied by the NAG Library (147), which finds a least-squares solution of M non-linear equations in N variables by minimising the sum of squares of residuals. In this particular case, M = 2 (the two criticality conditions) and N = 2 (temperature and density).

5) The thermodynamic stability of the computed critical point is then tested by subroutine STABLE. This subroutine simply computes the value of the derivative G_{4x}. From classical thermodynamics:

$$G_{4x} \equiv \left(\frac{\partial G_{3x}[P,T,x]}{\partial x}\right)_{P,T} = \left(\frac{\partial G_{3x}[\rho,T,x]}{\partial x}\right)_{\rho,T} - \frac{\rho A_{x\rho}}{2A_{\rho} + \rho A_{2\rho}} \left(\frac{\partial G_{3x}[\rho,T,x]}{\partial \rho}\right)_{x,T} . \qquad (9\text{-}67)$$

The two partial derivatives, $(\partial G_{3x}/\partial x)_{\rho,T}$ and $(\partial G_{3x}/\partial \rho)_{x,T}$, are obtained by numerical differentiation of the function $G_{3x}[\rho,T,x]$. If $G_{4x} < 0$, the critical point is unstable; otherwise, it may be either stable or metastable, but these two cases are not differentiated in the present analysis of stability.

6) Intermediate and final results for the current value of x are printed out.

7) If subroutine E04FAF is not successful in finding a solution of the criticality conditions, the program is aborted; otherwise, the whole procedure is repeated for a new value of the mole fraction x, until the whole range of composition values has been covered.

(.../)

8) After computing the critical curve for one set of values of the parameters (ξ_{12}, η_{12}), the values of ξ_{12} and/or η_{12} are changed, and a new critical line is computed by the same procedure, until the whole set of values of (ξ_{12}, η_{12}) has been covered.

The solution of the criticality conditions using the minimisation subroutine E04FAF requires a knowledge of the thermodynamic quantities in equations (9-31) and (9-32). In subroutine RESID, all the relevant derivatives of the configurational Helmholtz free energy of the mixture are obtained in terms of the scaling parameters $h^{e.s.}$ and $f^{e.s.}$, their derivatives up to third order in composition x, and the configurational properties of the reference substance, following the method described in section 9.1.4. The values of $h^{e.s.}$, $f^{e.s.}$, $h_x^{e.s.}$, $f_x^{e.s.}$, etc., are computed in subroutine SHAPE, using the method outlined in section 9.1.5. Finally, all the relevant configurational properties of the reference substance are computed in subroutine REFSUB, in accordance with the method described in section 9.1.6.

Chapter 10

COMPUTER RESULTS AND CONCLUSIONS

10.1 Introduction

The algorithm described in the previous chapter was used for the prediction of critical lines in mixtures of CF_4 and n-alkanes. In order to test the program, it was used initially for the CH_4 + n-alkane systems which were expected to be well represented by the corresponding states principle. Experimentally measured critical data for these systems were compared with the predictions, but unfortunately the agreement obtained was extremely poor. Even for simple systems, such as CH_4 + C_3H_8, it was not possible to predict the critical behaviour correctly, irrespective of the values chosen for the binary interaction parameters ξ_{12} and η_{12}. The results obtained for the higher n-alkanes, e.g. CH_4 + n-C_7H_{16}, were even more discouraging in that the algorithm would frequently diverge and no solution of the criticality conditions could be found.

Much time was spent checking the derivation of the equations given in chapter 9, and in trying to find possible mistakes in the computer program, but no errors were found. A breakthrough was finally made when the program was run with the shape factors ϕ_{ii} and θ_{ii} set to unity, which is equivalent to assuming that the components of the mixture and the reference substance form a set of conformal substances. Although this assumption is obviously incorrect for most of the systems studied, the results obtained were surprisingly good. The critical behaviour of the CH_4 + n-alkane systems could now be correctly predicted, and the agreement obtained for the CF_4 + n-alkane systems was generally very good. In particular, the liquid-liquid and gas-gas critical lines observed experimentally for some of these systems were correctly predicted by this simplified model.

It is clear that the problems with the original version of the program were caused by the molecular shape factor equations of Leach and Leland (equations 9-24). For some reason, the problem of finding a

solution of the criticality conditions becomes mathematically ill-conditioned when these equations are employed. Szczepanski (144) has recently encountered the same problem when trying to apply the van der Waals one-fluid model to the prediction of thermodynamic properties for chemical process design. Saville (148) has compared the shape factors derived from Leach's equations with values calculated from pure component data on methane and several other substances and found that the Leach shape factors provide a poor representation of the data at high temperatures. It is beyond the scope of this investigation to enquire into the reasons for the failure of the molecular shape factor equations, but undoubtedly a detailed investigation of this matter is urgently required.

In view of the limitations of the molecular shape factor equations, it was decided to discard them and to analyse the predictions of the model when the shape factors ϕ_{ii} and θ_{ii} are set to unity. A simplified version of subroutine SHAPE was therefore written to replace the original version containing the shape factor equations (see Appendix H); all the results and diagrams presented in this chapter were obtained with this simplified version of the program for the calculation of critical points of binary mixtures.

10.2 Correlation of Critical Data for Carbon Tetrafluoride + n-Alkane Systems

Experimentally measured critical data for binary mixtures normally consist of scattered values of (P^C, T^C) or (P^C, T^C, x^C); values of ρ^C or V^C are seldom available. Ideally, therefore, the values of the binary interaction parameters ξ_{12} and η_{12} should be obtained from a fit in three-dimensional (P-T-x) phase space. Unfortunately, this was not possible with the present structure of the algorithm, and the curve-fitting had to be confined to two dimensions, on any of the three main planes. Since the experimental values of P^C and T^C are usually more accurate than the corresponding values of x^C, the values of (ξ_{12}, η_{12}) quoted in this chapter refer to the curves that best fitted the experimental data on the (P-T) projection of the phase diagram. In only one case

(CF_4 + n-C_7H_{16}) was an attempt made to obtain the values of (ξ_{12}, η_{12}) that produced the best fit of the experimental critical data on the (P-x) plane.

The calculated critical curves for carbon tetrafluoride + n-alkane mixtures are shown in Figs. 10.1 to 10.6. In all these diagrams, the solid lines represent the stable or metastable portions of the predicted critical curve, whilst the unstable portions of the same curves are shown dotted; pure component critical points are represented by circles and experimental mixture critical points by crosses. Typical values of the predicted critical mole fraction of carbon tetrafluoride and of the critical density of the mixture (in mol.dm^{-3}) are shown in brackets along the various curves.

10.2.1 The systems carbon tetrafluoride + methane and carbon tetrafluoride + ethane

The predicted liquid-liquid critical curve for the CF_4 + CH_4 system is shown in Fig. 10.1 for ξ_{12} = 0.900 and η_{12} = 1.034. It fits the experimental critical data of Paas (67) surprisingly well. The critical mole fraction remains almost constant along the curve, varying from x^c = 0.404 at $P^c \simeq$ 100 bar to x^c = 0.409 at $P^c \simeq$ 2 000 bar. Paas also obtained an experimental (P^c - x^c) curve which was almost vertical, although the value of the critical mole fraction quoted by him ($x^c \simeq$ 0.43) differs slightly from the predicted value.

The gas-liquid critical curve shown on the right-hand side of Fig. 10.1 was predicted using the values of the binary interaction parameters determined from liquid-liquid critical data. It joins the critical points of the pure components and has a very shallow pressure maximum. No comparison with experimental values was possible since no gas-liquid critical data exist for this system. It is, however, unlikely that the values of (ξ_{12}, η_{12}) needed to fit the gas-liquid critical data will be the same as those needed to fit the liquid-liquid critical data. It must be borne in mind that the shape factors have been set to unity, which means that their dependence on temperature, density and composition has been transferred to the binary interaction parameters ξ_{12}

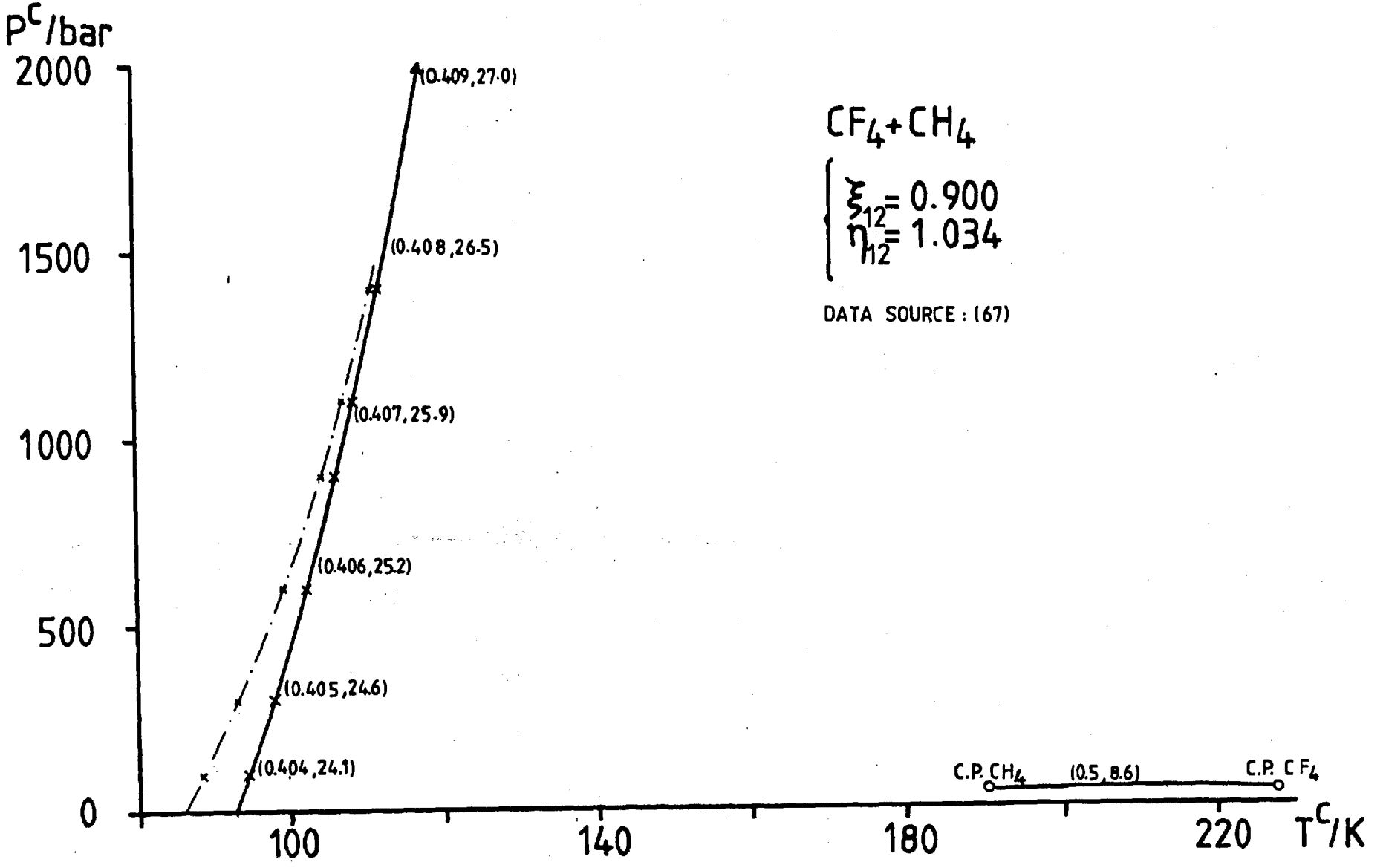


FIG. 10.1. Predicted (P^c-T^c) projection of the critical locus for the CF_4 + CH_4 system.

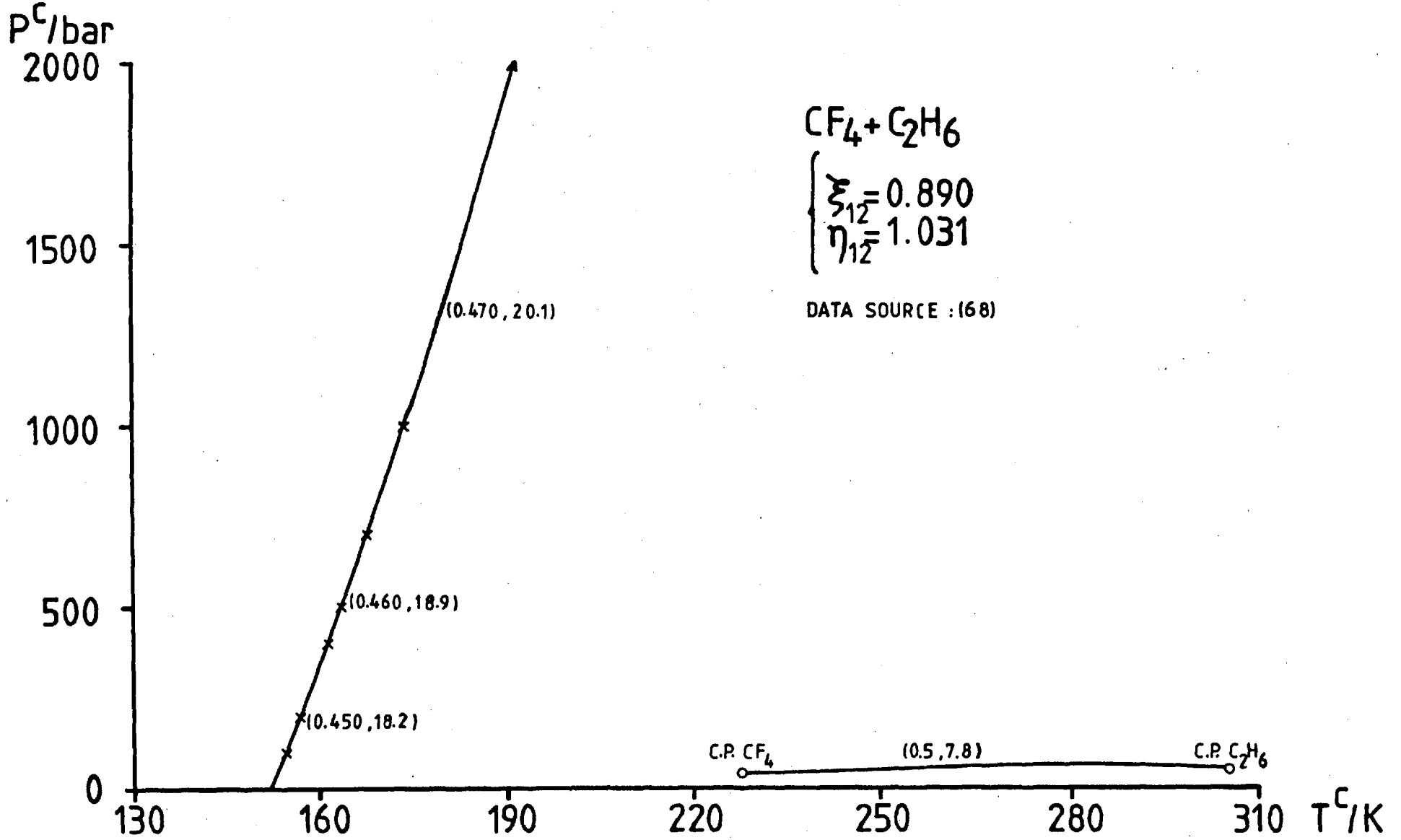


FIG. 10.2. Predicted (P^c-T^c) projection of the critical locus for the CF_4 + C_2H_6 system.

and η_{12}. In other words, it is unlikely that the same values of ξ_{12} and η_{12} will fit experimental critical data in regions of phase space very far apart.

Also depicted in Fig. 10.1 as a dot-dashed line is the three-phase (liquid-liquid-solid) line experimentally determined by Paas. According to him, the three-phase line and the liquid-liquid critical line should terminate at a critical end point at a pressure of ca. 1 900 bar.

The predicted curve for the CF_4 + C_2H_6 system is shown in Fig. 10.2. The liquid-liquid critical data determined by Peter (68) were used, and the values of the binary interaction parameters that provide the best fit of these data are ξ_{12} = 0.890, η_{12} = 1.031. This system is similar to the previous one, but the discrepancy between experimental and predicted values of the critical mole fraction is more noticeable: according to Peter, the critical mole fraction remains almost constant at $x^c \simeq 0.35$ up to 1 000 bar. For the same system, however, Croll and Scott (149) report a value of $x^c \simeq 0.50$ for the critical mole fraction at atmospheric pressure, which is closer to the predicted value.

The gas-liquid critical curve for this system was predicted by assuming again the same values of the binary interaction parameters, as determined from liquid-liquid critical data. The curve thus obtained is shown on the right-hand side of the diagram in Fig. 10.2: it has a shallow maximum at P^c = 54.7 bar and x^c = 0.24.

10.2.2 The systems carbon tetrafluoride + n-pentane, carbon tetrafluoride + n-hexane and carbon tetrafluoride + n-heptane

The predicted critical line for the CF_4 + n-C_5H_{12} system is shown in Fig. 10.3. The experimental critical points were obtained by Mukherjee (69) and the binary interaction parameters that give the best fit of these data are ξ_{12} = 0.803, η_{12} = 1.040. The curve has two branches: the branch starting at the critical point of pure n-pentane goes through a minimum critical temperature ($T^c \simeq 272$ K) at $P^c \simeq 500$ bar, and then proceeds to higher pressures and temperatures, being almost vertical at 2 000 bar. The other branch of the critical line,

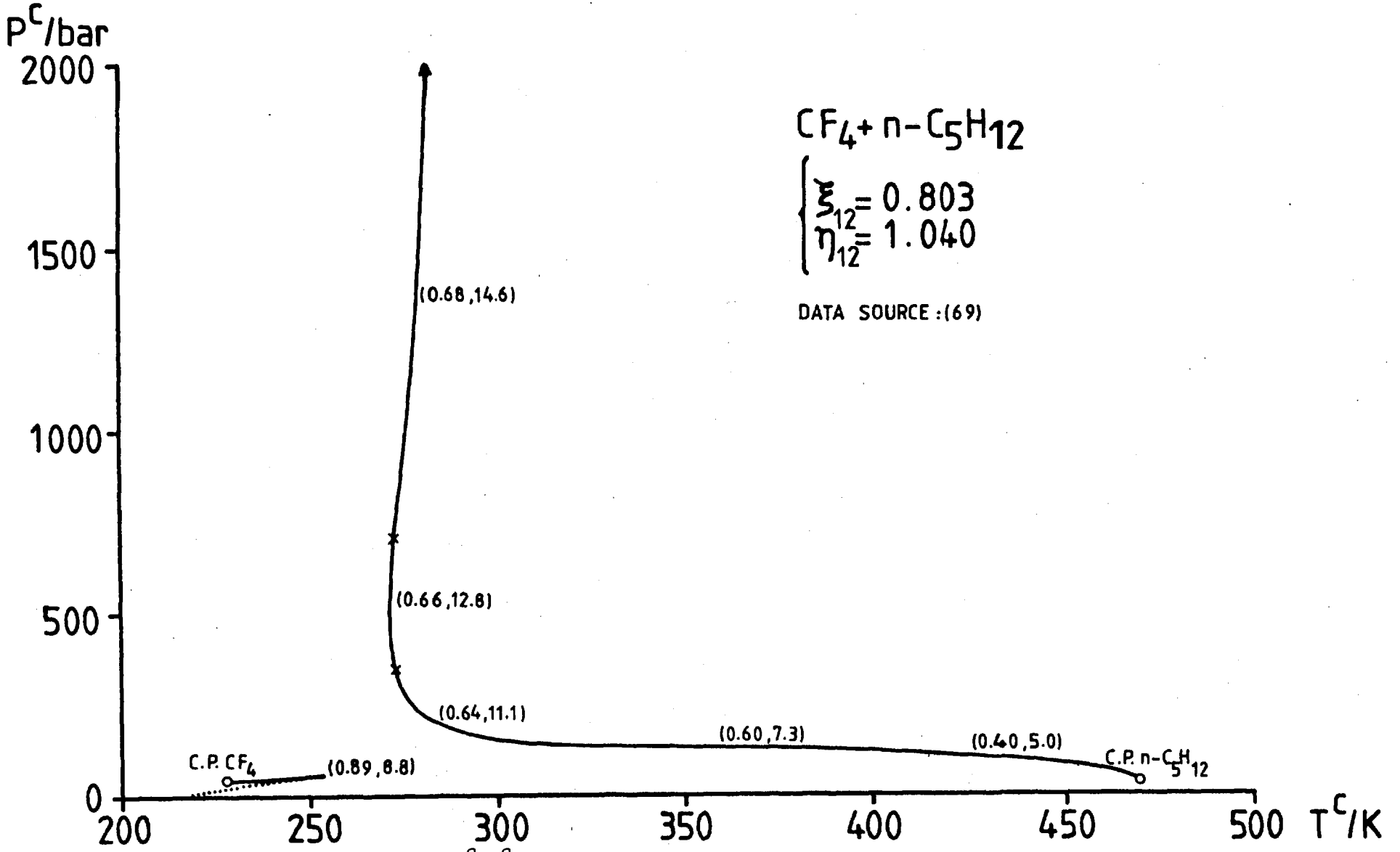


FIG. 10.3. Predicted (P^c-T^c) projection of the critical locus for the CF_4 + $n\text{-}C_5H_{12}$ system.

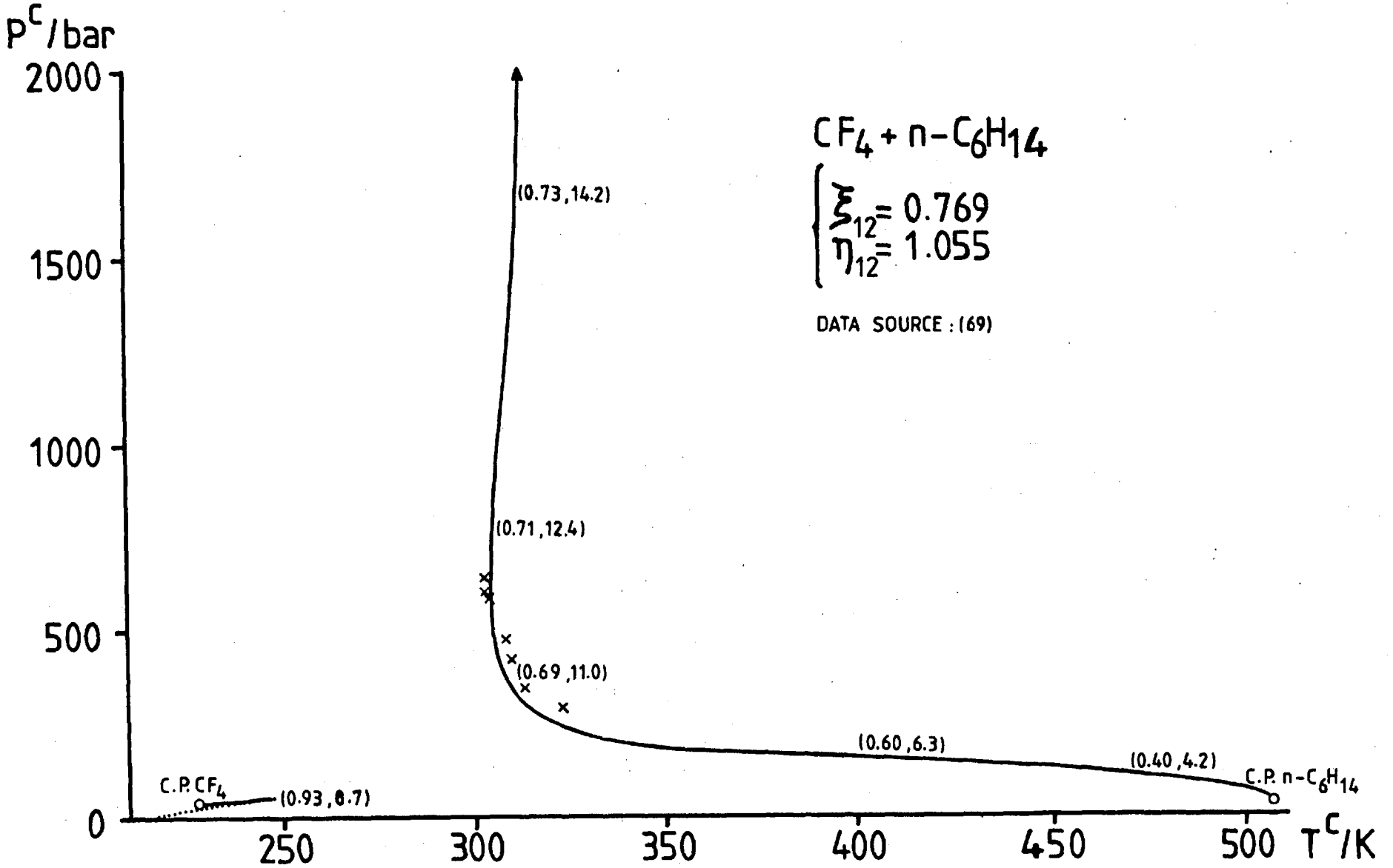


FIG. 10.4. Predicted (P^c-T^c) projection of the critical locus for the CF_4 + $n\text{-}C_6H_{14}$ system.

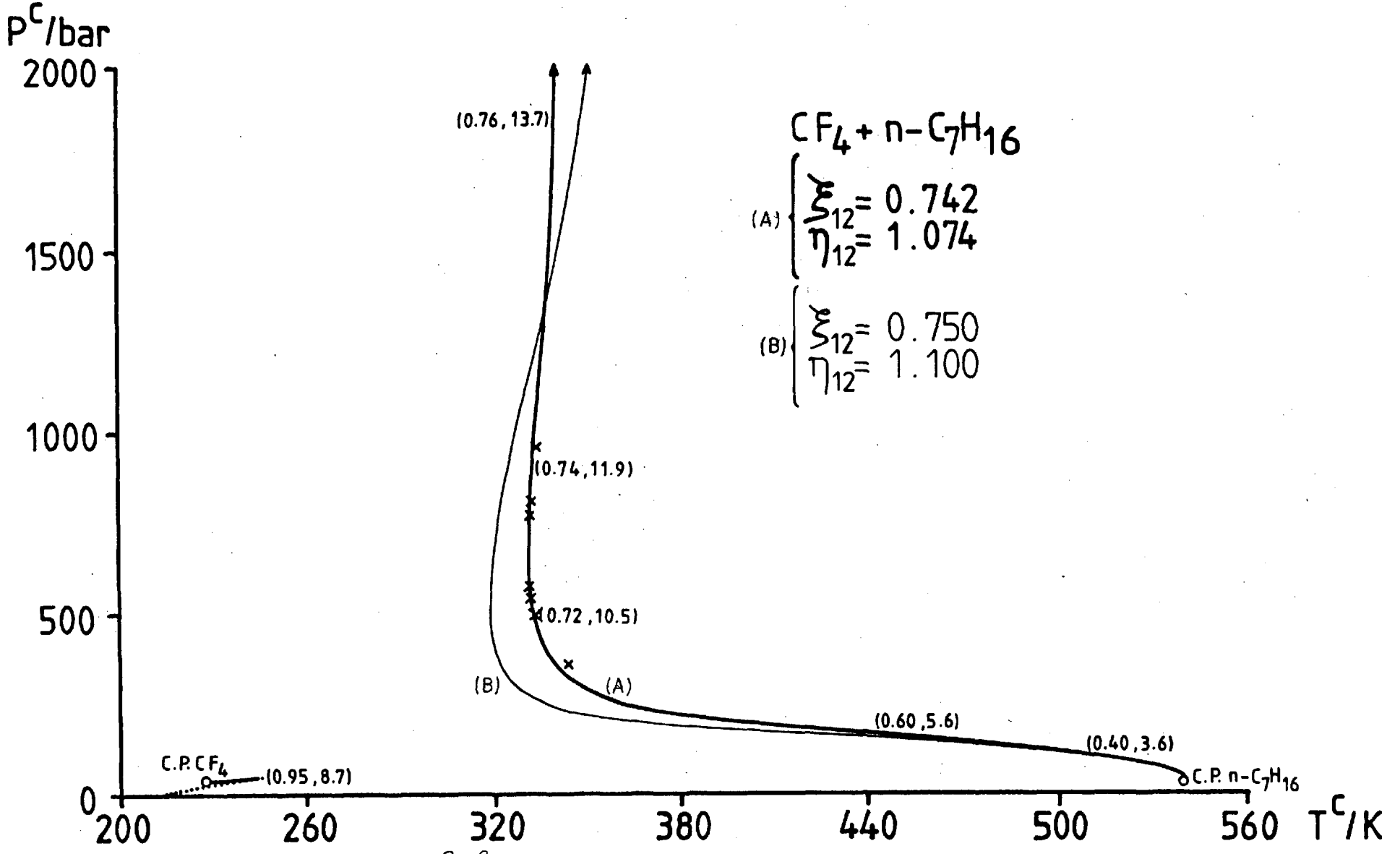


FIG. 10.5. Predicted (P^C-T^C) projection of the critical locus for the CF_4 + $n\text{-}C_7H_{16}$ system.

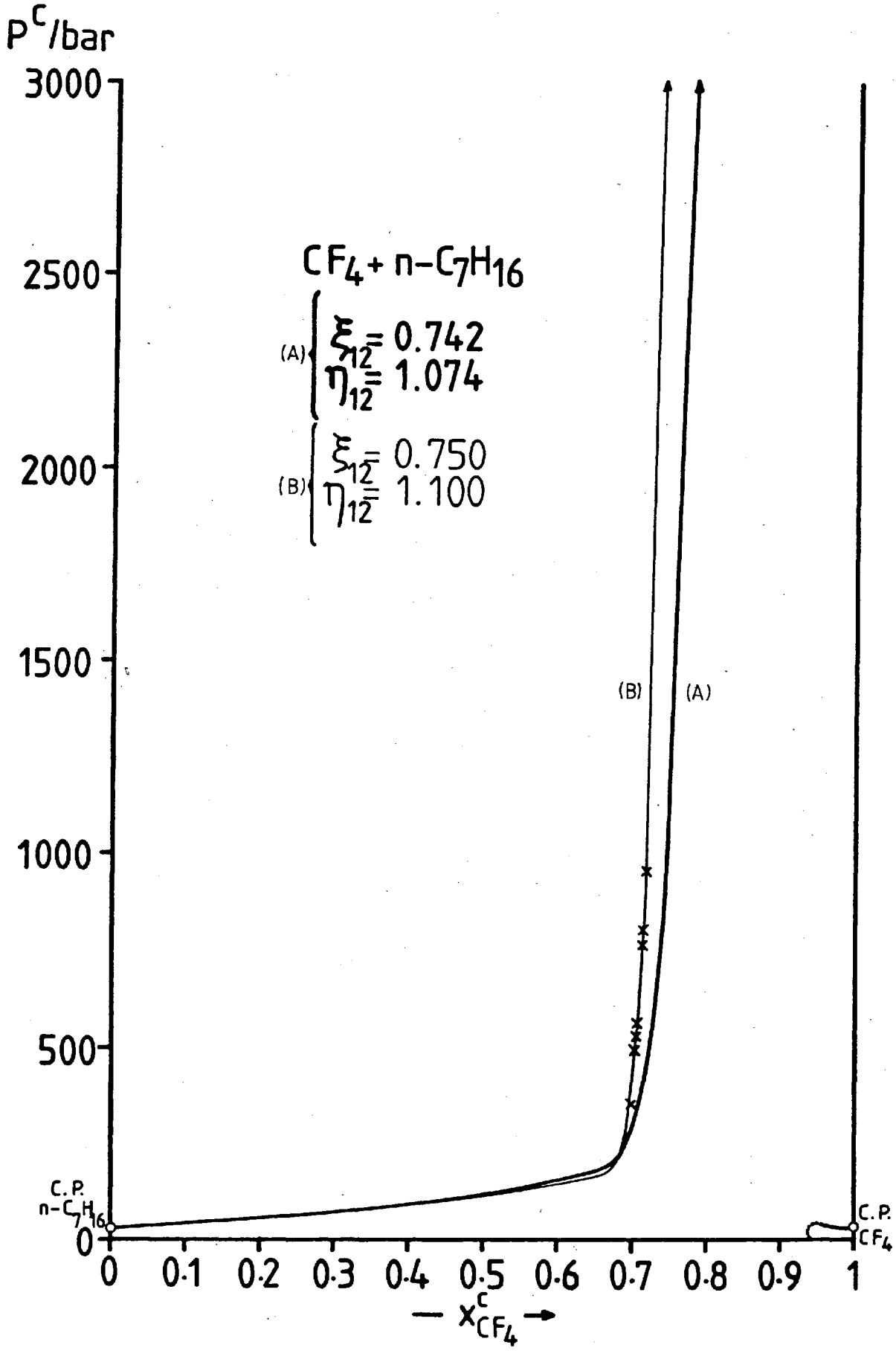


FIG. 10.6. Predicted (P^c-x^c) projection of the critical locus for the CF_4 + n-C_7H_{16} system.

which starts at the critical point of pure CF_4, goes through a "cusp-like" turning point at $x^c = 0.89$ and then proceeds to lower temperatures and negative pressures. This branch of the critical line is unstable for $x^c < 0.91$.

Similar results were obtained for the CF_4 + n-C_6H_{14} system, depicted in Fig. 10.4. The data were measured by Mukherjee (69), and the best fit was obtained with $\xi_{12} = 0.769$ and $\eta_{12} = 1.055$. This system gave the poorest results of all those investigated, possibly because the quality of the experimental data was not comparable to that of the other systems studied. The branch of the critical line starting at the critical point of pure n-hexane is displaced to higher temperatures, the minimum critical temperature being $T^c = 304$ K at $P^c = 620$ bar. The other branch of the critical line, which starts at the critical point of pure CF_4, is unstable for $x^c < 0.94$ and goes through a "cusp" at $x^c = 0.93$.

Finally, the results for the CF_4 + n-C_7H_{16} system measured as part of this investigation are shown in Figs. 10.5 (P^c-T^c diagram) and 10.6 (P^c-x^c diagram). The numerical values of the binary interaction parameters that gave the best fit on both the (P-T) and the (P-x) planes are not very different: $\xi_{12} = 0.742$, $\eta_{12} = 1.074$ for the (P-T) fit and $\xi_{12} = 0.750$, $\eta_{12} = 1.100$ for the (P-x) fit. The curves obtained differ significantly, however, especially in the region around the temperature minimum. This confirms the need for developing a procedure to obtain the binary interaction parameters by three-dimensional least-squares curve-fitting in (P-T-x) phase space. As with the two previous systems, the branch of the critical line starting at the critical point of pure CF_4 goes through a "cusp-like" turning point on the (P^c-T^c) diagram (see Fig. 10.5) which corresponds to a maximum critical pressure on the (P^c-x^c) diagram (see Fig. 10.6). The curve then proceeds to lower temperatures and negative pressures via a minimum in the critical mole fraction ($x^c = 0.938$) which can be seen clearly in Fig. 10.6. This branch is unstable for $x^c < 0.952$.

(.../)

10.3 Prediction of the Critical Lines for the Systems Carbon Tetrafluoride + Propane and Carbon Tetrafluoride + n-Butane

So far in this thesis, the binary interaction parameters ξ_{12} and η_{12} have been used simply as adjustable parameters whose numerical values are obtained by fitting available experimental data. With a "family" of binary systems in which one of the components is common and the others are members of a series of similar substances (e.g. the n-alkanes), it is well known that when the numerical values of ξ_{12} and η_{12} are plotted against a quantity characteristic of the member in the series definite trends are exhibited. Teja (150) has shown that, to a good approximation, the value of ξ_{12} can be correlated with the number of carbon atoms in the n-alkane molecule in "families" of systems such as CH_4 + n-alkanes, C_2H_6 + n-alkanes and CO_2 + n-alkanes. He also attempted to correlate ξ_{12} with various functions of the critical volume of the n-alkane, and obtained the best correlations when plotting ξ_{12} against $(V_2^c)^{\frac{1}{2}}$ or $(V_2^c)^{-\frac{1}{2}}$.

In order to obtain an estimate of the values of ξ_{12} and η_{12} for the binary systems CF_4 + C_3H_8 and CF_4 + n-C_4H_{10}, correlations similar to those proposed by Teja were used for the CF_4 + n-alkane "family" of systems. The results obtained confirmed that the correlation of ξ_{12} and η_{12} with the number of carbon atoms in the n-alkane molecule provided smooth curves suitable for interpolation, although the other correlations might have been used for this purpose. The binary interaction parameters for CF_4 + C_3H_8 and CF_4 + n-C_4H_{10} estimated using Fig. 10.7 are given in Table 10.1, together with the values previously obtained for the other members of the "family":

TABLE 10.1

Binary interaction parameters for CF_4 + n-alkane systems

System	ξ_{12}	η_{12}
CF_4 + CH_4	0.900	1.034
CF_4 + C_2H_6	0.890	1.031
CF_4 + C_3H_8	0.870*	1.030*
CF_4 + n-C_4H_{10}	0.840*	1.032*
CF_4 + n-C_5H_{12}	0.803	1.040
CF_4 + n-C_6H_{14}	0.769	1.055
CF_4 + n-C_7H_{16}	0.742	1.074

* = estimated values

(.../)

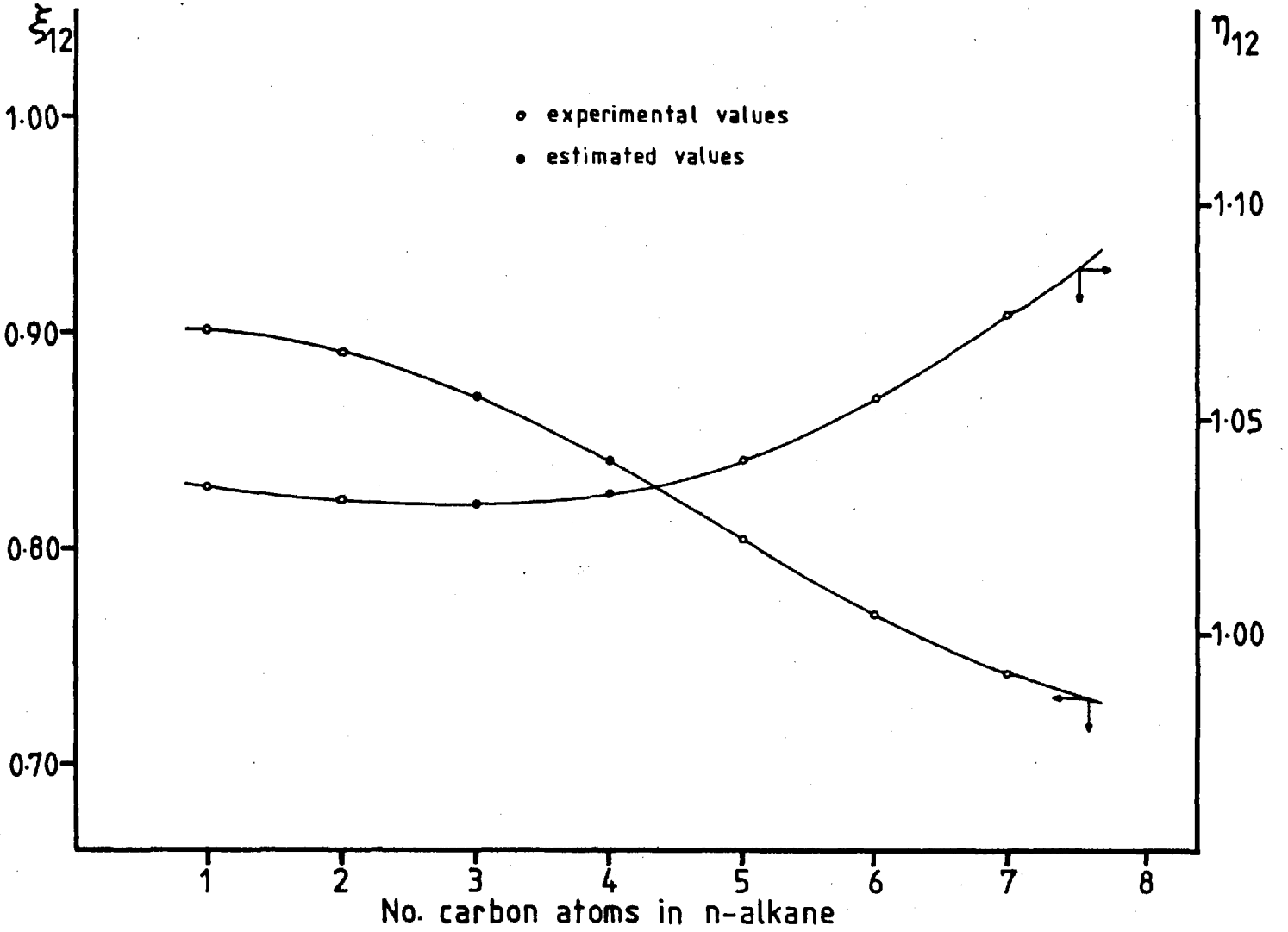


FIG. 10.7. Correlation of the binary interaction parameters ξ_{12} and η_{12} with the number of carbon atoms in the n-alkane molecule for CF_4 + n-alkane binary systems.

The critical curve predicted for the CF_4 + C_3H_8 system using the values of ξ_{12} and η_{12} given in Table 10.1 is shown in Fig. 10.8. It is similar to the curves shown in Figs. 10.1 and 10.2, in that this system shows a liquid-liquid critical curve distinct from the gas-liquid critical curve. There are, however, two important differences: the liquid-liquid critical curve is displaced to higher temperatures (closer to the critical point of pure CF_4) and goes through a minimum critical temperature (T^c = 184.1 K, P^c = 28.5 bar) before proceedings to higher pressures with $(dP/dT)^c > 0$.

The model still predicts the same type of critical line for the CF_4 + n-C_4H_{10} system, as shown in Fig. 10.9, but the shape of the liquid-liquid critical line is rather unusual. As the pressure is decreased, it goes successively through a minimum in T^c (T^c = 225.15 K, P^c = 277.5 bar), then a minimum in x^c ($x^c \simeq 0.605$, T^c = 229 K, P^c = 110 bar), and finally a "cusp-like" point (x^c = 0.692, T^c = 265.2 K, P^c = 58.26 bar), before turning towards lower temperatures and negative pressures. The diagram in Fig. 10.9 is misleading, since it appears that the liquid-liquid and gas-liquid critical curves intersect at low pressures. This is not so: the diagram represents the projection of the two critical curves on to the (P-T) plane, and the critical mole fraction at the "point of intersection" does not have the same value. Thus the curves are distinct and do not intersect in (P-T-x) space.

If the value of ξ_{12} is decreased slightly to ξ_{12} = 0.832 (keeping η_{12} constant), the predicted critical line is of the same type as that in Figs. 10.3 to 10.5 for the CF_4 + higher n-alkanes. This is shown in more detail in the enlarged diagram of Fig. 10.10, where the (P^c - T^c) curves have been plotted for the CF_4 + n-C_4H_{10} system in the vicinity of the critical point of pure CF_4 for ξ_{12} = 0.840, η_{12} = 1.032 (the estimated values) and for ξ_{12} = 0.832, η_{12} = 1.032. Clearly, this system represents the transition between the type of behaviour shown by the CF_4 + lower n-alkane systems and that of the CF_4 + higher n-alkane systems. The way in which this transition takes place as ξ_{12} is decreased is even more obvious from the (P^c - ρ^c) diagram for this system, shown in Fig. 10.11 for values of ρ^c greater than the density of pure CF_4.

(.../)

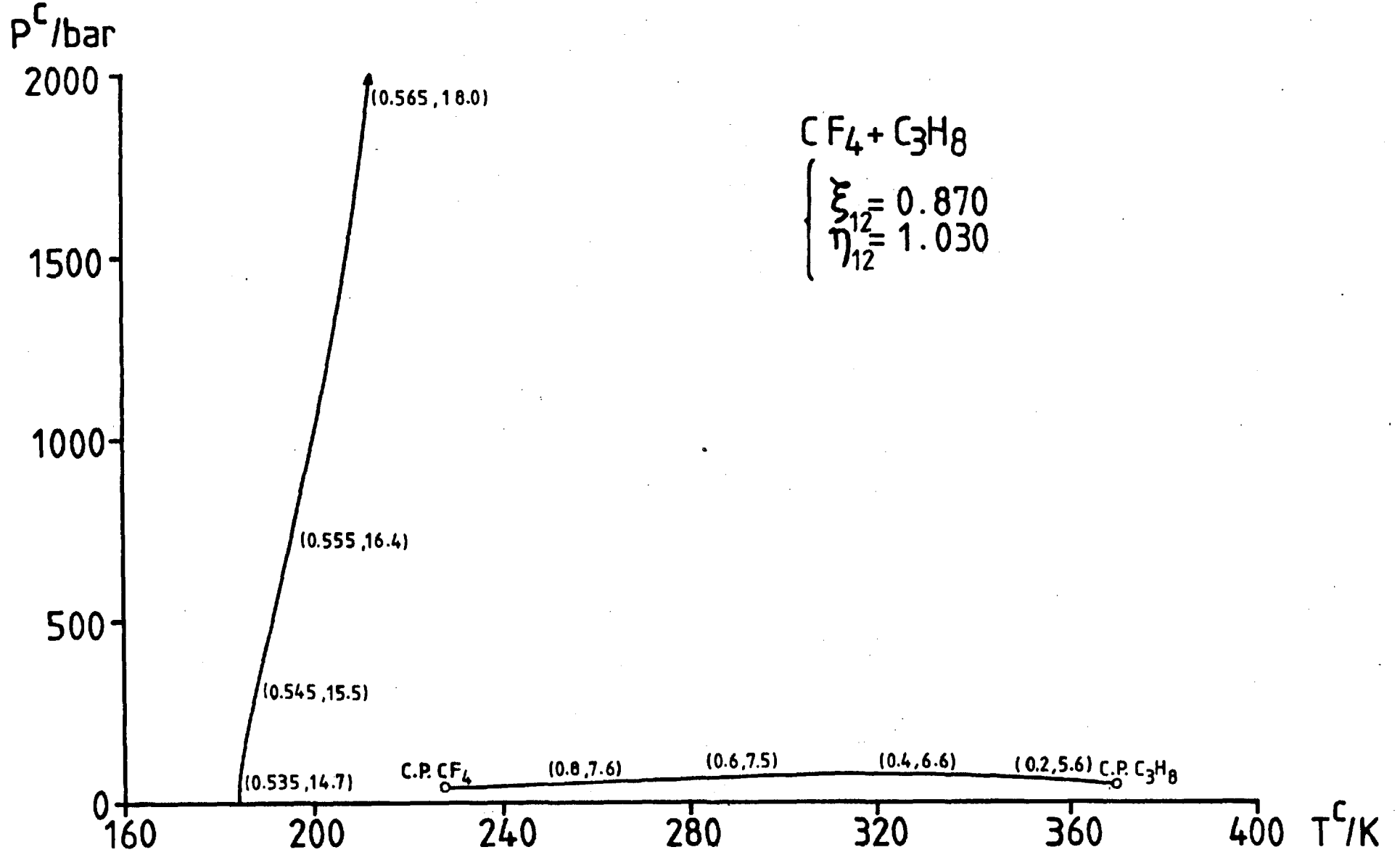


FIG. 10.8. Predicted (P^c-T^c) projection of the critical locus for the CF_4 + C_3H_8 system.

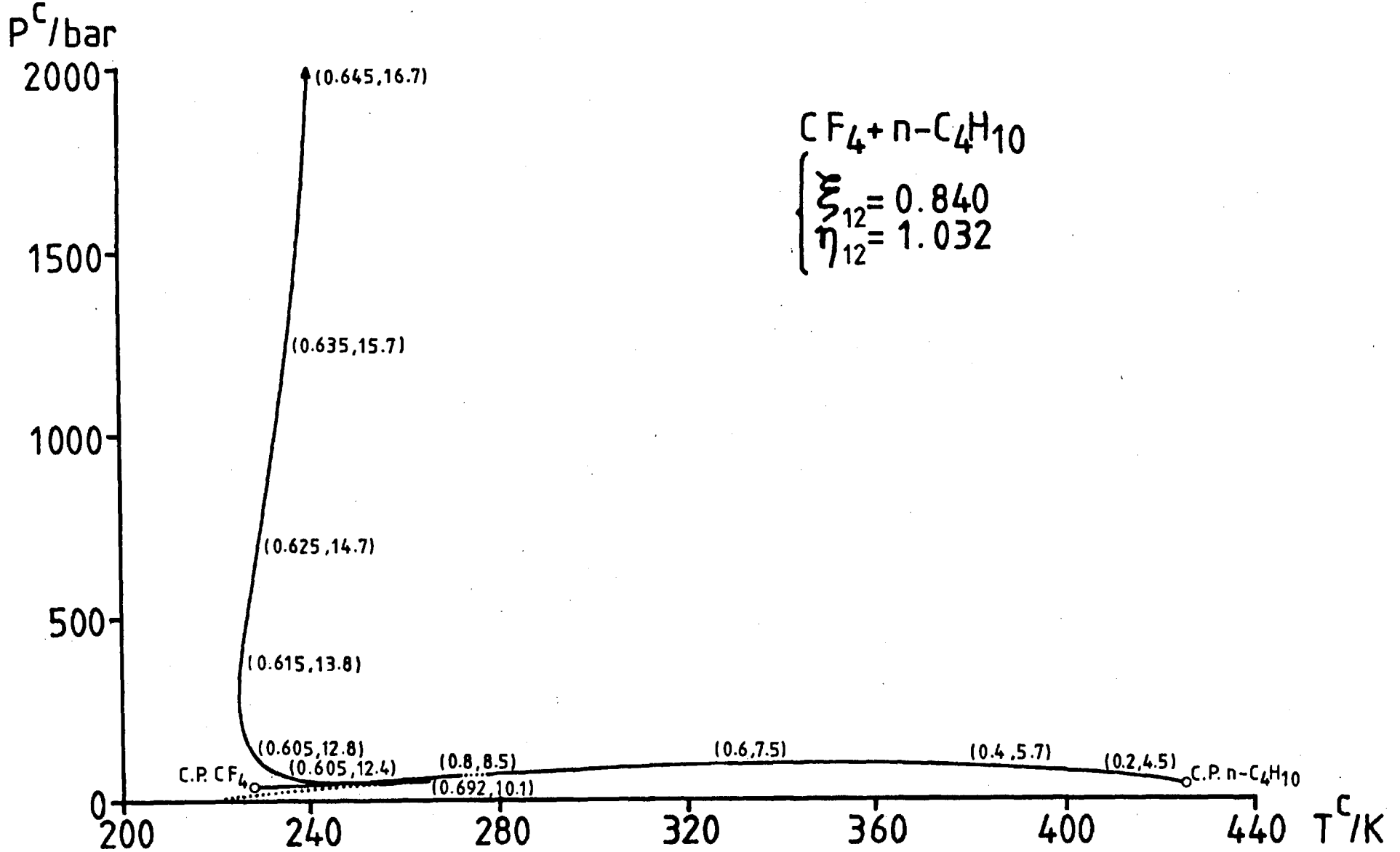


FIG. 10.9. Predicted (P^C-T^C) projection of the critical locus for the CF_4 + n-C_4H_{10} system.

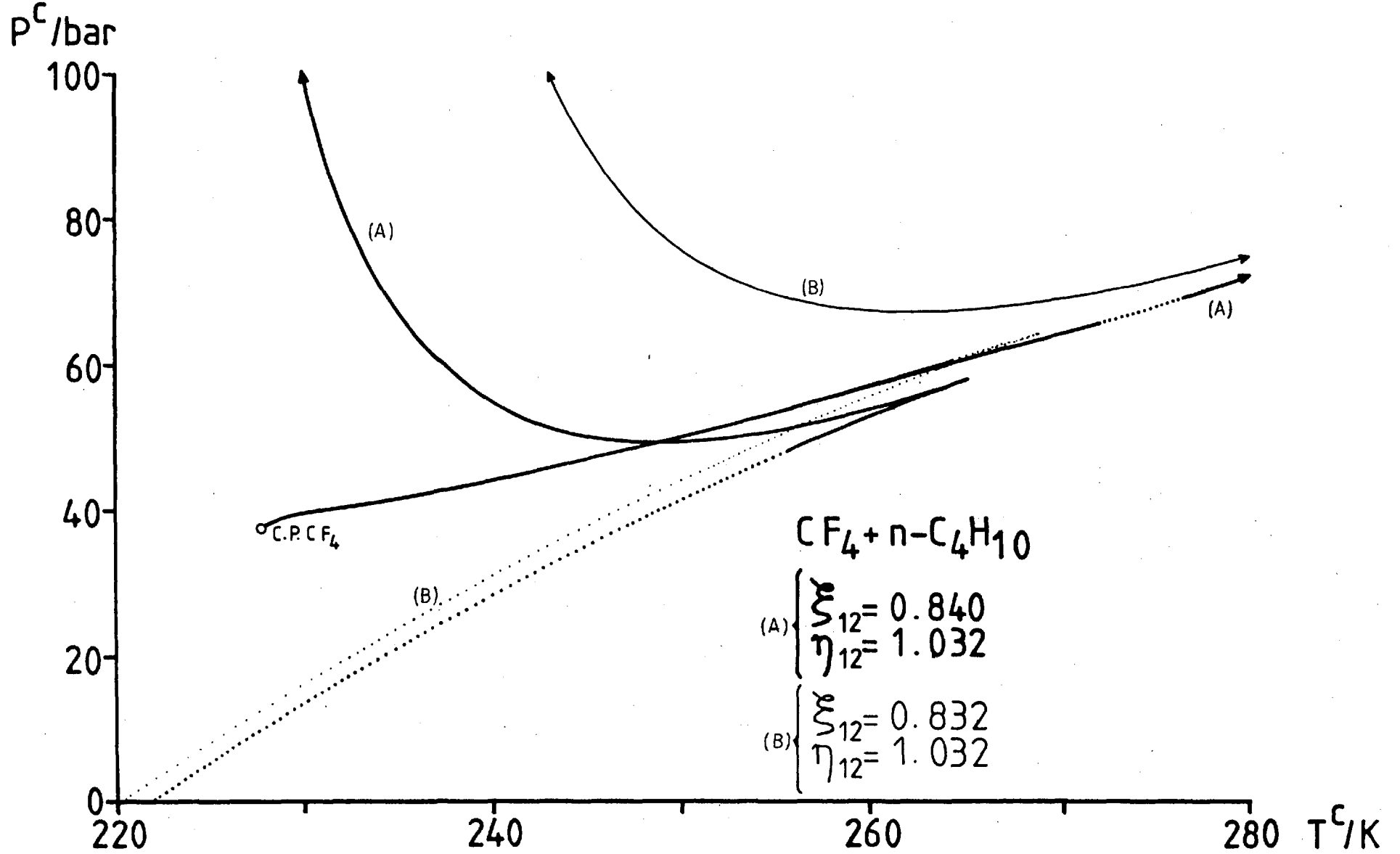


FIG. 10.10. Enlarged view of Fig. 10.9 in the vicinity of the critical point of pure CF_4.

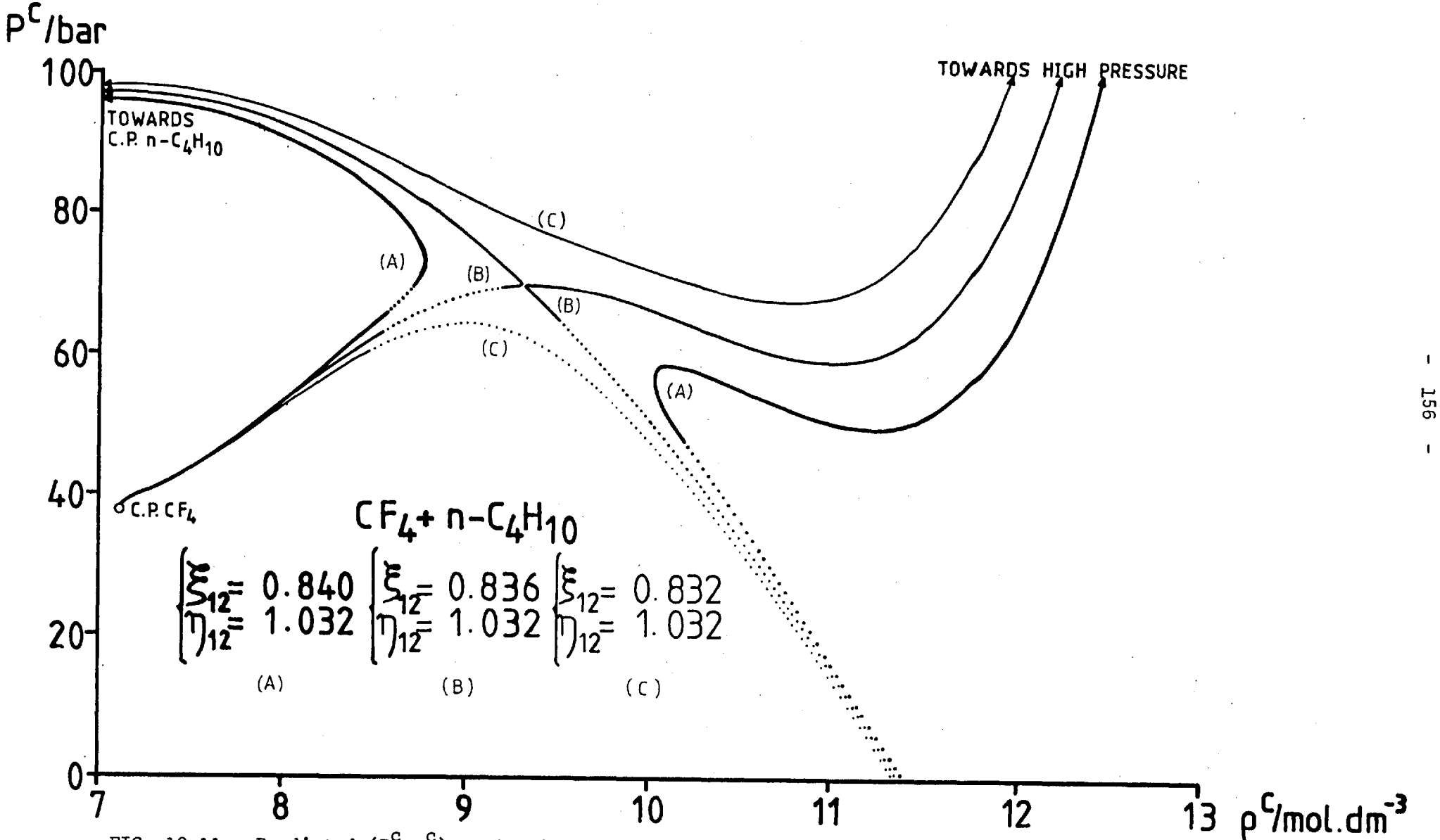


FIG. 10.11. Predicted (P^c-ρ^c) projections of the critical locus for the CF_4 + n-C_4H_{10} system in the vicinity of the critical point of pure CF_4.

On this diagram, it can be seen that the liquid-liquid (high density) branch of the critical curve approaches the gas-liquid (low density) branch ($\xi_{12} = 0.840$), until the two branches eventually merge into each other ($\xi_{12} \simeq 0.836$). If ξ_{12} is further decreased, the critical curve again separates into two branches, but of a different type ($\xi_{12} = 0.832$): one of these branches starts at the critical point of pure n-C_4H_{10} and goes towards high densities and pressures (via a minimum in critical temperature, not shown in Fig. 10.11), whilst the other branch starts at the critical point of pure CF_4 and goes through the usual "cusp-like" turning point (on the P^c - T^c projection) before proceeding to lower temperatures and negative pressures (higher densities). Hence the predictions of the van der Waals one-fluid model confirm the views put forward by Schneider concerning the nature of this transition (see chapter 2).

The enlarged diagram in Fig. 10.10 reveals a possible inconsistency in the algorithm. The inconsistency concerns the "cusp" observed in some of the (P^c - T^c) diagrams in this chapter, and its relation to the stable and unstable portions of the computed critical lines. In mathematical terms, the critical line of a binary system is a curve in (P-T-x) space defined by the two implicit equations

$$\left.\begin{aligned} G^c_{2x}[P,T,x] &= 0 \\ \text{and} \qquad G^c_{3x}[P,T,x] &= 0 \end{aligned}\right\} \quad . \tag{10-1}$$

Differentiation of these two equations gives

$$\left.\begin{aligned} (dG_{2x} &= 0 = V_{2x}\,dP - S_{2x}\,dT + G_{3x}\,dx)^c \\ \text{and} \qquad (dG_{3x} &= 0 = V_{3x}\,dP - S_{3x}\,dT + G_{4x}\,dx)^c \end{aligned}\right\} \quad . \tag{10-2}$$

These two simultaneous equations can be solved to give the expressions for the derivatives along the critical line:

$$\left(\frac{dP}{dT}\right)^c = \left(\frac{S_{2x}}{V_{2x}}\right)^c \quad , \tag{10-3}$$

$$\left(\frac{dP}{dx}\right)^c = \left(\frac{S_{2x}G_{4x}}{S_{3x}V_{2x} - S_{2x}V_{3x}}\right)^c \qquad (10\text{-}4)$$

and

$$\left(\frac{dT}{dx}\right)^c = \left(\frac{V_{2x}G_{4x}}{S_{3x}V_{2x} - S_{2x}V_{3x}}\right)^c, \qquad (10\text{-}5)$$

the three derivatives being related by

$$\left(\frac{dP}{dT}\right)^c = \frac{(dP/dx)^c}{(dT/dx)^c} . \qquad (10\text{-}6)$$

If the critical curve in (P-T-x) space is to show a "cusp" only on its projection on the (P-T) plane, then the projection of the curve on each of the other two planes must go through a stationary point. Hence at the "cusp"

$$\left(\frac{dP}{dx}\right)^c = 0 \quad \underline{\text{and}} \quad \left(\frac{dT}{dx}\right)^c = 0. \qquad (10\text{-}7)$$

From equations (10-4) and (10-5), this is equivalent to the condition:

$$G_{4x} = 0. \qquad (10\text{-}8)$$

But this condition represents the transition from unstable to metastable and stable critical points, which should therefore be associated with a "cusp" on the (P-T) projection of the critical line. This is clearly not the case in Fig. 10.10, nor in Figs. 10.3 to 10.5. The reasons for this inconsistency are not immediately obvious; although subroutine STABLE was checked, it is possible that an error may have been overlooked. Since G_{4x} is obtained from G_{3x} by numerical differentiation, the inconsistency is more likely to be caused by rounding errors in the numerical method than by thermodynamic inconsistencies in the model. Clearly, further work is needed to determine the cause of this problem.

(.../)

10.4 Predicted Critical Behaviour at Very High Pressures

The predictions of the van der Waals one-fluid model were extended to very high pressures and densities by following the branches of the various critical lines in Figs. 10.1 to 10.5, 10.8 and 10.9, up to a maximum pressure of 10 kbar. The resulting curves are labelled from 1 to 7 in Fig. 10.12, in accordance with the number of carbon atoms in the n-alkane molecule. Curves 1 to 4 represent liquid-liquid critical curves, whereas curves 5 to 7 could be termed gas-gas critical curves, since they start at the critical point of the corresponding pure n-alkane and go through a minimum in critical temperature before proceeding to high pressures.

Curves 1 and 2 show the normal type of behaviour, i.e. upper critical solution temperatures (UCST) that rise with increasing pressure, $(dP/dT)^c$ remaining positive up to the highest pressure attained. Curve 3, however, goes through a maximum in temperature ($T^c \approx 233.8$ K, $P^c \approx$ 7 kbar) above which the UCST decreases with increasing pressure. According to Schneider (9), this type of behaviour has not yet been found experimentally.

Curves 4 to 7 are even more unusual. The model predicts that these systems will also go through a maximum in critical temperature, at pressures of the order of 2 to 3 kbar. As the pressure is increased above that corresponding to this maximum temperature, the UCST will decrease, until the curves eventually go through a maximum in critical pressure located at about 7 to 8 kbar. Finally, as the mole fraction of CF_4 is further increased, the curves turn sharply down towards very low temperatures (ca. 60 K) and negative pressures. Obviously the portions of curves 4 to 7 to the left of the pressure maxima represent lower critical solution temperatures (LCST).

Not much significance should be attached to the predicted critical behaviour at very low temperatures, because this region of the phase diagram is probably outside the range of validity of the equation of state for the reference substance. Even if the behaviour of the real systems is as depicted in Fig. 10.12, the critical curves are much more likely to terminate at critical end points of the type S_2-L_1-L_2

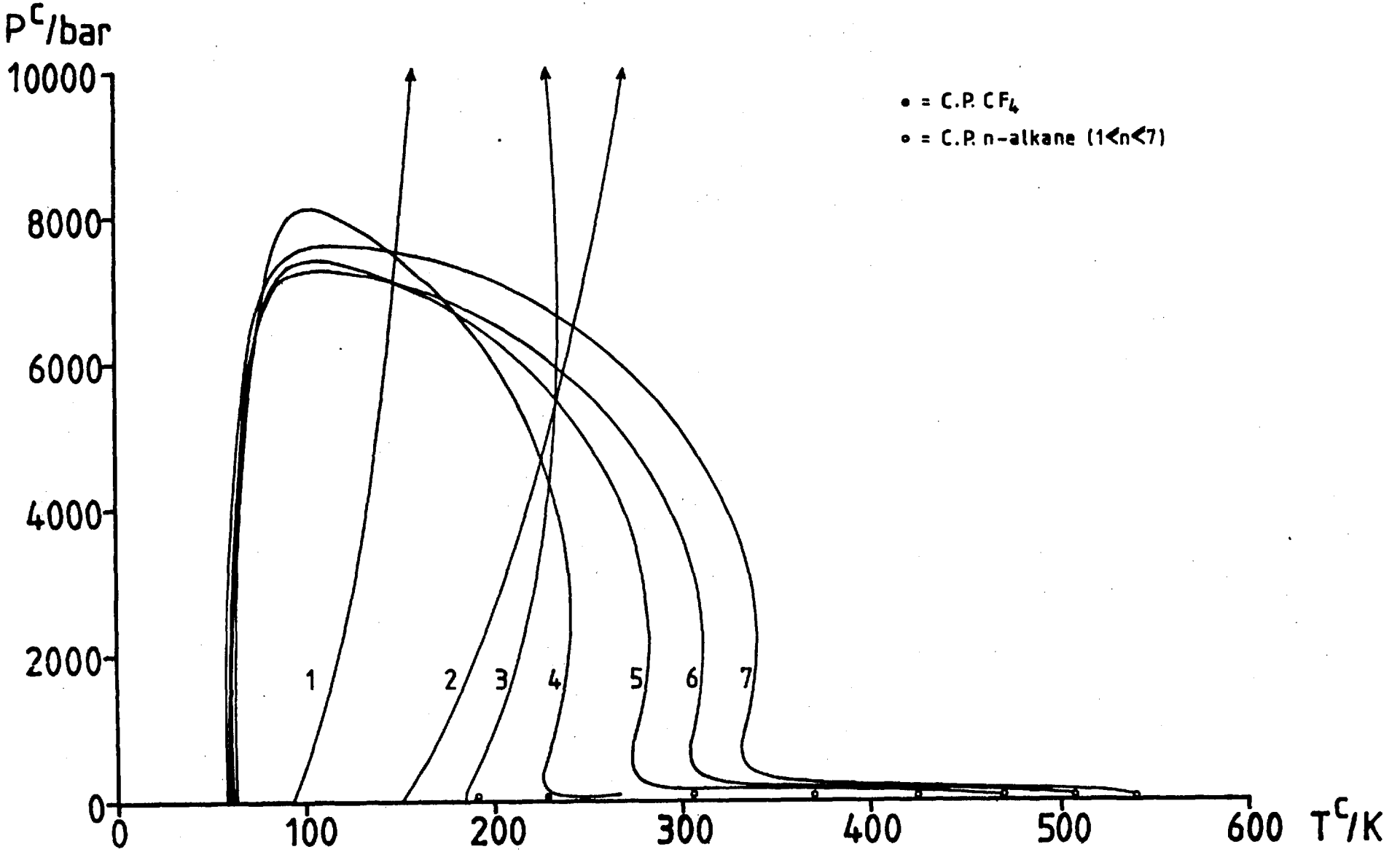


FIG. 10.12. Predicted behaviour of CF_4 + n-alkane systems at very high pressures.

(or S_2-G_1-G_2) long before reaching the maxima in pressure (25).

The predicted maxima in critical temperature cannot, however, be discarded so easily, because the results are well within the range of validity of the equation of state for the reference substance. Thus two possibilities arise:

1) The prediction of the model is incorrect, and the actual critical curves continue to higher temperatures as the critical pressure is increased, rather than going through temperature maxima. This is the normal behaviour observed for this type of system. On the other hand, it seems unlikely that the van der Waals one-fluid model will fail so drastically in view of the good results achieved at lower pressures.

2) The behaviour depicted in Fig. 10.12 corresponds to the actual behaviour of the real systems. Although there is no experimental evidence to support this, it is nevertheless thermodynamically possible (6). Since S^c_{2x} must be negative for a UCST (151), it follows from equation (10-3) that all that is required is that V^c_{2x} changes sign from negative to positive as the pressure is increased, being exactly zero at the maximum critical temperature.

These two possibilities can only be resolved when further experimental evidence at higher pressures becomes available for these systems.

10.5 Conclusions and Suggestions for Further Work

An algorithm based on the van der Waals one-fluid model, originally developed by Teja and Rowlinson (85, 86), was used for the prediction of critical lines in binary mixtures of carbon tetrafluoride and n-alkanes. The method has been improved considerably in terms of flexibility, range of application and efficiency.

In its original form, the calculation procedure made use of the molecular shape factor equations of Leach and Leland (124) to account for departures from the simple principle of corresponding states caused by non-sphericity of the component molecules. The poor results

obtained with this version of the program, however, raised serious doubts as to the validity of these equations, and a simplified version of the algorithm had to be used in which the shape factors were set to unity. It is becoming increasingly clear that the present shape factor equations are inadequate at both high and low temperatures, and that improved equations valid over a much wider temperature range are urgently required. Work should therefore be directed towards obtaining the extremely accurate experimental data on non-spherical molecules which are required in order to produce equations which can be used with confidence in the knowledge that this will not yield physically absurd results.

The simplified version of the algorithm was used to correlate the existing critical data on CF_4 + n-alkane mixtures and the results obtained were surprisingly good. In particular, the method correctly predicts the experimentally observed liquid-liquid and gas-gas critical lines for these systems. By correlating the binary interaction parameters with the number of carbon atoms in the n-alkane molecule, it was possible to obtain estimates for the numerical values of ξ_{12} and η_{12} for the CF_4 + C_3H_8 and CF_4 + n-C_4H_{10} systems, for which no experimental critical data exist at present. The critical locus predicted for the latter system is particularly interesting, since it clearly demonstrates the transition from liquid-liquid to gas-gas equilibria. Experimental critical data on this system would certainly provide invaluable information concerning the nature of this transition, as well as providing a means of testing the predicting capabilities of the van der Waals one-fluid model.

The calculation procedure was extended to its limits when the high-pressure branches of the predicted critical lines in the CF_4 + n-alkane systems were followed to pressures as high as 10 kbar. This produced some unexpected results, such as the prediction of UCST that go through a maximum as the pressure is increased. Although such behaviour has never been observed experimentally, it is not thermodynamically impossible, and further experimental evidence at higher pressures is needed to resolve this problem.

(.../)

The present structure of the algorithm, even in its simplified version, leaves much to be desired. Further work should be directed towards improving the stability tests, and in particular the inclusion in the procedure of van Konynenburg's method for the computation of critical end points (12) seems essential, since this would make it possible to distinguish between the stable and metastable portions of the computed curves. It would also be advantageous to compute analytically the derivatives given in equation (10-3) to (10-5), since this would provide an extremely useful test for the thermodynamic consistency of the algorithm.

The present minimisation subroutine fails to find a solution of the criticality conditions whenever the critical mole fraction x^c goes through an extreme value because in the search procedure the mole fraction is varied parametrically. In order to overcome this problem, additional work should be directed towards developing a more general search procedure, which would compute all the local minima of a given objective function.

Finally, as has been mentioned before, the present method of trial-and-error curve fitting is not only tedious and inaccurate, but can only be used in two dimensions. If this algorithm is to be used for practical applications, the structure of the program should be changed so as to allow for the determination of the best values of ξ_{12} and η_{12} by least-squares curve fitting in two and/or three dimensions, in order to cover all the possible types of critical data for binary mixtures.

REFERENCES

(1) ROWLINSON, J.S., and WATSON, I.D., Chem. Engng. Sci., 24, 1565 (1969).

(2) SCOTT, R.L., J. Phys. Chem., 62, 136 (1958).

(3) SIDERAS, G.M., M.Sc. Thesis, University of London (1970).

(4) ROWLINSON, J.S., "Liquids and Liquid Mixtures", 2nd edition, Butterworths, London (1969).

(5) SCHNEIDER, G.M., Ber. Bunsenges. phys. Chem., 70, 497 (1966).

(6) SCHNEIDER, G.M., in "Advances in Chemical Physics", vol. XVII, pp. 1-42, Interscience Publishers, John Wiley (1970).

(7) SCHNEIDER, G.M., Fortschritte der Chemischen Forschung, 13, 559 (1970).

(8) SCHNEIDER, G.M., in "Water. A Comprehensive Treatise", vol.2, pp. 381-404, ed. Felix Franks, Plenum Press (1973).

(9) SCHNEIDER, G.M., in "Chemical Thermodynamics", vol.2, pp. 105-146, Specialist Periodical Reports, The Chemical Society, London (1978).

(10) HICKS, C.P., and YOUNG, C.L., Chemical Reviews, 75, 119 (1975).

(11) PRAUSNITZ, J.M., Advances in Chemical Engineering, 7, 139 (1968).

(12) Van KONYNENBURG, P.H., Ph.D. Thesis, University of California, Los Angeles (1968).

(13) MICHAELS, S., GREEN, M.S., and LARSEN, S.Y., "Equilibrium Critical Phenomena in Fluids and Mixtures: A Comprehensive Bibliography with Key-Word Descriptors", N.B.S. Special Publication 327, Washington (1970).

(14) KUENEN, J.P., Commun. phys. Lab. Univ. Leiden, No. 4 (1892).

(15) ONNES, H.K., and KEESOM.,W.H., Commun. phys. Lab. Univ. Leiden, Nos. 96a, 96b, 96c (1906); Suppl. Nos. 15, 16 (1907); Koninkl. Ned. Akad. Wetenschap. Proc., Ser. B, 9, 786 (1907); 10, 231 (1907).

(16) LINDROOS, A.E., and DODGE, B.F., Chem. Engng. Prog. Symp. Ser. No. 3, 48, 10 (1952).

(.../)

(17) MICHELS, A., DUMOULIN, E., and van DIJK, J.J., Physica, 25, 840 (1959); 27, 886 (1961).

(18) SCOTT, R.L., and van KONYNENBURG, P.H., Discuss. Faraday Soc., 49, 87 (1970).

(19) SCOTT, R.L., Ber. Bunsenges. phys. Chem., 76, 296 (1972).

(20) Van der WAALS, J.D., Zittingsversl. Koninkl. Akad. Wetenschap. Proc., Ser. B, 133 (1894).

(21) KRICHEVSKII, I.R., Acta phys.-chim. URSS, 12, 480 (1940).

(22) TSIKLIS, D.S., Dokl. Akad. Nauk SSSR, 86, 1159 (1952).

(23) ZERNIKE, J., "Chemical Phase Theory", Kluwer, Antwerp (1956).

(24) De SWAAN ARONS, J., and DIEPEN, G.A.M., J. Chem. Phys., 44, 2322 (1966).

(25) STREETT, W.B., Can. J. Chem. Engng., 52, 92 (1974).

(26) TSIKLIS, D.S., Dokl. Akad. Nauk SSSR, 91, 1361 (1953).

(27) TSIKLIS, D.S., and ROTT, L.A., Russ. Chem. Rev., 36, 351 (1967).

(28) MASLENNIKOVA, V.Ya., GORJUNOVA, N.P., and TSIKLIS, D.S., Dokl. Akad. Nauk SSSR, 178, 886 (1968).

(29) TSIKLIS, D.S., MASLENNIKOVA, V.Ya., and GORJUNOVA, N.P., Zhur. Fiz. Khim., 41, 1804 (1967).

(30) LENTZ, H., and FRANCK, E.U., Ber. Bunsenges. phys. Chem., 73, 28 (1969).

(31) STREETT, W.B., Chem. Engng. Prog. Symp. Ser. No. 81, 63, 37 (1967).

(32) STREETT, W.B., Trans. Faraday Soc., 65, 696 (1969).

(33) TRAPPENIERS, N.J., and SCHOUTEN, J.A., Physics Letters, 27a, 340 (1968).

(34) STREETT, W.B., J. Chem. Phys., 46, 3282 (1967).

(35) SCHNEIDER, G.M. ALWANI, Z., HEIM, W., HORVATH, E., and FRANCK, E.U., Chem. Ingr. Tech., 39, 649 (1967).

(36) TSIKLIS, D.S., and MASLENNIKOVA, V.Ya., Dokl. Akad. Nauk SSSR, 161, 645 (1965).

(.../)

(37) TÖDHEIDE, K., and FRANCK, E.U., Z. phys. Chem., 37, 387 (1963).

(38) TAKENOUCHI, S., and KENNEDY, G.C., Amer. J. Sci., 262, 1055 (1964).

(39) DANNEIL, A., TÖDHEIDE, K., and FRANCK, E.U., Chem. Ingr. Tech., 39, 816 (1967).

(40) TSIKLIS, D.S., and MASLENNIKOVA, V.Ya., Dokl. Akad. Nauk SSSR, 157, 426 (1964).

(41) CONNOLLY, J.F., J. Chem. Engng. Data, 11, 13 (1966).

(42) PETER, K., Diplomarbeit, University of Karlsruhe, Germany (1968).

(43) REBERT, C.J., and HAYWORTH, K.E., A.I.Ch.E. Journal, 13, 118 (1967).

(44) REBERT, C.J., and KAY, W.B., A.I.Ch.E. Journal, 5, 285 (1959).

(45) ALWANI, Z., and SCHNEIDER, G.M., Ber. Bunsenges. phys. Chem., 71, 633 (1967).

(46) ALWANI, Z., and SCHNEIDER, G.M., Ber. Bunsenges. phys. Chem., 73, 294 (1969).

(47) ALWANI, Z., Ph.D. Thesis, University of Karlsruhe, Germany (1969).

(48) SWINTON, F.L., in "Chemical Thermodynamics", vol. 2, pp. 147-173, Specialist Periodical Reports, The Chemical Society, London (1978).

(49) THORP, N., and SCOTT, R.L., J. Phys. Chem., 60, 670 (1956).

(50) CROLL, I.M., and SCOTT, R.L., J. Phys. Chem., 62, 954 (1958).

(51) SIMON, M., and KNOBLER, C.M., J. Chem. Thermodynamics, 3, 657 (1971).

(52) LEWIS, K.L., and STAVELEY, L.A.K., J. Chem. Thermodynamics, 7, 847 (1975).

(53) DUNLAP, R.D., BEDFORD, R.G., WOODBREY, J.C., and FURROW, S.D., J. Amer. Chem. Soc., 81, 2927 (1959).

(54) WILLIAMSON, A.G., and SCOTT, R.L., J. Phys. Chem., 65, 275 (1961).

(55) BEDFORD, R.G., and DUNLAP, R.D., J. Amer. Chem. Soc., 80, 282 (1958).

(56) DYKE, D.E.L., ROWLINSON, J.S., and THACKER, R., Trans. Faraday Soc., 55, 903 (1959).

(.../)

(57) DOUSLIN, D.R., HARRISON, R.H., and MOORE, R.T., J. Phys. Chem., 71, 3477 (1967).

(58) DANTZLER-SIEBERT, E.M., and KNOBLER, C.M., J. Phys. Chem., 75, 3863 (1971).

(59) BATTINO, R., and CLEVER, H.L., Chemical Reviews, 66, 395 (1966).

(60) MASLENNIKOVA, V.Ya., EMELYANOVA, E.A., and TSIKLIS, D.S., Russ. J. Phys. Chem., 45, 448 (1971).

(61) JORDAN, L.W., and KAY, W.B., Chem. Engng. Prog. Symp. Ser. No. 44, 59, 46 (1963).

(62) HICKS, C.P., and YOUNG, C.L., Trans Faraday Soc., 67, 1605 (1971).

(63) BARBER, J., Ph.D. Thesis, Ohio State University (1968).

(64) MOUSA, A.E.H.N., KAY, W.B., and KREGLEWSKI, A., J. Chem. Thermodynamics, 4, 301 (1972).

(65) PETER, K.H., PAAS, R., and SCHNEIDER, G.M., J. Chem. Thermodynamics, 8, 731 (1967).

(66) PAAS, R., PETER, K.H., and SCHNEIDER, G.M., J. Chem. Thermodynamics, 8, 741 (1976).

(67) PAAS, R., Ph.D. Thesis, University of Bochum, West Germany (1977).

(68) PETER, K.H., Ph.D. Thesis, University of Bochum, West Germany (1974).

(69) MUKHERJEE, A., Ph.D. Thesis, University of London (1978).

(70) HUDSON, G.H., and McCOUBREY, J.C., Trans. Faraday Soc., 56, 761 (1960).

(71) MUNN, R.J., Trans. Faraday Soc., 57, 187 (1961).

(72) GOOD, R.J., and HOPE, C.J., J. Chem. Phys., 53, 540 (1970).

(73) SIKORA, P.T., J. Phys. B: Atom. Molec. Phys., 3, 1475 (1970).

(74) HIZA, M.J., and DUNCAN, A.G., A.I.Ch.E. Journal, 16, 733 (1970).

(75) KONG, C.L., J. Chem. Phys., 59, 2464 (1973).

(76) PESUIT, D.R., Ind. Eng. Chem. Fundam., 17, 235 (1978).

(77) REYNOLDS, R.G., Ph.D. Thesis, University of London (1964).

(.../)

(78) GRAHAM, E.B., Ph.D. Thesis, University of London (1958).

(79) BETT, K.E., and REYNOLDS, R.G., J. of Scientific Instruments, 42, 642 (1965).

(80) SAVILLE, G., in "Experimental Thermodynamics, Volume II: Experimental Thermodynamics of Non-Reacting Fluids", Chap. 6, Le Neindre, B., and Vodar, B., ed., Butterworths, London (1975).

(81) HILL, T.L., "An Introduction of Statistical Thermodynamics", Addison-Wesley, Reading, Massachusetts, U.S.A. (1960).

(82) DIN, F., "The Thermodynamic Functions of Gases", Butterworths, London (1956).

(83) BARTIS, J.T., and HALL, C.K., Physica, 78, 1 (1974).

(84) LIPHARD, K.G., and SCHNEIDER, G.M., J. Chem. Thermodynamics, 7, 805 (1975).

(85) TEJA, A.S., and ROWLINSON, J.S., Chem. Engng. Sci., 28, 529 (1973).

(86) TEJA, A.S., Ph.D. Thesis, University of London (1971).

(87) GIBBS, J.W., "Collected Works, Volume I: Thermodynamics", Yale Univ. Press, New Haven (1948).

(88) MÜNSTER, A., "Classical Thermodynamics", Wiley-Interscience, New York (1970).

(89) HICKS, C.P., and YOUNG, C.L., J.C.S. Faraday II, 73, 597 (1977).

(90) McDONALD, I.R., in "Statistical Mechanics", vol. 1, pp. 134-193, Specialist Periodical Reports, The Chemical Society, London (1973).

(91) KURATA, F., and KATZ, D.L., Trans. Am. Inst. Chem. Engrs., 38, 995 (1942).

(92) ORGANICK, E.I., Chem. Engng. Prog. Symp. Ser. No. 6, 49, 81 (1953).

(93) DAVIS, P.C., BERTUZZI, A.F., GORE, T.L., and KURATA, F., Petrol. Trans. Am. Inst. Mech. Engrs., 201, 245 (1954).

(94) REID, R.C., and SHERWOOD, T.K., "The Properties of Gases and Liquids", 2nd edition, McGraw-Hill, New York (1966); REID, R.C., PRAUSNITZ, J.M., and SHERWOOD, T.K., "The Properties of Gases and Liquids", 3rd edition, McGraw-Hill, New York (1977).

(.../)

(95) SPENCER, C.F., DAUBERT, T.E., and DANNER, R.P., A.I.Ch.E. Journal, 19, 522 (1973).

(96) CHUEH, P.L., and PRAUSNITZ, J.M., A.I.Ch.E. Journal, 13, 1107 (1967).

(97) PRAUSNITZ, J.M., and CHUEH, P.L., "Computer Calculations for High-Pressure Vapour-Liquid Equilibria", Prentice Hall, Englewood Cliffs (1968).

(98) TEMKIN, M.I., Russ. J. Phys. Chem., 33, 275 (1959).

(99) Van der WAALS, J.D., "Die Kontinuität des gasförmigen und flüssigen Zustandes", vol. 2, chap. 1, Leipzig (1900).

(100) BOBERG, T.C., and WHITE, R.R., Ind. Eng. Chem. Fundam., 1, 40 (1962).

(101) REDLICH, O., and KISTER, A.T., J. Chem. Phys., 36, 2002 (1962).

(102) REDLICH, O., and KISTER, A.T., Indust. Engng. Chem., 40, 341 (1948); REDLICH, O., and TURNQUIST, C.E., Chem. Engng. Prog. Symp. Ser. No. 2, 48, 49 (1952).

(103) REDLICH, O., and KWONG, J.N.S., Chemical Reviews, 44, 233 (1949).

(104) ACKERMAN, F.J., and REDLICH, O., J. Chem. Phys., 38, 2740 (1963).

(105) BENEDICT, M., WEBB, G.B., and RUBIN, L.D., J. Chem. Phys., 8, 334 (1940); 10, 747 (1942); Chem. Engng. Prog., 47, 419 (1951).

(106) ARAI, Y., and SAITO, S., J. Chem. Eng. Japan, 3, 253 (1970).

(107) SARASHINA, E., NOHKA, J., ARAI, Y., and SAITO, S., J. Chem. Eng. Japan, 7, 219 (1974).

(108) PROKHOROV, V.M., Russ. J. Phys. Chem.,44, 1713 (1970).

(109) JOFFE, J., and ZUDKEVITCH, D., Chem. Engng. Prog. Symp. Ser. No. 81, 63, 43 (1967).

(110) HISSONG, D.W., and KAY, W.B., A.I.Ch.E. Journal, 16, 580 (1970).

(111) PAK, S.C., and KAY, W.B., Ind. Eng. Chem. Fundam., 11, 255 (1972).

(112) HURON, M.-J., Chem. Engng. Sci., 31, 837 (1976).

(.../)

(113) SPEAR, R.R., ROBINSON, R.L., and CHAO, K.C., Ind. Eng. Chem. Fundam., 8, 2 (1969).

(114) DEITERS, U., and SCHNEIDER, G.M., Ber. Bunsenges. physik. Chem., 80, 1316 (1976).

(115) SPEAR, R.R., ROBINSON, R.L., and CHAO, K.C., Ind. Eng. Chem. Fundam., 10, 588 (1971).

(116) PENG, D.-Y., and ROBINSON, D.B., A.I.Ch.E. Journal, 23, 137 (1977).

(117) REID, R.C., and BEEGLE, B.L., A.I.Ch.E. Journal, 23, 726 (1977).

(118) SCHOUTEN, J.A., TEN SELDAM, C.A., and TRAPPENIERS, N.J., Physica, 73, 556 (1974).

(119) GUGGENHEIM, E.A., "Mixtures", Clarendon Press, Oxford (1952).

(120) MERMIN, N.D., Phys. Rev. Letters, 26, 957 (1971).

(121) CLARK, R.K., and NEECE, G.A., J. Chem. Phys., 48, 2575 (1968); WHEELER, J.C., and WIDOM, B., J. Amer. Chem. Soc., 90, 3064 (1968); WHEELER, J.C., Ber. Bunsenges. physik. Chem., 76, 308 (1972).

(122) GUNNING, A.J.,and ROWLINSON, J.S., Chem. Engng. Sci., 28, 521 (1973).

(123) HICKS, C.P., J.C.S. Faraday II, 72, 423 (1976).

(124) LELAND, T.W., CHAPPELEAR, P.S., and GAMSON, B.W., A.I.Ch.E. Journal, 8, 482 (1962); LEACH, J.W., CHAPPELEAR, P.S., and LELAND, T.W., Proc. Am. Petrol. Inst., 46, 223 (1966); A.I.Ch.E. Journal, 14, 568 (1968); REID, R.C., and LELAND, T.W., A.I.Ch.E. Journal, 11. 228 (1965); FISHER, G.D., and LELAND, T.W., Ind. Eng. Chem. Fundam., 9, 537 (1970).

(125) HICKS, C.P., and YOUNG, C.L., J.C.S. Faraday I, 72, 122 (1976); J.C.S. Faraday II, 73, 597 (1977); HURLE, R.L., JONES, F., and YOUNG, C.L., J.C.S. Faraday II, 73, 613 (1977); HURLE, R.L., TOCZYLKIN, L., and YOUNG, C.L., J.C.S. Faraday II, 73, 618 (1977); HICKS, C.P., HURLE, R.L., and YOUNG, C.L., J.C.S. Faraday II, 73, 1884 (1977).

(126) McGLASHAN, M.L., STEAD, K., and WARR, C., paper presented at the 3rd International Conference on Chemical Thermodynamics, Vienna (1973); J.C.S. Faraday II, 73, 1889 (1977).

(.../)

(127) SCOTT, R.L., paper presented at the 3rd International Conference on Chemical Thermodynamics, Vienna (1973).

(128) SNIDER, N.S., and HERRINGTON, T.M., J. Chem. Phys., 47, 2248 (1967).

(129) SMITH, W.R., in "Statistical Mechanics", vol. 1, pp. 71-132, Specialist Periodical Reports, The Chemical Society, London (1973).

(130) RIGBY, M., ALDER, B.J., SAPSE, A.M., and HECHT, C.E., J. Chem. Phys., 52, 3665 (1970).

(131) SCHOUTEN, J.A., DEERENBERG, A., and TRAPPENIERS, N.J., Physica, 81A, 151 (1975).

(132) MANSOORI, G.A., DARNAHAN, W.F., STARLING, K.E., and LELAND, T.W., J. Chem. Phys., 54, 1523 (1971).

(133) MYRAT, C.D., TRAPPENIERS, N.J., and SCHOUTEN, J.A., Physica, 94A, 559 (1978).

(134) NEFF, R.O., and McQUARRIE, D.A., J. Phys. Chem. 79, 1022 (1975).

(135) WEEKS, J.D., CHANDLER, D., and ANDERSON, H.C., J. Chem. Phys., 54, 5237 (1971).

(136) KREGLEWSKI, A., and KAY, W.B., J. Phys. Chem., 73, 3359 (1969).

(137) TAN, P.Y., LUKS, K.D., and KOZAK, J.J., J. Chem. Phys., 55, 1012 (1971).

(138) GUBBINS, K.E., and TWU, C.H., Chem. Engng. Sci., 33, 863 (1978); TWU, C.H., and GUBBINS, K.E., Chem. Engng. Sci., 33, 879 (1978).

(139) PITZER, K.S., and CURL, R.F., "Thermodynamic and Transport Properties of Fluids", Institution of Mechanical Engineers, London (1958).

(140) CANFIELD, F.B., and GUNNING, A.J., Chem. Engng. Sci., 26, 1136 (1971).

(141) LELAND, T.W., ROWLINSON, J.S., and SATHER, G.A., Trans. Faraday Soc., 64, 1447 (1968).

(142) ANGUS, S., ARMSTRONG, B., and de REUCK, K.M., "International Thermodynamic Tables of the Fluid State - 5. Methane", Pergamon Press, Oxford (1978).

(.../)

(143) STEWART, R.B., and JACOBSEN, R.T., "Preliminary thermodynamic property formulation for oxygen", Center for Applied Thermodynamic Studies, Report No. 76-5, University of Idaho (1976).

(144) SZCZEPANSKI, R., Ph.D. Thesis, University of London (1979).

(145) BETT, K.E., ROWLINSON, J.S., and SAVILLE, G., "Thermodynamics for Chemical Engineers", The Athlone Press, University of London (1975).

(146) VENNIX, A.J., and KOBAYASHI, R., A.I.Ch.E. Journal, 15, 930 (1969).

(147) NAG Fortran Library Manual, Mark 6 (FLM 6), Volume 1 (1977).

(148) SAVILLE, G., Dept. of Chem. Eng., Imperial College, London, private communication (1979).

(149) CROLL, I.M., and SCOTT, R.L., J. Phys. Chem., 68, 3853 (1964).

(150) TEJA, A.S., Chem. Engng. Sci., 33, 609 (1978).

(151) PRIGOGINE, I., and DEFAY, R., "Chemical Thermodynamics", transl. D.H. Everett, Longmans (1954).

(152) CARRUTH, G.F., and KOBAYASHI, R., J. Chem. Engng. Data, 18, 115 (1973).

(153) VARGAFTIK, N.B., "Tables on the Thermophysical Properties of Liquids and Gases", 2nd edition, Hemisphere Publishing Co., Washington (1975).

(154) SIMON, M., KNOBLER, C.M., and DUNCAN, A.G., Cryogenics, 7, 138 (1967).

(155) Encyclopédie des Gaz, L'Air Liquide, Division Scientifique, Elsevier, Amsterdam (1976).

APPENDIX A

PURITY OF MATERIALS

Carbon Tetrafluoride

This was supplied by BOC Limited to the following specification:

G.L.C. analysis: Minimum purity of 99.7%;
Specific volume at 20 ^{o}C: 0.14 $m^{3}.kg^{-1}$;
Boiling point: -128 ^{o}C.

n-Heptane

This was supplied by B.D.H. Chemicals Ltd. to the following specification:

G.L.C. analysis: Not less than 99.5%;
Density at 20 ^{o}C: 0.682 to 0.684 $g.ml^{-1}$;
Refractive index: 1.3880 to 1.3885;
Boiling range: Note more than 1 ^{o}C between 97 ^{o}C and 99 ^{o}C.

APPENDIX B - PHYSICAL PROPERTIES OF PURE SUBSTANCES

SUBSTANCE	MOLECULAR WEIGHT	T^c (K)	ρ^c (mol.dm^{-3})	P^c (bar)	z^c	ω	NORMAL BOILING POINT (^oC)	NORMAL MELTING POINT (^oC)
CARBON TETRAFLUORIDE CF_4	88.01	227.67	7.1073	37.39	0.2770	0.191	-128.0	-186.8
METHANE CH_4	16.04	190.555	10.1095	45.97	0.2870	0.013	-164.0	-182.5
ETHANE CH_3CH_3	30.07	305.43	6.7510	48.86	0.2850	0.105	-88.6	-183.3
PROPANE $CH_3CH_2CH_3$	44.11	369.82	4.9210	42.52	0.2810	0.152	-42.1	-189.7
n-BUTANE $CH_3(CH_2)_2CH_3$	58.13	425.16	3.9230	37.99	0.2740	0.201	-0.5	-138.4
n-PENTANE $CH_3(CH_2)_3CH_3$	72.15	469.65	3.2850	33.65	0.2623	0.259	36.1	-129.7
n-HEXANE $CH_3(CH_2)_4CH_3$	86.18	507.40	2.7040	30.12	0.2640	0.290	68.9	-95.0
n-HEPTANE $CH_3(CH_2)_5CH_3$	100.21	540.20	2.3150	27.35	0.2630	0.352	98.4	-90.6

APPENDIX C - TABULATED EXPERIMENTAL RESULTS

TABLE C.1 - T = 323.15 K

	DENSE PHASE				LIGHT PHASE			
Pressure (bar)	Mass of $n\text{-}C_7H_{16}$(g)	Volume of CF_4 (cm^3)	Mole fraction CF_4	Molar density ($mol.dm^{-3}$)	Mass of $n\text{-}C_7H_{16}$(g)	Volume of CF_4 (cm^3)	Mole fraction CF_4	Molar density ($mol.dm^{-3}$)
22	2.9387	27.7	0.041	6.8	0.1323	172.9	0.854_5	0.9
45	2.8663	59.4	0.085	7.0	0.1322	390.0	0.930	1.9
70	2.8028	91.2	0.127_5	7.2	0.1479	654.3	0.952	3.1
89	2.7497	116.8	0.160	7.3	0.1852	875.8	0.955	4.1
113	2.6668	147.6	0.199	7.4	0.2685	1159.8	0.951	5.5
138	2.6007	179.1	0.236	7.6	0.3737	1434.8	0.945	6.8
154	2.5220	194.8	0.255	7.6_5	0.4484	1574.9	0.940	7.5
212	0.3100	858.9	0.926	9.3	5.4868	558.2	0.314	8.0
267	0.4067	939.5	0.912	10.3	5.2862	649.7	0.356	8.2
399	0.5955	1011.2	0.884	11.5	4.9973	841.5	0.431	8.7
440	0.6423	1025.9	0.878	11.7	4.9138	891.9	0.449	8.9
583	0.7358	1068.6	0.867	12.4	4.7626	1021.4	0.491	9.3
640	0.7560	1081.7	0.865	12.5	4.7595	1044.3	0.496	9.4
660	0.7765	1084.0	0.862_5	12.6	4.7672	1051.9	0.498	9.4_5
699	0.7720	1103.6	0.865	12.8	4.7921	1056.1	0.497_5	9.5
850	0.7661	1160.6	0.872	13.3_5	4.9605	1037.7	0.484_5	9.6
936	0.7000	1217.2	0.886_5	13.8	5.0677	1011.6	0.473	9.6
976	0.6815	1236.1	0.891	13.9	5.1314	993.9	0.465	9.5_5
990	0.6830	1243.1	0.891	14.0	5.1540	987.9	0.463	9.5_5
1254	0.5412	1366.9	0.919	14.9	5.5289	878.5	0.416_5	9.4

TABLE C.2 - T = 330.15 K

	DENSE PHASE				LIGHT PHASE			
Pressure (bar)	Mass of $n\text{-}C_7H_{16}$ (g)	Volume of CF_4 (cm^3)	Mole fraction CF_4	Molar density ($mol.dm^{-3}$)	Mass of $n\text{-}C_7H_{16}$ (g)	Volume of CF_4 (cm^3)	Mole fraction CF_4	Molar density ($mol.dm^{-3}$)
293	0.4777	926.9	0.897	10.4	4.9554	754.1	0.406	8.3
343	0.5861	943.3	0.878_5	10.8	4.7651	855.2	0.446_5	8.6
400	0.7133	948.1	0.856_5	11.1	4.5637	976.2	0.490	8.9
456	0.8485	940.7	0.833	11.3	4.3773	1082.2	0.526	9.2
512	0.9895	914.5	0.806	11.4	4.1553	1207.5	0.566	9.5_5
575	1.1300	885.6	0.779	11.4	3.9132	1348.1	0.607_5	9.9
652	1.2354	868.7	0.759_5	11.5	3.6730	1500.5	0.647	10.4
700	1.2333	880.2	0.762	11.6	3.7128	1517.5	0.647_5	10.5
750	1.2050	915.8	0.773_5	11.9	3.8464	1485.6	0.634_5	10.5
775	1.1673	944.3	0.784	12.1	3.9322	1460.6	0.625	10.4_5
804	1.1274	964.0	0.793_5	12.2	4.0435	1428.6	0.613_5	10.4
850	1.0747	1007.4	0.808	12.5	4.1792	1387.2	0.598_5	10.4
901	1.0286	1045.2	0.820	12.8	4.3666	1329.7	0.578	10.3
1003	0.9190	1121.2	0.846	13.3	4.6110	1262.3	0.551_5	10.2_5

TABLE C.3 - T = 330.75 K

	DENSE PHASE				LIGHT PHASE			
Pressure (bar)	Mass of $n\text{-}C_7H_{16}$(g)	Volume of CF_4 (cm^3)	Mole fraction CF_4	Molar density ($mol.dm^{-3}$)	Mass of $n\text{-}C_7H_{16}$(g)	Volume of CF_4 (cm^3)	Mole fraction CF_4	Molar density ($mol.dm^{-3}$)
318	0.5488	927.9	0.884	10.5	4.7775	834.1	0.439_5	8.5
450	0.8538	934.5	0.831	11.3	4.2938	1112.7	0.538	9.2_5
475	0.9126	925.4	0.820	11.3	4.1786	1174.7	0.558	9.4
496	0.9764	912.4	0.807_5	11.3	4.1206	1219.8	0.571	9.5_5
523	1.0610	888.4	0.790	11.3	3.9669	1302.6	0.596	9.8
549	1.1602	853.2	0.768	11.1_5	3.7262	1409.2	0.629_5	10.0
559	1.2417	827.3	0.749_5	11.1	3.5302	1494.9	0.655_5	10.2
SINGLE PHASE REGION								
785	1.3079	873.3	0.750	11.7	3.5502	1641.2	0.675	10.9
798	1.2757	896.4	0.759_5	11.8_5	3.6945	1587.2	0.659	10.8
825	1.2011	937.0	0.778	12.1	3.9065	1512.8	0.635	10.6_5
846	1.1645	960.1	0.787_5	12.2	4.0397	1467.9	0.620	10.6
875	1.1106	995.0	0.801	12.4_5	4.1615	1424.7	0.606	10.5
902	1.0710	1022.2	0.811	12.6_5	4.2548	1387.3	0.594	10.4_5

TABLE C.4 - T = 331.15 K

	DENSE PHASE				LIGHT PHASE			
Pressure (bar)	Mass of $n\text{-}C_7H_{16}$(g)	Volume of CF_4 (cm^3)	Mole fraction CF_4	Molar density ($mol.dm^{-3}$)	Mass of $n\text{-}C_7H_{16}$(g)	Volume of CF_4 (cm^3)	Mole fraction CF_4	Molar density ($mol.dm^{-3}$)
213	0.3278	831.7	0.919	9.1	5.3069	583.9	0.331	7.9
263	0.4190	897.8	0.906	9.9_5	5.0840	697.2	0.381	8.2
347	0.6310	936.2	0.869_5	10.8	4.7173	888.6	0.458_5	8.7
400	0.7449	937.8	0.850	11.1	4.4854	1008.4	0.502_5	9.0
450	0.8896	917.6	0.822_5	11.2	4.2478	1138.1	0.546	9.3
476	0.9685	902.0	0.807	11.2	4.0782	1224.7	0.574	9.5_5
500	1.0625	876.0	0.787_5	11.1_5	3.8939	1308.0	0.601_5	9.7
512	1.1150	862.0	0.776_5	11.1_5	3.8277	1349.2	0.613	9.8_5
522	1.1797	843.0	0.762_5	11.1	3.6537	1425.0	0.636_5	10.0
SINGLE PHASE REGION								
825	1.3167	885.9	0.751_5	11.8	3.6181	1648.5	0.672	11.0
848	1.2372	929.2	0.771_5	12.1	3.8307	1558.1	0.646	10.8
878	1.1652	972.5	0.789_5	12.3_5	4.0175	1482.2	0.624	10.6
900	1.1206	1001.3	0.800_5	12.5_5	4.1103	1448.3	0.613	10.6
924	1.0750	1022.1	0.810	12.6_5	4.2440	1405.0	0.598	10.5
945	1.0535	1044.1	0.816_5	12.8	4.3293	1377.0	0.588	10.5
1000	0.9735	1092.3	0.834_5	13.1	4.5074	1318.2	0.568	10.4
1118	0.8706	1174.3	0.858	13.7	4.8475	1209.9	0.528_5	10.2_5
1230	0.7822	1242.6	0.877	14.2	5.0680	1140.5	0.503	10.1_5

TABLE C.5 - T = 333.15 K

	DENSE PHASE				LIGHT PHASE			
Pressure (bar)	Mass of $n\text{-}C_7H_{16}$(g)	Volume of CF_4 (cm^3)	Mole fraction CF_4	Molar density ($mol.dm^{-3}$)	Mass of $n\text{-}C_7H_{16}$(g)	Volume of CF_4 (cm^3)	Mole fraction CF_4	Molar density ($mol.dm^{-3}$)
20	2.8869	23.4	0.035	6.7	0.1376	150.4	0.831	0.8
41	2.8235	52.2	0.077	6.8	0.1299	344.3	0.922_5	1.7
67	2.7400	89.2	0.127_5	7.0	0.1463	602.1	0.949	2.8_5
86	2.7030	113.0	0.158	7.2	0.1802	802.4	0.952_5	3.8
106	2.6350	140.6	0.193	7.3	0.2370	1033.3	0.951_5	4.8_5
127	2.5790	165.4	0.224	7.4	0.3298	1256.3	0.945	5.9_5
146	2.5257	191.5	0.254	7.5_5	0.4326	1434.5	0.937	6.8_5
158	2.4973	205.8	0.270	7.6_5	0.4965	1523.7	0.932_5	7.3
168	2.4743	217.9	0.283_5	7.7	0.5250	1592.4	0.931_5	7.6_5
176	2.4419	229.7	0.297	7.7_5	0.5740	1646.7	0.928	7.9_5
205	0.3195	797.2	0.918	8.7	5.3055	580.1	0.329_5	7.9
220	0.3559	826.0	0.912_5	9.1	5.1800	618.3	0.349	7.9
247	0.4175	865.1	0.903	9.6	5.1115	670.6	0.371	8.1
269	0.4532	890.1	0.898	9.9_5	4.9950	722.4	0.394	8.2
277	0.4814	896.8	0.893	10.1	4.9388	748.5	0.405	8.3
301	0.5460	911.2	0.882	10.3_5	4.8225	805.1	0.428_5	8.4
317	0.5670	917.2	0.879	10.5	4.7610	845.1	0.444	8.5
353	0.6705	920.1	0.860_5	10.7	4.5700	942.0	0.481	8.8
377	0.7349	915.3	0.848_5	10.8	4.5143	982.7	0.494_5	8.9
402	0.8055	910.4	0.835_5	10.9	4.3435	1057.9	0.522_5	9.0_5
426	0.8875	898.0	0.820	11.0	4.1790	1140.5	0.551	9.3
456	0.9758	881.4	0.802	11.0	3.9945	1233.7	0.581	9.5
473	1.0670	854.4	0.782_5	10.9_5	3.8340	1315.7	0.606_5	9.7
483	1.1390	829.8	0.766	10.9	3.6550	1393.3	0.631_5	9.9
490	1.2120	808.5	0.750	10.8	3.5190	1456.0	0.650	10.0

(cont. over)

TABLE C.5 (continued)

Pressure (bar)	DENSE PHASE				LIGHT PHASE			
	Mass of $n\text{-}C_7H_{16}$(g)	Volume of CF_4 (cm^3)	Mole fraction CF_4	Molar density ($mol.dm^{-3}$)	Mass of $n\text{-}C_7H_{16}$(g)	Volume of CF_4 (cm^3)	Mole fraction CF_4	Molar density ($mol.dm^{-3}$)
SINGLE PHASE REGION								
970	1.3250	909.4	0.755	12.1	3.6893	1686.3	0.672_5	11.2
983	1.2602	947.9	0.772	12.3	3.8000	1629.0	0.658	11.1
990	1.2269	963.1	0.779	12.4	3.9127	1583.7	0.645	11.0
998	1.2007	982.1	0.786	12.5	3.9960	1554.8	0.636	10.9_5
1023	1.1378	1019.0	0.801	12.7_5	4.1410	1493.6	0.618_5	10.8
1041	1.1139	1037.2	0.807	12.9	4.2348	1458.4	0.607_5	10.7_5
1064	1.0732	1062.7	0.816_5	13.0_5	4.3241	1417.5	0.595_5	10.6_5
1104	0.9950	1107.0	0.833	13.3	4.5175	1349.0	0.573	10.5_5
1143	0.9416	1146.6	0.845_5	13.6	4.6532	1298.3	0.556	10.4_5
1276	0.8230	1233.7	0.871	14.2	4.9915	1175.3	0.514	10.2

TABLE C.6 - T = 343.15 K

	DENSE PHASE				LIGHT PHASE			
Pressure (bar)	Mass of $n\text{-}C_7H_{16}$ (g)	Volume of CF_4 (cm^3)	Mole fraction CF_4	Molar density ($mol.dm^{-3}$)	Mass of $n\text{-}C_7H_{16}$ (g)	Volume of CF_4 (cm^3)	Mole fraction CF_4	Molar density ($mol.dm^{-3}$)
19	2.8295	24.2	0.037	6.5_5	0.1317	133.8	0.820	0.7
34	2.7978	43.2	0.065	6.7	0.1216	268.2	0.908	1.3
42	2.7893	52.1	0.077_5	6.7_5	0.1204	339.7	0.927	1.6_5
53	2.7382	72.4	0.106	6.8_5	0.1249	439.3	0.940_5	2.1
67	2.7190	88.7	0.128	6.9_5	0.1407	572.1	0.948	2.7
84	2.6621	113.3	0.160_5	7.1	0.1697	733.2	0.951	3.4_5
109	2.5873	145.8	0.202	7.2_5	0.2482	982.2	0.947	4.6_5
130	2.5209	176.6	0.239_5	7.4	0.3261	1181.1	0.942	5.6
150	2.4540	202.4	0.270	7.5	0.4268	1359.8	0.935	6.5
164	2.4049	222.4	0.293_5	7.6	0.5139	1465.6	0.927_5	7.1
175	2.3680	236.1	0.309_5	7.6_5	0.9826	1533.0	0.922	7.4_5
200	2.2730	272.7	0.350	7.8	0.7421	1676.3	0.910	8.2_5
224	0.4064	793.0	0.897_5	8.8_5	4.9105	678.0	0.383	7.9
248	0.4714	816.3	0.886	9.2_5	4.6980	751.1	0.418	8.0_5
262	0.5303	829.4	0.875_5	9.5	4.6328	790.9	0.434	8.1_5
283	0.5880	839.7	0.865	9.7_5	4.4467	860.6	0.465	8.3
299	0.6672	839.9	0.850	9.9	4.3223	926.2	0.490_5	8.4_5
315	0.7445	831.7	0.834	10.0	4.1509	1000.1	0.520	8.6
322	0.8018	821.6	0.821_5	10.0	4.0474	1041.1	0.536	8.7
329	0.8600	810.4	0.809	10.0_5	3.9350	1085.2	0.553_5	8.8
334	0.9064	799.6	0.798_5	10.0_5	3.8408	1129.6	0.569	8.9
339	0.9318	792.4	0.792_5	10.0	3.7254	1172.2	0.586	8.9_5
345	0.9966	775.1	0.777_5	10.0	3.6236	1215.9	0.601	9.0_5
352	1.0888	747.6	0.755	9.9	3.4186	1304.0	0.631_5	9.2_5

APPENDIX D

OUTLINE OF DERIVATION OF EQUATIONS (6-3) AND (6-4)

The volume of CF_4 at standard temperature and pressure is obtained from the experimental value measured at ambient temperature and pressure by assuming perfect gas behaviour:

$$(V)^{S.T.P.} = (V)^{A.T.P.} \times \left(\frac{P^{amb.} - P^{vac.}}{760}\right) \times \left(\frac{273.15}{t^{amb.} + 273.15}\right) \qquad (D\text{-}1)$$

where:

$(V)^{S.T.P.}$ = volume of CF_4, cm^3, reduced to standard conditions of temperature and pressure (0 °C, 1 atm);

$(V)^{A.T.P.}$ = volume of CF_4 experimentally measured at ambient temperature and pressure, cm^3;

$(P)^{amb.}$ = ambient pressure, mm of Hg;

$(P)^{vac.}$ = vacuum pressure, mm of Hg;

$(t)^{amb.}$ = ambient temperature, °C.

The fractional error in the value of $(V)^{S.T.P.}$ is therefore given by

$$\frac{\delta V^{S.T.P.}}{V^{S.T.P.}} = \left(\left(\frac{\delta V^{A.T.P.}}{V^{A.T.P.}}\right)^2 + \left(\frac{\delta(P^{amb.} - P^{vac.})}{P^{amb.} - P^{vac.}}\right)^2 + \left(\frac{\delta(t^{amb.} + 273.15)}{t^{amb.} + 273.15}\right)^2\right)^{\frac{1}{2}}, \qquad (D\text{-}2)$$

where the symbol δ has the same meaning as in equations (6-3) and (6-4). Since $P^{vac.} << P^{amb.}$ and the error in the measurement of $P^{vac.}$ is negligible, equation (D-2) can be written, to a good approximation:

$$\frac{\delta V^{S.T.P.}}{V^{S.T.P.}} \approx \left(\left(\frac{\delta V^{A.T.P.}}{V^{A.T.P.}}\right)^2 + \left(\frac{\delta P^{amb.}}{P^{amb.}}\right)^2 + \left(\frac{\delta t^{amb.}}{t^{amb.} + 273.15}\right)^2\right)^{\frac{1}{2}}. \qquad (D\text{-}3)$$

From section 6.2, the fractional errors in the measurement of the ambient pressure and temperature do not exceed 0.000 15 and 0.000 35 respectively, whereas the fractional error in the measurement of the

volume of CF_4 (A.T.P.) is of the order of 0.001. When these values are substituted in equation (D-3), it is obvious that the errors in the measurement of ambient temperature and pressure are negligible compared to the error in the measurement of $V^{A.T.P.}$. To all intents and purposes, therefore,

$$\frac{\delta V^{S.T.P.}}{V^{S.T.P.}} \approx \frac{\delta V^{A.T.P.}}{V^{A.T.P.}} \approx 0.001. \qquad \text{(D-4)}$$

The fractional error in the values of the mole fraction of CF_4 and molar density can now be obtained by using the formula for the propagation of random experimental errors:

$$(\delta x)^2 = \left(\frac{\partial x}{\partial V^{S.T.P.}}\right)^2 \left(\delta V^{S.T.P.}\right)^2 + \left(\frac{\partial x}{\partial W}\right)^2 (\delta W)^2 \qquad \text{(D-5)}$$

$$\text{and} \quad (\delta \rho)^2 = \left(\frac{\partial \rho}{\partial V^{S.T.P.}}\right)^2 \left(\delta V^{S.T.P.}\right)^2 + \left(\frac{\partial \rho}{\partial W}\right)^2 (\delta W)^2 + \left(\frac{\partial \rho}{\partial V_s}\right)^2 (\delta V_s)^2, \qquad \text{(D-6)}$$

where the symbols have the same meaning as in equations (6-1) and (6-2), and the various partial derivatives can be obtained from the same equations. When this is done, the following expressions are obtained for $(\delta x)^2$ and $(\delta \rho)^2$:

$$(\delta x)^2 = \frac{(V^*)^2}{M^2 V^2 \left(1 + \frac{V^* W}{MV}\right)^4} \left(\left(\frac{W}{V}\right)^2 (\delta V)^2 + (\delta W)^2\right) \qquad \text{(D-7)}$$

$$\text{and} \quad (\delta \rho)^2 = \left(\frac{1}{V^* V_s}\right)^2 (\delta V)^2 + \left(\frac{1}{MV_s}\right)^2 (\delta W)^2 + \left(\frac{\rho}{V_s}\right)^2 (\delta V_s)^2, \qquad \text{(D-8)}$$

where, for reasons of clarity, the superscript S.T.P. has been omitted from $(V^*)^{S.T.P.}$ and $(V)^{S.T.P.}$.

Equations (D-7) and (D-8) can be re-arranged to give, respectively:

$$\left(\frac{\delta x}{x}\right)^2 = \frac{(V^*)^2 W^2}{M^2 V^2 \left(1 + \frac{V^* W}{MV}\right)^2} \left(\left(\frac{\delta V}{V}\right)^2 + \left(\frac{\delta W}{W}\right)^2\right) \qquad \text{(D-9)}$$

(.../)

and

$$\left(\frac{\delta\rho}{\rho}\right)^2 = \left(\frac{V}{V^*\rho V_s}\right)^2\left(\frac{\delta V}{V}\right)^2 + \left(\frac{W}{M\rho V_s}\right)^2\left(\frac{\delta W}{W}\right)^2 + \left(\frac{\delta V_s}{V_s}\right)^2. \qquad \text{(D-10)}$$

Finally, by using equations (6-1) and (6-2), the following results are obtained for the fractional errors in the mole fraction x and density ρ respectively:

$$\left(\frac{\delta x}{x}\right) = (1 - x)\left(\left(\frac{\delta V}{V}\right)^2 + \left(\frac{\delta W}{W}\right)^2\right)^{\frac{1}{2}} \qquad \text{(D-11)}$$

and

$$\left(\frac{\delta\rho}{\rho}\right) = \left(x^2\left(\frac{\delta V}{V}\right)^2 + (1-x)^2\left(\frac{\delta W}{W}\right)^2 + \left(\frac{\delta V_s}{V_s}\right)^2\right)^{\frac{1}{2}}. \qquad \text{(D-12)}$$

APPENDIX E

OUTLINE OF DERIVATION OF EQUATIONS (9-36) - (9-44)

The configurational Helmholtz free energy of the equivalent substance is given by

$$\tilde{A}^{e.s.}[\rho,T,x] = f^{e.s.}[\rho,T,x]\tilde{A}_o[\rho_o,T_o] - RT\ln h^{e.s.}[\rho,T,x] \quad (E\text{-}1)$$

where

$$\rho_o \equiv \rho.h^{e.s.}[\rho,T,x] \quad (E\text{-}2)$$

and

$$T_o \equiv T/f^{e.s.}[\rho,T,x]. \quad (E\text{-}3)$$

By differentiation of (E-1) with respect to x, at constant ρ and T:

$$\tilde{A}^{e.s.}_x = f^{e.s.}_x \tilde{A}_o + f^{e.s.}\left(\frac{\partial \tilde{A}_o}{\partial x}\right)_{\rho,T} - RT\frac{h^{e.s.}_x}{h^{e.s.}}. \quad (E\text{-}4)$$

Since $\tilde{A}_o$ is a function of the independent variables ρ_o and T_o:

$$\left(\frac{\partial \tilde{A}_o}{\partial x}\right)_{\rho,T} = \left(\frac{\partial \tilde{A}_o}{\partial \rho_o}\right)_{T_o}\left(\frac{\partial \rho_o}{\partial x}\right)_{\rho,T} + \left(\frac{\partial \tilde{A}_o}{\partial T_o}\right)_{\rho_o}\left(\frac{\partial T_o}{\partial x}\right)_{\rho,T}. \quad (E\text{-}5)$$

From (E-2) and (E-3):

$$\left(\frac{\partial \rho_o}{\partial x}\right)_{\rho,T} = \rho h^{e.s.}_x \quad (E\text{-}6)$$

and

$$\left(\frac{\partial T_o}{\partial x}\right)_{\rho,T} = -T\frac{f^{e.s.}_x}{(f^{e.s.})^2} \quad (E\text{-}7)$$

and, from classical thermodynamics:

$$\left(\frac{\partial \tilde{A}_o}{\partial \rho_o}\right)_{T_o} = \frac{\tilde{P}_o}{\rho_o^2} = \frac{P_o}{\rho_o^2} \quad (E\text{-}8)$$

and

$$\left(\frac{\partial \tilde{A}_o}{\partial T_o}\right)_{\rho_o} = -\tilde{S}_o. \quad (E\text{-}9)$$

(.../)

Substitution of equations (E-6) to (E-9) into (E-5) gives:

$$\left(\frac{\partial \tilde{A}_o}{\partial x}\right)_{\rho,T} = \left(\frac{P_o}{\rho_o^2}\right)(\rho h_x^{e.s.}) + (\tilde{S}_o)\left(T\frac{f_x^{e.s.}}{(f^{e.s.})^2}\right)$$

$$= \left(\frac{P_o}{\rho_o}\right)\left(\frac{h_x^{e.s.}}{h^{e.s.}}\right) + (T_o\tilde{S}_o)\left(\frac{f_x^{e.s.}}{f^{e.s.}}\right). \qquad \text{(E-10)}$$

Substitution of this result in equation (E-4) finally gives:

$$\tilde{A}_x^{e.s.} = f_x^{e.s.}\tilde{A}_o + \left(\frac{f^{e.s.}h_x^{e.s.}}{h^{e.s.}}\right)\left(\frac{P_o}{\rho_o}\right)$$

$$+ f_x^{e.s.}(T_o\tilde{S}_o) - \left(\frac{f^{e.s.}h_x^{e.s.}}{h^{e.s.}}\right)(RT_o)$$

$$= \left(\frac{f^{e.s.}h_x^{e.s.}}{h^{e.s.}}\right)\left(\frac{P_o}{\rho_o} - RT_o\right) + f_x^{e.s.}(\tilde{A}_o + T_o\tilde{S}_o)$$

$$= \left(\frac{fh_x}{h}\right)^{e.s.}\left(\frac{P_o}{\rho_o} - RT_o\right) + f_x^{e.s.}\,\tilde{U}_o\ , \qquad \text{(E-11)}$$

which is equation (9-36).

Similarly, if equation (E-1) is differentiated with respect to ρ, at constant x and T:

$$\tilde{A}_\rho^{e.s.} = f_\rho^{e.s.}\tilde{A}_o + f^{e.s.}\left(\frac{\partial \tilde{A}_o}{\partial \rho}\right)_{x,T} - RT\frac{h_\rho^{e.s.}}{h^{e.s.}}\ . \qquad \text{(E-12)}$$

Again, since $\tilde{A}_o$ is a function of ρ_o and T_o:

$$\left(\frac{\partial \tilde{A}_o}{\partial \rho}\right)_{x,T} = \left(\frac{\partial \tilde{A}_o}{\partial \rho_o}\right)_{T_o}\left(\frac{\partial \rho_o}{\partial \rho}\right)_{x,T} + \left(\frac{\partial \tilde{A}_o}{\partial T_o}\right)_{\rho_o}\left(\frac{\partial T_o}{\partial \rho}\right)_{x,T}. \qquad \text{(E-13)}$$

From (E-2) and (E-3):

$$\left(\frac{\partial \rho_o}{\partial \rho}\right)_{x,T} = h^{e.s.} + \rho h_\rho^{e.s.} \qquad \text{(E-14)}$$

and

$$\left(\frac{\partial T_o}{\partial \rho}\right)_{x,T} = -T\frac{f_\rho^{e.s.}}{(f^{e.s.})^2}\ . \qquad \text{(E-15)}$$

(.../)

Substitution of (E-8), (E-9), (E-14) and (E-15) into equation (E-13) now gives:

$$\left(\frac{\partial \tilde{A}_o}{\partial \rho}\right)_{x,T} = \left(\frac{P_o}{\rho_o^2}\right)(h^{e.s.} + \rho h_\rho^{e.s.}) + (\tilde{S}_o)\left(T\frac{f_\rho^{e.s.}}{(f^{e.s.})^2}\right)$$

$$= h^{e.s.}\left(\frac{P_o}{\rho_o^2}\right) + \left(\frac{h_\rho^{e.s.}}{h^{e.s.}}\right)\left(\frac{P_o}{\rho_o}\right) + \left(\frac{f_\rho^{e.s.}}{f^{e.s.}}\right)(T_o\tilde{S}_o). \qquad \text{(E-16)}$$

Hence, from (E-12) and (E-16):

$$\tilde{A}_\rho^{e.s.} = f_\rho^{e.s.}\tilde{A}_o + (h^{e.s.}f^{e.s.})\left(\frac{P_o}{\rho_o^2}\right) + \left(\frac{f^{e.s.}h_\rho^{e.s.}}{h^{e.s.}}\right)\left(\frac{P_o}{\rho_o}\right)$$

$$+ f_\rho^{e.s.}(T_o\tilde{S}_o) - \left(\frac{f^{e.s.}h_\rho^{e.s.}}{h^{e.s.}}\right)(RT_o)$$

$$= (h^{e.s.}f^{e.s.})\left(\frac{P_o}{\rho_o^2}\right)$$

$$+ \left(\frac{f^{e.s.}h_\rho^{e.s.}}{h^{e.s.}}\right)\left(\frac{P_o}{\rho_o} - RT_o\right) + f_\rho^{e.s.}\,\tilde{U}_o\,. \qquad \text{(E-17)}$$

If, however, thermodynamic consistency is to be preserved, then clearly

$$\tilde{A}_\rho^{e.s.} = \frac{\tilde{P}^{e.s.}}{\rho^2} = \left(\frac{h^{e.s.}}{\rho_o}\right)^2\frac{f^{e.s.}}{h^{e.s.}}\,\tilde{P}_o$$

$$= (h^{e.s.}f^{e.s.})\left(\frac{P_o}{\rho_o^2}\right), \qquad \text{(E-18)}$$

since $\tilde{P}^{e.s.}$ and $\tilde{P}_o$ are related by

$$\tilde{P}^{e.s.} = \frac{f^{e.s.}}{h^{e.s.}}\,\tilde{P}_o. \qquad \text{(E-19)}$$

Comparison of (E-17) and (E-18) shows that the condition of thermodynamic consistency requires that the sum of the last two terms on the right-hand side of (E-17) must equal zero; thus

$$\left(\frac{fh_\rho}{h}\right)^{e.s.}\left(\frac{P_o}{\rho_o} - RT_o\right) + f_\rho^{e.s.}\,\tilde{U}_o = 0. \qquad \text{(E-20)}$$

(.../)

Equation (E-20) implies that the dependence of $h^{e.s.}$ and $f^{e.s.}$ on ρ is not arbitrary. Since the two scaling parameters are obtained via the molecular shape factor equations, a similar condition of thermodynamic consistency must apply to ϕ and θ. Canfield and Gunning (140) tested the Leach and Leland molecular shape factor equations for thermodynamic consistency and they managed to show, at least for pure substances, that equation (E-20) is very nearly satisfied for a wide range of values of reduced temperature and reduced volume.

As a final example, the derivation of equation (9-42) will be presented. This can be obtained from (E-11) by differentiation with respect to ρ or, alternatively, from (E-18) by differentiation with respect to x. The resulting equation should be the same whichever route is used, and this provides a convenient check for the derivation. Taking (E-18) as the starting point:

$$\tilde{A}^{e.s.}_{x\rho} = (h^{e.s.}_x f^{e.s.})\left(\frac{P_o}{\rho_o^2}\right) + (h^{e.s.} f^{e.s.}_x)\left(\frac{P_o}{\rho_o^2}\right) + (h^{e.s.} f^{e.s.})\left(\frac{\partial}{\partial x}\frac{P_o}{\rho_o^2}\right)_{\rho,T}. \qquad \text{(E-21)}$$

Using the same "chain-rule" as before in equation (E-5):

$$\left(\frac{\partial}{\partial x}\frac{P_o}{\rho_o^2}\right)_{\rho,T} = \left(\frac{\partial}{\partial \rho_o}\frac{P_o}{\rho_o^2}\right)_{T_o}\left(\frac{\partial \rho_o}{\partial x}\right)_{\rho,T} + \left(\frac{\partial}{\partial T_o}\frac{P_o}{\rho_o^2}\right)_{\rho_o}\left(\frac{\partial T_o}{\partial x}\right)_{\rho,T}, \qquad \text{(E-22)}$$

with

$$\left(\frac{\partial}{\partial \rho_o}\frac{P_o}{\rho_o^2}\right)_{T_o} = \frac{1}{\rho_o^2}\left(\frac{\partial P_o}{\partial \rho_o}\right)_{T_o} - 2\frac{P_o}{\rho_o^3} \qquad \text{(E-23)}$$

and

$$\left(\frac{\partial}{\partial T_o}\frac{P_o}{\rho_o^2}\right)_{\rho_o} = \frac{1}{\rho_o^2}\left(\frac{\partial P_o}{\partial T_o}\right)_{\rho_o}. \qquad \text{(E-24)}$$

Substitution of equations (E-6), (E-7), (E-23) and (E-24) into equation (E-22) gives:

$$\left(\frac{\partial}{\partial x}\frac{P_o}{\rho_o^2}\right)_{\rho,T} = \left(\frac{h_x^{e.s.}}{h^{e.s.}}\right)\left(\frac{1}{\rho_o}\left(\frac{\partial P_o}{\partial \rho_o}\right)_{T_o} - 2\frac{P_o}{\rho_o^2}\right)$$

$$- \left(\frac{f_x^{e.s.}}{f^{e.s.}}\right)\left(\frac{T_o}{\rho_o^2}\left(\frac{\partial P_o}{\partial T_o}\right)_{\rho_o}\right). \qquad \text{(E-25)}$$

Finally, substitution of this result into equation (E-21) gives the required derivative:

$$A_{x\rho}^{e.s.} = (h_x^{e.s.} f^{e.s.})\left(\frac{1}{\rho_o}\left(\frac{\partial P_o}{\partial \rho_o}\right)_{T_o} - \frac{P_o}{\rho_o^2}\right)$$

$$+ (h^{e.s.} f_x^{e.s.})\left(\frac{P_o}{\rho_o^2} - \frac{T_o}{\rho_o^2}\left(\frac{\partial P_o}{\partial T_o}\right)_{\rho_o}\right). \qquad \text{(E-26)}$$

The derivation of the remaining equations in the set (9-36) to (9-44) follows a similar pattern, the only difference being that the equations for the higher derivatives become more complex.

APPENDIX F

OUTLINE OF DERIVATION OF EQUATIONS (9-58) AND (9-59)

It is convenient to start by re-writing equations (9-50) to (9-53):

$$h_{ii} = \left(\frac{\rho_o^c}{\rho_i^c}\right) \cdot \phi_{ii}[V_i^R, T_i^R] \qquad (i = 1,2) \qquad \text{(F-1)}$$

$$f_{ii} = \left(\frac{T_i^c}{T_o^c}\right) \cdot \theta_{ii}[V_i^R, T_i^R] \qquad (i = 1,2) \qquad \text{(F-2)}$$

$$V_i^R = \frac{\rho_o^c \, \phi_{ii}}{\rho \, h^{e.s.}} \qquad (i = 1,2) \qquad \text{(F-3)}$$

$$T_i^R = \frac{T \, \theta_{ii}}{T_o^c \, f^{e.s.}} \, . \qquad (i = 1,2) \qquad \text{(F-4)}$$

If each of these four equations is differentiated with respect to x at constant ρ and T, the following results are obtained:

$$\frac{\Delta h_{ii}}{h_{ii}} = \frac{\Delta \phi_{ii}}{\phi_{ii}} \qquad (i = 1,2) \qquad \text{(F-5)}$$

$$\frac{\Delta f_{ii}}{f_{ii}} = \frac{\Delta \theta_{ii}}{\theta_{ii}} \qquad (i = 1,2) \qquad \text{(F-6)}$$

$$\frac{\Delta V_i^R}{V_i^R} = \frac{\Delta \phi_{ii}}{\phi_{ii}} - \frac{\Delta h^{e.s.}}{h^{e.s.}} \qquad (i = 1,2) \qquad \text{(F-7)}$$

$$\frac{\Delta T_i^R}{T_i^R} = \frac{\Delta \theta_{ii}}{\theta_{ii}} - \frac{\Delta f^{e.s.}}{f^{e.s.}} \qquad (i = 1,2), \qquad \text{(F-8)}$$

where the symbol Δ is again used to represent differentiation with respect to x at constant ρ and T. Since the ϕ_{ii} and θ_{ii} are functions of the independent variables V_i^R and T_i^R, by the "chain rule":

$$\frac{\Delta\phi_{ii}}{\phi_{ii}} = \frac{1}{\phi_{ii}}\left(\frac{\partial\phi_{ii}}{\partial V_i^R}\right)\Delta V_i^R + \frac{1}{\phi_{ii}}\left(\frac{\partial\phi_{ii}}{\partial T_i^R}\right)\Delta T_i^R \qquad (i = 1,2) \quad \text{(F-9)}$$

and $$\frac{\Delta\theta_{ii}}{\theta_{ii}} = \frac{1}{\theta_{ii}}\left(\frac{\partial\theta_{ii}}{\partial V_i^R}\right)\Delta V_i^R + \frac{1}{\theta_{ii}}\left(\frac{\partial\theta_{ii}}{\partial T_i^R}\right)\Delta T_i^R \qquad (i = 1,2) \quad \text{(F-10)}$$

Combining equations (F-7), (F-8) and (F-9):

$$\frac{\Delta\phi_{ii}}{\phi_{ii}} = \frac{V_i^R}{\phi_{ii}}\left(\frac{\partial\phi_{ii}}{\partial V_i^R}\right)\left(\frac{\Delta\phi_{ii}}{\phi_{ii}} - \frac{\Delta h^{e.s.}}{h^{e.s.}}\right) + \frac{T_i^R}{\phi_{ii}}\left(\frac{\partial\phi_{ii}}{\partial T_i^R}\right)\left(\frac{\Delta\theta_{ii}}{\theta_{ii}} - \frac{\Delta f^{e.s.}}{f^{e.s.}}\right) \qquad (i = 1,2). \quad \text{(F-11)}$$

Similarly, combining equations (F-7), (F-8) and (F-10):

$$\frac{\Delta\theta_{ii}}{\theta_{ii}} = \frac{V_i^R}{\theta_{ii}}\left(\frac{\partial\theta_{ii}}{\partial V_i^R}\right)\left(\frac{\Delta\phi_{ii}}{\phi_{ii}} - \frac{\Delta h^{e.s.}}{h^{e.s.}}\right) + \frac{T_i^R}{\theta_{ii}}\left(\frac{\partial\theta_{ii}}{\partial T_i^R}\right)\left(\frac{\Delta\theta_{ii}}{\theta_{ii}} - \frac{\Delta f^{e.s.}}{f^{e.s.}}\right) \qquad (i = 1,2). \quad \text{(F-12)}$$

If, for clarity, the following quantities are now defined:

$$\left(\frac{DL\phi}{DLV}\right)_i \equiv \frac{V_i^R}{\phi_{ii}}\left(\frac{\partial\phi_{ii}}{\partial V_i^R}\right)$$

$$\left(\frac{DL\phi}{DLT}\right)_i \equiv \frac{T_i^R}{\phi_{ii}}\left(\frac{\partial\phi_{ii}}{\partial T_i^R}\right)$$

$$\left(\frac{DL\theta}{DLV}\right)_i \equiv \frac{V_i^R}{\theta_{ii}}\left(\frac{\partial\theta_{ii}}{\partial V_i^R}\right)$$

and

$$\left(\frac{DL\theta}{DLT}\right)_i \equiv \frac{T_i^R}{\theta_{ii}}\left(\frac{\partial\theta_{ii}}{\partial T_i^R}\right)$$

$\Big\}$ $(i = 1,2)$, (F-13)

then equations (F-11) and (F-12) can be re-written as

$$\frac{\Delta\phi_{ii}}{\phi_{ii}} = \left(\frac{DL\phi}{DLV}\right)_i\left(\frac{\Delta\phi_{ii}}{\phi_{ii}} - \frac{\Delta h^{e.s.}}{h^{e.s.}}\right) + \left(\frac{DL\phi}{DLT}\right)_i\left(\frac{\Delta\theta_{ii}}{\theta_{ii}} - \frac{\Delta f^{e.s.}}{f^{e.s.}}\right) \quad (i = 1,2) \qquad \text{(F-14)}$$

and $$\frac{\Delta\theta_{ii}}{\theta_{ii}} = \left(\frac{DL\theta}{DLV}\right)_i\left(\frac{\Delta\phi_{ii}}{\phi_{ii}} - \frac{\Delta h^{e.s.}}{h^{e.s.}}\right) + \left(\frac{DL\theta}{DLT}\right)_i\left(\frac{\Delta\theta_{ii}}{\theta_{ii}} - \frac{\Delta f^{e.s.}}{f^{e.s.}}\right) \quad (i = 1,2). \qquad \text{(F-15)}$$

Using equations (F-5) and (F-6) to eliminate $\frac{\Delta\phi_{ii}}{\phi_{ii}}$ and $\frac{\Delta\theta_{ii}}{\theta_{ii}}$ from equations (F-14) and (F-15), we get:

$$\frac{\Delta h_{ii}}{h_{ii}} = \left(\frac{DL\phi}{DLV}\right)_i\left(\frac{\Delta h_{ii}}{h_{ii}} - \frac{\Delta h^{e.s.}}{h^{e.s.}}\right) + \left(\frac{DL\phi}{DLT}\right)_i\left(\frac{\Delta f_{ii}}{f_{ii}} - \frac{\Delta f^{e.s.}}{f^{e.s.}}\right) \quad (i = 1,2) \qquad \text{(F-16)}$$

and $$\frac{\Delta f_{ii}}{f_{ii}} = \left(\frac{DL\theta}{DLV}\right)_i\left(\frac{\Delta h_{ii}}{h_{ii}} - \frac{\Delta h^{e.s.}}{h^{e.s.}}\right) + \left(\frac{DL\theta}{DLT}\right)_i\left(\frac{\Delta f_{ii}}{f_{ii}} - \frac{\Delta f^{e.s.}}{f^{e.s.}}\right) \quad (i = 1,2). \qquad \text{(F-17)}$$

If these two simultaneous equations are now solved for $\frac{\Delta h_{ii}}{h_{ii}}$ and $\frac{\Delta f_{ii}}{f_{ii}}$, the results obtained, after some tedious but straightforward algebra, are precisely equations (9-58) and (9-59):

$$\frac{\Delta h_{ii}}{h_{ii}} = \frac{\left(\frac{DL\phi}{DLV}\frac{DL\theta}{DLT} - \frac{DL\theta}{DLV}\frac{DL\phi}{DLT} - \frac{DL\phi}{DLV}\right)_i \frac{\Delta h^{e.s.}}{h^{e.s.}} - \left(\frac{DL\phi}{DLT}\right)_i \frac{\Delta f^{e.s.}}{f^{e.s.}}}{\left(1 - \frac{DL\theta}{DLT} - \frac{DL\phi}{DLV} + \frac{DL\phi}{DLV}\frac{DL\theta}{DLT} - \frac{DL\theta}{DLV}\frac{DL\phi}{DLT}\right)_i} \quad (i = 1,2) \qquad \text{(F-18)}$$

and

$$\frac{\Delta f_{ii}}{f_{ii}} = \frac{\left(\frac{DL\phi}{DLV}\frac{DL\theta}{DLT} - \frac{DL\theta}{DLV}\frac{DL\phi}{DLT} - \frac{DL\theta}{DLT}\right)_i \frac{\Delta f^{e.s.}}{f^{e.s.}} - \left(\frac{DL\theta}{DLV}\right)_i \frac{\Delta h^{e.s.}}{h^{e.s.}}}{\left(1 - \frac{DL\theta}{DLT} - \frac{DL\phi}{DLV} + \frac{DL\phi}{DLV}\frac{DL\theta}{DLT} - \frac{DL\theta}{DLV}\frac{DL\phi}{DLT}\right)_i} \quad (i = 1,2). \qquad \text{(F-19)}$$

APPENDIX G

COEFFICIENTS IN EQUATION OF STATE FOR THE REFERENCE SUBSTANCE

The coefficients listed below are for the equation of state for methane, which was the reference substance equation of state used throughout this investigation. The form of the equation is given in section 9.1.6, equation (9-61). The numerical values of the coefficients listed here give pressure in bar when the temperature is expressed in K and the density in $mol.dm^{-3}$.

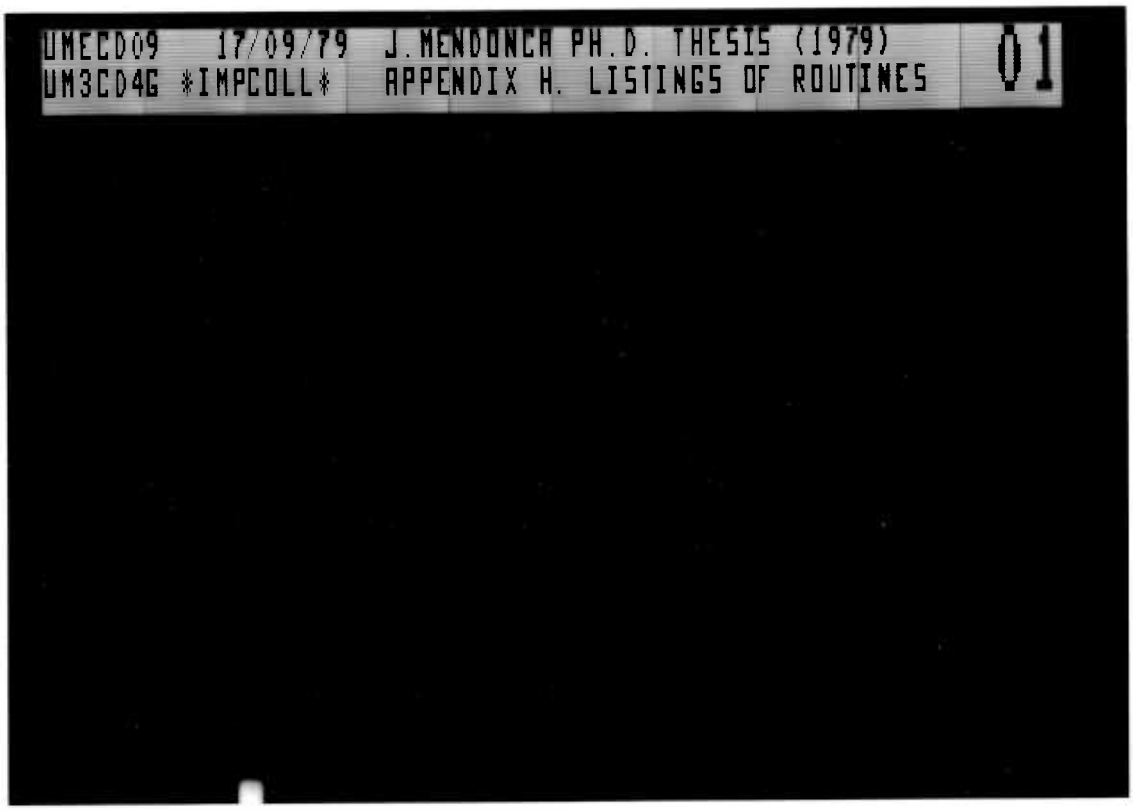
Coefficient	Numerical value
A_1	$.898183102418203 \times 10^{-3}$
A_2	$.188570883290667$
A_3	$-.507334853102101 \times 10^{1}$
A_4	$.242440372451133 \times 10^{3}$
A_5	$-.275937243280870 \times 10^{5}$
A_6	$.667706377937420 \times 10^{-4}$
A_7	$.659554690589554 \times 10^{-1}$
A_8	$-.475099859427983 \times 10^{2}$
A_9	$.941749168525057 \times 10^{4}$
A_{10}	$.203123055432435 \times 10^{-5}$
A_{11}	$-.882991375776145 \times 10^{-3}$
A_{12}	$.269841136358502 \times 10^{1}$
A_{13}	$.163105161848591 \times 10^{-3}$
A_{14}	$-.965840913440501 \times 10^{-2}$
A_{15}	$-.497527927565047$
A_{16}	$.388068765782800 \times 10^{-3}$
A_{17}	$-.447156684620678 \times 10^{-5}$
A_{18}	$.280554989023392 \times 10^{-3}$
A_{19}	$-.496671746902338 \times 10^{-6}$
A_{20}	$.427414662506472 \times 10^{4}$
A_{21}	$-.125241753249749 \times 10^{7}$
A_{22}	$-.102133310575650 \times 10^{3}$
A_{23}	$.788608202448113 \times 10^{6}$
A_{24}	$-.374931459166889 \times 10^{-1}$

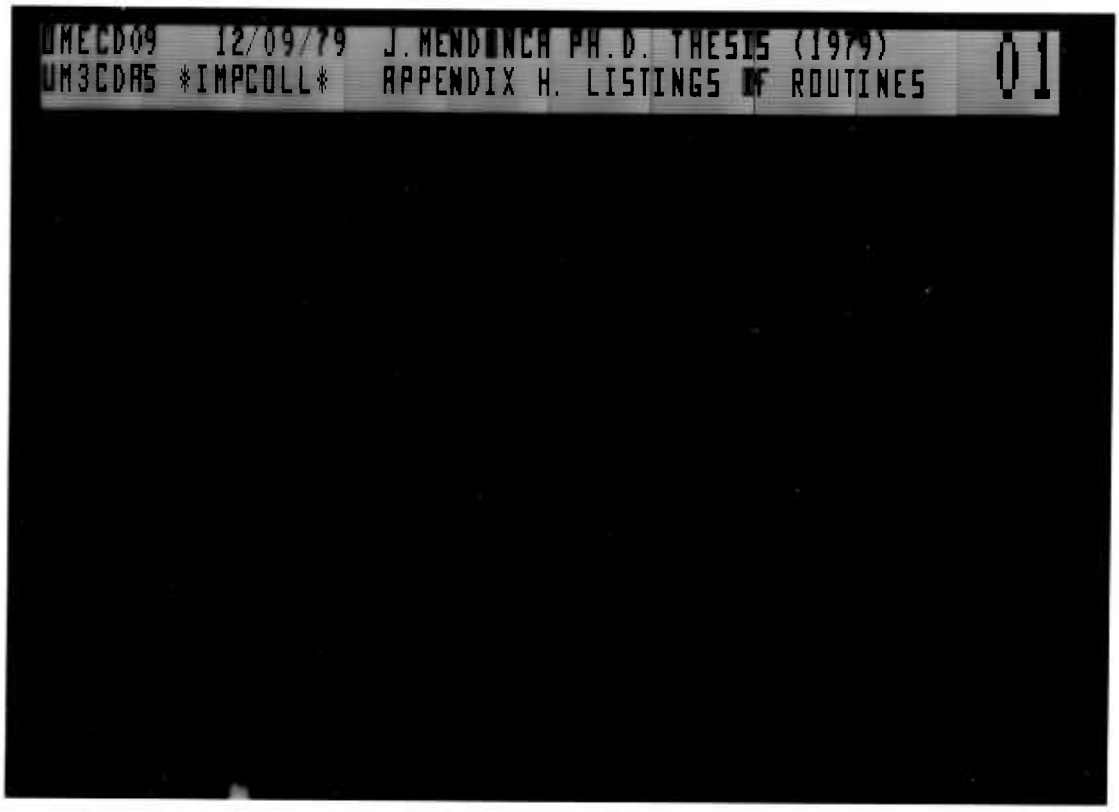
(.../)

Coefficient	Numerical value
A_{25}	$.127111849576157 \times 10^{2}$
A_{26}	$-.236364400068937 \times 10^{-2}$
A_{27}	$-.123455321378684 \times 10^{2}$
A_{28}	$.204715659218475 \times 10^{-5}$
A_{29}	$.406242840085238 \times 10^{-3}$
A_{30}	$-.873417429882791 \times 10^{-8}$
A_{31}	$-.381661132664854 \times 10^{-6}$
A_{32}	$.532641296926859 \times 10^{-5}$
γ	$.97 \times 10^{-2}$

The gas constant in these units is:

$$R = .0831434 \text{ bar.dm}^{3}.(\text{mol.K})^{-1}.$$


UMECD09 17/09/79 J.MENDONCA PH.D. THESIS (1979)
UM3CD4G *IMPCOLL* APPENDIX H. LISTINGS OF ROUTINES
01


UMECD09 12/09/79 J.MENDONCA PH.D. THESIS (1979)
UM3CDA5 *IMPCOLL* APPENDIX H. LISTINGS OF ROUTINES
01